Engineering geology and geohydrology of the magnesian limestone of Northern England

A. S. Burgess

ENGINEERING GEOLOGY AND GEOHYDROLOGY OF THE MAGNESIAN LIMESTONE OF NORTHERN ENGLAND

by

A. S. Burgess

Being a Thesis submitted to the University of Durham in Fulfilment of the Requirements for the Degree of Doctor of Philosophy

Durham, 1970.

CONTENTS

CONTENTS (Cont'd) Page

CONTENTS (Cont'd)

Page

SECTION IV SUMMARY AND CONCLUSIONS

FIGURES

SECTION I GEOLOGY

SECTION II GEOHYDROLOGY

FIGURES (Cont'd)

FIGURES (Cont'd).

SECTION III ENGINEERING GEOLOGY

FIGURES (Cont'd).

ACKNOWLEDGEMENTS

The author wishes to acknowledge:

D. B. Smith, Institute of Geological Sciences, Leeds, for invaluable information on the geological stratigraphic interpretation of the Permian of the north-east England.

The Northumbrian River Authority, and in particular, Dr. T. Cairney, for the finance, data, and useful discussion they provided for analogue simulation.

Dr. R. Herbert, Civil Engineering Department, University of Birmingham, and A. Hunter-Blair, Water Research Association, for advice on electrical analogue models.

Sunderland and South Shields Water Company, and Hartlepools Water Company, for making available their well and pumping records.

Quarry owners and managers, for assistance in sampling and blast vibration recording, in particular, Slaters Ltd. (N.E. Division), Steetly Dolomite, Raisby Hill Quarries Ltd., Tarmac Roadstone Ltd., (Stockton), Turner and Newalls Ltd., Hawthorn Aggregates Ltd., Dobsons Ltd.

Fellow students, technical and academic staff of the Department of Geology, for their help in the field and laboratory, and critical discussion of the results and deductions contained in this thesis.

The work was carried out during the tenure of a Natural Environment Research Council research studentship.

SYNOPSIS

The Permian of Northern England consists of over 1800 feet of dolomites, limestones, marls and evaporites, with arenaceous deposits at the base. Although of limited areal extent, a wide variety of lithologies are represented, largely interpretable in terms of the depositional environment at the western margin of the Zechstein Sea. The structure consists of a low east to south-easterly dip, together with faults, the largest of which trend east-west and attain maximum development in the south of Co. Durham.

The geohydrology is controlled by the lithology and the structure. To the north of the Hartlepool Fault System the aquifer is unconfined, and represented chiefly by the Lower Magnesian Limestone and Basal Permian Sands. It has been indiscriminately developed in the past, and at present 24 m.g.d. are licensed for abstraction. In the south and around Hartlepool, the Middle Magnesian Limestone forms the main aquifer, being confined for most of its extent by drift or marls of the Lower Evaporite Group. A groundwater investigation of this area by the Northumbrian River Authority showed that analysis and extrapolation was made difficult by the presence of hydrological barriers due to faulting and basement 'highs'. Digital and analogue simulation techniques have been used, and results from the latter indicate a net 12 m.g.d. to be available without depleting resources.

The strength and rheological parameters of the Magnesian Limestone are controlled principally by the rock lithology. However, since the strata is usually highly fractured, the effect of discontinuities on the rheology, and on the failure characteristics in both biaxial and triaxial stress fields has been examined. Laboratory tests have been undertaken to establish typical parameters for various lithologies, and most correlate

with the unconfined compressive strength, even though the latter may be erroneous on an absolute stress basis due to sample-platen interaction. Results from the various lithologies may be utilised in the quarrying industry where a knowledge of the probable rock types at a locality is invaluable. Although slope stability is not a large scale problem, slope degradation may be arrested by designing on a 'semi-discontinuum' basis. Foundation properties of the Magnesian Limestone are generally good, although remedial measures may be necessary where there is a significant thickness of leached material.

SECTION 1

GEOLOGY

CHAPTER 1

INTRODUCTION AND REGIONAL SETTING

1.1. Introduction

The Magnesian Limestone of northern England, although outcropping over what amounts to a very small fraction of the total area of the British Isles (Fig 1.1), nevertheless affords an interesting study on account of the many variations in occurrence, lithology and properties which are exhibited within a relatively small area.

The Magnesian Limestone underlies Co. Durham east of a sinuous line from South Shields in the north, through Ferryhill to west of Darlington and then south towards Scotch Corner, where it becomes discontinuous. Further south in Yorkshire, glacial drift blankets much of the solid geology, although from both borehole evidence and the limited exposures, it appears that the outcrop narrows to some 5 miles due to the overstep of the Trias. In the Midlands, the Magnesian Limestone becomes attenuated until, in the Nottingham area, it is represented by only a thin bed of arenaceous dolomite. The precise stratigraphic correlations between areas are difficult to determine due to the absence of palaeontological evidence and the replacement of the marine limestones by the diachronous Bunter Sandstones (Sherlock, 1926, 1928). To the west of the Pennines, a thin equivalent of the Magnesian Limestone occurs in a few restricted localities, notably near Appleby in Westmorland and around Manchester (Wells et al, 1966).

In the north of Co. Durham, the eastward dipping strata produces a well defined westward facing escarpment, but in the south of the county and in Yorkshire glacial drift masks the effects of the structure upon the topography.

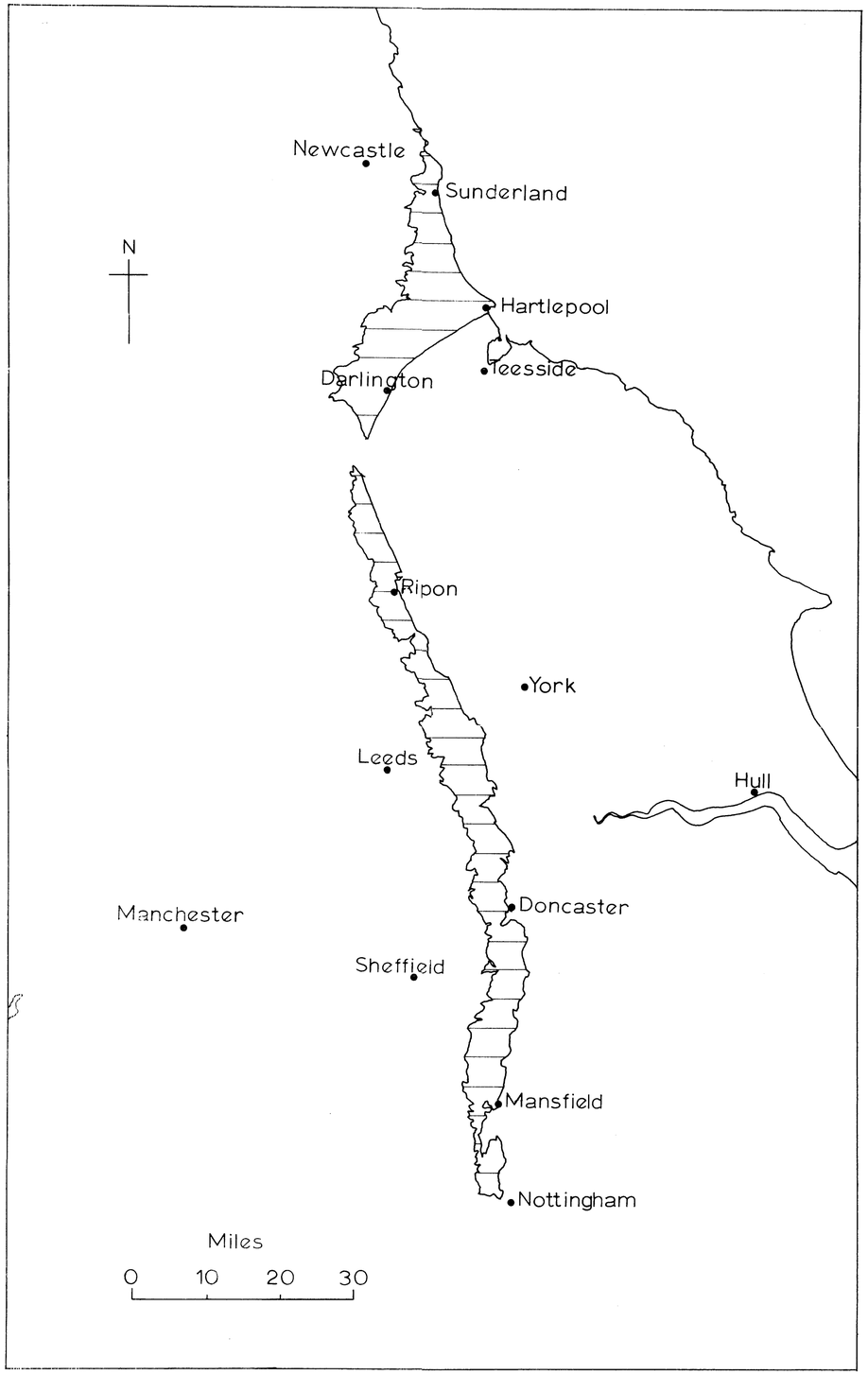

Fig.1.1. Permian of Eastern England.

The Permian hills are small in comparison with their Pennine neighbours, attaining 600 feet or over in only a few isolated places.

Over most of the area, the drainage is post-Pleistocene, drift controlled, although some of the deeply incised coastal denes are re-excavating pre-glacial valleys and locally flow in the Magnesian Limestone. Recent boreholes in the south of the county have located the positions of tributaries of the proto-Tees, but it is not yet possible to produce a complete picture of the pre-glacial terrain.

1.2. Previous work

Much of the first geological mapping and stratigraphic correlation of the Permian was carried out early this century by Trechmann (1914, 1925), with further contributions by Woolacott (1919), and Hodge (1932). A resurvey of the Durham and West Hartlepool sheet by the Institute of Geological Sciences in the 1950's, coupled with evidence from N. C. B. land and offshore boreholes (Magraw et al, 1963) resulted in a reappraisal of the difficult stratigraphy in terms of the palaeogeography (Smith and Francis, 1968). The succession as outlined in the above memoir, together with personal communications from D. B. Smith concerning the as yet unpublished Sunderland sheet, has been used as reference throughout this thesis.

The hydrology of the area has received only sparse attention, although the implementation of the Water Resources Act (1963), and the work of the River Authorities should eventually lead to a more complete understanding. A wartime pamphlet,(Anderson, 1941), lists the localities of wells together with rudimentary information on the geological succession, rest water levels, pumped water levels and yields. More recent information on abstraction is given in the Wear and Tees Hydrological Survey (Ministry of Housing, 1961),

and although it contains no quantitative data on the aquifer parameters, it seeks to indicate the over-developed areas, and those areas where future development should be concentrated.

A report by the Water Resources Board (1967) on the resources of northern England indicates a possible deficiency in the Northumbrian River Authority area, based on existing supplies, of 30 million gallons per day (m.g.d.) by 1971, and 205 m.g.d. by the year 2001. The investigation and simulation of an area around Darlington (Northumbrian River Authority, 1969; Burgess and Cairney, in press) to offset this deficit is considered at length elsewhere in this thesis.

The influence of the geohydrology of the Permian on the working of the underlying coal was the subject of two papers resulting from work carried out by the National Coal Board (Armstrong et al, 1959; Clarke, 1962). It was concluded that resources in the Chilton-Rushyford area could be extracted providing there was dewatering of the overlying Permian. Clarke showed that there was a correlation between the pumping required in the mines, and the degree of fracturing and faulting and hydraulic head. The actual instigation of these schemes, however, was dependent upon the economics of the situation.

As far as the engineering geology of the Magnesian Limestone is concerned, there have been no published reports in the literature.

1.3. Objects

The aims of the present research have been threefold:-

(i) To assess techniques for investigating and evaluating a highly variable material, often very fractured and jointed.

(ii) To apply these methods to the Magnesian Limestone in particular, and to arrive at representative values for the engineering and hydrological parameters.

(iii) On the basis of these results to consider the area as a geological, engineering and hydrological entity, and to be able to predict at any locality the possible nature of the geology and geological material, engineering and hydrological problems likely to be encountered, groundwater potential, suitability of the rock for aggregates, and other relevant particulars.

The first of these objectives is considered the most important, since applications are by no means limited to the succession studied. Where required, contemporary methods of analysis and data processing have been employed, particularly the I. B. M. System 360/67 NUMAC computing facilities.

CHAPTER 2

GEOLOGY OF NORTH EASTERN ENGLAND

2.1. Regional Geology

In the north east of England, the broad geological succession is:-

Recent & Pleistocene		
Trias	)	
	)	Permo-Trias
Permian	)	
Coal Measures	)	
	)	
Millstone Grit Series	)	Carboniferous
	)	
Carboniferous Limestone Series	)	
Lower Palaeozoic		

2.1.1. Lower Palaeozoic

The basement series of slates, grits and volcanics occur as faulted inliers in a few Pennine localities at Horton-in-Ribblesdale, Langdon Beck and Cross Fell (Eastwood, 1963), and have been proved in a borehole at Crook (Woolacott, 1923). In some areas, Devonian granites appear to have intruded the basement, and borehole evidence at Rookhope substantiated geophysical evidence of a granite at depth (Bott, 1967).

2.1.2. Carboniferous

The Carboniferous strata is deposited unconformably upon the Lower Palaeozoics in all areas. At the base, cyclothemic sedimentation was developed on the block areas of Alston and Askrigg, and these thicken greatly across hinge-lines into arenaceous and argillaceous successions in the trough

areas of Northumberland, south Durham and north Lancashire. The Millstone Grit deltaic facies is less developed in the northern Pennines than in the Lancashire-Yorkshire area, attaining a thickness of only 400 feet. The succeeding Coal Measures, however, are represented by Lower and Middle Coal Measures up to the upper A. similis - A pulchra zone. The initial extraction of coal was located on the exposed coalfield of west Durham, with expansion into the concealed coalfield taking place in the mid 19th century. The difficulty of shaft sinking through the Permian was highlighted by the abandoning of the first Haswell sinking with a loss of £60,000 (Galloway, 1898). It was not until techniques for freezing difficult ground conditions were adopted in the early years of this century that full exploitation was realised, especially in the coastal areas where most of todays 'long life' pits are situated working undersea reserves.

2.1.3. Permian

At the end of the Coal Measures, considerable denudation under very arid conditions reduced the area to a peneplain. The slight unconformity at the base of the Permian is marked by breccias and dune sandstones. Locally, to the north-east of Darlington and around Billingham, Carboniferous 'highs' result in attenuation or complete absence of Permian sediments (Wood, 1950).

The Permo-Triassic succession in Co. Durham (Fig 2.1) consists fundamentally of a marine transgression over a desert peneplain, followed by cycles of evaporite formation. Since Co. Durham represented the western marginal area of the Zechstein Sea, the full development of the more soluble evaporites occurs only in the south-east of the county on Tees-side. In the Whitby area of the North Yorkshire Moors potash salts have been proved an economic proposition, and work is currently in progress on the shaft sinking and drilling connected with their abstraction. The oil and gas exploration

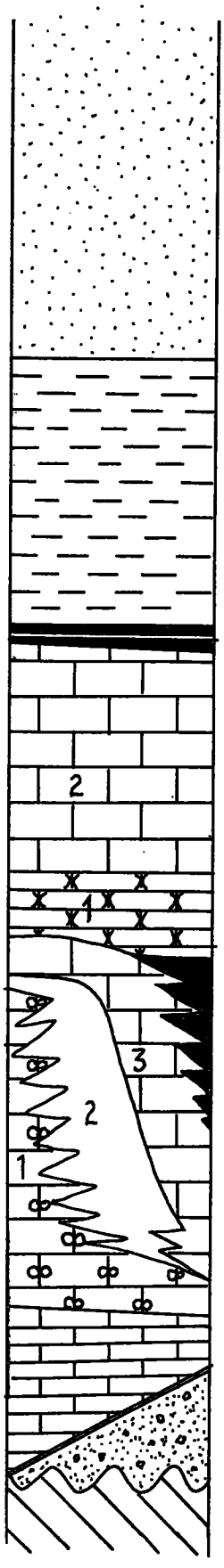

Bunter Sandstone up to 700 ft.

Upper Permian Marls, with interbedded evaporites up to 430 ft.

Upper Anhydrite
Billingham Main Anhydrite

Upper Magnesian Limestone up to 430 ft.

2. Hartlepool and Roker Dolomite

1. Concretionary Limestone with Flexible Limestone at base

Middle Magnesian Limestone up to 515 ft.

3 Post-reef dolomite with interbedded evaporites

2 Reef dolomite and off-reef equivalent

1 Transitional and Lagoonal dolomite

Lower Magnesian Limestone 0–250 ft.
Marl Slate at base

Basal Permian Sands and Breccias 0–?161 ft.

Carboniferous

Fig. 2.1. Generalized Permo-Trias succession (from Smith and Francis, 1967)

programme at present being undertaken in the North Sea has led to a more complete understanding of the stratigraphic relationships between the Permian of northern England and the rest of Europe, even though details of many of the wells and boreholes have been withheld for obvious industrial security reasons.

2.1.4. Pleistocene and recent

The interpretation of the Pleistocene of Co. Durham is complicated by its position, being influenced by Pennine, Cheviot and Scandinavian ice sheets. Pre-Pleistocene, the drainage was radial from the Pennine uplands, with the headwaters of the River Wear flowing via Shildon-Newton Aycliffe into the River Tees, and the River Browney flowing directly into the sea via Shadforth Beck (Smith and Francis, op. cit.) However, a tributary of the River Tyne, cutting south, intersected first the River Browney and then the River Wear, to produce the pre-glacial River Team, this being the drainage pattern immediately prior to glaciation.

Over the central Durham area there is evidence of only one period of glaciation, although in the coastal area it seems probable that there were three, the oldest of which, the Scandinavian Drift, occurs at the base of clefts in the Magnesian Limestone. The Lower Boulder Clay, however, represents the ice sheet which covered the whole of the region, moving from north to south, and is up to 120 ft thick. This is succeeded by the Middle Sands, Gravels and Clays, indicative of a period of sub-aerial erosion of the pre-existing deposits. The Upper Boulder Clay extended westwards only as far as an approximate north-south line through Shotton and Wingate, and during this period, sub-aerial erosion continued with deposition of sands, gravels and laminated clays in ice and boulder clay dammed lakes, such as Lakes Edderacres and Wear (Smith and Francis, op. cit). Many of the lakes overflowed creating distinct channels, the most striking of which is the

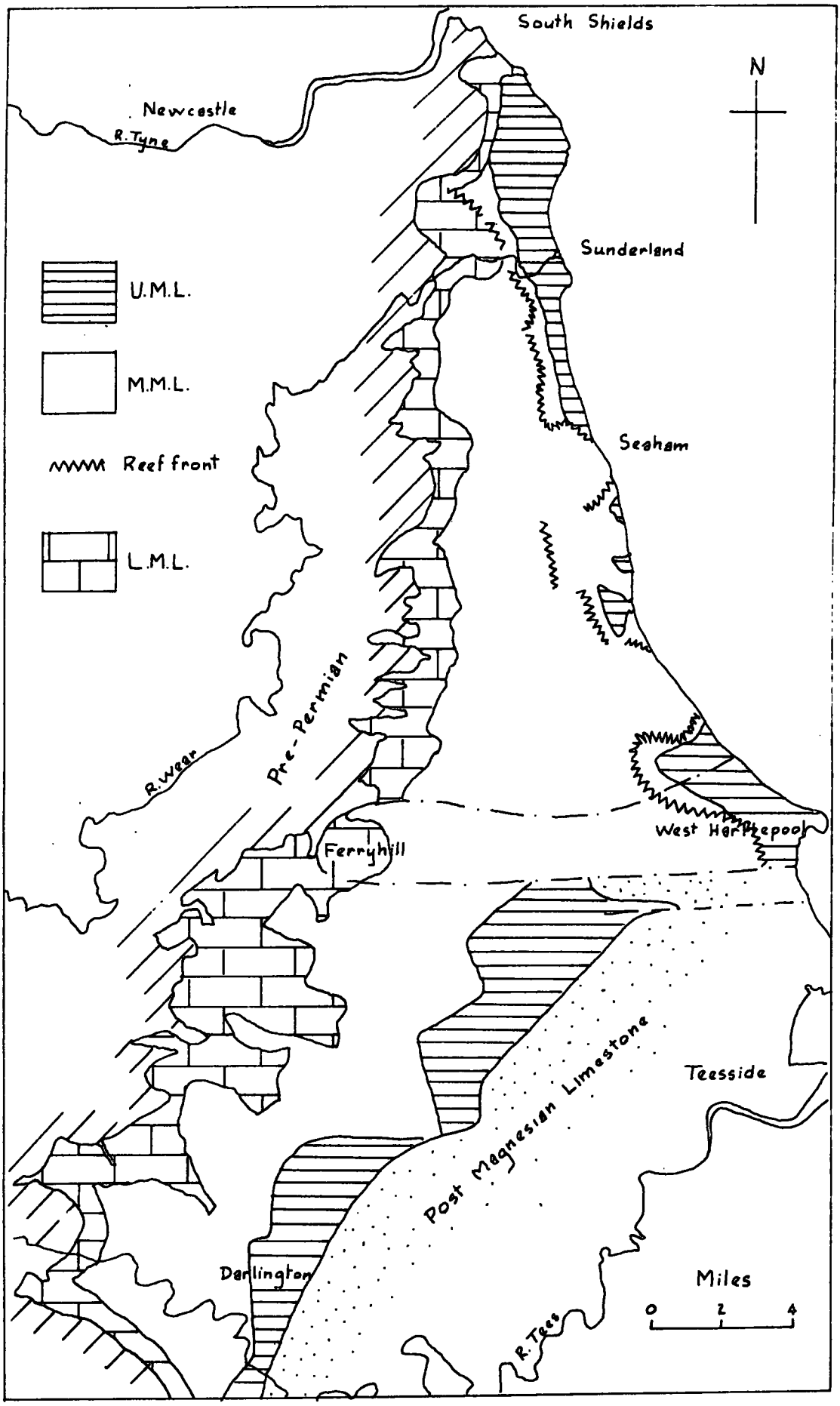

Fig. 2.2. Permian outcrop in County Durham.

Ferryhill Gap, produced when Lake Wear spilled southwards. In central Durham, the succeeding deposit, the Upper Stony Clays, is probably indicative of a solifluxion phenomena, rather than of further ice sheets, since the underlying laminated clays are not usually contorted. The laminated clays of the Tees-side area are probably produced by ice damming from the receding Upper Boulder Clay sheet, and may thus be contemporaneous with the Morainic Drift and Upper Gravels.

In post-glacial times, many of the rivers have adopted different courses, the River Wear, for example, cutting gorges in solid rock, notably at Durham, Chester-le-Street and Sunderland, and thus leaving their old channels infilled with drift deposits. In the coastal area, there is evidence of the pre-glacial denes having a much lower base level, with slopes in the Magnesian Limestone generally at 10^{o} to 20^{o} (Smith and Francis, op. cit), which is considerably less than the present day streams that now occupy many of the former courses.

2.2. Permian stratigraphy and lithologies

The stratigraphy of the Permian is considered below in a palaeogeographical context and the various lithologies outlined. A generalized map of the Permian outcrop is given in Fig 2.2., and Fig 2.3 shows the southern area in detail.

2.2.1. Basal Sands and Breccias

The Permian Basal Sands and Breccias represent reworked arid terrestrial deposits, and are thus highly variable in thickness and occurrence. South of a sinuous line from Blackhall Rocks to Rushyford the often incoherent, running Yellow Sands are replaced by breccias.

2.2.1.1. Palaeogeography - The age of the basal deposits is difficult to determine due to the obvious lack of palaeontological evidence. Smith et al (op. cit.) suggests that by analogy with the Russian type area as described by Nalivkin (1937)

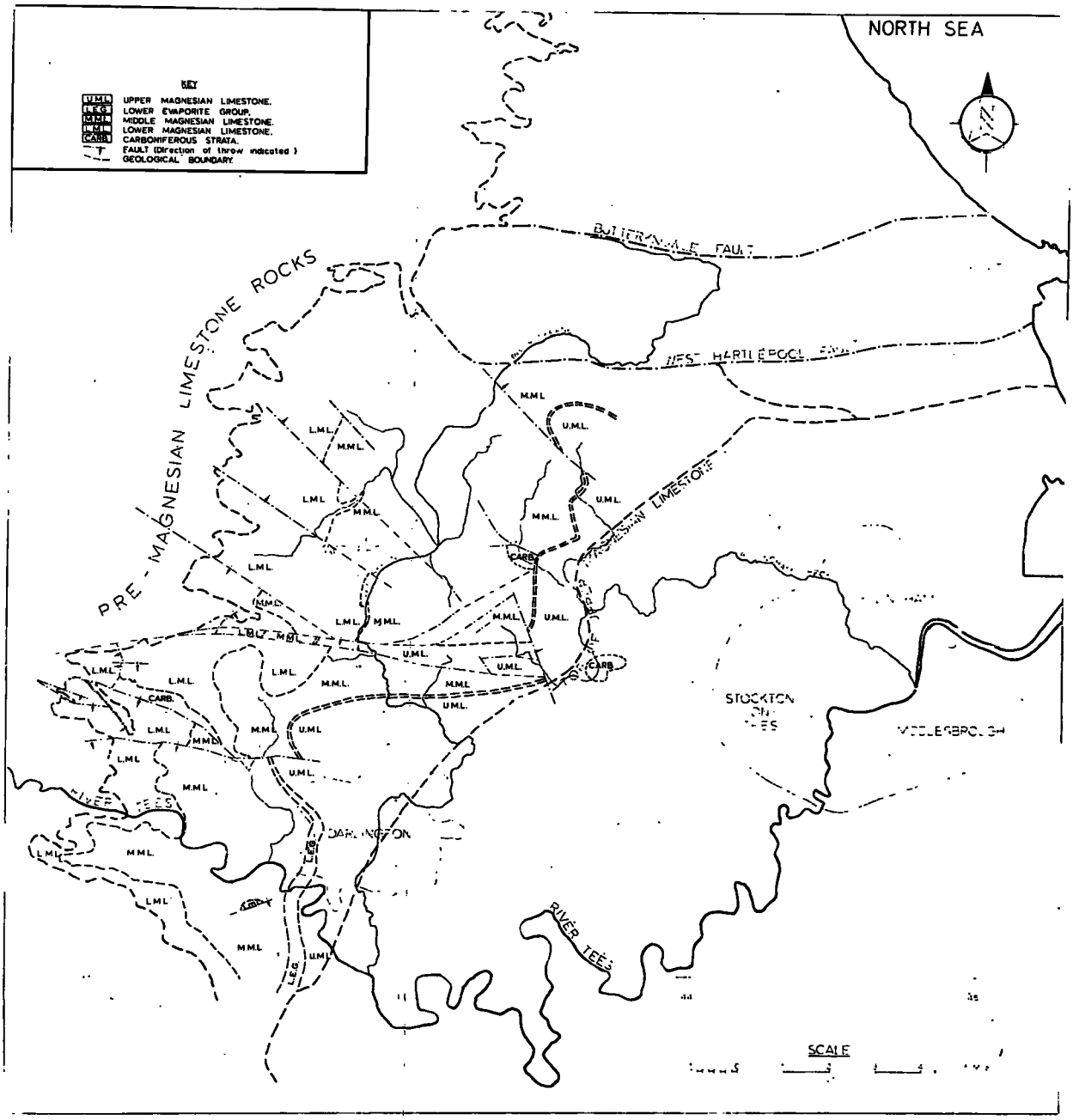

Fig. 2.3. Detailed geology of south-east Co. Durham.

the basal beds should be ascribed to the Kungurian Stage of the Lower Permian.

The thickness and distribution of the Yellow Sands are very variable reaching a possible 196 feet near Easington, but being completely absent elsewhere.

From borehole data and cross bedding preserved within the Yellow Sands it is possible to reconstruct the desert landscape, and it appears that large dunes similar to present day sief dunes were reworked during the Zechstein Transgression. From the orientation of the axis of a dune mapped in the Chilton-Raisby Hill area and using Bagnold's hypothesis for the generation of barchan dunes (Bagnold, 1941), palaeo-winds with a prevailing direction of E 10^{o} N, with a subordinate direction of E 40^{o} N have been postulated by Smith et al (op. cit.) . These directions agree closely with the present day equatorial regimes, and thus yield independent evidence in support of polar wandering and/or continental drift derived from palaeomagnetic evidence.

Information on the breccias which occur in the south of Co. Durham is at present too limited to enable a detailed distribution to be determined, although the variable thickness may indicate deposition as debris fans and wadi infillings.

2.2.1.2. Lithology - Sizing analysis of the Yellow Sands shows a bimodal distribution indicative of aeolian transport (Hodge, 1932). The heavy mineral assemblage shows the material to be derived partly from the immediate vicinity, and partly from an area to the north containing granites and metamorphic rocks. Usually the Yellow Sands are virtually cohesionless, although the silt-clay loessic fraction does impart some cohesive strength. At outcrop the material is bright brownish-yellow, but fresh samples from

depth are greenish in colour, the change being attributed to oxidation of the pyrite to limonite near the surface. Towards the base and top of the sands, secondary cementation by calcite leached from the overlying limestone produces a more competent material. Near Easington Colliery, the complete 90 feet thickness of Basal Sands penetrated in a National Coal Board boring has been cemented into a low porosity, grey sandstone.

The Basal Breccias consist of angular fragments embedded in a sandy matrix. The provenance is fairly local, being derived from the Carboniferous 'highs' of North Cleveland and the Tees Valley.

2.2.2. Marl Slate

The Marl Slate, a silty dolomitic shale was first considered by Sedgewick (1829) to be the English equivalent of the German Kupferschifer.

In north eastern England it reaches a maximum thickness of 18 feet near Rushyford, but attenuates rapidly in all directions, 2 feet to 5 feet being general over the majority of the Permian outcrop, but decreasing to zero in the area around Hartlepool and offshore. It outcrops near the base of the Permian escarpment, but because of its nature and thickness is rarely well exposed, except in quarry sections. At depth it is massive but on weathering becomes brown-grey and develops typical shale laminations.

2.2.2.1. Palaeogeography - The Zechstein Transgression was followed by a period of quiescent, stagnant marine conditions. High base metal concentrations have been shown to be present (Hirst and Dunham, 1963), and are believed to have been responsible for the extermination of the marine fauna. The origin of the mineralizing fluids is not known, although the widespread spatial occurrence would seem to suggest submarine exhalations possibly similar to those recently noted in the Salton Sea (Skinner et al, 1967).

2.2.2.2. Lithology - The Marl Slate consists of a silt grade dolomite in a clay matrix. X-ray texture analysis (Attewell et al, 1968) shows that the fissility is due to the orientation of illite and kaolinite with the basal (001) planes sub-parallel to the bedding. The dolomite rhombs are largely aligned with their c-axes perpendicular to the bedding, and there is no evidence of non-hydrostatic stresses in a horizontal plane.

2.2.3. Lower Magnesian Limestone

The resistant Lower Magnesian Limestone produces the westward facing escarpment, and is well exposed in the numerous quarries along this line. Further east, however, it is located in depth only from boreholes. Its maximum thickness of 225 feet is reached at Mill Hill near Easington, but at outcrop in the Houghton-le-Spring to Shildon area it is usually 150 feet thick. In the area around Sunderland, and to the north of the River Wear, the Lower Magnesian Limestone thins drastically, being at maximum 20 feet thick and in places completely absent.

2.2.3.1. Palaeogeography - The Lower Magnesian Limestone represents the carbonate-dolomite phase of the first evaporite cycle. The increasingly saline nature is evidenced by the fauna becoming stunted and impoverished. Over much of the county there is a gradual transition into the overlying Middle Magnesian Limestone, but in Yorkshire a thin sequence of intratidal clays and dolomites, the Hampole Beds, have been recognized (Smith, 1968). The basal beds at outcrop from South Shields to the Tees often show signs of slumping producing disturbed beds and turbidites (Smith, in preparation). The much reduced thickness in the Sunderland area and to the north, reflecting a removal of up to 75 feet of strata, is interpreted as a submarine slide (Smith, op. cit.), occurring towards the end of Lower Magnesian Limestone deposition. By comparison with documented contemporary submarine slides it

appears to be due to a rapid increase in pore pressure, probably from an earthquake, producing an unstable condition (Morgenstern, 1967).

2.2.3.2. Lithology - At the western escarpment outcrop three distinct units may be recognized, but these are not easily identifiable in boreholes to the east (Smith and Francis, op. cit.).

The lowest unit, 4-12 feet thick and massively bedded, ranges from a calcitic dolomite to a pure calcite limestone, and having a granular to finely crystalline texture.

The middle unit consists of dolomites with the bedding varying from 3 ins. to 2 ft. In many places, for example at Thrislington, it has a mottled appearance (Fig 2.4), representing a partial segregation of calcitic and/or organic material. Locally, this horizon is completely undolomitized, notably at Raisby Hill Quarry, near Coxhoe, and at East Thickley, near Shildon. In the Houghton-le-Spring area, it is extremely cavernous and autobrecciated (Fig 2.5) with very distinct bedding about 2 ins. thick.

The upper unit consists of silt grade granular dolomite, often very pure and homogeneous(Fig 2.6). The bedding is very distinct, about 2 ins. thick, and there is a considerable reduction in the amount of autobrecciation and vughs.

This sequence of lithologies in the Lower Magnesian Limestone is interpreted as indicating pre-diagenetic dolomitisation of the upper unit, with post-diagenetic dolomitisation of the lower units becoming incomplete near the base. This hypothesis is compatible with an increasingly saline environment and downward percolation of hyper-saline solutions producing dolomitisation downwards. The competent nature of the lower micritic strata would prevent easy passage, except along lines of weakness such as bedding planes, thus giving rise to the characteristic mottled appearance of the partially dolomitised limestones.

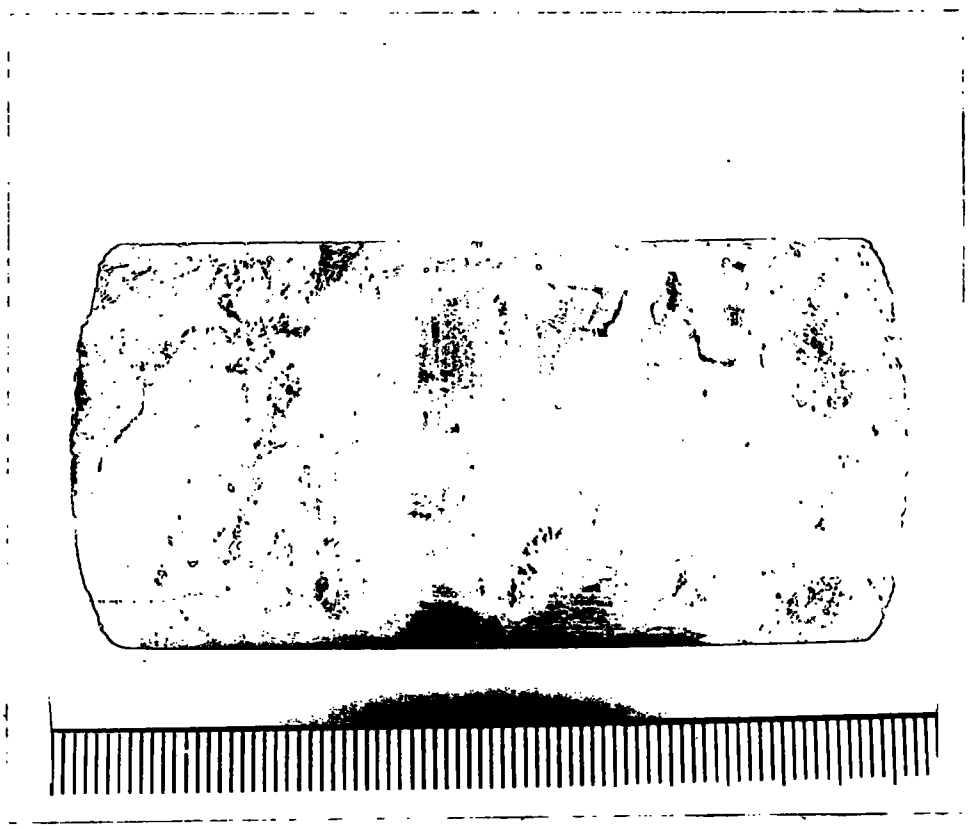

Fig. 2.4. Lower Magnesian Limestone, dolomitised limestone (TH2).

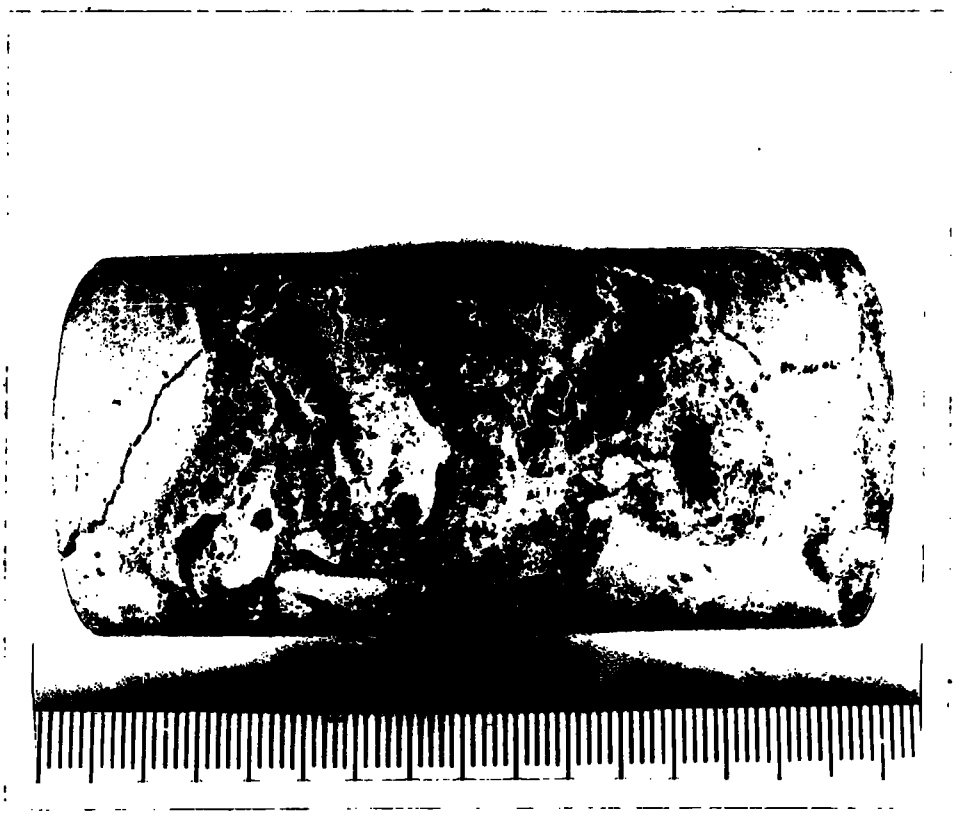

Fig. 2.5. Lower Magnesian Limestone, cavernous dolomite (H01).

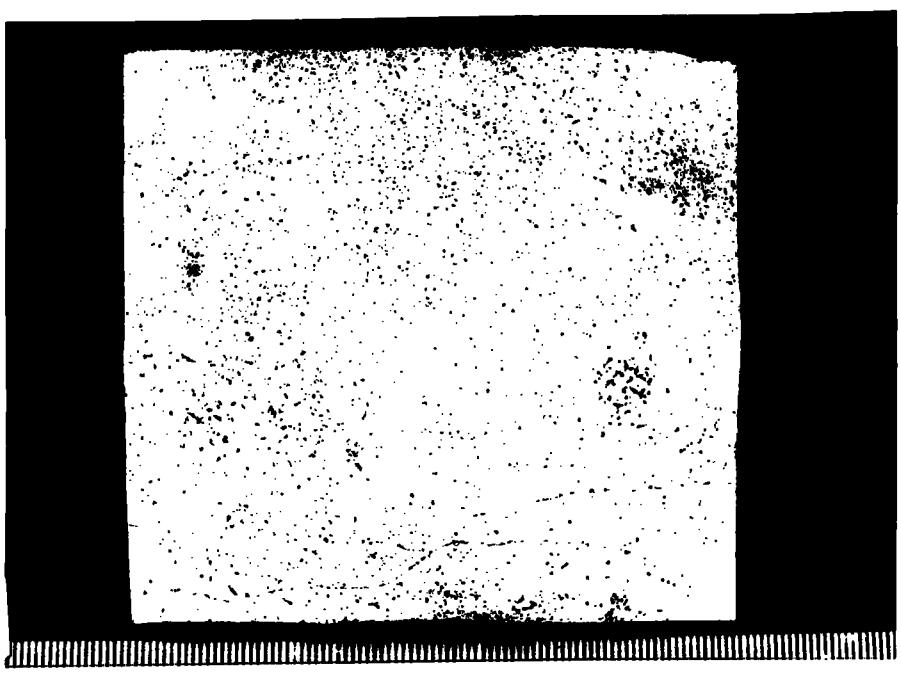

Fig. 2.6. Lower Magnesian Limestone, granular dolomite. (TH1).

2.2.4. Middle Magnesian Limestone

On an areal basis, the Middle Magnesian Limestone occupies most of the Permian outcrop. However, the poorly resistant nature results in few exposures. Because of the different depositional environments, the Middle Magnesian Limestone exhibits a great variety of lithology, with thicknesses ranging from 30 feet offshore to over 250 feet near Easington Colliery.

2.2.4.1. Palaeogeography - The influence of the palaeogeography on the nature of the sediment is more marked in the Middle Magnesian Limestone than elsewhere in the Permian succession.

There are essentially three facies divisions: in the west, lagoonal, passing eastwards into reef, and this into basinal sediments. The dominant feature is thus the fringing reef, which followed a generally north-south line, from Downhill through Humbledon, Ryhope and Peterlee to Blackhall Rocks, and south to Hartlepool, where it became much subdued. Embayments occur in some areas, notably around Hesleden Dene and Horden.

Initially the reef was composed of a low shell bank, forming first of all in the north where there is some evidence that it may have existed in Lower Magnesian times. As the salinity increased, the brachiopod fauna was replaced by bryozoa and algae, as only these latter could withstand the hypersaline environment. South of Sunderland, the reef as now exposed, consists largely of algal stromatolites. It is probable that the reef existed longest in the central area where it is developed to its maximum thickness of 250 feet. To the west of the reef, lagoonal conditions with quiet waters produced oolites and pisolites to a maximum thickness of 200 feet. Overlying these in the south, marls and evaporites of the Lower Evaporite Group occur. They are unknown north of the Hartlepool Fault system, but this is probably an erosional feature resulting from the southern downthrow, since nowhere to the north has the

actual top of the oolitic dolomites been identified (Jones, in preparation).

To the east of the reef, basinal dolomites and evaporites were deposited. In many areas subsequent solution has left only a thin residue bed, especially in the Sunderland area. In the N. C. B. Offshore Borehole No. 2, however, over 500 feet of anhydrite was logged (Magraw et al, 1963), giving an indication of the thickness dissolved.

2. 2. 4. 2. Lithology - (a) Lagoon. The lagoonal facies consists almost entirely of dolomites, often oolitic or pisolitic and weakly cemented (Fig 2. 7), together with granular silt-grade dolomites similar to the upper unit of the Lower Magnesian Limestone. Where oolitic horizons occur beneath a thick impermeable cover of marls in the southern area, the pores are invariably infilled with evaporites. It thus appears likely that the open textured oolites represent strata from which the interstitial evaporite cement has been leached by groundwater movement. Very locally, dedolomitisation has occurred, producing crystalline limestones, but the zones affected are limited and unpredictable although in many cases they appear to be related to faults.

(b) Reef. The nature of the reef building material is the main factor determining the resultant lithology. In the Sunderland area, and especially at Ford Quarry, shells constitute the main material, producing a highly porous, dolomitized rock (Fig 2. 8). As the salinity increases, bryozoa and algae become the dominant builders, and the resultant rock is more massive, often with distinct algal domes and stromatolitic crenulations (Fig 2. 9).

(c) Basin. The Lower Evaporite Group is included in this division since the beds are lithologically more akin to the true basinal sediments than to the lagoonal oolites. Close to the reef, buff, bioclastic, dolomitic calcarenites are found. Further offshore, to the south around Tees-side and in Yorkshire, evaporites up to the sylvine stage are found. The Lower

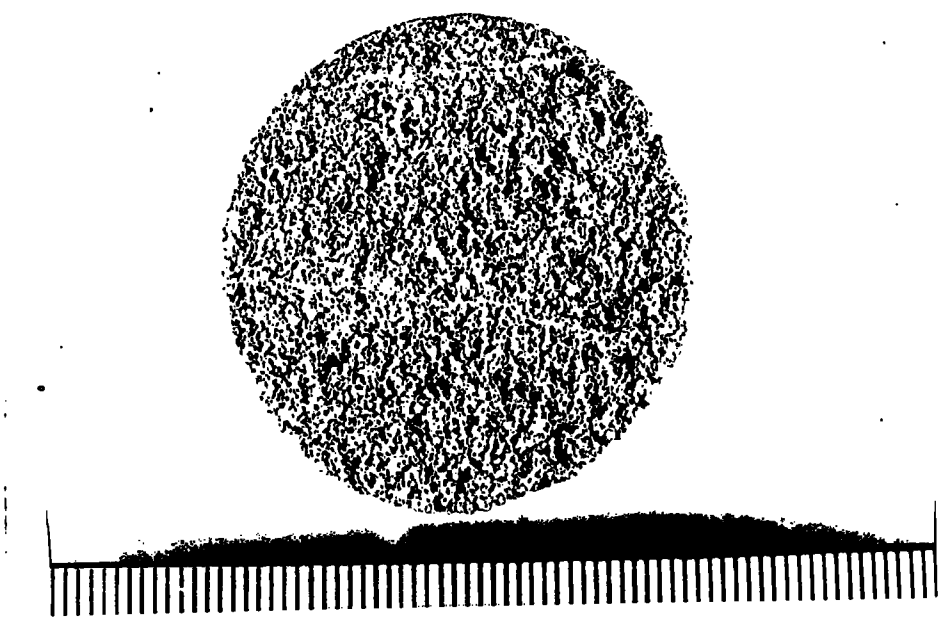

Fig. 2.7. Middle Magnesian Limestone, oolitic dolomite (HA1).

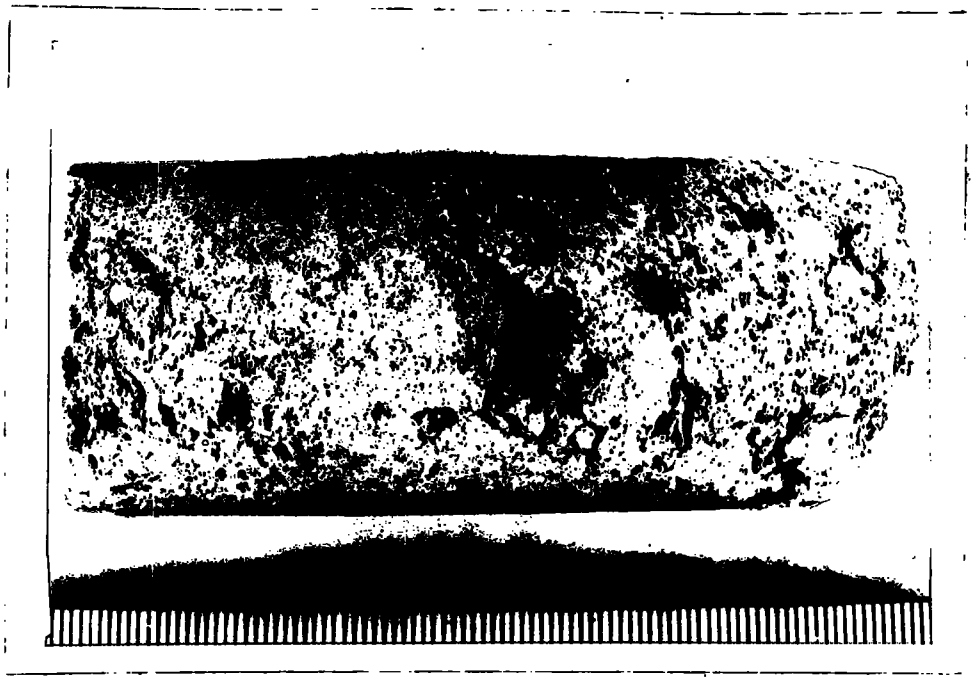

Fig. 2.8. Middle Magnesian Limestone, shelly reef dolomite (F01).

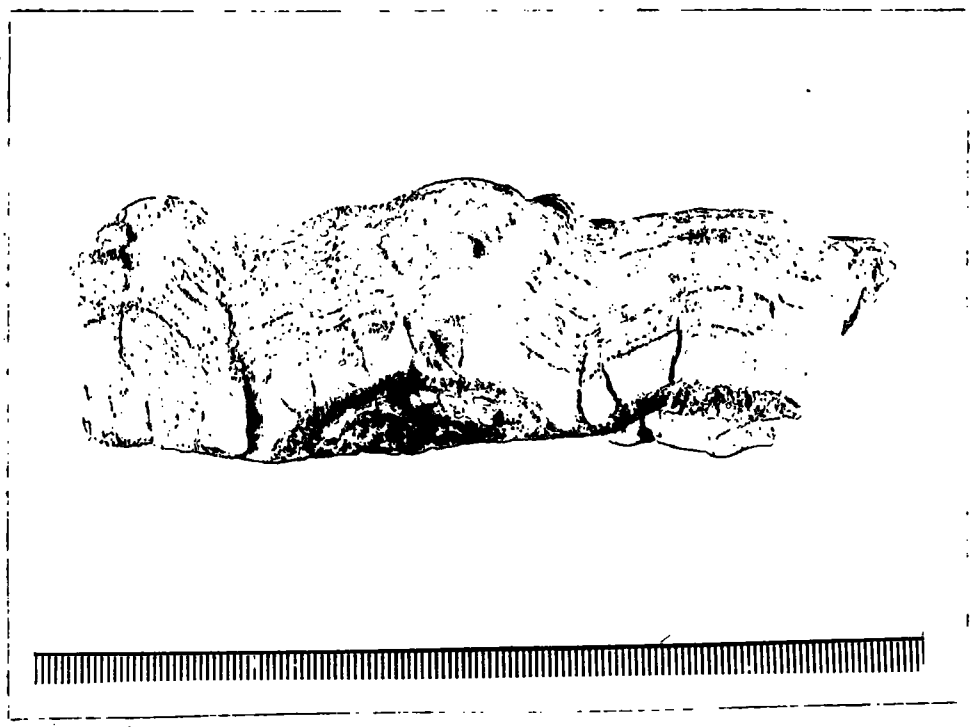

Fig. 2.9. Middle Magnesian Limestone, algal reef dolomite.

Evaporite Group of the south of the county is generally marly, but the evaporites increase eastward to produce the Hartlepool Anhydrite. Immediately beneath the drift, and to a lesser extent beneath the Upper Magnesian Limestone, leaching of the evaporites occurs.

2.2.5. Upper Magnesian Limestone

The outcrop area of the Upper Magnesian Limestone is limited in extent due to the easterly dip and the proximity of the reef to the coast. Its maximum thickness is known from Offshore Borehole No. 2 to be 412 feet, but on land it is a maximum of 200 feet and generally less than 150 feet thick (Smith and Francis, op. cit.).

2.2.5.1. Palaeogeography - The base of the Upper Magnesian Limestone represents the start of an evaporite cycle. As with the first, the conditions are initially stagnant marine, but the presence of clay minerals and organic material is secondary to the dolomite. Limited fossil evidence indicates that fish did exist in this environment, and the basal Flexible Limestone has occasionally yielded identifiable remains. The majority of the succession consists of buff, granular dolomites, with some oolitic and cross-bedded strata.

2.2.5.2. Lithology. - The division of the Upper Magnesian Limestone into Flexible Limestone and Concretionary Limestone at the base, and Roker and Hartlepool Dolomite above, is based almost entirely on lithologic characteristics. The Flexible Limestone exhibits shale-like laminations (Fig 2.10) and was originally thought to be a chronostratigraphic unit, but it now appears to be a lithostratigraphic unit, since beds with similar features occur above the base of the sequence.

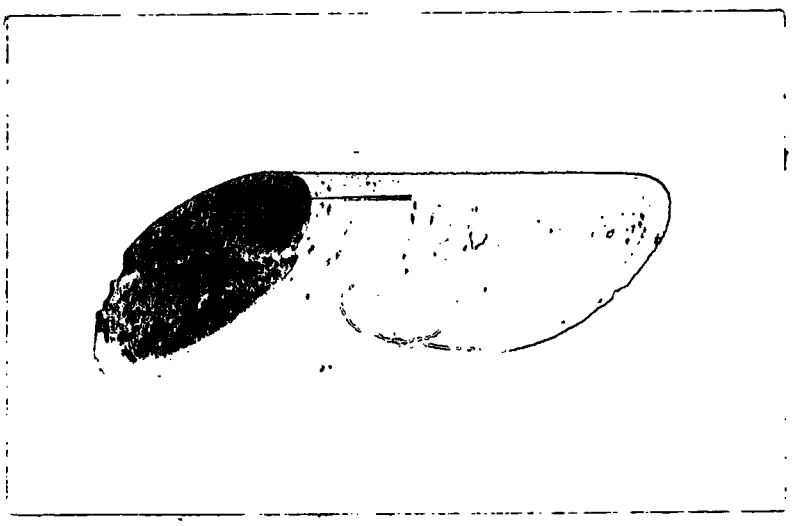

Fig. 2.10. Upper Magnesian Limestone, Flexible Limestone, (MA2).

The succeeding strata are noted for the diverse sperical and pseudo-coralline concretions (Fig 2.11), best known and first described from Fulwell Quarry, near Sunderland. The concretions are wholly calcite, and appear to be the result of dedolomitization by suitable circulating waters. Their occurrence throughout the lower part of the Upper Magnesian Limestone is widespread, although they are most typically developed in the Sunderland area, and the distribution appears to be related to areas of large scale collapse brecciation (Smith, in press). The solution of underlying Middle Magnesian Limestone evaporites by groundwater may have taken place as late as Tertiary times. The result was analogous to coal mining subsidence, although on a cataclysmic scale due to the great thickness dissolved, the incompetent nature of the strata, and the probably thin cover. Similar effects may be seen today in parts of Cheshire where solution of the Upper Keuper Saliferous Beds at outcrop has produced linear and crater subsidence features (Evans et al, 1968). In the Whitburn-Marsden area the effect of collapse becomes more intense northwards, beginning as an increase in joint frequency, leading to gash brecciation, and finally to widespread collapse brecciation. The high porosity and permeability of these beds (Fig 2.12) would readily allow circulation of sulphate rich solutions derived from the evaporites, leading to dedolomitisation of the breccias and surrounding strata.

The Hartlepool and Roker Dolomites consist generally of soft, granular dolomites, with some oolites showing slightly more cementation than in the Middle Magnesian Limestone.

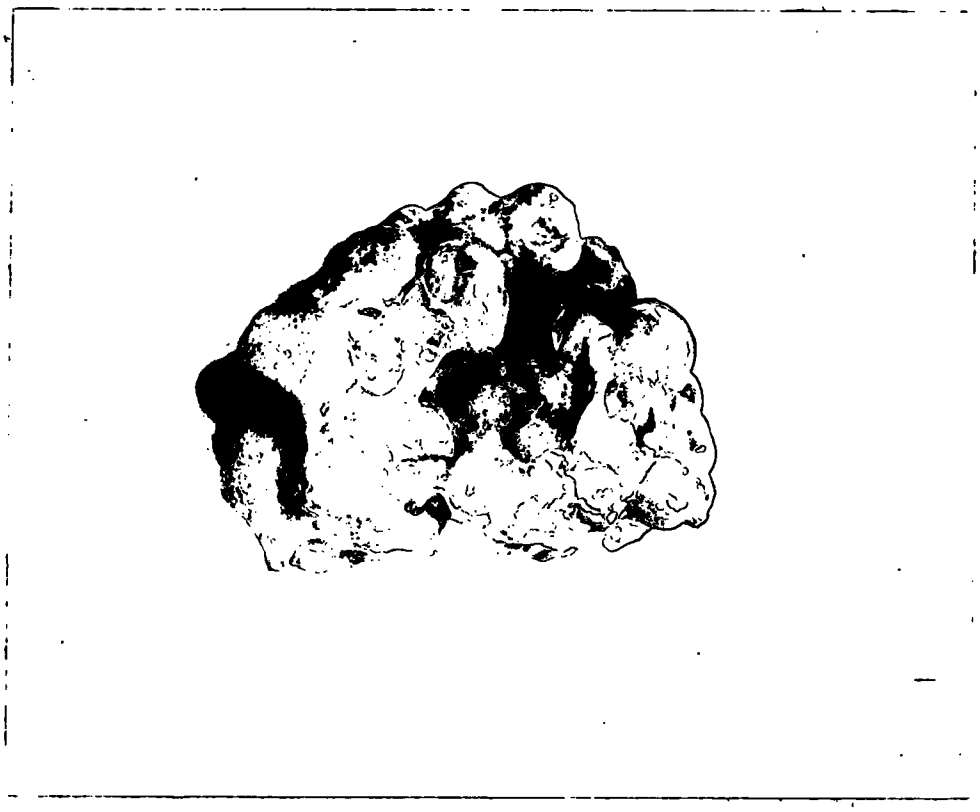

Fig. 2.11. Upper Magnesian Limestone, Concretionary Limestone.

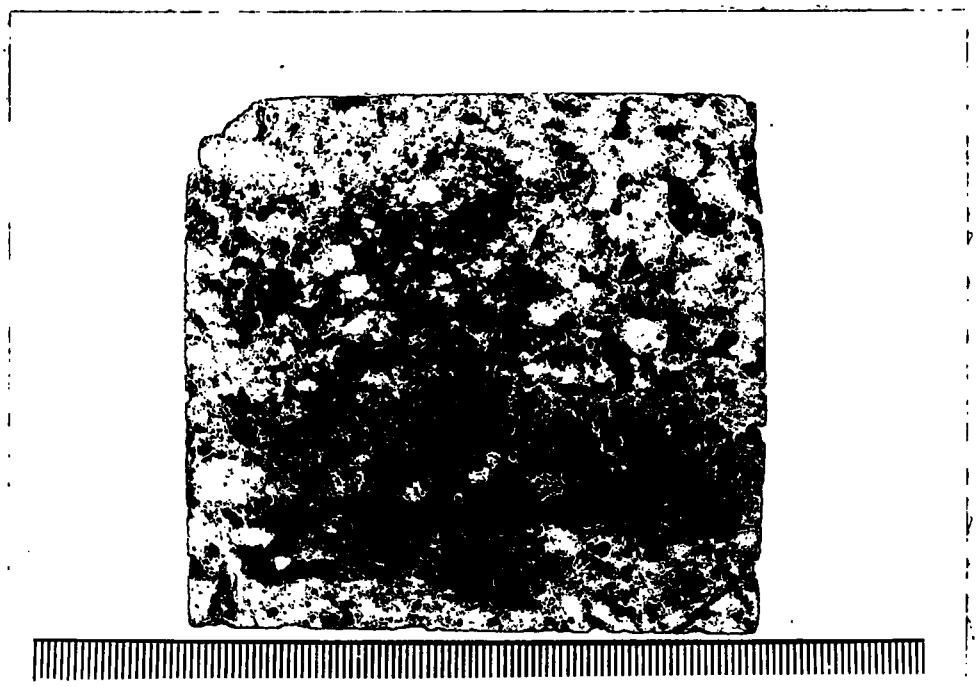

Fig. 2.12. Upper Magnesian Limestone, cellular breccia, (TR2).

2.2.6. Upper Permian Marls

These represent the final silting up of the British Zechstein Sea. Nowhere are the marls exposed on the surface although underground evidence suggests that they represent portions of two evaporite cycles producing the Upper Anhydrite and the Billingham Main Anhydrite, both of which are extensively mined by Imperial Chemical Industries Limited at Billingham. The maximum thickness of the Upper Permian Marls is 370 feet, and upwards they become increasingly arenaceous and grade into the succeeding Bunter Sandstone.

2.3. Structure

The structural history of the area is divided by Smith and Francis (op. cit.) into three phases. Evidence for the first, pre-Upper Carboniferous, is purely geophysical, and is based on the interpretation of gravity anomalies as thickening of sediments southwards across and east-north-easterly hinge line from Horden to Ferryhill (Bott and Masson-Smith, 1957). The second phase is Carboniferous-Permian, and produced the Butterknowle Fault approximately along the line of the previous hinge belt. The period of erosion following these movements resulted in the angular disconformity between the Carboniferous and Permian, and isolated Carboniferous 'highs' over which little or no Permian sediments were deposited. Post-Permian movements gave the strata its easterly dip of about 125 feet per mile, and rejuvenated many of the faults, extending them upwards with much decreased throws, as well as producing further flexuring along the Butterknowle line. The most important features of this episode, however, occur in the south of the county, where the West Hartlepool, Seaton Carew and Butterwick faults produce en-echelon downthrow to the south of over 1,000 feet.

2.3.1. Faulting

In the Chilton-Wingate area of Co. Durham, analysis of fault frequency and orientation by Clarke (1962) has shown strike maxima in directions E-W and NNW-SSE. Most of the large throw faults (greater than 100 feet) are aligned east-west, for example the Easington Fault, Blackhall Fault and Seaham Harbour Fault. Many show monoclinic flexuring on the downthrow side so reducing the overall throw. Trough faults, generally trending north-north-west are notable in the Castle Eden and Wingate areas. The faulting in the south of the county is largely drift obscured and is interpreted from borehole evidence and barrier effects delineated during well testing (see later). The most important feature is the east-west trough fault in the Aycliffe area, but further north the directions become more north-westerly. Due to thick drift cover the exact lines of the West Hartlepool Fault and the Seaton Carew Fault are largely unknown, their positions being located by the associated gravity anomalies.

2.3.2. Folding

Besides the folding associated with many of the larger east-west faults, high dips are restricted to the reef front area, where there is evidence of penecontemporaneous movement to produce a talus slope at the foot. Over most of the area there is gentle flexuring of the Magnesian Limestone, and in the south of the county a broad anticline has been located in boreholes, running north-west south-east through Preston-le-Skerne.

2.3.3. Jointing

In general the joint directions agree closely with the fault directions. Moseley and Ahmed (1967) show that post-Carboniferous joints exhibit the same directional frequency as those of the underlying strata. Joint frequency is very variable, but the spacing is generally similar to the bed thickness (Price, 1966).

SECTION II

GEOHYDROLOGY

CHAPTER I

INTRODUCTION AND THEORY OF AQUIFERS

1.1. Introduction

An investigation of the groundwater regime such as that undertaken in this study has a twofold object. First, the nature and disposition of the aquifers must be determined using the available surface and subsurface information, the results of pumping tests and routine abstraction, and details of the recharge areas. Second, a synthesis of this information must be made in order to arrive at as complete an understanding as possible of the areal behaviour of the aquifers, and on this basis, conservation and management schemes may be constructed so as to obtain the optimum return from the available resources.

Until the mid-1950's the study of groundwater and well hydraulics was apparently divided between engineers, mathematicians, and geologists, with the result that the latter approached the problem on a qualitative basis, whereas the others endeavoured to construct complex mathematical models, often with scant regard for either the geology or the workability of the solution. However, the pioneer work of Southwell (1946) on the application of numerical relaxation techniques created possibilities of reconciliation between the two sides. Karplus (1958) recognized the potential of electrical analogue methods for the solution of field problems, and Stallman (1963) applied the techniques to groundwater. With the advent of third generation computers, direct methods of solution are being investigated.

In many ways the present study has been a precis of this evolution. Initially the investigation employed analytical techniques developed in the late 19th century, followed by the non-steady state concept of Theis (1935).

Latterly analogue and digital methods of simulation have been used, resulting, it is hoped, in a contemporary evaluation of the aquifers.

1.2. Theoretical Basis and Definitions

1.2.1. Darcy's Law and the Laplace Equation

The flow of water through a porous medium was investigated by Darcy in 1856 when he showed that for low rates of flow, the discharge velocity varied directly with the loss of head per unit length of sand column through which the flow occurred. He thus established the empirical law, expressed as

$$V = K\Delta h / l \qquad (1.1)$$

where V = discharge velocity

Δh = head difference

l = length of column

K = constant, dependent upon the material.

For the general case of any liquid, this becomes

$$V = i k \gamma / \eta \qquad (1.2)$$

where i = hydraulic gradient

k = intrinsic permeability

γ = density

η = kinematic viscosity

The constant K in Darcy's original equation is thus a function of both the material and the fluid. However, if the fluid is water, the changes in its physical parameters are negligible over the range of conditions encountered in groundwater, and thus variations in K, the hydraulic conductivity or permeability, may be reasonably referred directly to the material.

By a consideration of the laminar-to-turbulent transition in pipeflow and the inertial forces, Lindquist (1933) has defined values N* at which digression from Darcy's Law starts, given by

$$N^* = VD/\eta \qquad (1.3)$$

where D = average grain diameter

He showed that for a material with grain diameters between 1mm and 5mm and a porosity of 38%, N* was about 4. For most groundwater conditions laminar flow conditions will obtain; however, around a well, high discharge velocities may result in localised turbulent flow leading to 'well losses'. The discharge velocity around a well is determined by

$$V = Q / 2\pi r_w h_w \qquad (1.4)$$

where Q = rate of flow

r_w = well radius

h_w = depth of water in well

An assessment of the flow conditions may therefore be made, assuming a knowledge of the relevant parameters of the surrounding material.

The similarity between the laws governing the flow of water, electricity and heat was recognized in the mid-19th century. It is here that two basic concepts in groundwater hydraulics, namely, steady state and non-steady state, cause a slight divergence of solution.

Partial differential equations of the general two-dimensional form

$$a \frac{\partial^2 u}{\partial x^2} + b \frac{\partial^2 u}{\partial x \partial y} + c \frac{\partial^2 u}{\partial y^2} = f \qquad (1.5)$$

where a, b, c, are functions of x and y, and f is a function of x, y, u, $\partial u/\partial x$, $\partial u/\partial y$, occur widely in engineering (c.f. James et al, 1967). There are three basic forms, elliptic, parabolic and hyperbolic, but only the first two have relevance in groundwater hydraulics.

(a) Elliptic partial differential equations. This type is defined by

$$b^2 - 4ac < 0 \qquad (1.6)$$

and thus the Laplace Equation

$$\frac{\partial^2 h}{\partial x^2} + \frac{\partial^2 h}{\partial y^2} = 0 \qquad (1.7)$$

is of this form. The solution is represented by two sets of orthogonal lines, one set being the equipotential lines, the other being the flow lines. The solution domain is closed, with the implication that steady state conditions exist, and in this way Laplace's equation is basically different from the open-ended domain solution of the parabolic equation.

(b) Parabolic partial differential equation. In this case, the solution must satisfy the partial differential equation throughout the domain determined by time, as well as the initial and boundary conditions. Such an equation represents the non-steady flow of water through an aquifer, subject to recharge at a steady rate of accretion, W,

$$\frac{\partial^2 h}{\partial x^2} + \frac{\partial^2 h}{\partial y^2} = \frac{S}{T}\frac{\partial h}{\partial t} - \frac{W}{T} \qquad (1.8)$$

where S = storage coefficient

T = transmissibility

W = rate of accretion

Equations 1.7 and 1.8 form the theoretical basis for the study of groundwater hydraulics; the resulting differences are thus a reflection on the solution adopted and the field of application.

1.2.2. Definition of aquifer parameters

The usage of the various terms adopted in this thesis are outlined below.

1.2.2.1. Hydraulic conductivity or permeability, K - It is implicit in the application of Darcy's Law that the value of the constant K takes account of the properties of the fluid as well as the porous material. The units are generally expressed as LT^{-1}. However, alternative units which take account of the true dimensional nature of K are sometimes used, especially in the U.S.A., where their application is usually limited to the hydraulics of

oil reservoirs in which the different properties of the fluids involved are as important as the characteristics of the reservoir rocks. In general, values obtained from tests will be expressed in gallons per day per (foot)^2, or in centimetres per second (1 g.p.d. /ft^2 = 5.65 x 10^{-5} cm/sec).

1.2.2.2. Coefficient of storage, S. - This is defined as the volume of water released or taken into storage per unit surface area of the aquifer.

(a) Confined case. The release of water from a confined aquifer due to a change in head is entirely a function of the compressibility of the aquifer skeleton and the water. Assuming no leakage into contiguous beds, Jacob (1950) deduced the relationship:

$$S = \gamma_w \, n \, D(\beta + \frac{\alpha}{n}) \qquad (1.9)$$

where γ_w = density of water

n = porosity

D = aquifer thickness

β = compressibility of water

α = compressibility of aquifer skeleton

From a knowledge of the elastic parameters, porosity and thickness of the aquifer, it is thus possible to compute the storage coefficient. Where recordable, the barometric efficiency, BE, and tidal efficiency, TE, may also be used to derive the storage coefficient.

(b) Unconfined case. In the unconfined aquifer, actual dewatering takes place, the elastic effects due to changes in ambient pressures being negligible in comparison. Thus the storage coefficient is often equated with the porosity, but this appears to be somewhat optimistic except in coarse sands and gravels.

Capillary effects due to pore geometry can greatly reduce the quantity of water able to drain freely, and thus a saturated clay in

equilibrium with the saturated moisture which exists above it would lose very little of its held moisture.

1.2.2.3. Transmissibility, T. - This is simply defined as hydraulic conductivity X saturated thickness of aquifer, and for a confined, homogeneous aquifer it is, of course, constant. However, in the water table aquifer near wells it will be a function of the position of the free surface induced by pumping, and will therefore be variable. In general, it is the transmissibility which is determined from aquifer tests, and the conversion to the equivalent permeability merely represents the overall average permeability of an ideal homogeneous aquifer which behaves similarly to the one tested. The value of permeability obtained by analysis of pumping test data is, by assumption, for the horizontal direction. This average value obtained is a composite of the individual bed thicknesses and hydraulic conductivities. In some cases the average may be reduced to its constituents by the relationship

$$KH = K_1 H_1 = K_2 H_2 \ldots\ldots\ldots + K_n H_n \qquad (1.10)$$

where K = average hydraulic conductivity

$K_1 \ldots . K_n$ = hydraulic conductivity of individual beds

H = total thickness

$H_1 \ldots . H_n$ = thickness of individual beds

1.2.2.4. Specific capacity, SC - This is defined as the yield in gallons per day, per foot of drawdown under steady state conditions. For a confined aquifer, the specific capacity is constant for drawdowns less than the artesian head. For an unconfined aquifer, the specific capacity is a function of the percentage drawdown of maximum, or percentage dewatered. Because of this, specific capacity values have been normalized to the value represented

by 50% dewatered, using a relationship derived from the graph of Johnson (1966)

$$SC_{50} = SC\left(\frac{0.75}{1 - \%dw/200}\right) \qquad (1.11)$$

where SC_{50} = specific capacity at 50% dewatered

SC = calculated specific capacity

%dw = percentage of aquifer dewatered

1.3. Aquifer tests

The theory of aquifer tests is based on either a steady or non-steady state condition of flow within the aquifer.

1.3.1. Steady state

The steady state concept provided the framework for analysis of well hydraulics started at the end of the nineteenth century.

1.3.1.1. Confined flow - (Fig 11). The Thiem formula linking discharge with the potential around the well is given by

$$K = \frac{Q}{2\pi D} \cdot \frac{\log_e (r_2/r_1)}{h_2 - h_1} \qquad (1.12)$$

where D = aquifer thickness

r_1, r_2 = radial distances from well

h_1, h_2 = heads at distances r_1, r_2

The derivation of the formula for steady state is based on the following assumptions:

a) the aquifer is homogeneous, isotropic and of infinite areal extent,

b) the discharging well penetrates and receives water from the entire thickness of aquifer,

c) the transmissibility is constant at all times and at all places,

d) pumping has continued for a sufficient time to allow the system to have reached steady state conditions, i.e. no change in drawdown as a function of time,

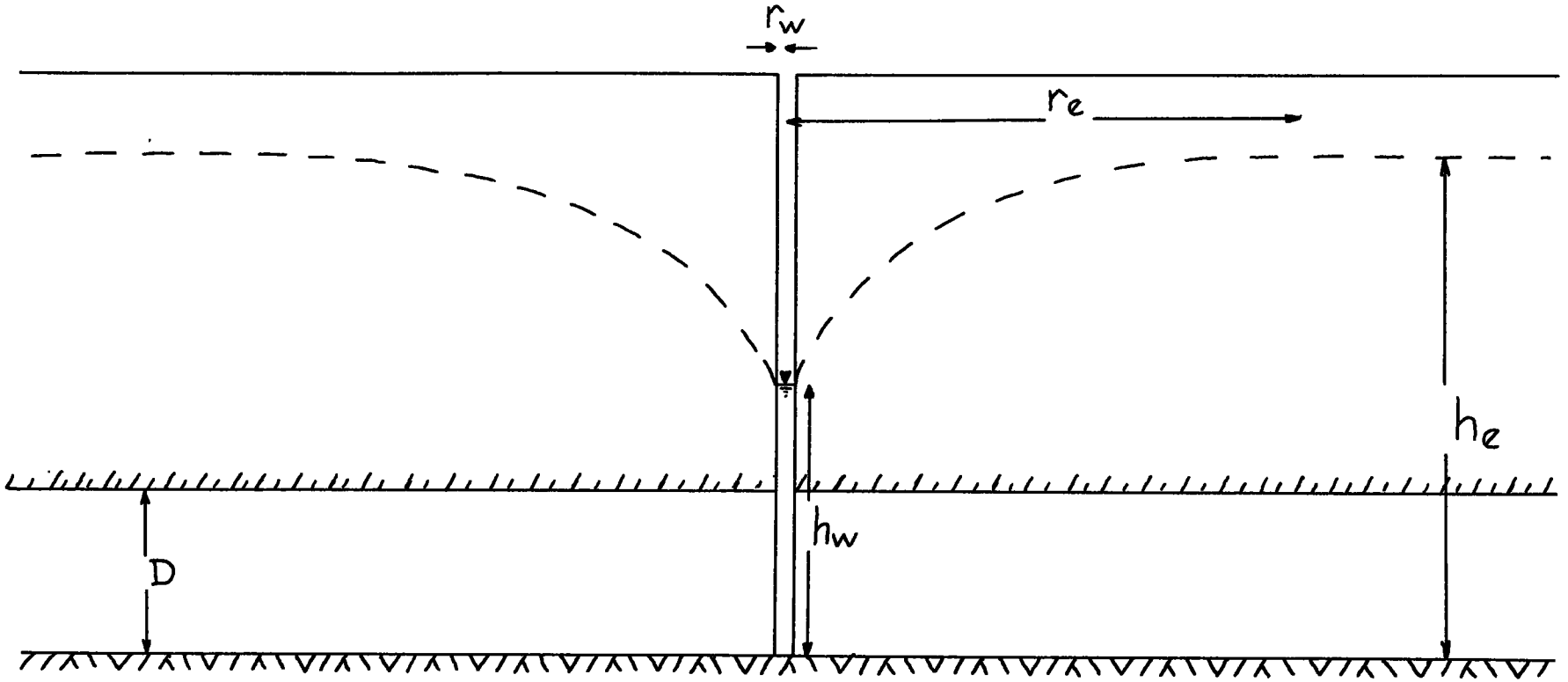

Fig 1.1. Confined aquifer: radial well flow.

e) the flow is laminar.

Despite these limitations, the formula has quite widespread applications.

1.3.1.2. Unconfined flow - (Fig 1.2). The corresponding equation for unconfined flow is generally attributed to Dupuit-Forchheimer, and is limited by similar assumptions to the Thiem equation above:-

$$K = \frac{Q}{\pi} \cdot \frac{\log_e (r_2/r_1)}{h_2^2 - h_1^2} \qquad (1.13)$$

Whilst this equation may be used to predict the discharge to within an error of 5%, Boulton (1951) has shown that it cannot be employed to determine the position of the free surface at a distance from the well of

$$r < 1.5\, h_e \qquad (1.14)$$

where r = radial distance from the well

h_e = undisturbed saturated aquifer thickness

Hantush (1964) has advanced a method for more accurately determining the free surface position using $\bar{h}$, the hydraulic head, defined as the height of water in a screened well completely penetrating the aquifer,

$$2h\bar{h} - h^2 = h_e^2 - \frac{Q}{\pi K} \cdot \log_e \frac{(r_e)}{r} \qquad (1.15)$$

As the distance from the well, r, increases, $\bar{h}$ approaches h and the equation becomes the same as the Dupuit-Forchheimer.

The main factor producing divergence of the free surface from that predicted by the Dupuit-Forchheimer is the existence of a seepage face in the well above the pumped water level. Boulton (1951) has shown by relaxation methods that the height of the seepage face may be determined from the well radius, amount pumped and hydraulic conductivity. Zee (1957) introduced dimensionless constants to express the combination of

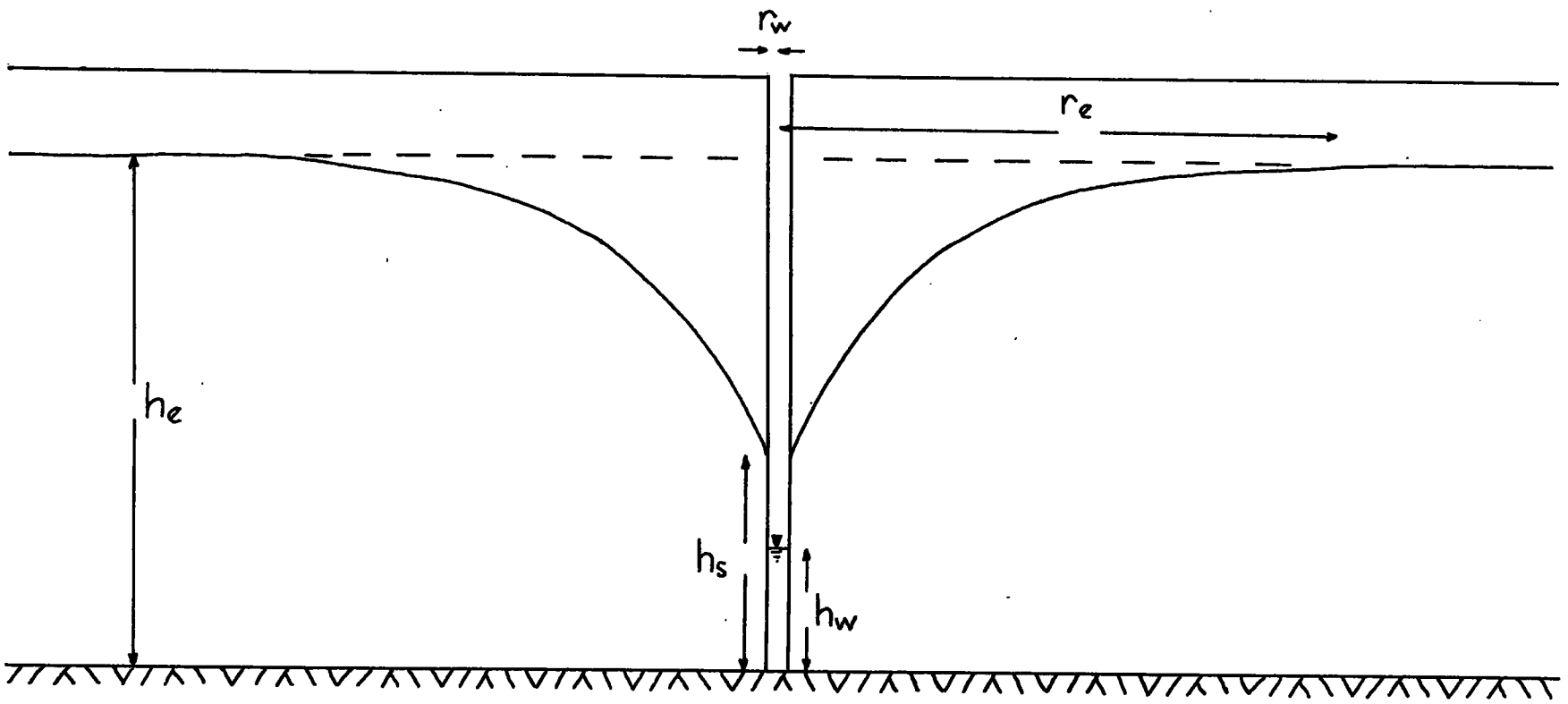

Fig 1.2. Unconfined aquifer: radial well flow.

parameters, and his work was further developed by Herbert (1965) who studied the disposition of the free surface around a steady state well using an electrical resistance analogue. From practically derived dimensionless number relationships he produced a graph of the correlation between Q/Kr_w^2 and $(h_{115} - h_s) / r_w$, where h_{115} is the height of the water table at a distance of 115 x r_w from the well, and h_s is the height of the seepage face. This, when used in conjunction with theoretically derived number relationships between Q/Kr_w^2 and h_w/r_w, enables the water table profile to be predicted from Zee's curves. Since it takes account of the seepage face it has been used as a method of analysis for cases where only the pumped water level is known. The process is iterative but converges very rapidly, and with practice takes little longer than the Dupuit-Forchheimer. Results obtained by the latter are generally higher than from the Herbert method due to the neglect of the seepage face by the former.

The application of steady state conditions has obvious attractions in its simplicity (Logan, 1964), but some of the limiting assumptions are too rigorous to allow more than an approximate solution for the parameters. By definition, the source of water under steady state conditions comes from lateral flow within the aquifer, rather than dewatering, and hence an estimate of the storage coefficient cannot be obtained. Boulton (1954) has shown that horizontal flow predominates for

$$\tau > 5 \qquad (1.16)$$

where $$\tau = Kt/Sh_e \qquad (1.17)$$

1. 3. 2. Non-steady state

The concept of time in groundwater hydraulics was first introduced by Theis in 1935, although the analogy with the conduction of heat had been recognized since the work of Slichter in 1899. In 1940, Jacob verified the non-equilibrium formula directly from hydraulic concepts. Stated in non-dimensional terms it is

$$s = \frac{Q}{4\pi T} \int_{\frac{r^2 S}{4tT}}^{\infty} \frac{e^{-u}}{u} \cdot du \qquad (1.18)$$

where $u = r^2 S/4tT$ (1.19)

The non-equilibrium formula is based on the following assumptions:-

a) the aquifer is homogeneous and isotropic,

b) the aquifer has infinite areal extent,

c) the discharge or recharge well penetrates or receives water from the entire thickness of aquifer,

d) the transmissibility is constant at all times and at all places,

e) the well has an infinitesimally small radius,

f) water removed from storage is discharged simultaneously with decline in head.

Since the expression cannot be directly integrated, solution is by matching a data curve of log (time) v log (drawdown) with the type curve of well function log (w(u)) v $\log(1/u)$. The match points are then substituted into the equations

$$s = \frac{Q}{T} \cdot w(u) \qquad (1.20)$$

$$u = \frac{S}{T} \cdot \frac{r^2}{t} \qquad (1.21)$$

allowing the storage coefficient and transmissibility to be calculated (De Wiest, 1965).

The value for the integral expression has been expanded (Jacob, 1950) into a series given by:-

$$\int_{\frac{r^2S}{4tT}}^{\infty} \frac{e^{-u}}{u} \cdot du = W(u) = -0.577216 - \log_e u - \frac{u^2}{2.2!}$$

$$+ \frac{u^3}{3.3!} - \frac{u^4}{4.4!} + \ldots\ldots\ldots \qquad (1.22)$$

Now for u 0.01 the terms beyond $\log_e u$ may be ignored, and the expression is thus reduced to

$$s = \frac{Q}{4\pi T} \left(\log_e \frac{4Tt}{r^2 S} - 0.5772\right)$$

$$s = \frac{Q}{4\pi T} \log_e \frac{2.25Tt}{r^2 S} \qquad (1.23)$$

This is known as the Jacob approximation, and the usual method of solution is to plot drawdown (s) v log (t) to produce a linear graph. Taking times t_1 and t_2 the respective drawdowns are s_1 and s_2 and thus

$$T = \frac{Q}{4\pi} \cdot \frac{\log_e (t_2/t_1)}{s_2 - s_1} \qquad (1.24)$$

If, for convenience, the time interval between t_1 and t_2 is taken as one log cycle, then

$$T = Q/\Delta s \qquad (1.25)$$

where Δs = change in drawdown, $s_2 - s_1$

The storage coefficient may be determined from the same plot, since when s = 0

$$s = \frac{Q}{4\pi Tt} \cdot \log_e \frac{2.25Tt}{r^2S}$$

thus $$S = \frac{2.25\ Tt_0}{r^2} \qquad (1.26)$$

where t_0 = intercept on time axis.

A development of the Jacob approximation allows the transmissibility to be calculated from the recovery of a pumped well. The cessation of pumping is considered analogous to the commencement of recharge at the same location and rate. Thus

$$s^1 = \frac{Q}{4\pi T}\left[\int_{\frac{r^2S}{4Tt}}^{\infty} \frac{e^{-u}}{u} \cdot du - \int_{\frac{r^2S}{4Tt^1}}^{\infty} \frac{e^{-u}}{u} \cdot du\right] \qquad (1.27)$$

where s^1 = residual drawdown

t^1 = time from end of pumping

Proceeding as before by expanding the integrals as series and neglecting all but the first two terms, then

$$s^1 = \frac{2.30\ Q}{4\pi T} \cdot \log_e\ (t/t^1) \qquad (1.28)$$

The most convenient method of solution is to plot the residual drawdown s^1 v log (t/t^1)

Taking $\Delta(\log(t/t^1))$ over one cycle, then

$$T = Q/\Delta s^1 \qquad (1.29)$$

It is not possible to determine with any accuracy the coefficient of storage from the recovery method.

Theoretically, the substitution of the well radius in the expression should produce a result, but the error in the determination of the effective well radius results in a large range of possible storage coefficient values. This is hardly

surprising since one of the assumptions for the Theis solution is a well of infinitesimally small radius.

The results of analyses based on recovery are usually reliable since errors due to variation in pumping rates which may be inherent in drawdown tests are not present. If howe ver the cone of depression intersects a barrier or recharge zone, then the results should be treated with caution, although they may be considered as giving the 'effective' transmissibility for the area around the well.

The Theis non-equilibrium equation was originally formulated for the confined aquifer case. It has, however, been employed ubiquitously and the results accepted with no more than the usual reservations. Ineson (1953) working on chalk aquifers which are sometimes unconfined, considers its application justifiable in such instances.

The first attempt to apply non-equilibrium conditions specifically to a water-table aquifer was made by Boulton (1954), who devised a solution based on two dimensionless parameters, defined by

$$\tau = \frac{Kt}{She} \qquad (1.17)$$

$$\theta = \frac{r}{h_e} \qquad (1.30)$$

The boundary conditions for which the solution was determined limits the drawdown to $s \leq 0.5\, h_e$, and was not therefore directly applicable to any of the cases studied.

Jacob (1963) produced a development of the Theis non-equilibrium formula for the recovery of pumped water-table wells, enabling the transmissibility to be determined with greater accuracy. The method of

solution is graphical and similar to the confined Jacob approximation, except that the residual drawdown, s^1, is replaced by $s^1 - (s^1)^2/2h_e$. Proceeding as before therefore, and taking the time interval, Δt, between t_1 and t_2 as one log cycle

$$T = \frac{Q}{\Delta (s^1 - (s^1)^2/2h_e)} \qquad (1.31)$$

1.4. Summary and conclusions

The methods of analysis that may be employed are largely dictated by the type of data available, and thus in the Sunderland and Hartlepool areas, unconfined, steady state models have been used. Of the non-equilibrium methods applicable, the recovery analysis has proved the most useful. In a more recent, controlled investigation of the south-east Durham area (see later) confined, non-steady methods have been used. However, since the values obtained by a similar method may be relative, rather than absolute, comparisons must be restricted to areas using similar models.

CHAPTER 2

PERMIAN GEOHYDROLOGY: FIELD AND LABORATORY TESTS

The dominant factor affecting all aspects of the geohydrology has proved to be the variation and distribution of the Permian lithologies, thus requiring a thorough assessment of the geology. Inevitably, extrapolation from borehole and exposure evidence has been required and grossly over-simplified models have been used to enable data to be analysed, with the result that the values obtained for the aquifer parameters are, on an absolute basis, suspect. In a subsequent chapter, alternative methods of analysis by simulation techniques will be discussed, and the results presented and compared with those obtained below from a theoretical treatment of an ideal aquifer.

In groundwater investigations, laboratory methods have largely been neglected compared with the sophisticated techniques employed by petroleum reservoir engineers, possibly due to the larger number of variables the latter is required to take into account. Nevertheless, determination of aquifer parameters by laboratory methods can afford an insight into the in-situ aquifer by comparing these values with those obtained by field tests.

The Permian of Co. Durham is divided hydrogeologically by an east-west line formed by the Hartlepool Fault and its westward extrapolation from Sedgefield to Chilton. North of this line, unconfined Lower Magnesian Limestone constitutes the major aquifer. The area has been overdeveloped, 24 m.g.d. being at present licensed for abstraction, and thus there appears to be little potential. South of the line, however, the aquifer is the far more permeable Middle Magnesian Limestone, and following a recent investigation under the auspices of the Northumbrian River Authority, is to be developed as a further source of water for the expanding industry of Tees-side.

The study of the geohydrology may be conveniently divided into:

(a) the determination of the areal and vertical distribution of groundwater,

(b) the analysis of data from pumping tests and routine abstraction, coupled with laboratory results, to ascertain the aquifer parameters,

(c) the overall assessment of the groundwater regime, especially with respect to water balance, to enable future development to be planned.

2.1. Groundwater distribution

The groundwater flow pattern is determined by the positions and potentials of the natural source and sink. Where the surface deposits are thin (less than 25 feet say) then accretion to the water table may take place by downward percolation of surface water. As outlined in the description of the Pleistocene deposits (Section I, 2.1.4), over much of the area the drift cover is so thick that it must be considered an impermeable blanket.

2.1.1. Recharge and discharge

The location of recharge is difficult to locate from limited detail. However, the distribution of groundwater level contours (Fig. 2.1) suggests that areas close to the escarpment constitute the major source, since usually they have only a thin veneer of drift. In addition to this, there are numerous quarries and diggings on or near to the scarp slope, and the bare rock exposed must greatly facilitate percolation. If the total rainfall per annum over the area is taken as 27 ins (Ministry of Housing and Local Government, 1961), of which 14 ins p.a. is lost in evapotranspiration (Institution of Water Engineers, 1961), a maximum of 13 ins p.a. is thus available for percolation, which represents 0.62 m.g.d./ $mile^2$. An estimate of the areas where percolation of this magnitude may be expected is both difficult and doubtful. Nevertheless, using Trechmann's map of the Permian (1925) a value of 51.5 $mile^2$ of thinly covered or exposed strata

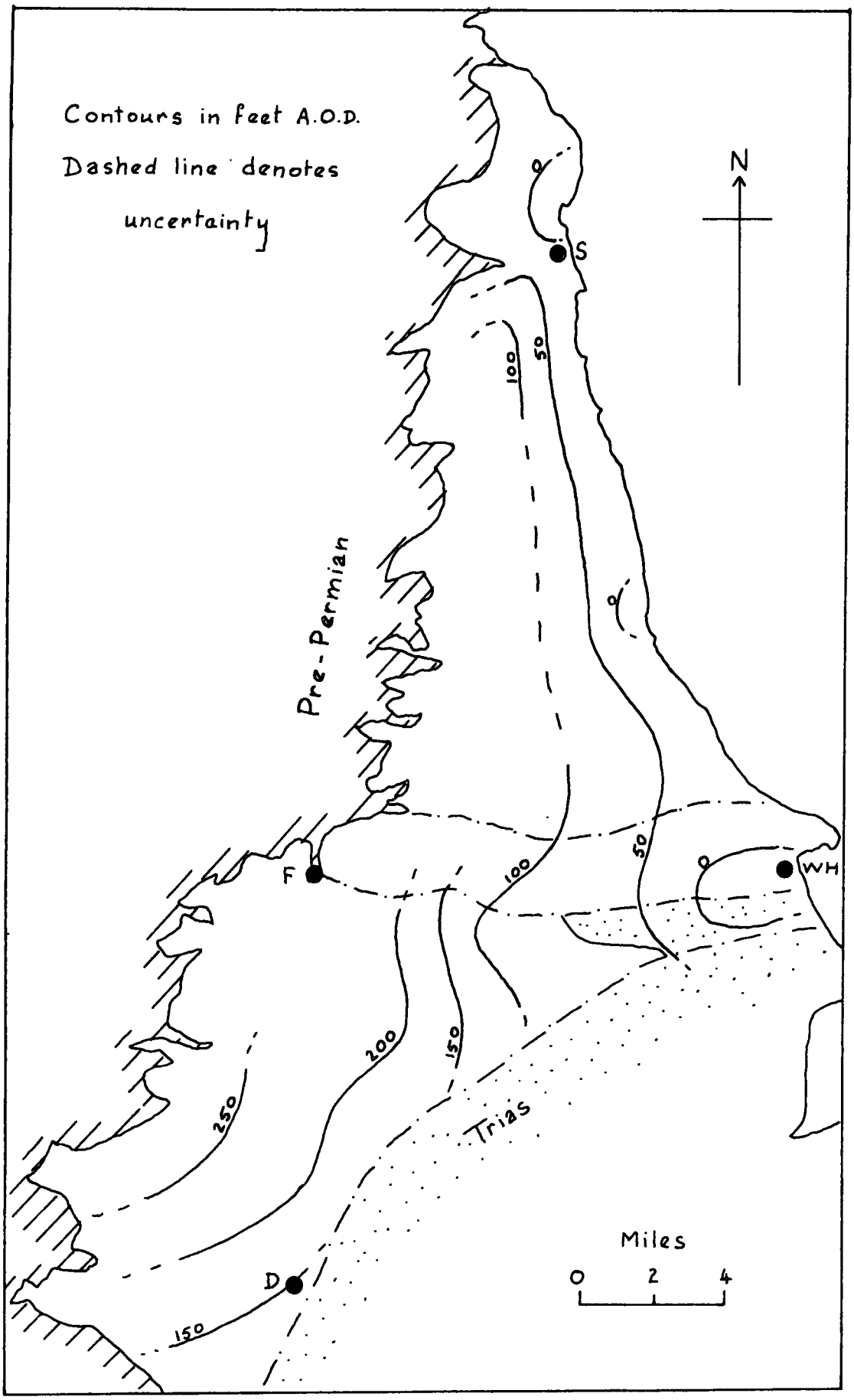

Fig. 2.1. Present-day ground-water levels.

was calculated using a simple gridding method. This constitutes a recharge of 32.08 m.g.d. Since this map was published more data from the south of the county has shown that areas such as Bradbury Carrs are locally thinly drift covered. At the present time, the Northumbrian River Authority is gauging the River Skerne, Billingham Beck, Rushyford Beck and Woodham Burn in an attempt to gain a more detailed and quantitiative knowledge of recharge in the area. Observations to date of the latter indicate that at least 1 m.g.d. is discharging into the aquifer during low flow conditions just north of Newton Aycliffe. An estimate of some 45 m.g.d. may thus be made for the total recharge over the whole of the Permian, although this may be in error either way by some 10 m.g.d.

Licensed abstraction from the Permian north of the Hartlepool Fault is at present 24 m.g.d., although this does not include losses from the Permian due to pumping from the underlying Coal Measures. In the southern area, a peak abstraction of 13 m.g.d. is at present under consideration, but since this would be only for part of the year, the average annual abstraction would be much lower.

The water balance for the whole area is thus extremely difficult to establish, but by breaking it down into small catchment basins it is hoped that a more detailed picture will emerge.

2.1.2. Groundwater level map

Since the recharge areas appear to be located towards the western edge of the Permian outcrop, and the strata dips gently eastwards or south-eastwards, the flow pattern is largely predictable, and does, in fact, behave as expected (Fig 2.1). Assuming the base of the outcrop, therefore, as the maximum elevation, north of Sunderland this would be at about 120 feet A.O.D. near Downhill. South of the River Wear, it lies at about 250 feet A.O.D. near

Houghton-le-Spring, rising southwards to over 500 feet A. O. D. near Coxhoe. From Ferryhill to Shildon it is at about 400 feet A. O. D. and reaches a maximum of 450 feet A O. D. neigh Heighington before decreasing to 250 feet A O. D. at the River Tees. Under balanced steady state conditions the groundwater level at the coast should be approximately Ordnance Datum. However, pit dewatering and overpumping have resulted in sub-O. D. groundwater levels around Whitburn, Sunderland, Ryhope, Horden and Hartlepool.

If the aquifer were isotropic and of uniform transmissibility with recharge along the western margin and discharge into the sea in the east, the equipotentials would be regularly spaced. Divergence from this is therefore attributable to a variation in transmissibility and/or recharge effects. Considering the piezometric map of the southern area (Fig 2. 2) and comparing it with the geological map (Section I, Fig. 2. 3) it can readily be seen that the wider spacing of contours occurs where the Middle Magnesian Limestone is present beneath the drift. Superimposed on this, in the Rushyford-Aycliffe area, is recharge, resulting in a very low potential gradient. The groundwater level contour map is thus a valuable indicator of the relative transmissibility and recharge conditions, and as such is used initially in simulation studies as a guide to the aquifer properties (see later).

The pre-war groundwater level map (Fig. 2. 3), based on the rest water levels given in the Wartime Pamphlet No. 19 (Anderson, 1941), shows some significant variations from the present day. A decrease in the number of private abstractors, coupled with an increasing use of surface water supplies by the Sunderland and South Shields Water Company, has resulted in a rise in the groundwater level in the Sunderland area. However, in the Hartlepools area, increased abstraction has produced a fall in the groundwater level of over 20 feet, and the associated sea water intrusion, although not yet

FIG. 2.2. PIEZOMETRIC CONTOURS OVER THE MODEL AREA

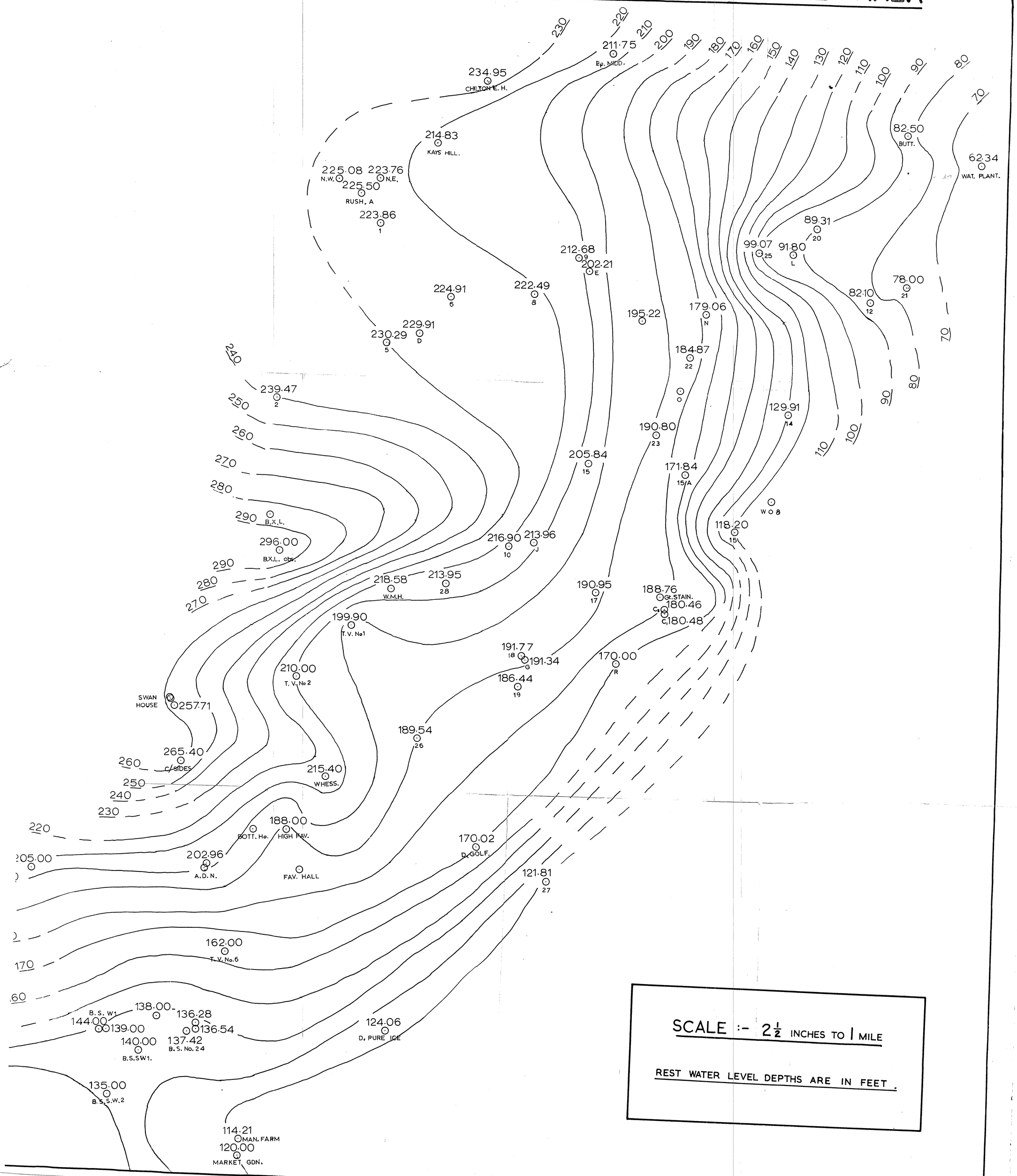

SCALE :- 2½ INCHES TO 1 MILE

REST WATER LEVEL DEPTHS ARE IN FEET.

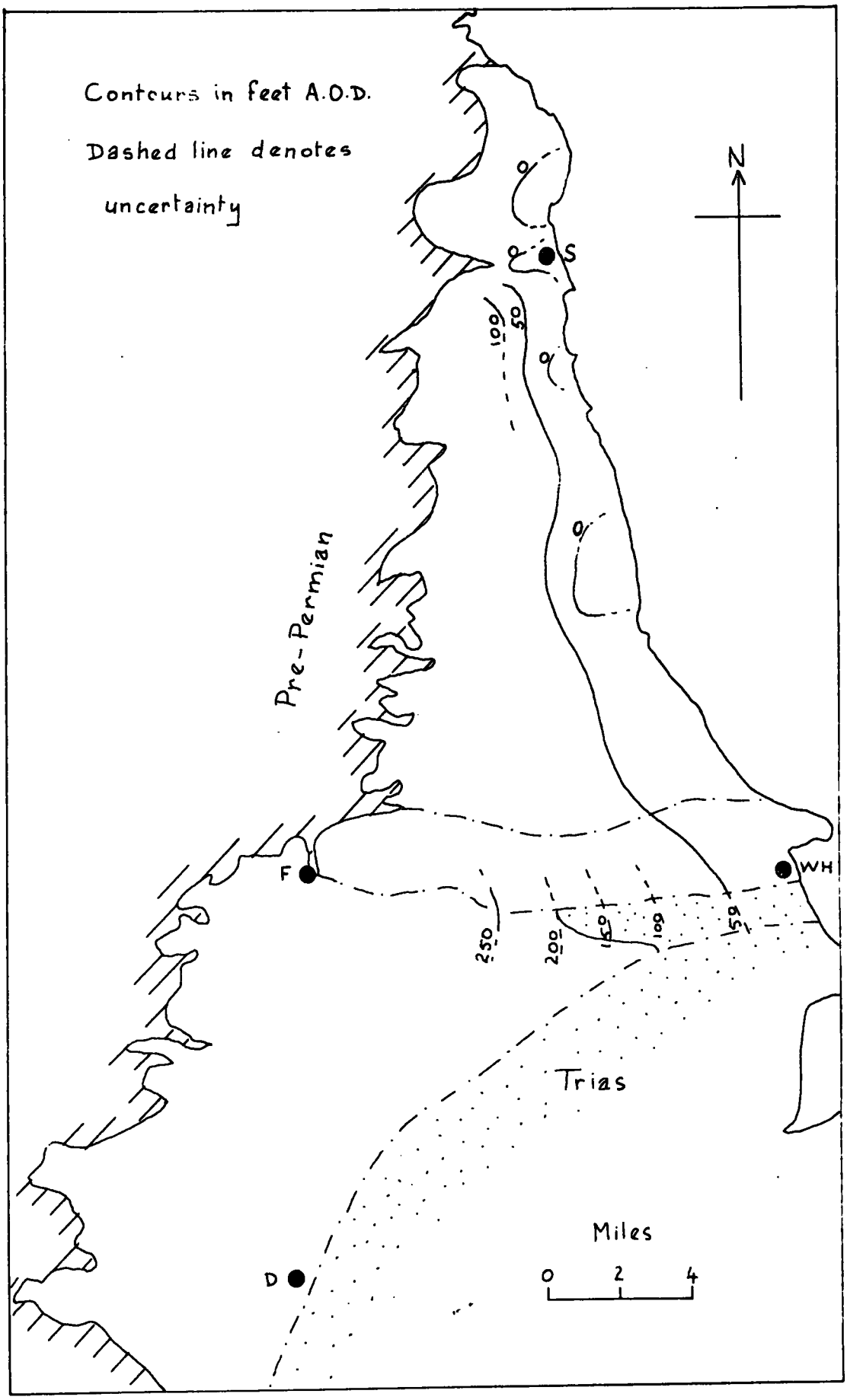

Fig. 2.3. Pre-war ground-water levels.

apparent, must be considered a possibility in the near future. The areas affected by mine dewatering have also changed, the most dramatic effect being in the Sedgefield area where pumping from workings at the nearby Fishburn Colliery has lowered the groundwater level an estimated 150 feet since 1935. Wood (1923) noted an 80 feet fall in the groundwater level between 1870 and 1915, and believed that some of the subsidence attributed to mining was in fact due to water abstraction. As yet, the long term groundwater disposition for the area south of Sedgefield is unavailable, and to help predict it model simulation has been employed (see later).

2.2. Analysis of pumping data

The data from the Sunderland and South Shields Water Company, and the Hartlepools Water Company was originally collected and processed in 1967. Many of the wells had been in constant use since the turn of the century, although the commissioning of the Derwent Reservoir in 1967 enabled some of the former's to be shut-down until increased demand requires additional supplies. Since there were no records of pumping tests with time-drawdown results and observation wells analysis was largely based on steady state assumptions. Where possible, recovery curves have been used as an independent method of assessing the transmissibility, but the lack of observation wells meant that storage coefficients could not be computed.

The details of each well and the derivation of the associated parameters where possible is contained in Appendix A, and a comparative selection is presented in Table 2.1.

In the northern area, the evidence for unconfined conditions comes from the geology and is confirmed by the yield-drawdown curves (Fig 2.4).

Peterlee Borehole

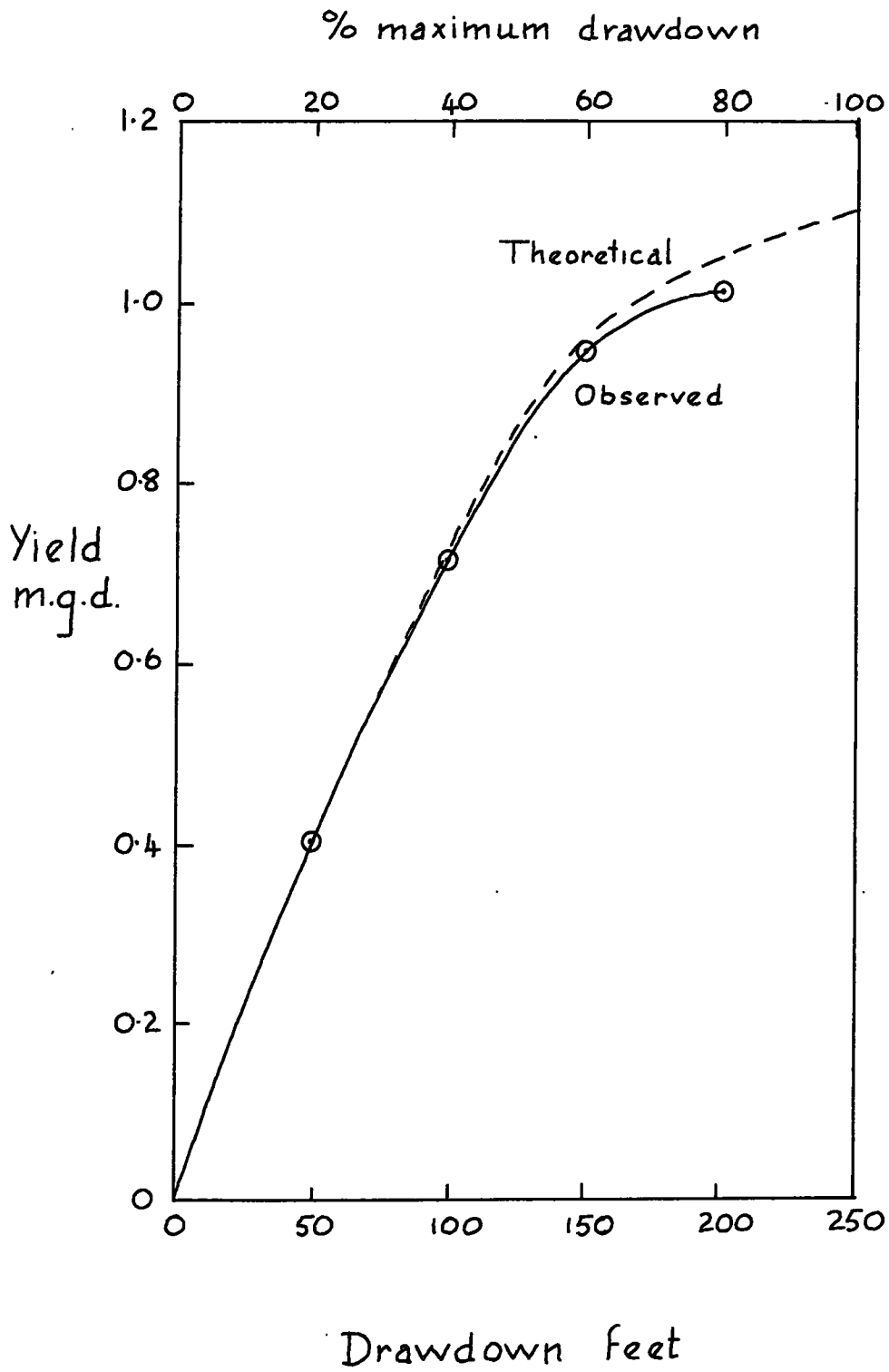

Fig. 2.4. Yield-drawdown curve.

TABLE 2.1.

	Aquifer(s)	h_e ft	Dupuit-Forchheimer g. p. d. /ft^2 K_1	Herbert K_1 g. p. d. /ft^2	Jacob recovery (g. p. d. /ft^2)	SC_{50} g. p. d. /ft
Humbledon	L. M. L. & M. M. L.	40	291. 5	205	244. 4	10371
Fulwell	L. M. L. & U. M. L.	84. 8	268. 9	275	118. 8	20280
Cleadon	L. M. L. & U. M. L.					36544
Ryhope	L. M. L.	31. 6	2679	430		80457
Dalton	L. M. L.	154	109. 7	111. 5		16239
Seaton	L. M. L.	82	59. 1	66	40. 9	4533
Stonygate	L. M. L.	105. 3	109. 6	95		10624
Thorpe	L. M. L.	102	107. 1	124	56. 4	10891
Burdon	L. M. L. & B. P. S.					
North Dalton	L. M. L. & B. P. S.	215	99. 4			
New Winning No. 1	L. M. L.	151	90. 7			12177
Hawthorn	L. M. L.	218	46. 5	48	33. 1	7181
Herrington	L. M. L.					

/Continued overleaf.

TABLE 2.1. (Continued)

	Aquifer(s)	h_e ft	Dupuit-Forchheimer g.p.d./ft^2 K_1	Herbert K_{21} g.p.d./ft^2	Jacob recovery (g.p.d./ft^2)	SC_{50} g.p.d./ft
Peterlee	L.M.L. & B.P.S.	250	36.6	25		6238
Mill Hill	L.M.L. & B.P.S.	166.5	93.3	120		10589
Coal Lane	M.M.L. & L.M.L.	145	297.1			29205
Naisberry	M.M.L. & L.M.L.	125	370.8			30417
Butterwick	L.M.L.	120	61.1	46	20.4	4543

The particular well, Peterlee, from which this example was taken, penetrates Lower Magnesian Limestone, Marl Slate and Basal Permian Sands beneath the groundwater level. The influence of the impermeable Marl Slate as a confining bed appears to be minimal, probably due to the abundance of faults which, for throws greater than the Marl Slate thickness of about 2 feet, would allow passage of water between the Lower Magnesian Limestone and the Basal Sands. The yield-drawdown curve does, however, show a slight divergence from the theoretical (Johnson, 1966) at large drawdowns. This could be due to either a decrease in the hydraulic conductivity towards the base, or anisotropy resulting in a lower horizontal than vertical permeability, the effect of which would become increasingly apparent with large drawdowns as the flow lines diverge from the horizontal. In practice the cause may be a combination of these two mechanisms. A water-table model has been used for all wells north of the Hartlepool-Chilton line.

South of the Hartlepool-Chilton line the main aquifer, the Middle Magnesian Limestone, is invariably confined by drift deposits or marls of the Lower Evaporite Group. The underlying Lower Magnesian Limestone has a sufficiently low hydraulic conductivity in comparison that it may be considered the basal aquiclude. Since investigation of this area could be carried out on a more ordered basis, the results obtained have been more comprehensive and reliable, and the aquifer parameters determined, by Dr. T. Cairney of the Northumbrian River Authority, from pumping tests in this area are contained in Appendix A.

In examining hydraulic conductivities for different localities and horizons it should be noted that only values based on similar models can be usefully compared. Since the most ubiquitous solution available is based on

steady state conditions, with an assumed radius of influence of 1000 feet, this will be used for interpretation of the northern area. Similar conclusions, differing in magnitude rather than meaning would be drawn by using a radius of influence of 5000 feet, or by comparing values obtained from analyses by the Herbert method. In the southern area, a more rigorous approach could be used, and the aquifer parameters cited are based on a non-steady Theis-type model. Direct comparison between the areas across the Hartlepool-Chilton line is thus difficult, although judging by results from the northern area the relationship

$$K \text{ (non steady)} = 0.763 \cdot K \text{ (steady)} - 20.4 \qquad (2.1)$$

(Fig 2.5) allows an approximate comparison to be made.

2.3. Interpretations

The hydraulic conductivities given in Appendix A and in Table 2.1 represent the hydraulic conductivity of an ideal isotropic aquifer which would, under the restrictions imposed by the assumed model, behave similarly to the aquifer tested. The subsequent interpretation of these values is the result of an effort to break them down into their constituent parts.

2.3.1. Northern area

The hydraulic conductivities calculated by the Dupuit-Forchheimer method with an assumed radius of influence of 1000 feet, together with a diagrammatic representation of the well and strata penetrated beneath the water table, is given in Fig. 2.6, and from this the relationships between the aquifers and hydraulic conductivities may be deduced.

Where the Middle Magnesian Limestone or the brecciated Upper Magnesian Limestone represents over half the saturated thickness, the hydraulic conductivity is greater than 250 g.p.d./ft^2. However, where the Lower Magnesian Limestone is the only aquifer, the hydraulic conductivity is

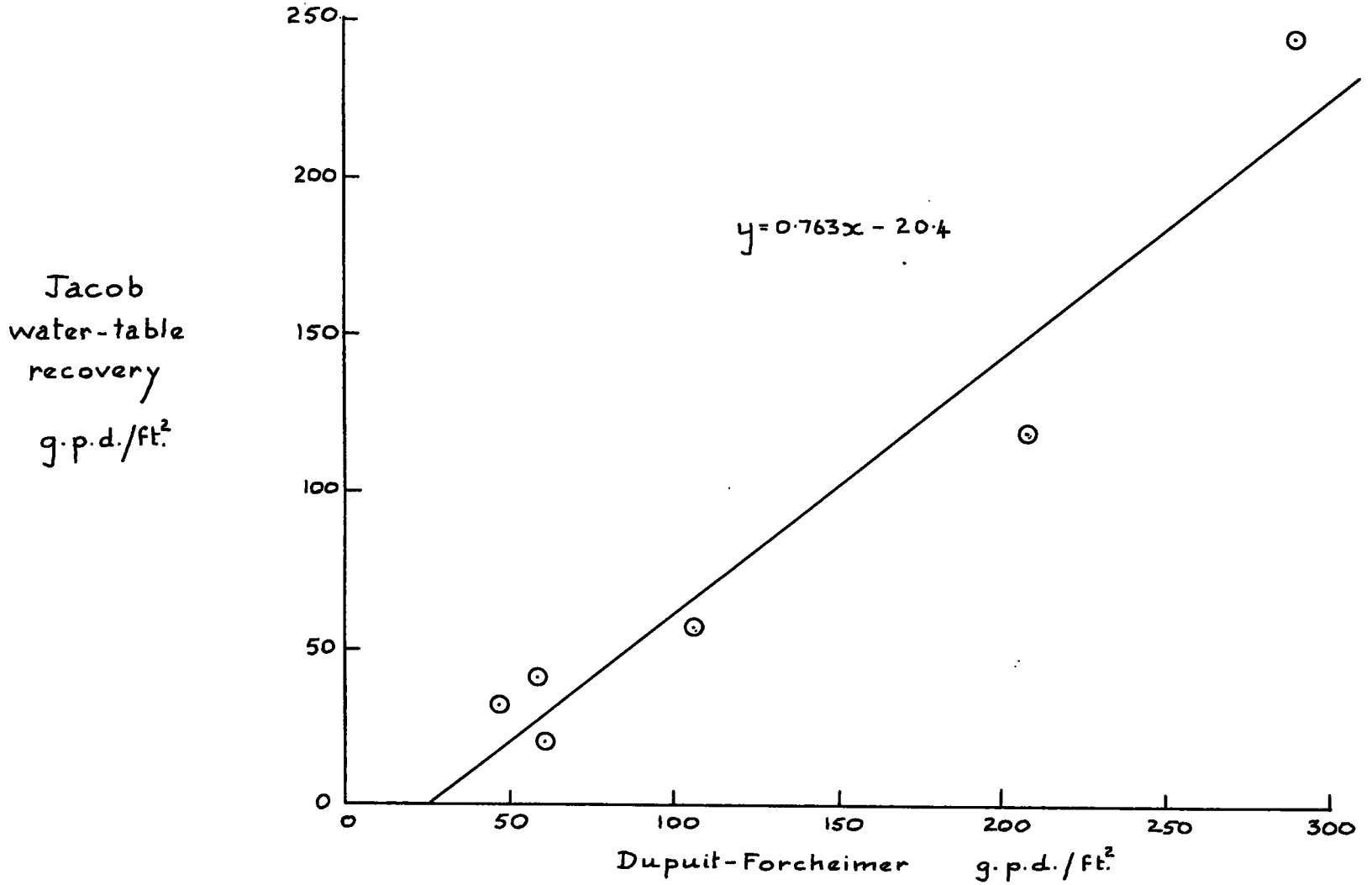

Fig. 2.5. Hydraulic conductivity: steady state — non-equilibrium relationship.

Well	Humbledon	Fullwell	Cleadon	Ryhope	Dalton	Seaton	Stonygate	Thorpe	North Dalton	New Winning No.1.	Hawthorn	Peterlee	Mill Hill	Butterwick	Coal Lane	Naisberry
SC_{50} gpd/ft	10371	20280	36544	80457	16239	4533	10624	10891		12177	7181	6238	10589	4543	29205	30417
Hydraulic conductivity gpd/ft^2	29.5	268.9		26.79	109.7	59.1	109.6	107.1	99.4	90.7	46.5	36.6	93.3	61.1	297.1	370.8
Recalc. hydraulic conductivity gpd/ft^2	300	255.3	300	300	110	90.4	110	93.3	103.2	105.4	89.7	71.0	101.3	92.5	241.0	219.4

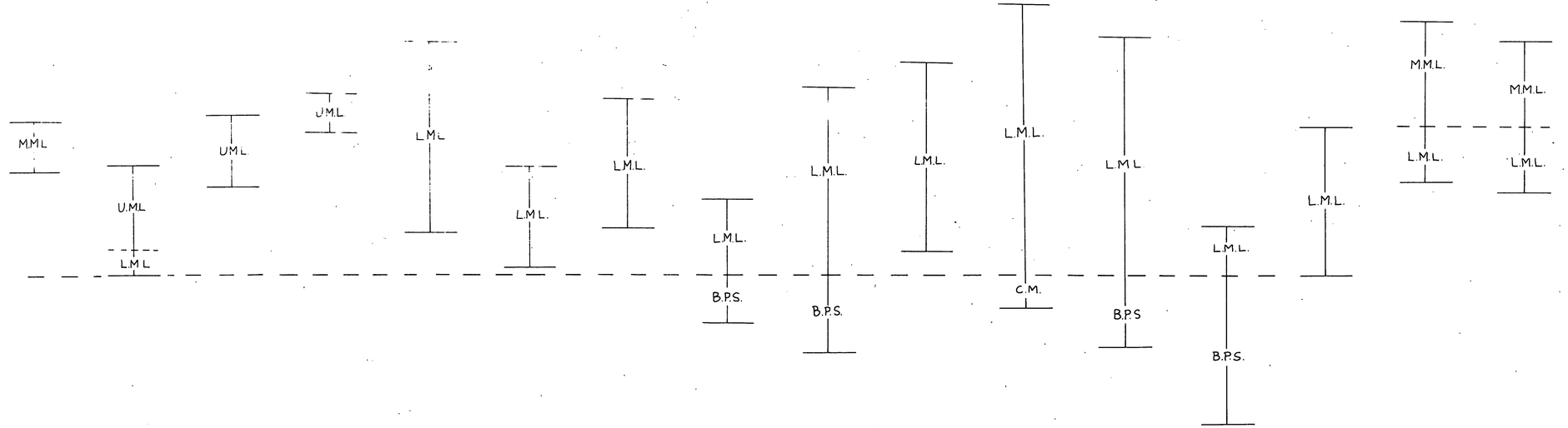

Saturated succession 1cm. = 20ft

Fig. 2.6 Well parameters

less than 110 g. p. d. /ft^2. The more competent lithology of the Lower Magnesian Limestone results in a much lower hydraulic conductivity than the more open textured Middle or brecciated Upper Magnesian Limestones. The very high value for Ryhope is believed to be due to recharge from the sea which limits the growth of the cone of depression in that direction: further evidence is the very high chloride content recorded in this well.

The Lower Magnesian Limestone itself appears to show a variation in hydraulic conductivity with depth, becoming less permeable near the base, (compare Stonygate and Dalton with Butterwick and Seaton). This could be a reflection of the more massive and often calcitic beds which occur towards the base of the succession, as noted in Section I.

The Basal Permian Sands appear, in general, to have a hydraulic conductivity similar to the bulk of the Lower Magnesian Limestone. However, the very low value at Peterlee can only be interpreted as indicating low hydraulic conductivity of the Basal Permian Sands as well as the Lower Magnesian Limestone, (c.f. section II, 2. 2. for evidence of low hydraulic conductivity towards the base from yield-drawdown curve).

Values for the hydraulic conductivities of the various formations may thus be deduced from the evidence outlined above, and these are:-

Upper Magnesian Limestone, brecciated,	300 g. p. d. /ft^2
Middle Magnesian Limestone,	300 g. p. d. /ft^2
Lower Magnesian Limestone, except basal unit,	110 g. p. d. /ft^2
Lower Magnesian Limestone, basal unit	40 g. p. d. /ft^2
Basal Permian Sands	40-120 g. p. d. /ft^2

On this basis, the 'theoretical' hydraulic conductivity for each well may be calculated from Equation 1. 10. and the result compared with the observed value.

However, before this can be done, the extent of the basal low permeability unit of the Lower Magnesian Limestone must be fixed. Since Stonygate and Dalton both penetrate to within about 30 feet of the Marl Slate, figures of 20 feet, 30 feet and 40 feet have been taken, and the results are given in full in Appendix A. Some of the 'best fit' combinations are given in Fig. 2.6 but these merely represent one of an infinite number of possible solutions, and must therefore be viewed accordingly. Nevertheless, the pattern does suggest that the hypothesis of variable hydraulic conductivities, certainly between different units, and possibly within the same unit, is viable. However, the large variation in lithologies and hence properties within, say, the Lower Magnesian Limestone over the area studied means that the values can be applied areally only on a semi-quantitative basis.

The specific capacity value for each well has been calculated for the relevant drawdown, and the value normalized to 50% maximum drawdown (SC_{50}). The correlation with hydraulic conductivity is good (Fig. 2.7) and may be approximated by the linear equation:-

$$SC_{50} = 84.4 . K_1 \qquad (2.2)$$

Since, when $K_1 = 0$, $SC_{50} = 0$, the line was constrained to pass through the origin by using dummy reflection co-ordinates about the origin, for each point.

The transmissibility values are in themselves rather meaningless since many of the wells do not achieve maximum penetration of the saturated aquifers. Since maximum yield is basically a function of transmissibility, increased abstraction could be obtained at some wells by deepening. However, the increased cost of pumping due to the higher lift required may not be offset by the yield if the strata has a low hydraulic conductivity.

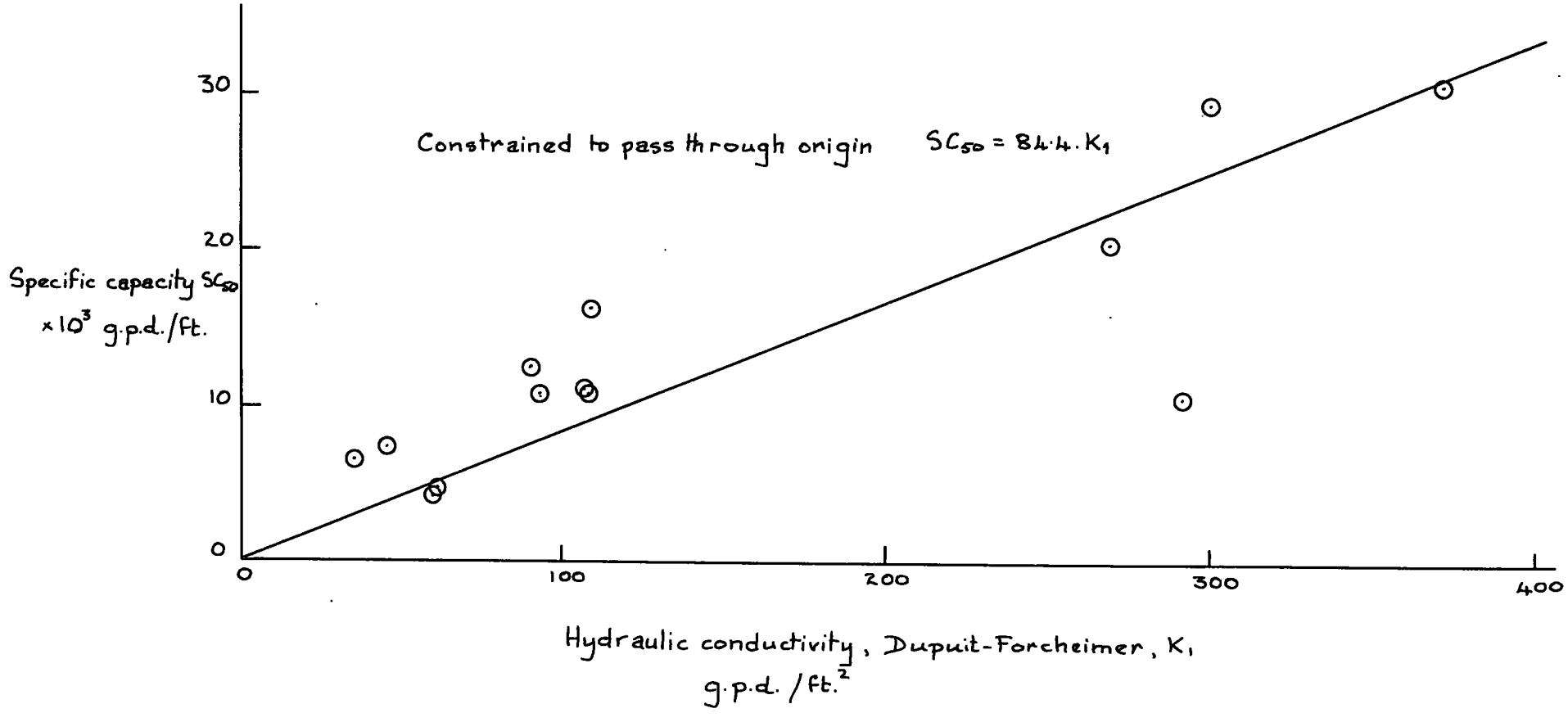

Fig. 2.7. Normalised specific capacity - hydraulic conductivity relationship.

2.3.2. Southern area

The results of the investigation undertaken in this area are fully documented in an internal report of the Northumbrian River Authority (1969). However, since this area represents the subject of the simulations, a brief summary of the results will be given here.

The suitability of the area (Fig. 2.8) for groundwater supply was investigated by drilling 42 primary and 15 large diameter holes, as well as utilising and testing existing boreholes. The details of the individual large diameter holes are given in Appendix A.

The transmissibilities calculated by non-equilibrium methods of analysis showed that there were large variations, even around a single hole, and that impermeable and semi-impermeable barriers due to faulting and basement 'highs' had a profound effect upon the development of the cone of depression (Fig. 2.9). The pumped hole recovery transmissibilities varied from 4000 g.p.d./ft (K) to 36,000 g.p.d./ft (D), but averaged 13410 g.p.d./ft. Analysis in the planes from the pumped well to observation wells showed a much wider range, from 2000 g.p.d./ft (L-K) to 48000 g.p.d./ft (9-18). Using the Jacob recovery value at the pumped well, the average permeability was 215.7 g.p d./ft^2 for the Middle Magnesian Limestone.

Where there is a thick cover of impermeable marls above the Middle Magnesian Limestone and the interstitial cement has not been leached, the porosity and hence permeability, is reduced.

In order to limit dewatering of the aquifer, the pumping rates are being limited so that drawdown does not exceed the artesian head. This is highest in the trough fault area and around Broken Scar, where it is over 100 feet. It reduces to about 30 feet at D and the aquifer is water table at b.h. 2. The maximum safe yield available for a well is thus given by

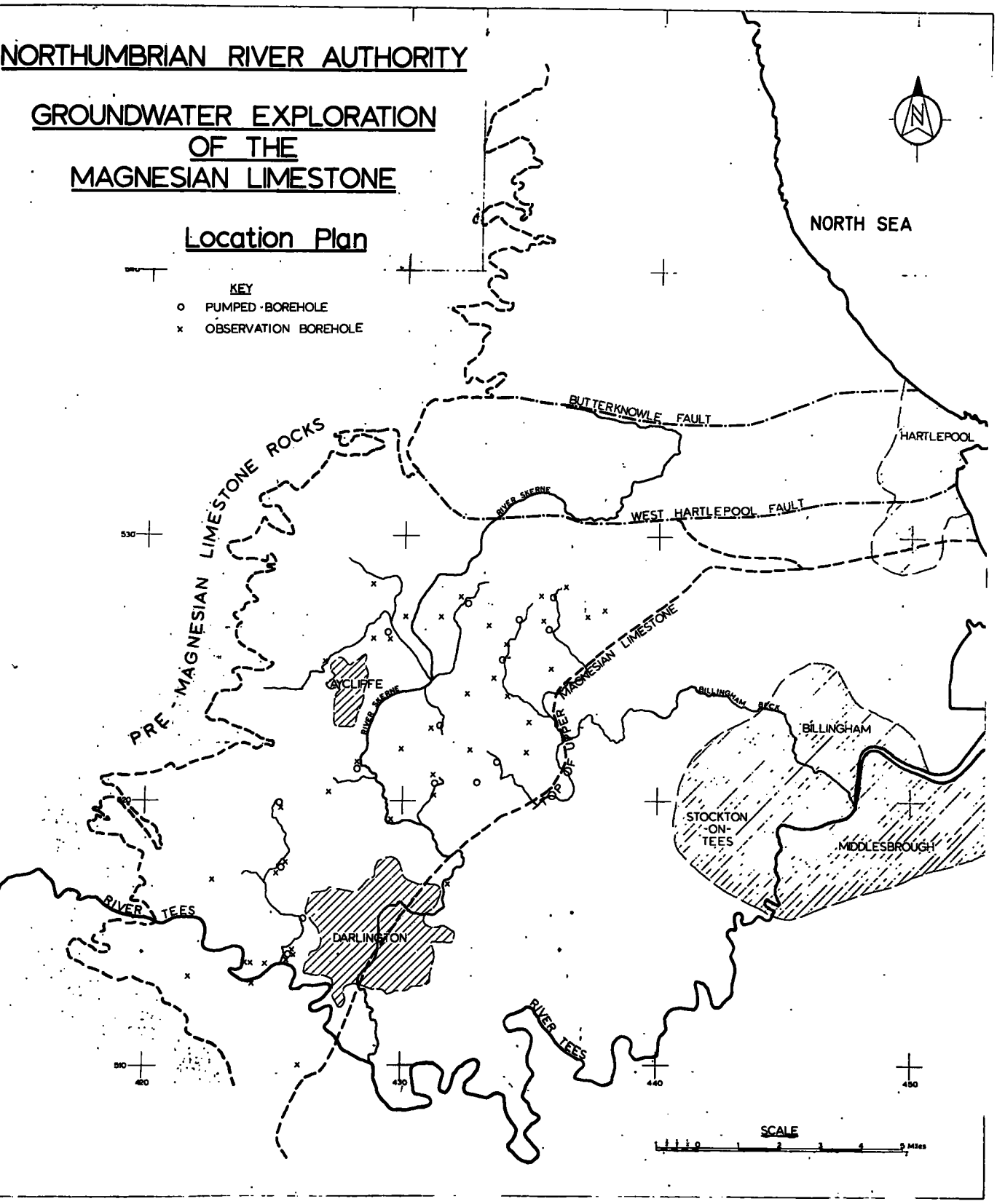
NORTHUMBRIAN RIVER AUTHORITY
GROUNDWATER EXPLORATION OF THE MAGNESIAN LIMESTONE
Location Plan
KEY
PUMPED - BOREHOLE
OBSERVATION BOREHOLE
NORTH SEA
BUTTERKNOWLE FAULT
HARTLEPOOL
RIVER SKERNE
WEST HARTLEPOOL FAULT
PRE-MAGNESIAN LIMESTONE ROCKS
TOP OF UPPER MAGNESIAN LIMESTONE
AYCLIFFE
BILLINGHAM BECK
BILLINGHAM
STOCKTON -ON- TEES
MIDDLESBROUGH
RIVER TEES
DARLINGTON
RIVER TEES
SCALE
530
510
420
430
440
450

Fig. 2.8

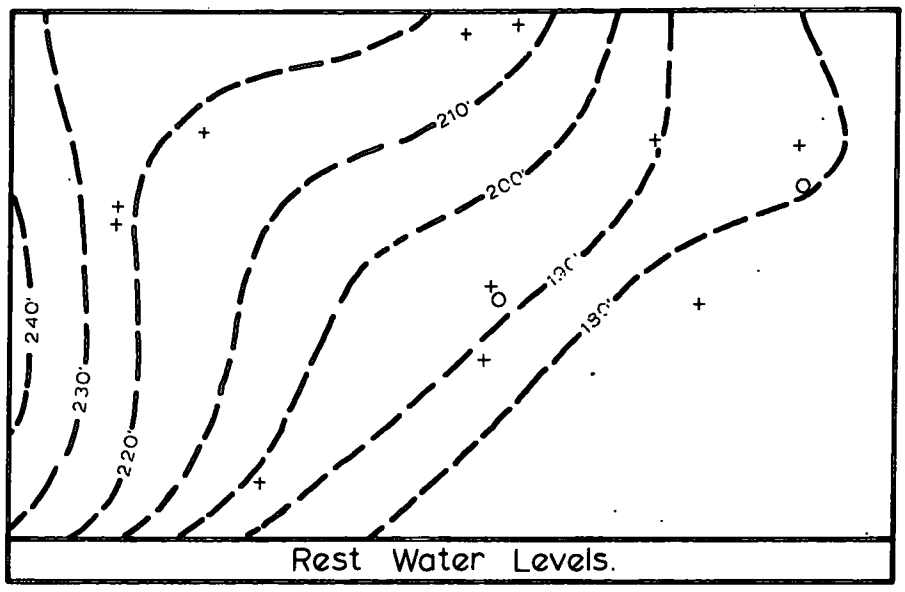

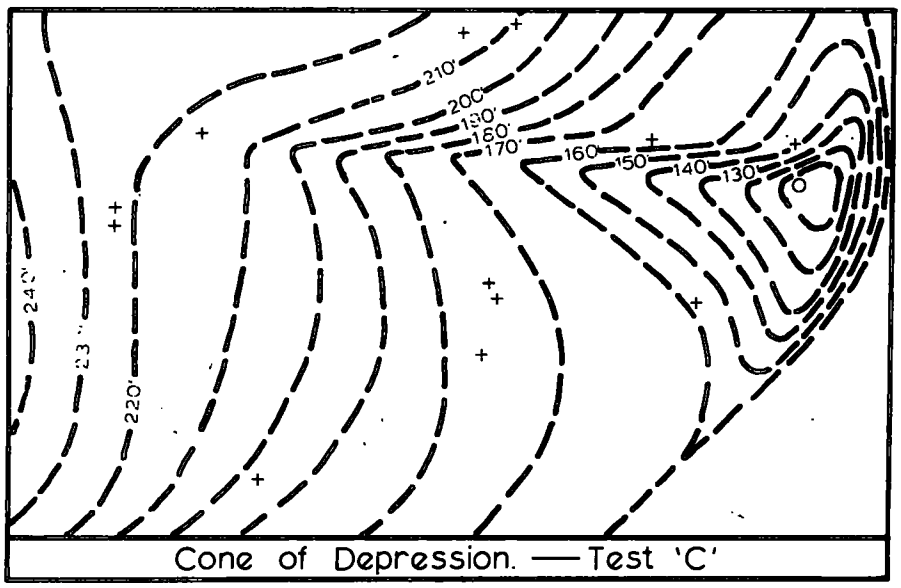

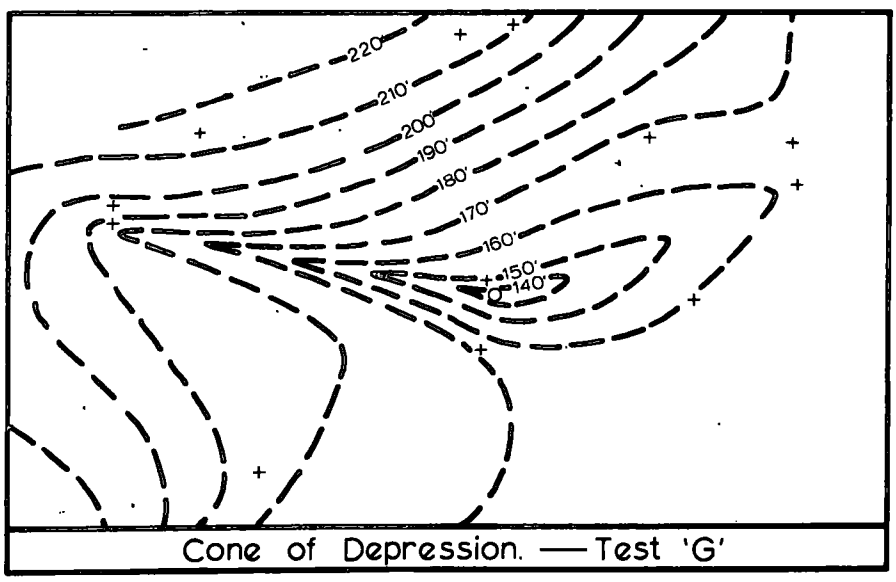

Fig. 29. Barrier effects.

$$Q_{max} = h_a . SC \qquad (2.3)$$

where h_a = artesian head.

Where there are a number of wells pumping and the cones of depression interfering, h_a is effectively reduced.

For the southern area, the relationship between hydraulic conductivity, K, and specific capacity, SC, (Fig. 2.10) shows a similar trend to the northern area, and is given by

$$SC = 65.5\ K \qquad (2.4)$$

2.4. Field results: summary and conclusions

1) The Permian may be divided by an east-west line along the Hartlepool Fault and its western extrapolation, into two areas, northern and southern. These are hydrologically different: the former fully exploited and abstracting largely from the unconfined Lower Magnesian Limestone and Basal Permian Sands; the latter underdeveloped, with the usually confined Middle Magnesian Limestone constituting the aquifer.

2) Recharge originates near the scarp, and is estimated at some 45 ± 10 m.g.d. for the whole of the Permian, based on theoretical percolation figures.

3) For the northern area, steady state analysis enables values for the saturated horizons to be calculated.

4) For the southern area, non-steady state methods have been similarly employed.

5) The aquifer in the south is complicated by hydrologic barriers and recharge zones, making analysis difficult, and extrapolation and prediction of multiple pumping schemes dubious.

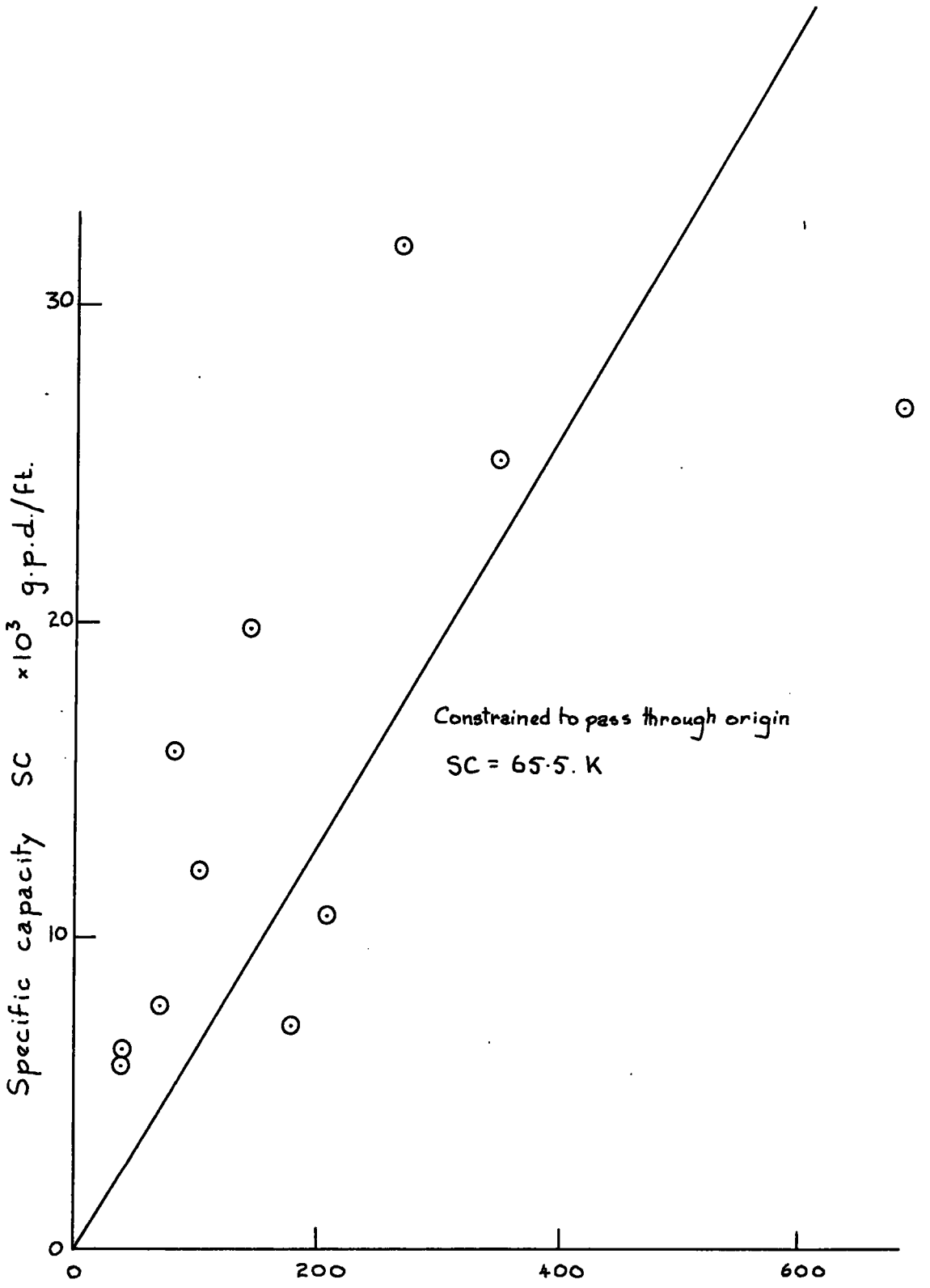

Fig. 2.10. Specific capacity v hydraulic conductivity.

2.5 Laboratory tests

The benefit of laboratory tests is limited by the errors involved in extrapolation from a small sample to in-situ conditions. Nevertheless, the difference between the field and laboratory values for hydraulic conductivity is partially an indication of the proportion of flow which is not through the intact material, but rather through fissures and joints.

2.5.1. Techniques

The determination of porosity and permeability is based on well tried methods used in soil mechanics (Akroyd, 1964).

2.5.1.1. - Porosity - The porosity, n, may be calculated from combination of the dry density, γ_d, saturated moisture content, w_s, specific gravity, G, saturated density, γ_s, using the following relationships:

$$n = 1 - (\gamma_d / G\,\gamma_w) \qquad (2.5)$$

$$n = (G\gamma_w - s)/\gamma_w(G-1) \qquad (2.6)$$

$$n = w_s G/(1 - w_s G) \qquad (2.7)$$

$$n = (\gamma_s - \gamma_d)/\gamma_w \qquad (2.8)$$

$$n = w_s \gamma_d/\gamma_w \qquad (2.9)$$

$$n = w_s \gamma_s/(1 - w_s)\,\gamma_w \qquad (2.10)$$

(a) Dry density. Since dry density is defined by oven dry weight/total volume, it is resolved into a determination of volume. This may be done directly by measuring a regularly shaped sample such as a cylinder, or indirectly by Archimedes' principal. For the latter, an irregularly shaped sample is coated with 'Lowerite' to prevent water entering the pores when weighed submerged.

(b) Saturated density. This is determined by either of the above methods, with the weight of the sample taken after at least 24 hours vacuum saturation.

(c) Saturated moisture content. This is calculated from the loss in weight from vacuum saturation after oven drying for at least 24 hours at 110°C.

(d) Specific gravity. S. G. bottle methods are generally preferred to the pycnometer since they allow for a more precise determination providing precautions are taken, especially if water is used, to see that the sample and liquid have been thoroughly de-aired.

2. 5. 1. 2. 24 hour absorption - This test merely consisted of leaving the cold, oven dried sample immersed in water for 24 hours and then determining the moisture content.

2. 5. 1. 3. Hydraulic conductivity - The permeability determinations used methods based on the familiar direct techniques of constant head or falling head, or by indirect methods.

(a) Constant head - In general, the head available with normal laboratory apparatus is about 6 feet and is insufficient for low permeability samples. Mercury compensated constant head apparatus designed for soil triaxial testing (Bishop and Henkel, 1957) was therefore used, but since a maximum of 300 cc of water was available, conditions had to be carefully controlled. Two types of sample holder were employed. The first is a commercially available high pressure permeameter manufactured by Clockhouse Engineering Ltd. The sample in the form of a cylinder is encased in Beeswax to form an impermeable sheath and the rate of flow of water from the constant head apparatus measured. The equipment suffers from a number of drawbacks. Wax may enter and block some of the peripheral pores if they are large and especially if the sample is hot, thus decreasing the effective cross sectional area. If the sample is saturated prior to the

test, the molten wax causes steam and 'blow holes' develop which allow water to pass through the wax. However, if the sample is not saturated, bubbles of air in the pores reduce the cross sectional area available for flow. Problems also occurred with the wax blocking up the interstices of the porous disc, although carbon tetrachloride proved to be an effective solvent cleanser. In conclusion, it was felt that the requirements for a precise determination of permeability were incompatible with the design and recommended use of the equipment.

Apparatus described by Chakrabarti & Taylor (1968), however, gave better results. In this a sample disc, about 1 cm thick, is securely held by 'O' rings, and the rate of flow of water from the constant head apparatus measured after passing through the sample. By judicious arrangement of the pressure, the flow can be adjusted so that its velocity potential is negligible. The advantage of this method is that the sample may be thoroughly saturated before testing, and hydraulic conductivities between 10^{-4} cm/sec and 10^{-8} cm/sec may be measured. A full description of the apparatus and suggested experimental technique is given by Jackson (1968).

(b) Falling head - In soil mechanics, the falling head method is used for samples with hydraulic conductivities less than 10^{-3} cm/sec, and may be simply adapted for rock samples. Beeswax was tried for sheathing the sample but was rejected for the reasons outlined above in favour of rubber sheaths as used in standard soil triaxial tests. The very low values obtained in some tests are attributed to carborundum powder from lapping blocking the end pores: subsequently samples were sawn. By plotting log (Δ h) v time, the hydraulic conductivity may be calculated from the straight line position of the graph.

(c) In direct methods - The grading of a sample may be used as a guide to the permeability, Hazen's empirical law being the simplest (Terzaghi & Peck, 1967)

$$K = C_1 D_{10}^{2} \qquad (2.11)$$

where K = hydraulic conductivity, cm/sec

C_1 = constant varying from 100-150

D_{10} = effective size in cm

Application is, however, limited to sands, and obviously cannot be applied to coherent material.

2.5.1.5. Storage release - An attempt was made to estimate the release of water under free draining conditions by allowing a saturated sample to equilibriate with its own saturated vapour at atmospheric pressure. This is thus equivalent to the moisture content at atmospheric pressure on the drying-out portion of the pF curve, the 24 hr. absorption being the corresponding position on the wetting-up curve. The saturated samples were placed on a No. 7 sieve, covered, and placed in a tray with the water surface just below the mesh. For most of the samples, the reduction in moisture content was less than the experimental errors inherent in trying to weigh a surface dry, moist sample.

2.5.2. Results

A summary of results obtained by the present author and others using Magnesian Limestone samples is given in Table 2.2. It will immediately be obvious that values are at least an order of magnitude less than the field values, although the highly friable and poorly cemented horizons of the Middle Magnesian Limestone could not be tested due to its cohesionless nature. As expected the premeability of the Lower Magnesian Limestone is considerably less than that of the Middle Magnesian Limestone, although isolated samples

TABLE 2.2.

Sample No.	Horizon	No. tested	Hydraulic conductivity cm/sec	Method	Porosity %	Worker
HO1(V)	L.M.L.	18	7.36×10^{-5}	F.H.	15.2	R.S.J.
HO1(H)	L.M.L.	1	6.57×10^{-5}	F.H.	22.6.	"
TH4(H)	L.M.L.	1	2.76×10^{-6}	F.H.	10.6	"
HA1(V)	M.M.L.	18	2.23×10^{-4}	F.H.	20.9	"
HA2(V)	M.M.L.	5	5.22×10^{-5}	F.H.	23.4	"
FO1(V)	M.M.L.	1	4.29×10^{-5}	F.H.	22.6	"
CH1(V)	M.M.L.	7	6.07×10^{-6}	F.H.	6.4	"
CH2(V)	M.M.L.	1	3.70×10^{-6}	F.H.	10.3	"
BL1(V)	U.M.L.	1	1.44×10^{-6}	F.H.	7.3	"
MH1(V)	L.M.L.	4	1.01×10^{-3}	H.P.P.	11.1	A.S.B.
MH4(H)	L.M.L.	3	2.71×10^{-3}	H.P.P.	32.4	"
MH8(V)	M.M.L.	2	3.40×10^{-4}	H.P.P.	38.6	"
MH8(H)	M.M.L.	1	1.89×10^{-5}	F.H.	38.6	"
MH8(H)	M.M.L.	3	6.49×10^{-4}	H.P.P.	38.6.	"
MH9(V)	M.M.L.	1	2.88×10^{-3}	H.P.P.	14.4	"
UP 44 H		1	1.11×10^{-6}	H.P.C.H.	19.95	K.J.
UP 160 H		1	4.62×10^{-8}	H.P.C.H.	15.84	"
UP 182 H		1	1.50×10^{-5}	H.P.C.H.	30.07	"
UP 155 H		1	3.73×10^{-7}	H.P.C.H.	17.20	"
UP 162 H		1	1.88×10^{-7}	H.P.C.H.	17.28	"
UP 30 H		1	4.98×10^{-6}	H.P.C.H.	24.54	"
K 84 H		1	1.00×10^{-9}	H.P.C.H.	5.00	"
UP 157 H		1	1.51×10^{-7}	H.P.C.H.	16.90	"

/Continued .....

TABLE 2.2. (Continued)

Abbreviations

U. M. L.	Upper Magnesian Limestone
M. M. L.	Middle Magnesian Limestone
L. M. L.	Lower Magnesian Limestone
F. H.	Falling Head
H. P. C. H.	High Pressure Constant Head (Chakrabarti & Taylor, 1968)
H. P. P.	High Pressure Permeameter (Clockhouse)
R. S. J.	(Jackson, 1968)
K. J.	(Jones, in preparation)

occasionally show high hydraulic conductivities, doubtless due to the presence of large cavities.

Jackson (1968) attempted to deduce relationships between porosity and permeability for the Magnesian Limestone. However, the samples taken were not representative enough of all horizons to allow any statistically viable conclusions to be reached. Nevertheless, some trends were established: the pre-diagenetic dolomites showed a different porosity-permeability relationship to post-diagenetic ('mineralized' of Jackson) dolomites.

2.6 Laboratory tests: summary and conclusions

1) Porosity can be measured by standard soil testing techniques.
2) Permeability may be measured by specially constructed constant head apparatus, or by a modification of the normal falling head method.
3) The parameters obtained are not independent of the method used.
4) Porosity-permeability relationships are a function of the diagenetic history of the sample.
5) Since cohesionless samples are difficult to obtain, the values obtained are biased towards low porosity-permeability examples.

CHAPTER 3

SIMULATION

3.1. Introduction & theoretical basis

The application of simulation techniques to groundwater studies has developed largely over the last decade. Its great advantage lies in its fundamental analytical fidelity, although the ultimate accuracy is a function of user-determined parameters and the inherent approximations of the numerical methods upon which it is based.

3.1.1. Previous work

The use of numerical techniques in the study of field problems has largely stemmed from the pioneering work of Southwell (1946) and his relaxation techniques, although electrical analogue methods had been used in the study of groundwater over ten years previously (Wyckoff & Read, 1935). Up to the present time, most of the development has been of electrical resistance-capacitance models, especially in the USA by Skibitzke (1963), Stallman (1963), Walton & Prickett (1963) and Zee (1957), and by Herbert (1968) and Hunter-Blair (in press) in this country. However, with the advent of large storage, high speed, digital computers, the way is open for direct solution methods (Pinder and Bredehoeft, 1968). Even so, it is doubtful if the many advantages of the electrical analogue will be surpassed by the increased accuracy of digital solutions, for the former method is simple, cheap, versatile, and may be operated by inexperienced personnel. Digital computers on the other hand are expensive to run, and require skilled operators and programmers, although one well designedpiece of software may ultimately be versatile enough to analyse many different problems with various boundary conditions.

3.1.2. Theoretical basis

The two-dimensional steady state flow of a fluid through a confined, homogeneous, isotropic, porous medium in which the algebraic sum of the boundary flows is zero is represented by the Laplace equation, a partial differential equation of the form

$$\frac{\partial^2 h}{\partial x^2} + \frac{\partial^2 h}{\partial y^2} = 0 \qquad (3.1)$$

Adopting the nomenclature of Fig. 3.1 then the finite difference form of Equation 3.1 may be written as:

$$\frac{H_1 + H_3 - 2Ho}{a^2} + \frac{H_2 + H_4 - 2Ho}{b^2} = 0 \qquad (3.2)$$

In the normal case of a square mesh, this therefore reduces to:

$$H_1 + H_2 + H_3 + H_4 - 4Ho = 0 \qquad (3.3)$$

This is the basic equation for the five point solution of potential utilised in many field problems governed by the Laplace equation, such as heat flow, electric potential and water. In the latter, however, complete isotropy is the exception rather than the rule, and this requires a modification of Equation 3.2. If the respective transmissibilities are constant over the distances 2a and 2b, then:

$$Tx \frac{\partial^2 h}{\partial x^2} + Ty \frac{\partial^2 h}{\partial y^2} = 0 \qquad (3.4)$$

which becomes, in finite difference form:

$$Tx \frac{b}{a} (H_1 + H_3 - 2Ho) + Ty \frac{a}{b} (H_2 + H_4 - 2Ho) = 0 \qquad (3.5)$$

In representing actual aquifers, the effects of pumping and recharge must be simulated. Leakage into the aquifer at W g. p. d. /ft^2 is represented by a nodal flow, Q_0, given by:

$$Q_0 = W.a.b. \qquad (3.6)$$

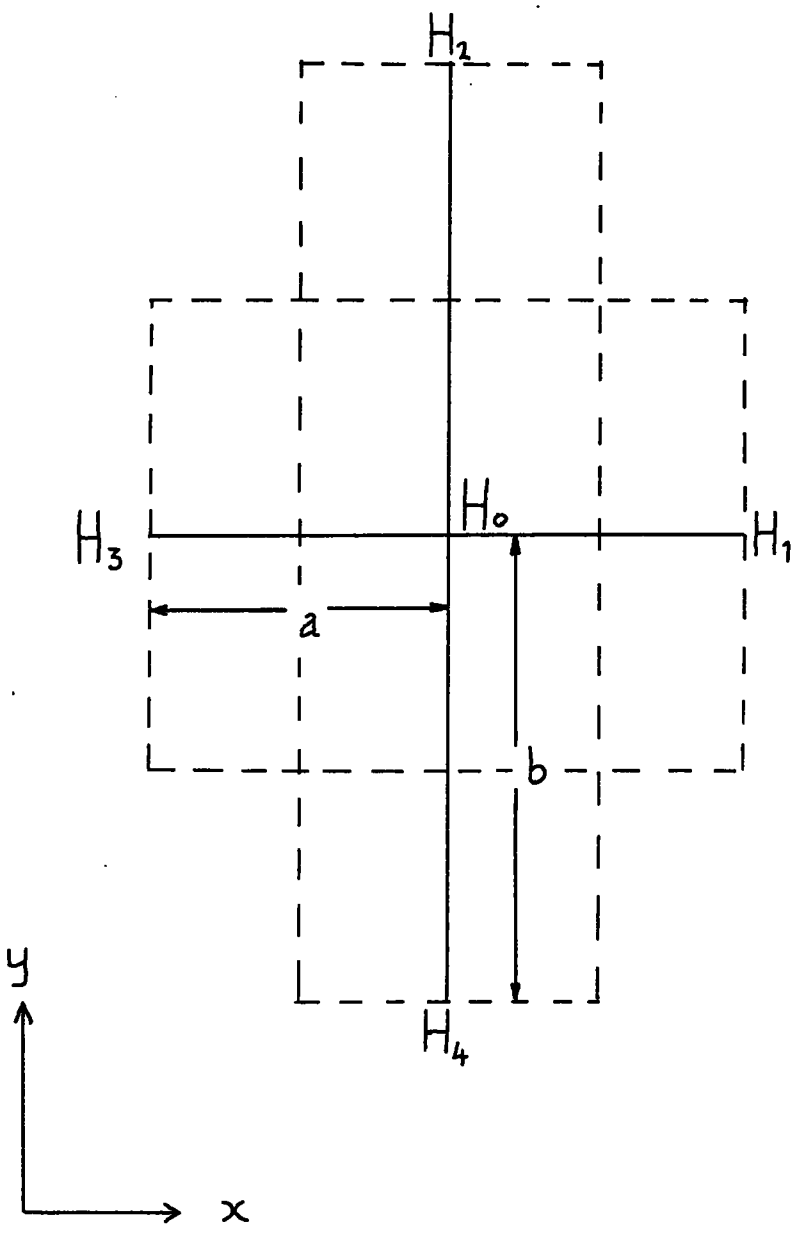

Fig. 3.1. Mesh nomencleture.

Abstraction from a well is measured directly as a quantity, $-Q_0$ g. p. d. but by the corollary of the above, correction must be made so that the true well cross sectional area is simulated (see later).

The general finite difference equation, allowing for nodal recharge and discharge, is thus:

$$Tx.\frac{b}{a}(H_1 + H_3 - 2Ho) + Ty\frac{a}{b}(H_2 + H_4 - 2Ho) = Q_0 \qquad (3.7)$$

3.1.2.1. Boundaries - Boundary conditions are of two types; (a) the potential, H, is known at nodal positions on the boundary (Fig. 3.2a). The cross sectional area in the x-direction is therefore half the cross sectional area in the equivalent five point arrangement, and the finite difference equation thus becomes:

$$Tx.\frac{1}{2}\frac{b}{a}(H_1 + H_3 - 2Ho) + Ty.\frac{a}{b}(H_4 - Ho) = Q_0 \qquad (3.8)$$

(b) Impermeable boundary; defined by $\frac{\partial h}{\partial y} = 0$ (Fig. 3.2b)

The potentials are unknown, and proceeding as before, except that $Q_0 = 0$.

$$Tx.\frac{1}{2}\frac{b}{a}(H_1 + H_3 - 2Ho) + Ty.\frac{a}{b}(H_4 - Ho) = 0 \qquad (3.9)$$

Equations 3.8 and 3 9 and their variants for different boundary dispositions and combinations form the basis for solution of the potential distribution.

3.1.2.2. Truncation errors (Noble, 1964) - Since the finite difference method is, by its nature, an approximation, an evaluation of the errors is necessary. This is best studied by expanding the heads as Taylor's series, thus:

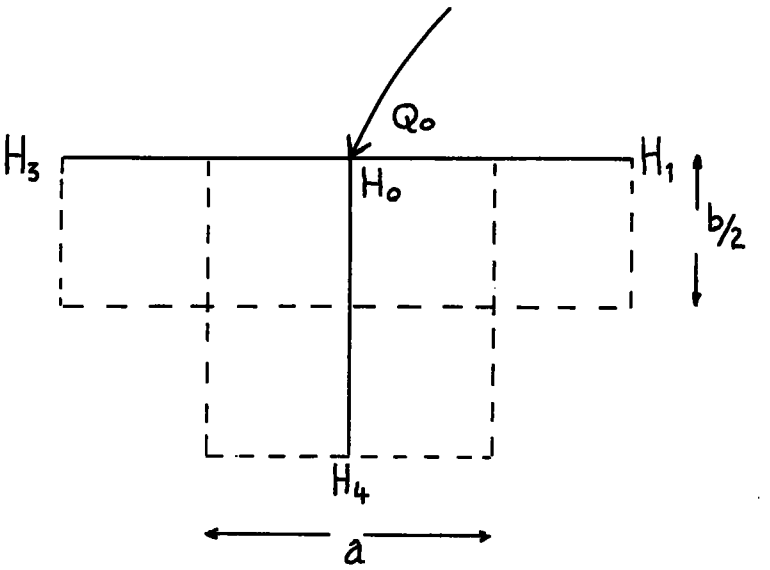

a. Permeable

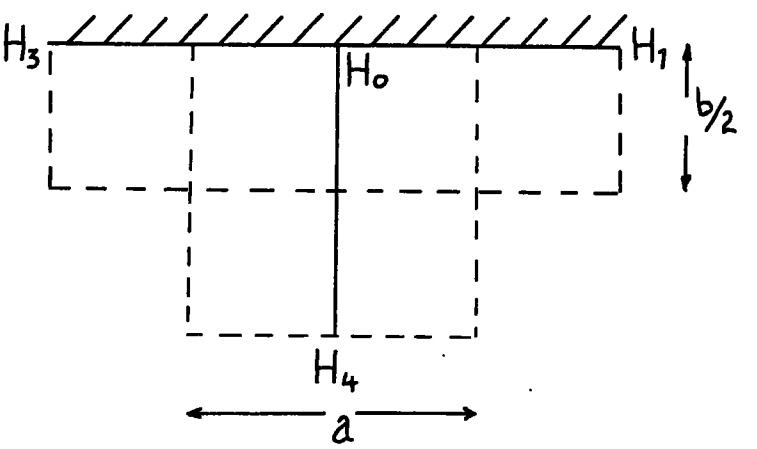

b. Impermeable

Fig. 3.2. Boundaries.

$$H_1 = Ho + a\left(\frac{\partial H}{\partial x}\right)_o + \frac{a^2}{2!}\left(\frac{\partial^2 H}{\partial x^2}\right)_o + \frac{a^3}{3!}\left(\frac{\partial^3 H}{\partial x^3}\right) + \frac{a^4}{4!}\left(\frac{\partial^4 H}{\partial x^4}\right) + \ldots\ldots \quad (3.10)$$

$$H_3 = Ho - a\left(\frac{\partial H}{\partial x}\right)_o + \frac{a^2}{2!}\left(\frac{\partial^2 H}{\partial x^2}\right)_o - \frac{a^3}{3!}\left(\frac{\partial^3 H}{\partial x^3}\right) + \frac{a^4}{4!}\left(\frac{\partial^4 H}{\partial x^4}\right) - \ldots\ldots \quad (3.11)$$

$$H_2 = Ho + b\left(\frac{\partial H}{\partial y}\right)_o + \frac{b^2}{2!}\left(\frac{\partial^2 H}{\partial y^2}\right)_o + \frac{b^3}{3!}\left(\frac{\partial^3 H}{\partial y^3}\right) + \frac{b^4}{4!}\left(\frac{\partial^4 H}{\partial y^4}\right)_o + \ldots\ldots \quad (3.12)$$

$$H_4 = Ho - b\left(\frac{\partial H}{\partial y}\right)_o + \frac{b^2}{2!}\left(\frac{\partial^2 H}{\partial y^2}\right)_o - \frac{b^3}{3!}\left(\frac{\partial^3 H}{\partial y^3}\right) + \frac{b^4}{4!}\left(\frac{\partial^4 H}{\partial y^4}\right) - \ldots\ldots \quad (3.13)$$

Adding, and if a = b

$$H_1 + H_2 + H_3 + H_4 - 4Ho = a^2\left(\frac{\partial^2 H}{\partial x^2} + \frac{\partial^2 H}{\partial y^2}\right) + \frac{a^4}{12}\left(\frac{\partial^4 H}{\partial x^4} + \frac{\partial^4 H}{\partial y^4}\right) + \ldots. \quad (3.14)$$

The second and subsequent terms thus represent the major error in the finite difference equation. Considering terms beyond the second negligible, typical error values may be determined from a study of the finite difference forms of some simple potential - spatial functions, Table 3.1.

The potential distribution around a well is of the form $H = x^{\frac{1}{2}}$, and thus the finite difference approach leads to large errors around a well or similar singularity. In some instances benefit is gained by reducing a. Thus for x = 1000 and a = 500, the corresponding truncation error for $H = x^{3/2}$ is reduced to 1.6%, and that for $H = x^{\frac{1}{2}}$ reduced to 12.5%.

3.1.2.3 Singularities - Where the change in potential is so rapid that it cannot be represented by the Laplace equation, a singularity exists. Examples are given by Herbert et al (1966) as the toe of a pile and a pumping well. To model the latter on a finite difference mesh, for $r_w < a$, the transmissibility elements should be replaced by 'effective' well elements calculated from

$$T_w = T/\left(\frac{2}{\pi} \cdot \log_e(a/r_w)\right) \quad (3.15)$$

TABLE 3.1

Function $x = 1000,\ a = 1000$	$a^2 \frac{d^2H}{dx^2}$	$a^4 \frac{d^4H}{dx^4}$	$a^4 \frac{d^4H}{dx^4} \quad a^2 \frac{d^2H}{dx^2}$	Truncation error %
$H = x$	0	0	0	0
$H = x^2$	$2a^2$	0	0	0
$H = x^3$	$6xa^2$	0	0	0
$H = x^4$	$12x^2a^2$	$2a^4$	$1/6 . a^2/x^2$	16.7
$H = x^{\frac{1}{2}}$	$-\frac{1}{4}x^{-3/2} . a^2$	$-5/64 . x^{-7/2}a^4$	$3/8 . a^2/x^2$	37.5
$H = x^{3/2}$	$\frac{3}{4}x^{-\frac{1}{2}} a^2$	$3/64 . x^{-5/2}a^4$	$1/16 . a^2/x^2$	6.3
$H = x^{5/2}$	$15/4x^{\frac{1}{2}} a^2$	$-5/64 . x^{-3/2} a^4$	$-1/48 . a^2/x^2$	2.1

3.1.2.4. Non-steady state - So far, only steady state conditions have been considered. Non-equilibrium conditions are described by the partial differential equation

$$\frac{\partial^2 H}{\partial x^2} + \frac{\partial^2 H}{\partial y^2} = \frac{\partial H}{\partial t} \cdot \frac{S}{T} + \frac{W}{T} \qquad (3.16)$$

From this, it can be seen that as $t \rightarrow \infty$, the equation becomes equivalent to the Laplace equation. The finite difference approximation and solution by an alternating direction implicit procedure has been fully described by Pinder et al (op. cit.) . It was not, however, employed in the present study.

3.2. Digital solution

A digital solution was attempted as an independent check on the electrical analogue. The complete program listing and description is given in Appendix B.

3.2.1. The problem

The object of the program was ultimately twofold:

(a) solution of the linear equations formed by the finite difference approximation, and hence determination of the potentials within the system,

(b) by utilising all the available data including piezometric contours, pumping test drawdowns and recharge values to investigate the possibility of assigning unique values to the transmissibility elements.

3.2.2. Formulation of matrices

Considering the arrangement in Fig. 3.3, the nodal flow is given by:

$$\frac{b}{a} Tk\,(Hi,j+1 - Hi,j) + \frac{a}{b} Tl(Hi-1,j - Hi,j) +$$

$$\frac{b}{a} Tm(Hi,j-1 - Hi,j) + \frac{a}{b} Tn\,(Hi+1,j - Hi,j) = Qi,j \qquad (3.17)$$

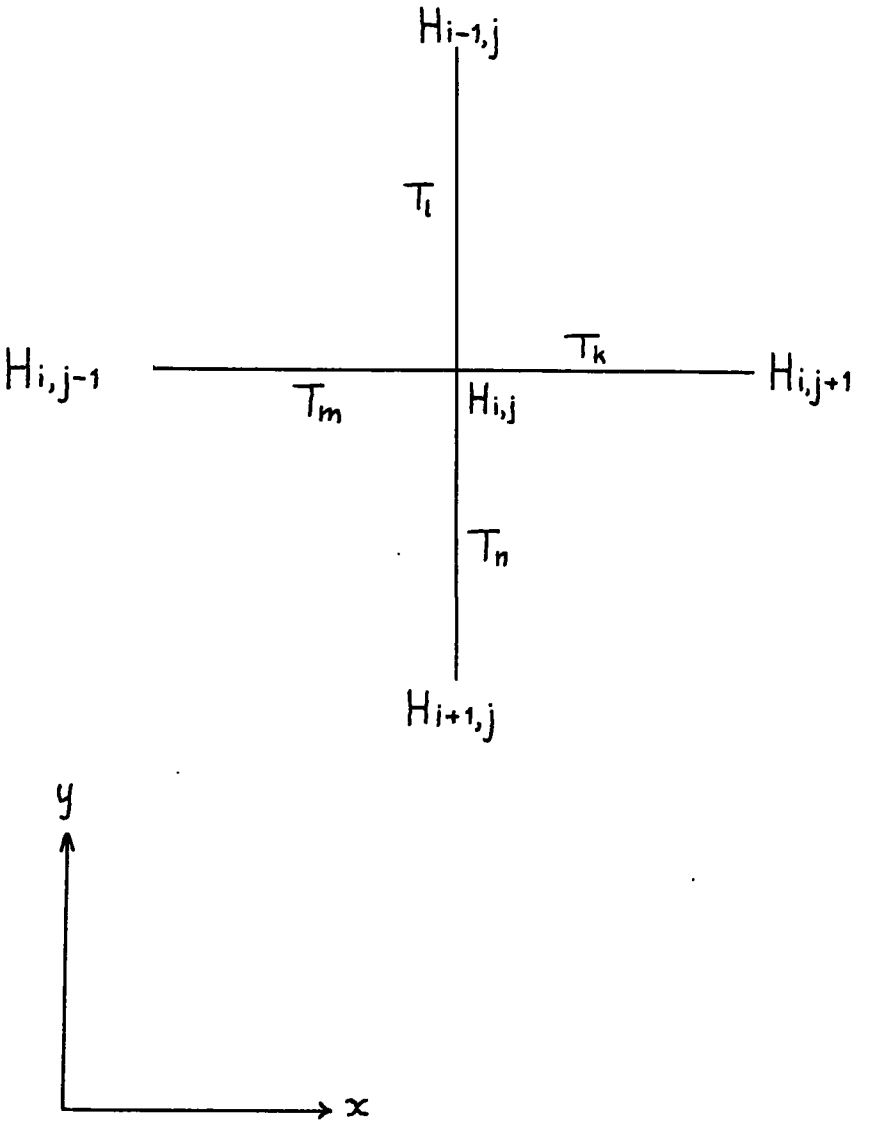

Fig 3.3. Digital solution nomencleture.

By numbering nodes and transmissibility elements consecutively from the top left to bottom right (Fig 3.4), Equation 3.17 may be rewritten as:

$$\frac{b}{a}.TkHe + \frac{a}{b}.TlHf + \frac{b}{a}.TmHg + \frac{a}{b}.TnHh + \left(-\frac{b}{a}.Tk - \frac{a}{b}.Tl - \frac{b}{a}.Tm - \frac{a}{b}.Tn\right)Hd = Qd \qquad (3.18)$$

or in general matrix form

$$[TA] \cdot \{H\} = \{Q\} \qquad (3.19)$$

It will be immediately obvious that $[TA]$ is symmetric with most off-diagonal elements zero, and a bandwidth determined by the difference between adjacent nodes.

3.2.2.1. Impermeable boundary - For this situation only one orientation will be considered, the others and combinations being similar. The equation thus becomes:

$$\frac{b}{2a}\,TkHe + \frac{b}{2a}\,TmHg + \frac{a}{b}\,TnHh + \left(-\frac{b}{2a}\,Tk - \frac{b}{2a}\,Tm - \frac{a}{b}\,Tn\right)Hd = 0 \qquad (3.20)$$

3.2.2.2. Fixed potential boundary - This is most easily treated by making all off-diagonal elements of the row zero in the coefficient matrix $[TA]$, and replacing the diagonal element by an arbitrary number of the same magnitude of others in $[TA]$. Qd is then put equal to TAd,d x Hd.

3.2.2.3. Fixed flow boundary - This is treated similarly to the impermeable boundary except that the zero flow is replaced by Qd. In many cases this is a more realistic way of determining the potential distribution within the model for different pumping conditions, since the amount of recharge available is not directly controlled by the amount abstracted. However, its use requires a knowledge of Qd which is rarely available, and the only alternative is to initially use a fixed boundary so positioned to be outside the area of influence of abstraction wells.

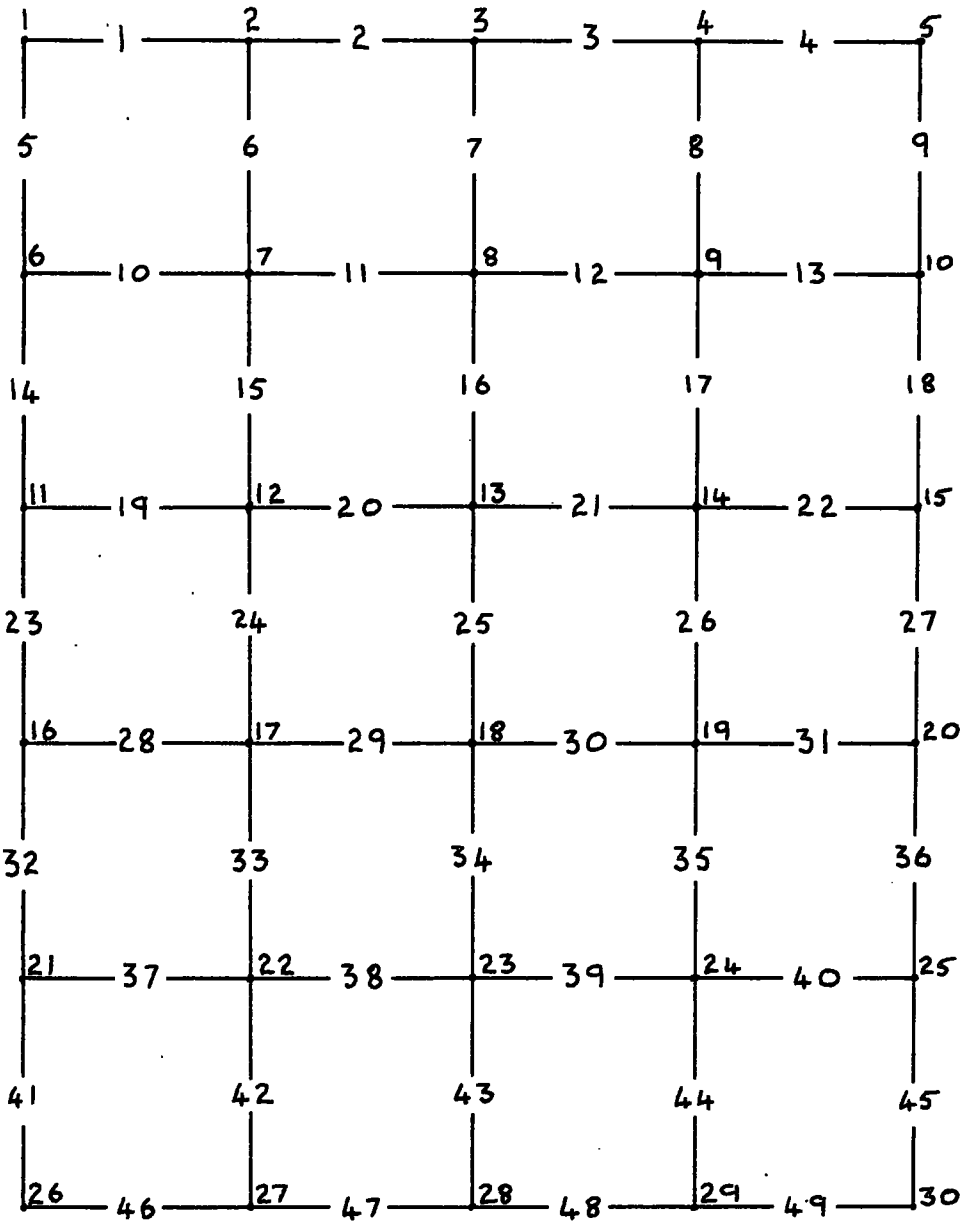

Fig 3.4. Node and element numbering

3.2.3. Solution of matrices

In a rectangular model of l columns and m rows, the potential distribution may be determined by the solution of (lm) nodal equations in (lm) unknowns. The techniques adopted are dictated by the computing facilities available, including library software. A number of different methods were tried in the present study, and even now, a significant improvement in the program could be effected by a more efficient method of solution of the linear equations.

3.2.3.1. Gauss-Jordan - This is the normally used method for systems of linear equations, solving by successive pivotal condensations. Its advantages lie in the ease of programming, and if the largest pivot element is used, it is accurate for a limited number of equations. However, where there may be up to 1000 unknowns, truncation errors become a serious drawback, even using double precision (16 digits). To some extent this may be reduced by using error equations (James et al, 1967), although this greatly increases computer time. Another disadvantage is that the complete $[TA]$ matrix must be formulated and stored before solution can begin. Methods may be devised for more economical storage, such as only half the matrix, or just the non-zero elements, but these complicate the programming. A user-written Gauss-Jordan subroutine including error equations was tried, but rejected for the reasons outlined above.

3.2.3.2. Gauss-Siedel - This is an iterative method (McCracken, 1967) and has been widely applied to the solution of field problems, the Southwell relaxation method being basically a variant. It entails an initial estimate of the potential at each node, which is then progressively adjusted to the final solution. Thus, for the simple case of all transmissibilities and mesh lengths equal, the non-trivial solution is obtained when

$$H_1 + H_2 + H_3 + H_4 - 4Ho = 0 \qquad (3.2.1)$$

Before solution

$$H_1^1 + H_2^1 + H_3^1 + H_4^1 - 4Ho^1 = HRo \qquad (3.22)$$

where HRo is termed the residual. The value of Ho^1 is adjusted, on the assumption that the surrounding values are correct, by a factor ΔH given by

$$\Delta H = -HRo/4 \qquad (3.23)$$

Thus

$$H_1^1 + H_2^1 + H_3^1 + H_4^1 - 4(Ho^1 + H) = 0 \qquad (3.24)$$

In general, since the early convergence is rapid, the choice of initial values for the potentials does not affect the solution, providing H = 0 is not used. Even more rapid convergence may be obtained by judicious choice of an over-relaxation factor, and a value of 1.7 has been employed. If too large a factor is used, the potentials oscillate about the true solution.

One great advantage of the Gauss-Siedel method is that it may be formulated a row at a time. Thus a model with n nodal points requires an n x n array for (TA) for the Gauss-Jordan method, but only an n x 1 array for the Gauss-Siedel.

3.2.3.3. Other methods - Since the solution of equations represents the largest operation in the program, more efficient methods would lead to a more economical performance. 'One shot' rather than iterative methods would reduce c.p.u. time, and of these, the Choleski method seems to offer the most potential.

3.2.3.4. Summary and conclusions - The development and choice of solution method ultimately requires a software expert. In many cases, library programs are sufficient and these will undoubtedly be extended within the future. For this particular study a small storage, long time method was chosen since, with the adoption of multi-tasking, low storage c.p.u.-bound jobs form a useful counterpart to the computing centre's principally i/o-bound batch jobs.

3.2.4. Solution for transmissibility

So far, only the determination of nodal potentials has been discussed, it being assumed that the values of the transmissibility elements were known. However, in many cases, it is the latter which is the most important since it enables predictions to be made to other areas and pumping regimes. In a rectangular model of l x m nodes, there are a total of (lm) nodes, but (2lm - l - m) transmissibility elements, and thus the system is under-determined with respect to the latter. The infinite number of solutions may be reduced by utilising all the information available from pumping tests at various locations, or by fixing a sufficient number of transmissibilities as to make the system determinate. This latter method was tried but was found to be unsuitable because (a) it involved making estimates, and (b) the coefficient array was (2lm - l - m) x (lm), and whilst being sparse, it was neither symmetric nor regular. Only a Gauss-Jordan method could be used for solution, and hence the errors were very large.

The shortage of time has precluded a completely satisfactory program being developed. The ultimate solution will be outlined, followed by details of progress to date.

3.2.4.1. Logic - Since, for the transmissibility determination, as much data as possible must be considered, it is essential that all processing from the raw data is done by computer. The piezometric contour map (Fig. 2.2) was drawn by linear interpolation between known points, and the nodal reference potentials interpolated from the contours. This method is both time-consuming and, to a certain extent, subjective. Since the sample locations are random, a program is required to interpolate between them. Probably the most suitable technique is to fit a least squares polynomial trend surface to the required accuracy, and use the equation to determine the

potential at given cartesian co-ordinates (Krumbein & Graybill, 1965). This would have other advantages in that, by fitting a similar surface to the topography, the siting of wells could be optimised.

With the data in a useable form, the values of the transmissibility elements must be adjusted until a unique arrangement is obtained which fits the various boundary and pumping conditions satisfactorily. For each set of conditions, starting with the piezometric potentials, this may be carried out as follows:

(a) Initially all the transmissibility elements are set to a value somewhere within the expected range, which was 10,000 g. p. d. /ft for the area studied.

(b) From the known boundary and flow conditions, the potentials are determined at every node within the model by the methods outlined above (3. 2. 3).

(c) The calculated and reference potentials are compared. If the residual is unacceptable the transmissibility elements around the node are adjusted. This is done by assuming that the current flowing through each element is a constant. Thus, if the calculated and reference potential drops across an element are ΔHc and ΔH_R respectively, then the new value is calculated from

$$T_{new} = T_{old} \cdot \frac{\Delta Hc}{\Delta H_R} \qquad (3.25)$$

(d) The new values of transmissibility are used and the process repeated until a satisfactory result is obtained.

(e) The transmissibility adjustment and determination is carried out on all the data sets and the resulting values from each compared and averaged. The whole process is then repeated until the necessary change in

the transmissibilities at the end of the total iteration is considered acceptable.

3.2.4.2. Developed program - This unfortunately falls short of the ultimate goal outlined above. Nevertheless, it is felt that some of the basic problems have been overcome.

The input data is prepared manually from well records and maps, and hence the reference potentials contain an error of $\pm$ 5ft, although the wells themselves can be gauged to $\pm$ 0.1ft. Only the piezometric data was prepared for input since the linear interpolation method used would have lead to grossly inaccurate results around a pumped well, where the piezometric surface would be second order.

Some improvements were made to the basic method of adjusting the transmissibility elements outlined above. It was noticed that the output often contained very high or very low transmissibilities which could not be interpreted in terms of potential gradient at those points. It was found that these arose where there was only a small potential drop across the element (Table 3.2). The residual between the reference and calculated potentials in A is probably acceptable, yet if adjustment is made by the method suggested above it requires the transmissibility to be doubled. On the other hand, the residuals in B are definitely unacceptable. Thus, A is very insensitive to changes in T_A whereas B is the opposite. A method or restricting the amount by which the element is altered is required being controlled by the potential drop across the element. This is most easily achieved by introducing a factor, the exact function of which must be decided by trial and error, but for example, may be unity when the potential drop is 50ft and 0.1 when the drop is 5ft.

TABLE 3.2

	Example A	Example B
Reference	T_A 100.5 — 100	T_B 150 — 100
Calculated	T = 10,000 101 — 100	T = 10,000 160 — 100
Trans-missibility adjustment	Therefore $T_A = \frac{(101-100)}{(100.5-100)} \cdot 10,000$ $T_A = 20,000$	Therefore $T_B = \frac{(160-100)}{(150-100)} \cdot 10,000$ $T_B = 12,000$

The obvious disadvantage is that convergence is delayed, or, with a poor choice, the solution may diverge. More research and experience is required to enable the optimum function for the transmissibility adjustment factor to be determined.

3.2.5. Results

The program was tested on a number of problems for which an analytical solution was available. An example is given in Fig. 3.5 which shows the cone of depression deduced by the Thiem equation, compared with the potentials determined by the finite difference solution. Two different mesh lengths of 1,000 ft and 500 ft were taken, and all results showed a good correlation with the theoretical solution.

A hypothetical model was constructed with variable transmissibility and realistic boundary potentials and the program used to deduce the piezometric nodal potentials. These values were then fed back into the program and the resulting transmissibility variations compared with the original. Although unable to assign exact values, the general trends were recognized.

The nodal potentials determined from the piezometric contour map was used to predict transmissibility variations over the modelled area (Fig 3.6) and these were used as a basis for recalibration of the electrical analogue model when required. Pumping tests using these values indicated that they were too low by a factor 2-5, and thus they could only be used on a relative basis. If this method had been available at the beginning of construction of the electrical analogue, many hours of resistor adjustment could have been eliminated.

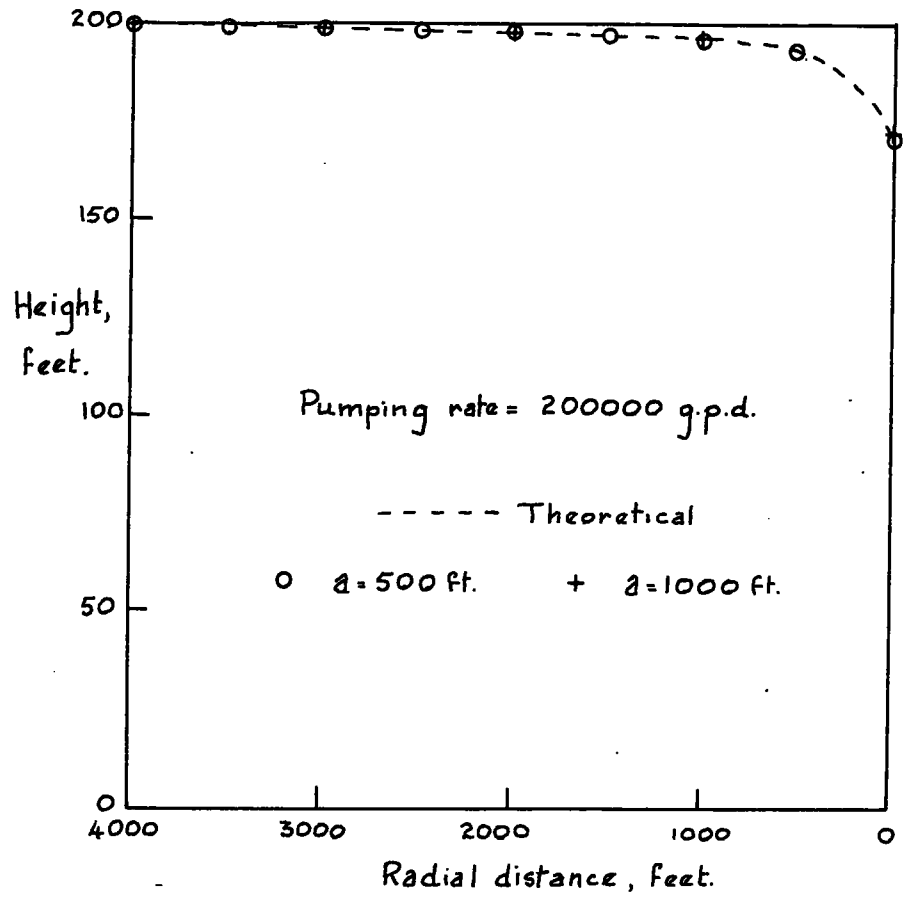

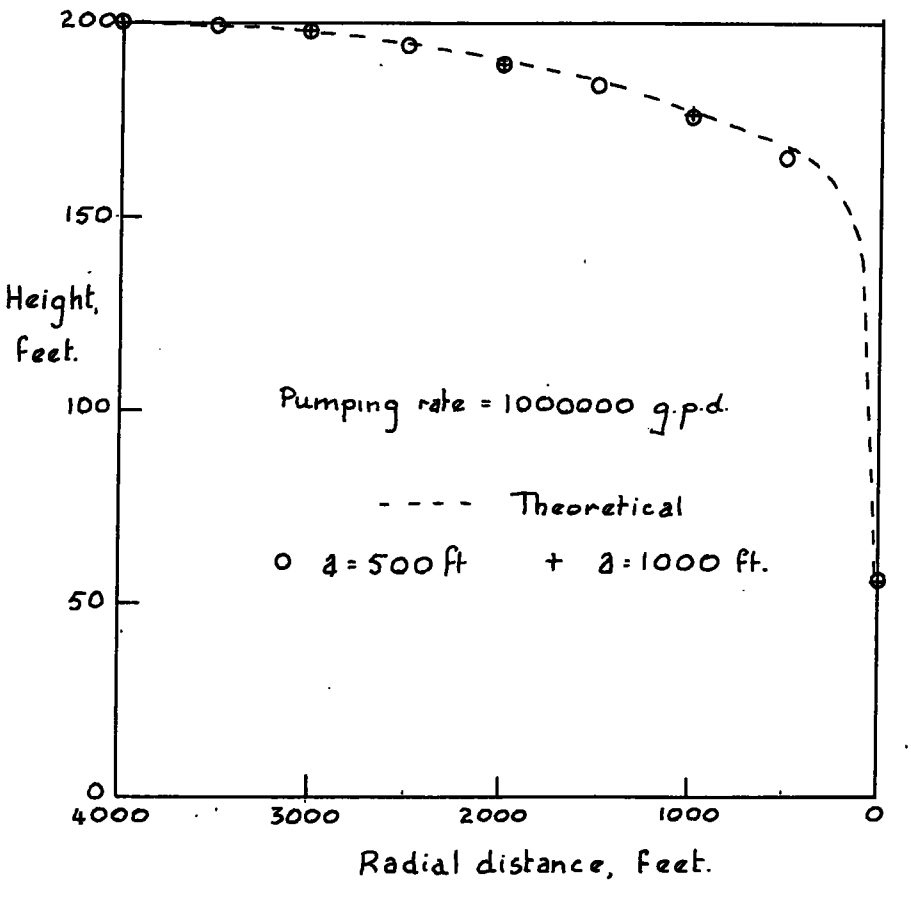

Fig. 3.5. Drawdown around pumped well: comparison of theoretical and digital solution.

3.2.6. Summary and conclusions

The digital method of analysis has inherent advantages where a large number of programmable iterations need to be executed. It may be best employed hybridised with an electrical analogue model to carry out the time consuming and tedious tasks associated with the calibration stage.

3.3. Electrical analogue

This represents the most popular method of examining field problems associated with heat, electricity, electrostatics, stress analysis, as well as fluid flow.

3.3.1. Theory

The electrical analogue may be considered either as a computer for the solution of linear equations, or as a true analogy between water flow and electricity (Fig. 3.7). Since the former has already been detailed, the latter approach will be adopted. The basic theory of electrical resistance - capacitance analogues has been described in numerous published works (see, for instance Skibitzke, 1963; Walton & Prickett, 1963; Herbert & Rushton, 1966; Herbert 1968; Hunter Blair, in press). Fundamental to the method are the four 'scaling factors', defined as:

$$q = K_1 . Ch. \qquad (3.26)$$

$$H = K_2 . V \qquad (3.27)$$

$$Q = K_3 . I \qquad (3.28)$$

$$td = K_4 . ts \qquad (3.29)$$

Thus K_1 = gallons per coulomb

K_2 = feet per volt

K_3 = gallons per day per amp

K_4 = time in days per model time in seconds.

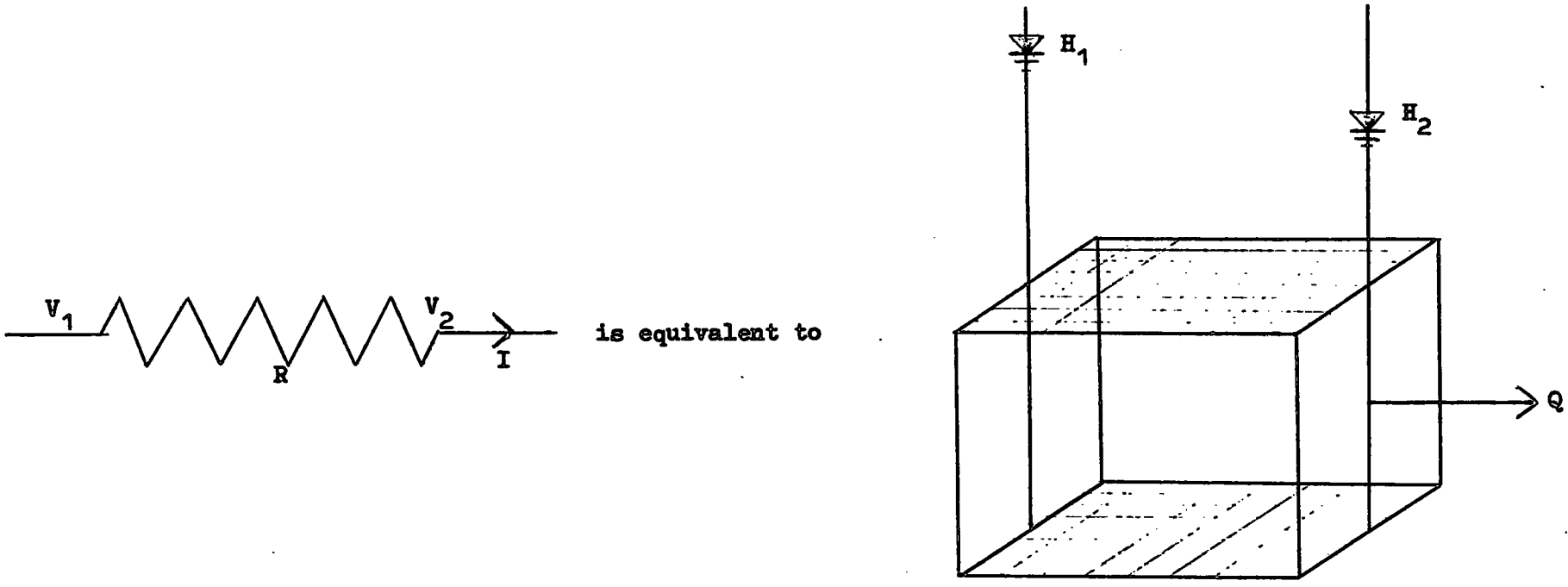

Fig 3.7. Electricity – water analogy

From these, the following identities hold (Walton & Prickett, op.cit.)

$$\frac{K_3 K_4}{K_1} = 1 \qquad (3.30)$$

$$R = \frac{K_3}{K_2} \cdot \frac{1}{T} \qquad (3.31)$$

$$C = 7.48 a^2 S . \frac{K_2}{K_1} \qquad (3.32)$$

where C= capacitance in farads

a = mesh length in feet

S = storage coefficient

Of the sealing factors, only K_2 can be fixed absolutely. However, knowing the range of transmissibilities expected, and the likely recharge and abstraction rates, a working value for K_3 can be chosen to allow convenient currents and resistors to be used.

3.3.2. Excitation-response apparatus

Since the model was constructed to simulate firstly steady state conditions, with provision for the addition of a time variant if and when necessary, the excitation-response apparatus necessary for each stage will be considered separately.

3.3.2.1. Steady state (Fig. 3.8). - The advantage of this type of model is that it is relatively easy to construct, requiring only resistors. The boundary conditions are simply applied and the necessary measuring equipment is readily available.

(a) Excitation - The boundary potentials are determined by extrapolation from the piezometric contour map. They are set from a bank of potential dividers with an input voltage large enough to enable the full range to be covered. A disadvantage of this simple arrangement is that both the potential

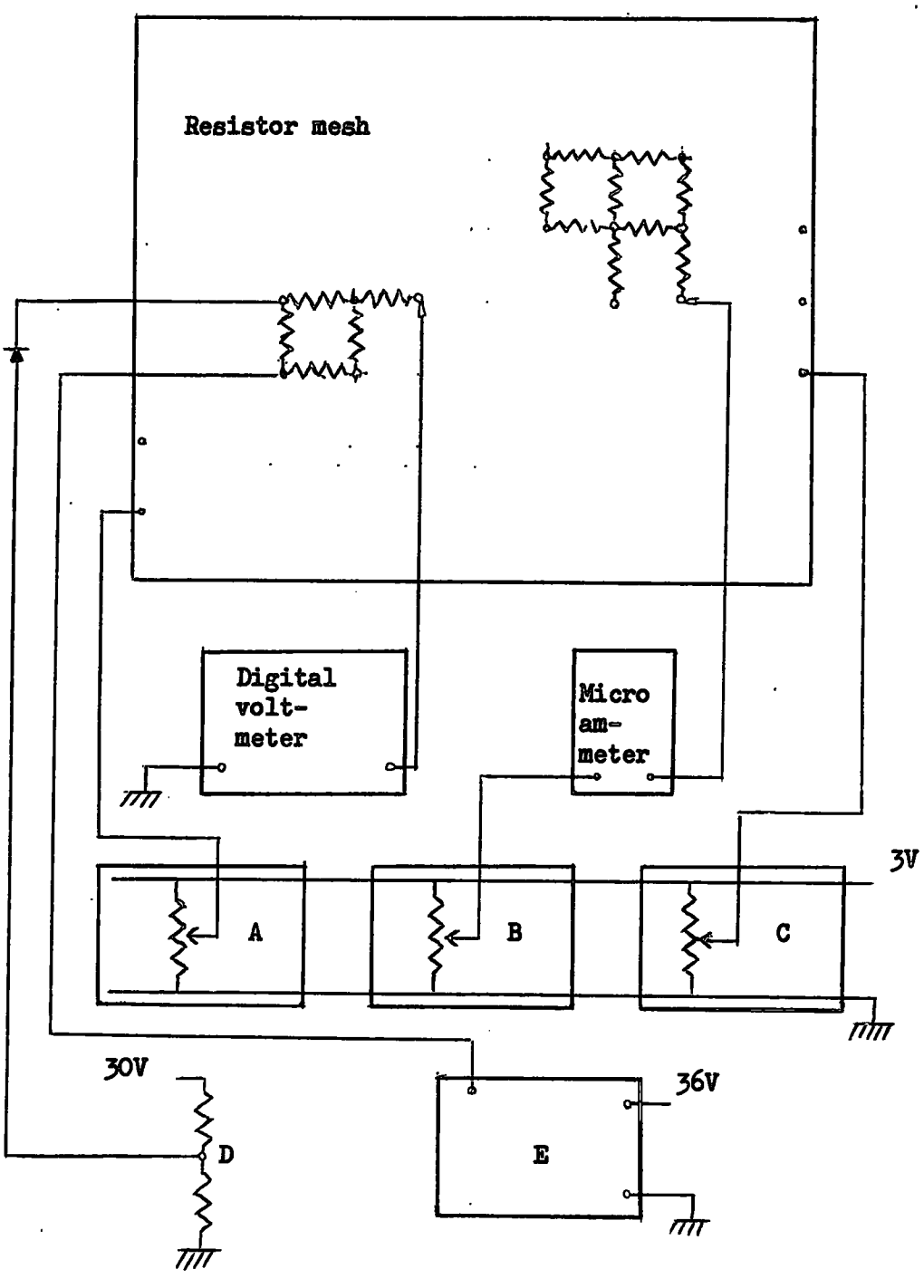

A,B,C Banks of 15 10K potentiometers

D Potential divider reference for spring discharge

E Positive constant current generator for recharge

Fig. 3.8. Steady state excitation-response arrangement.

and current are dependent upon the load, which may vary during simulation studies.

An alternative method is to estimate the recharge inflow and discharge over the area studied, and apply these as constant currents using factor K_3. Unfortunately, this pre-supposes a knowledge of the most elusive parameters, namely, recharge and discharge flows and locations. Positive and negative constant current generators (Fig. 3.9a) were constructed based on a simple bias emitter resistor circuit (from Water Research Association Internal Report). Alternatively, a simple voltage dropper circuit may be used (Fig. 3.9b) which will maintain a constant current within a determinable range. On the model constructed, V_L could range between 0 and 3V, ($K_2 = 10^2$ ft/volt). The current would thus vary from Vt/R to (Vt-3)/R. Providing Vt is high enough, say 50V, then the variation is acceptable, amounting to only 6% for extreme conditions.

Discharge areas on the model, such as spring lines, are simulated by means of a diode lead to a potential divider reference, equivalent to the topographic height at the location. When the nodal potential is greater than the reference, current drains from the model; but when the nodal potential drops below the reference under pumping conditions, the diode is negatively biased and no current is allowed to flow.

The final choice of excitation was a combination of the techniques outlined above. Initially, boundary conditions were fixed using the potential dividers, since they allowed for more versatility and rapid adjustment. When the model had been satisfactorily calibrated, these were replaced by constant current conditions; recharge fed from a high voltage line and discharge taken via a resistor to the common earth line.

This allowed large pumping schemes to be simulated and varied without the need for constant adjustment to the boundary conditions.

(b) Response. - The principal instrument required is a d.c. voltmeter with high input impedence. Modern solid-state digital voltmeters are the most suitable since the input impedence is commonly of the order of megohms. They are rapidly and objectively readable, and if necessary may be adapted for recording purposes. An ammeter capable of measuring currents over the anticipated range is required, and for this purpose an Avometer was found to be satisfactory.

3.3.2.2. Non-steady state - Since this contains a time variant, pulses and transients are input and measured. The time required for the input signal to decay determines whether the model is 'fast time' or 'slow time'. In the former the decay time may be up to a second and is thus monitored using a cathode-ray oscilloscope. However, when the decay period is measured in seconds and maybe minutes, a U.V. recorder is most suitable. Each type of model has its adherents, and each has advantages and disadvantages which must be considered before the model is constructed. A 'slow time' model can easily simulate complex pumping schemes using electro-mechanical switching arrangements: but the chief disadvantage lies in the large and expensive capacitors they require. On the other hand, 'fast time' models require purely electronic excitation apparatus, and complex abstraction and recharge needs involved and expensive equipment. However, cheap and readily available standard miniature capacitors may be used, and hence this type was favoured for the constructed model.

(a) Excitation. - The ideal arrangement of a battery of pulse generators able to simulate abstraction and recharge at different rates and times was beyond the budget and labour available for a small pilot investigation.

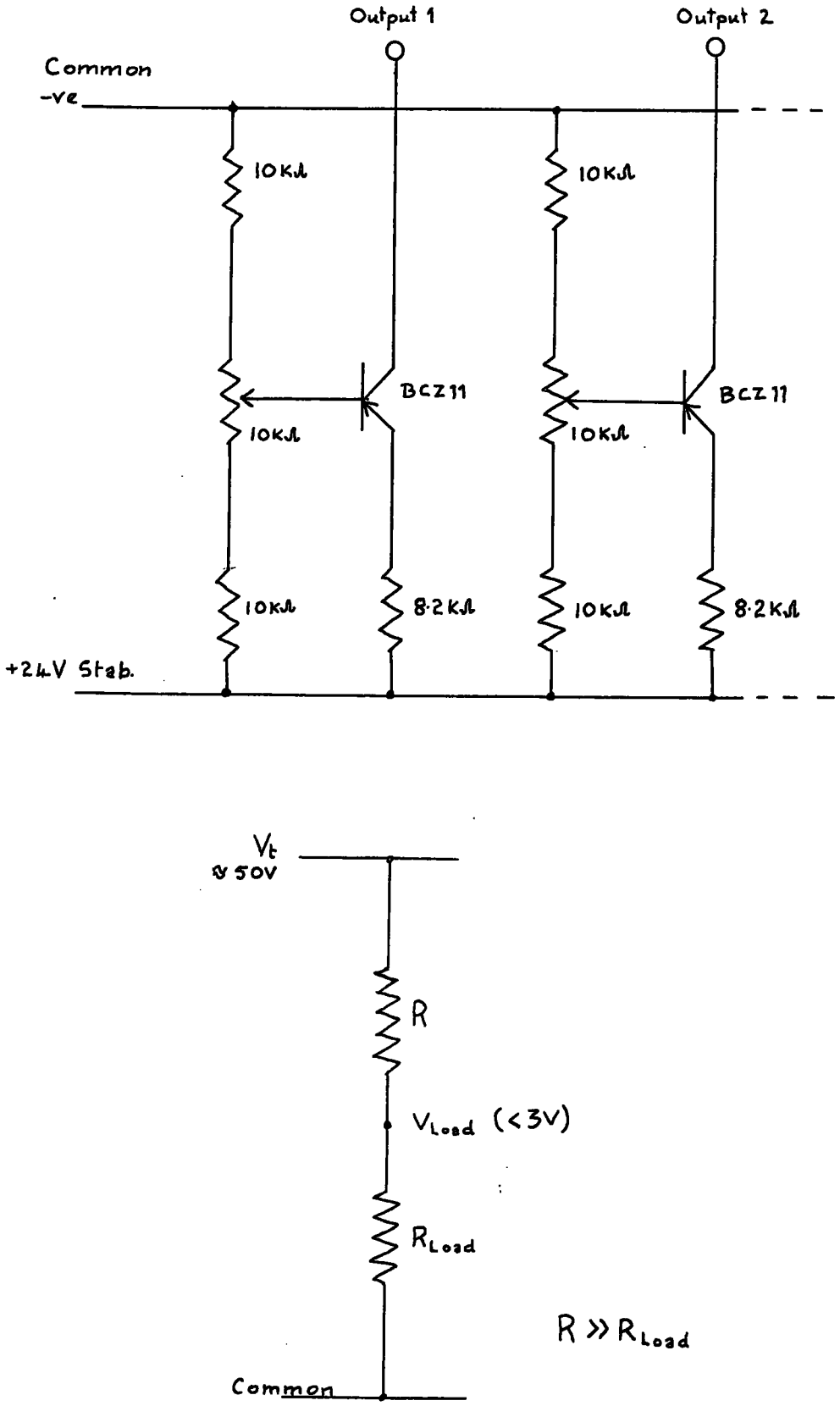

Fig. 3.9. Constant-current devices.

Time variant effects were therefore limited to abstraction. A constant current pulse to simulate pumping is obtained by applying a high voltage pulse (-50V) across a calculated fixed resistor on the same principle as that outlined above for d.c. constant current sources.

(b) Response. - A double beam cathode-ray oscilloscope is used, with a switched time-base variable from 0.5sec to 0.2μsec. Since many commercially available pulse generators have a pre-pulse output, this may be used to trigger the 'scope. An apparently continuous trace is obtained and different parts may be more closely examined by reducing the sweep time and altering the pre-pulse delay. Measurements may be made direct from the screen and recordings taken by tracing or photographs.

The complete excitation-response arrangement for non-equilibrium conditions is shown diagrammatically in Fig. 3.10.

3.3.3. Design and construction

The methods adopted in any investigation are dictated by the problem and resources. The former includes the amount and nature of the raw data. The resouces available are in terms of capital and equipment, and most importantly, man-hours.

3.3.3.1. Design - Since there was no-one directly connected with the project with experience in analogue simulation, it was decided to develop the model in stages, starting with steady state and subsequently adding the time variant, if required.

The area to be modelled lay in south Durham and the geological nature and hydrological parameters have already been discussed. Where possible, model boundaries were chosen to coincide with hydrological boundaries, and an area measuring 15 miles by 8 miles was covered (Fig. 3.11).

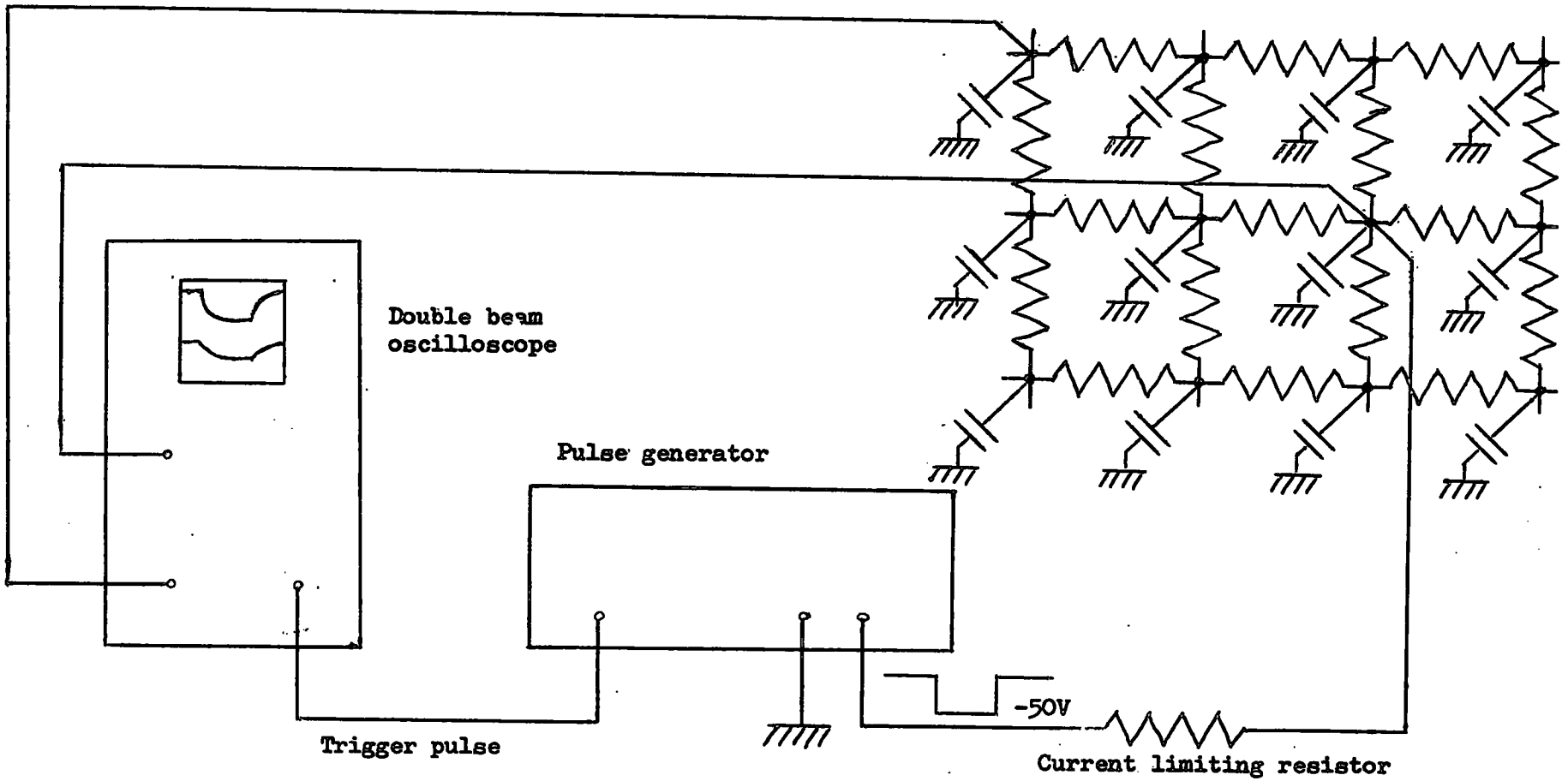

Fig. 3.10. Non-steady state excitation-response arrangement.

FIG. 3.11. S. E. DURHAM GROUNDWATER : AREA OF ANALOGUE MODEL.

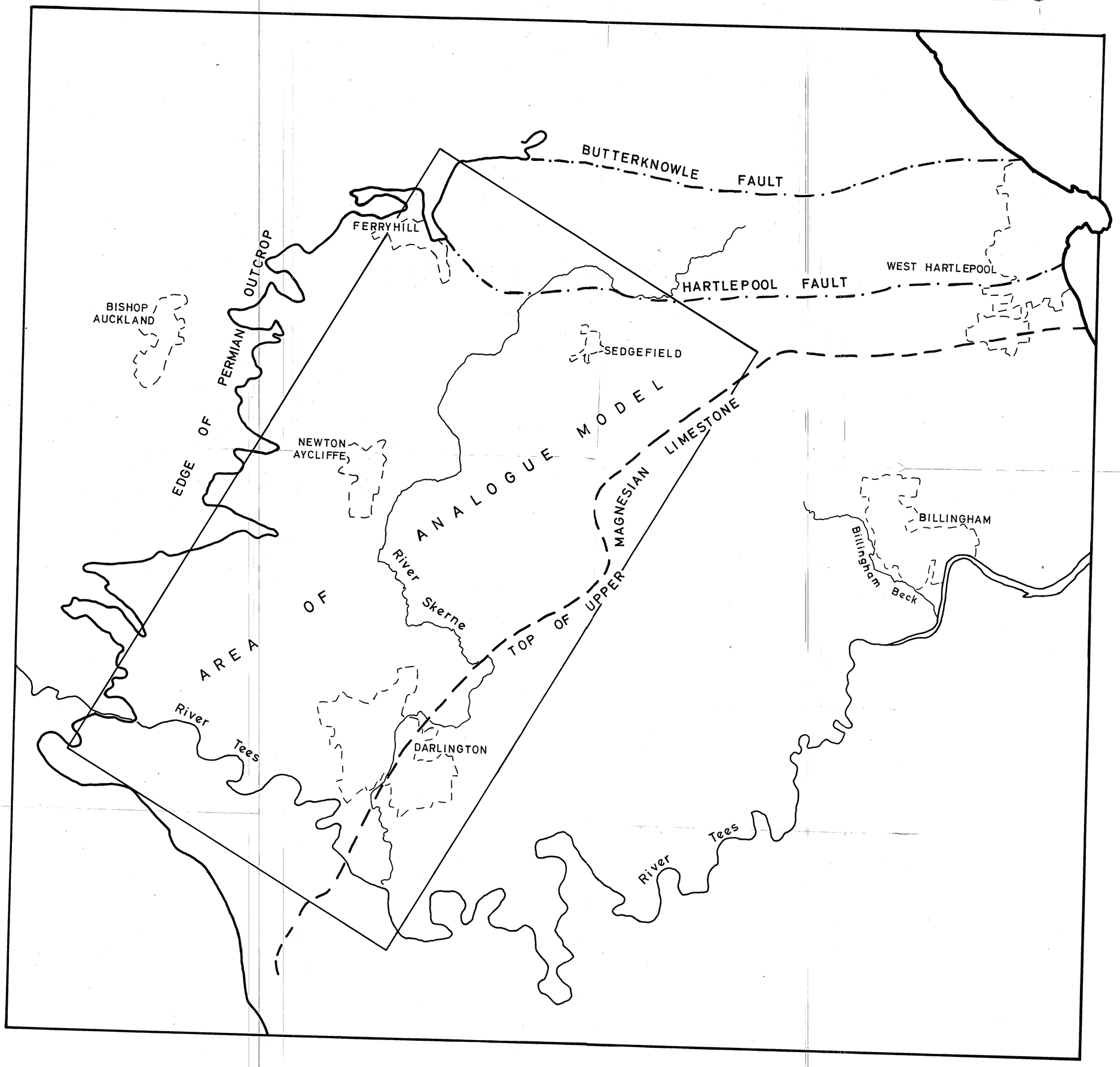

The terminal pin spacing was fixed at $1\frac{1}{2}$ ins to enable easy interchange of resistors and later addition of capacitors. Since 1:25,000 maps were readily available, and were used by the Northumbrian River Authority for much of their data plotting, they were adopted for the model, giving a mesh length, a, of 3,124 ft. Whilst a smaller mesh length would result in greater accuracy, the work entailed in iteratively adjusting the resistors to produce a good fit is greatly increased, and a compromise solution must be reached. It was felt that 600 resistors would be optimum, and if any area required a more detailed analysis, it could be 'blown-up' on a separate panel.

The scaling factors were tentatively fixed on the basis of a low voltage directly and easily convertible to feet, low currents, and a resistance of 10 KΩ being equivalent to a transmissibility of 10,000 g.p.d./ft. Upon calibration it was found that some of the values required slight adjustment, the final scaling factors being:

$$K_1 = 10^{14} \text{ gals/coulomb}$$

$$K_2 = 10^{2} \text{ ft/volt}$$

$$K_3 = 5.58 \times 10^{10} \text{ g.p.d/amp}$$

$$K_4 = 10^{4} \text{ days/sec}$$

$$a = 3,124 \text{ ft.}$$

The steady state excitation apparatus consisted of 2 banks, each of 15 10KΩ wire-wound potentiometers, together with a bank of 15 positive constant current generators. For abstraction schemes, a further bank of 15 potentiometers was available.

3.3.3.2. Construction - A 5ft x 4ft x $\frac{1}{4}$ins sheet of 'Perspex' was drilled 6BA clearance to take the node and capacitor terminals. It was held vertically be a 'Dexion' frame, and the terminal pins inserted. These were specially designed for electrical analogue models by the Civil Engineering Department, University of Birmingham and permit the easy interchange of components without the need for soldering. The steady state excitation apparatus was mounted at the bottom of the board, and the pre-set outputs connected to the back of the boundary terminal pins via leads. After calibration these were replaced by fixed resistors from the boundary nodes to

(i) a common high voltage line for recharge, or

(ii) an earth line for discharge.

All connections which were not permanent were by flying leads fitted with crocodile clips to the front of the board. The model is shown in Fig. 3.12 set for a non-steady pumping test simulation.

3.3.2. Results

The results from the model may be conveniently considered in two parts. The calibration of the model yields information on the quantities and locations of recharge and discharge. This is followed by simulation of pumping regimes to investigate the overall yields and the effects upon other abstractors.

3.3.2.1. Calibration - An initial estimate of the relative transmissibilites was made from the piezometric contour map and the corresponding resistors inserted using a working value for K_3 of 10^{10} g.p.d/amp. The boundary

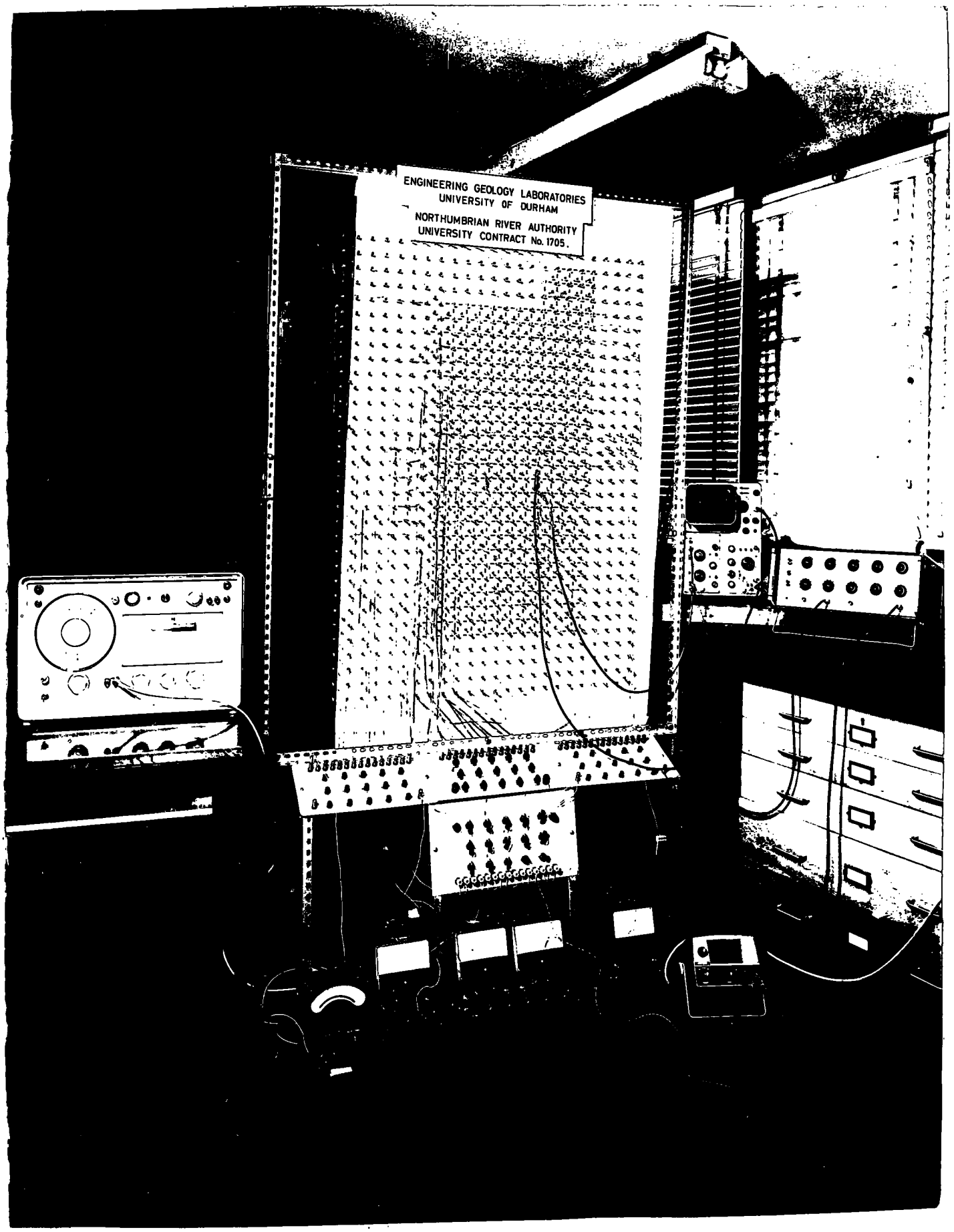

Fig. 3.12. Completed model under test.

potentials were applied with potentiometers and the resistors iteratively adjusted to obtain a reasonable agreement with the reference nodal potentials. Pumping tests were simulated by imposing the known drawdown at the pumped well, and altering the surrounding resistors until the drawdowns in the observation wells were reproduced. Where possible high resistors (low transmissibility) were only inserted if there was existing geological or hydrological evidence of boundaries. Following the first abortive attempt at calibration, low resistors (high transmissibility) were not used. For the second calibration, the digital solution was used as an initial guide in order to reduce the amount of adjustment required.

In some areas it proved very difficult to satisfy both the piezometric and the pumping conditions. This was especially noted in the Carr Lands and around Rushyford, where a solution using low resistors was inadequate. It was therefore concluded that the wide contour spacing in that area (see Fig. 2.2) should be interpreted as a function of recharge, and inputs were applied at selected nodes. Stream gauging has since substantiated the validity of this solution.

Surface discharge was apparent in only one area, in the valley of the River Skerne between Aycliffe and Coatham Mudeville. Seepages had been noted and a value of 0.3 m.g.d. was recorded from the model.

Following the final calibration, the nodal potentials were measured and plotted for comparison with the observed contours (Fig 3.13). The individual well tests are detailed in Table 3.3 and the resultant flow/current calibration shown in Fig. 3.14.

The boundary potentiometers were changed for fixed resistor devices as outlined above (3.3.3.2). The current flowing into and out of

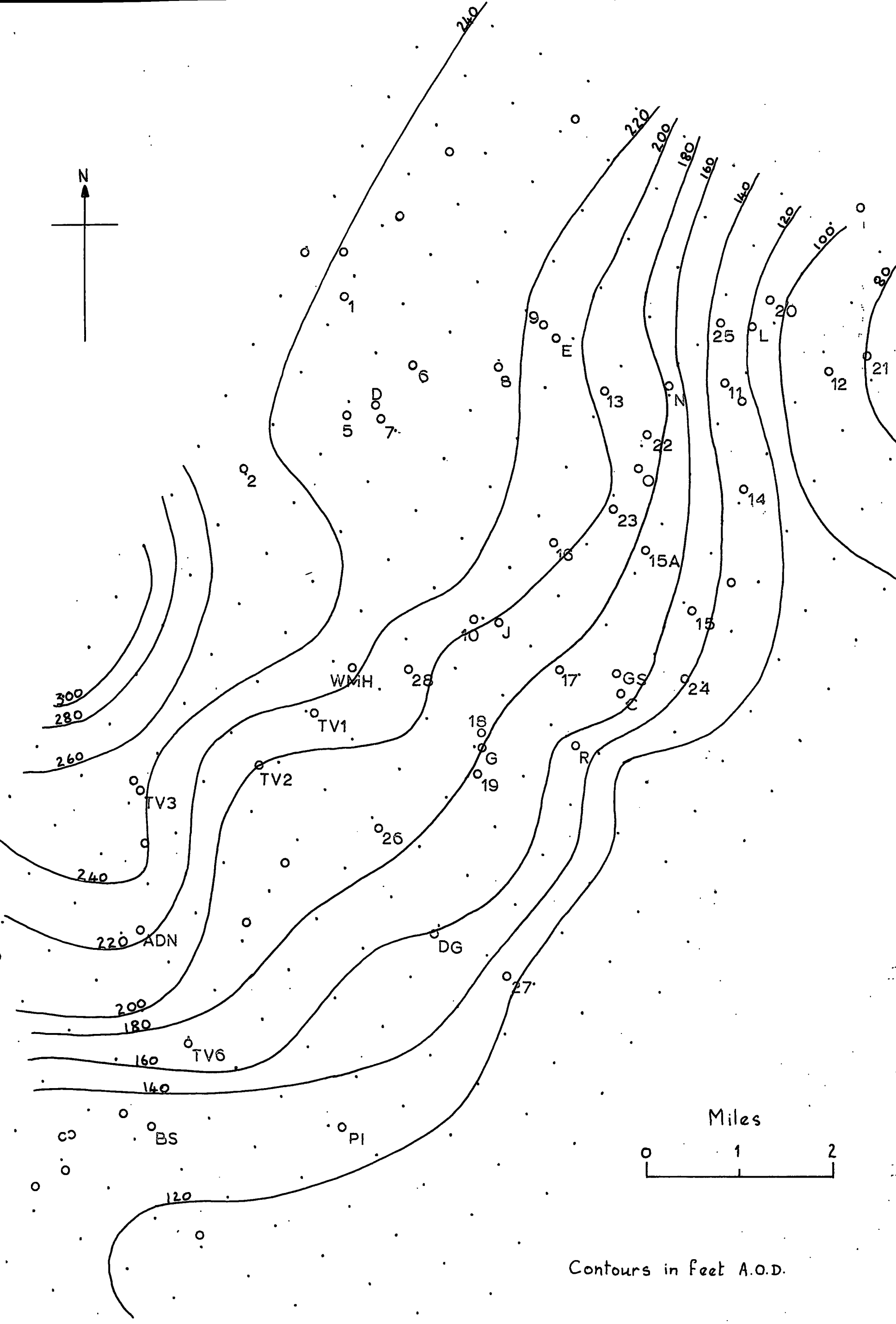

Fig 3.13. Calibrated model piezometric contours.

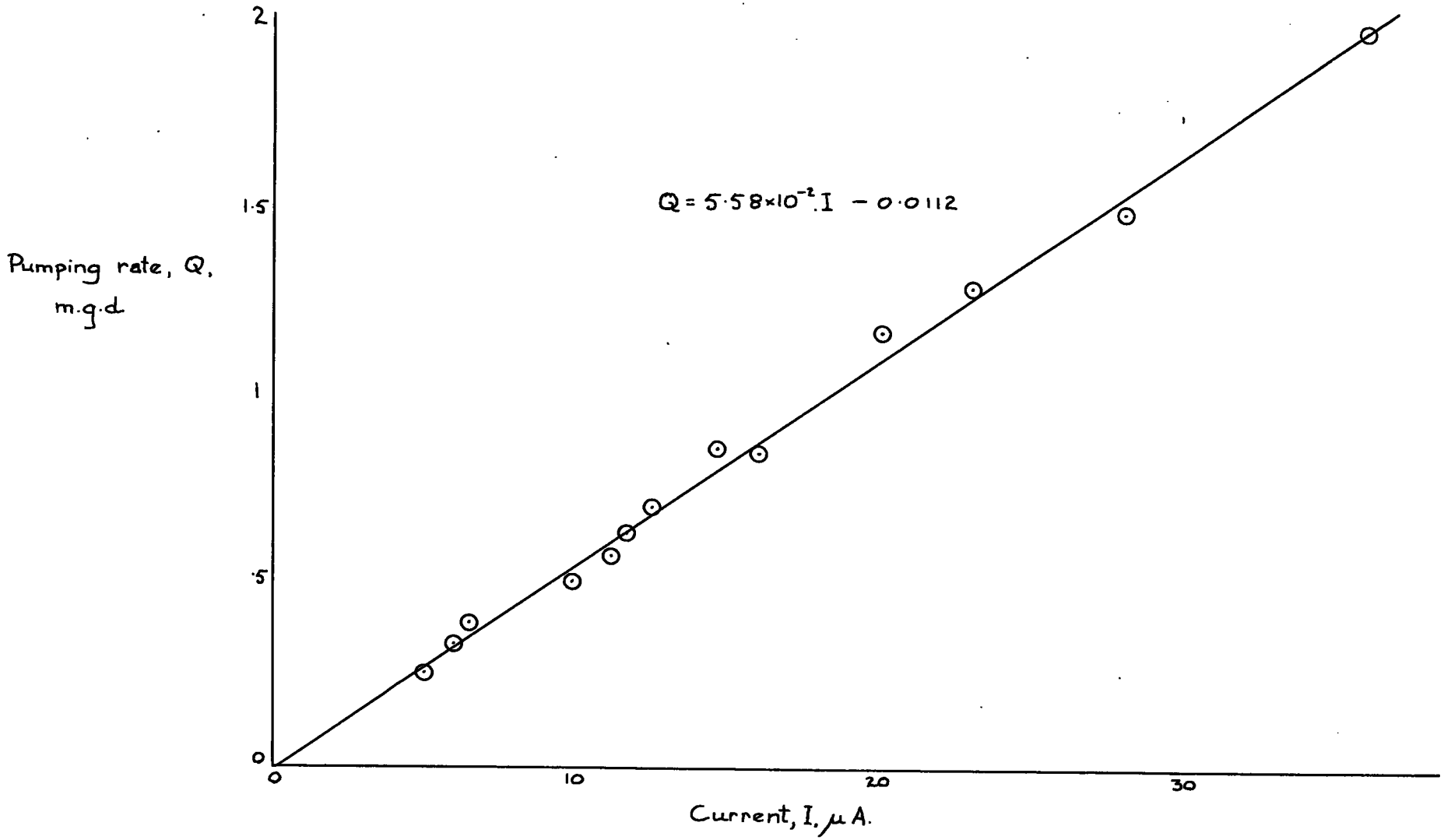

Fig. 3.14. Current-flow calibration.

TABLE 3.3.

Pumped hole	Drawdown Ft	Rate m.g.d.	Current μA	Obs. hole	Measured d.d. ft.	Model d.d. ft.
C	59	1.5	28	17	30.7	29
				G	25.6	19
				R	12.3	17
				24	3.0	4
				10	4.0	5
				15	3.0	3
				15A	5.2	3
				16	6.2	3
				18	24.7	19
				19	13.75	8
				Gt. Stnt.	42.7	40
				J	9.0	8
D	27.4	0.6907	12.5	5	3.3	1.5
				6	1.4	1
				7	6.6	6
				8	1.1	1
				9	n.a.	n.a.
				J	n.a.	n.a.
G	50.7	1.1755	20	17	19.7	16
				19	13.4	10
				26	5.9	4
				J	3.3	5
				R	8.8	8
				10	3.5	3
				C	18.3	15
				TV1	8.2	10
				Wml. Hse.	n.a.	n.a.
				Gt. Stnt.	18.7	15

Cont'd.

TABLE 3.3. (Cont'd)

Pumped hole	Drawdown Ft.	Rate m.g.d.	Current μA	Obs hole	Measured d.d. ft.	Model d.d. ft.
J	68.3	0.8921	16	10	12.9	11
				17	1.0	3
				16	n.a.	n.a.
				28	2.5	3
				G	n.a.	n.a.
				26	n.a.	n.a.
				D	0.35	1
				Wnl.Hse.	0.95	1.5
				18	n.a.	n.a.
				19	n.a.	1.5
				7	n.a.	1.2
				R	n.a.	n.a.
K	47.4	0.2493	5	0	0.79	1
				L	1.64	1.5
				12	1.41	1.5
				14	2.89	2.5
				15A	n.a.	n.a.
				20	1.38	1.5
				22	1.44	1.5
				25	1.58	1.5
				N	2.80	3
				13	0.75	1
L	estimated	variable	10	20	12.3n.s.	8
	24	av.0.5064		25	10.6n.s.	8
				11	6.6n.s.	6
				K	5.4n.s.	6
				12	5.6n.s.	5
				N	2.2n.s	2
				21	1.8	1.5
				0	0.7	n.a.

/Cont'd.

TABLE 3.3 (Cont'd)

Pumped hole	Drawdown Ft	Rate m.g.d.	Current μA	Obs. hole	Measured d.d. ft.	Model d.d. ft.
L (cont'd)				22	1.1	n.a.
				23	n.a.	n.a.
				13	0.95	1
				9	0.4	n.a.
				14	1.35	n.a.
				E	2.0	2.5
N	54.71	0.6324	11.5	11	9.2	8
				13	8.2	8.5
				0	8.0	6
				23	3.0	3.5
				14	2.0	3
				22	13.7	12
				12	2.3	2
				15A	2.5	2
				16	2.3	2
				20	5.4	4
R	54.6	0.8640	14.6	Gt. Stnt.	4.9	5
				15	n.a.	n.a.
				15A	n.a.	n.a.
				23	n.a.	n.a.
				24	7.1	7
				8	n.a.	n.a.
				C	no data	7
				17	10.1-4.5	7
				G	3.3	5
				19	3.3	2
				TV1	3	2

/Cont'd.

TABLE 3.3. (Cont'd)

Pumped hole	Drawdown Ft	Rate m.g.d.	Current μA	Obs. hole	Measured d.d. ft.	Model d.d. ft.
TV1	166.2	1.2720	23	TV1 obs	33	too close
				G	10	7
				17	1.1	5
				26	2.85	5
				Clds	2.9	5
				Gt. Stnt.	3.8	5
				10	n.a.	1
				B.X.L.	n.a.	0.5
				J	2.5	4

Abbreviations:

d.d. - drawdown
n.a. - not affected
n.s. - not stable

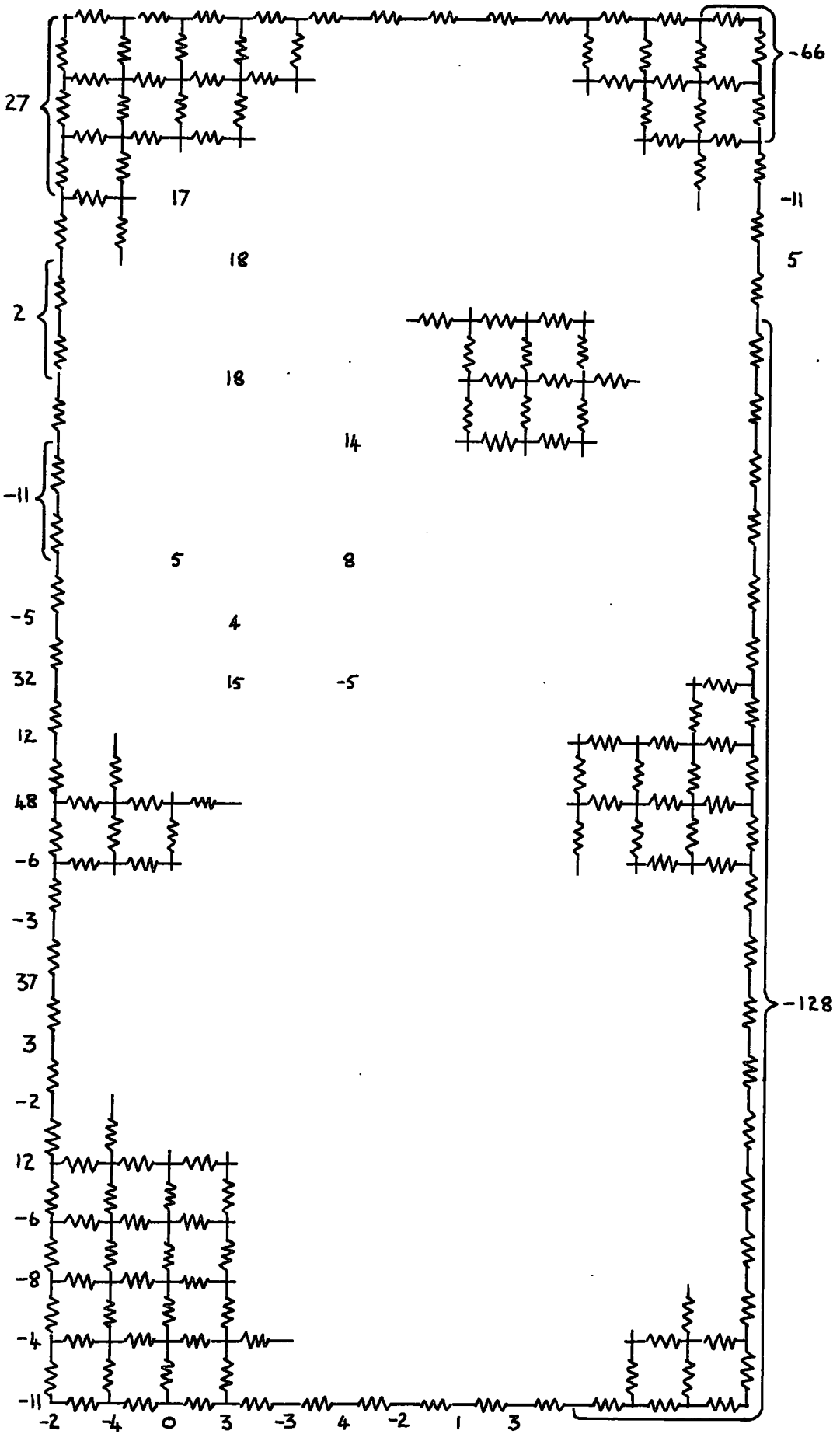

Fig. 3.15. Calibrated model currents (μA).

the model at each of the nodes can then be measured (Fig. 3.15) and converted into the corresponding water flow using factor K_3, determined as 5.58×10^{10} g.p.d/amp. This shows that some 16 m.g.d. represents the total daily flow through the area modelled.

The recharge areas are seen to be located along the western boundary, and in the Rushyford-Carr Lands area. High boundary inflows occur in the Rushyford, Newton Aycliffe and Walworth areas. One third of the recharge, however, occurs within the model area.

The discharge zone is located along the eastern margin, with minor amounts in the south and west. In the north-east a nett 4 m.g.d. flows eastwards, to be abstracted from the wells around Hartlepool. Since this flow must be maintained as high as possible so as not to deplete the Hartlepool area, pumping schemes must be designed to reduce the flow over the rest of the boundary rather than affect the north eastern corner.

3.3.2.2. Pumping scheme simulations - So far, four possible schemes have been simulated:

(a) Scheme No. 1. (Fig. 3.16)

Well	(mgd) Proposed pumping rate	Current (μ A)	Current available (μ A)	Suggested rate (m.g.d)
Broken Scar	4.0	73.0	50.0	2.7
TV	0.7	12.7	5.0	0.4
Archdeacon Newton	0.7	12.7	12.7	0.7
TV1	1.0	18.0	18.0	1.0
G	4.0	73.0	50.0	2.7
C	1.0	18.0	18.0	1.0
R	1.0	18.0	16.0	0.8

/Cont'd.

Well	Proposed pumping rate (m.g.d.)	Current (μA)	Current available (μA)	Suggested rate (m.g.d)
O	0.7	12.7	12.7	0.7
N	1.4	25.5	25.5	1.4

Total proposed yield 14.5 m.g.d.

Model yield 11.4 m.g.d.

The 3 m.g.d. deficiency is principally due to Broken Scar and G being unable to meet the 4 m.g.d. targets. The artesian head has been completely removed at most of the wells, and thus aquifer dewatering will be taking place. The 5 m.g.d. being abstracted from trough fault zone by TV1, G, C, R probably represents the maximum available for that area. In the southern area the yield is limited since the cones of depression of all the wells tend to develop northward and eastwards, towards Darlington Golf (DG). Thus little over 4 m.g.d. appears to be available from this part of the aquifer. In the north, the individual effects of O and N upon the Hartlepool flow are known to be small. However, with the high rate of abstraction in the central area, the piezometric level in the Carr Lands is decreased by 20-30ft and the nett outflow to Hartlepool reduced by just over 1 m.g.d.

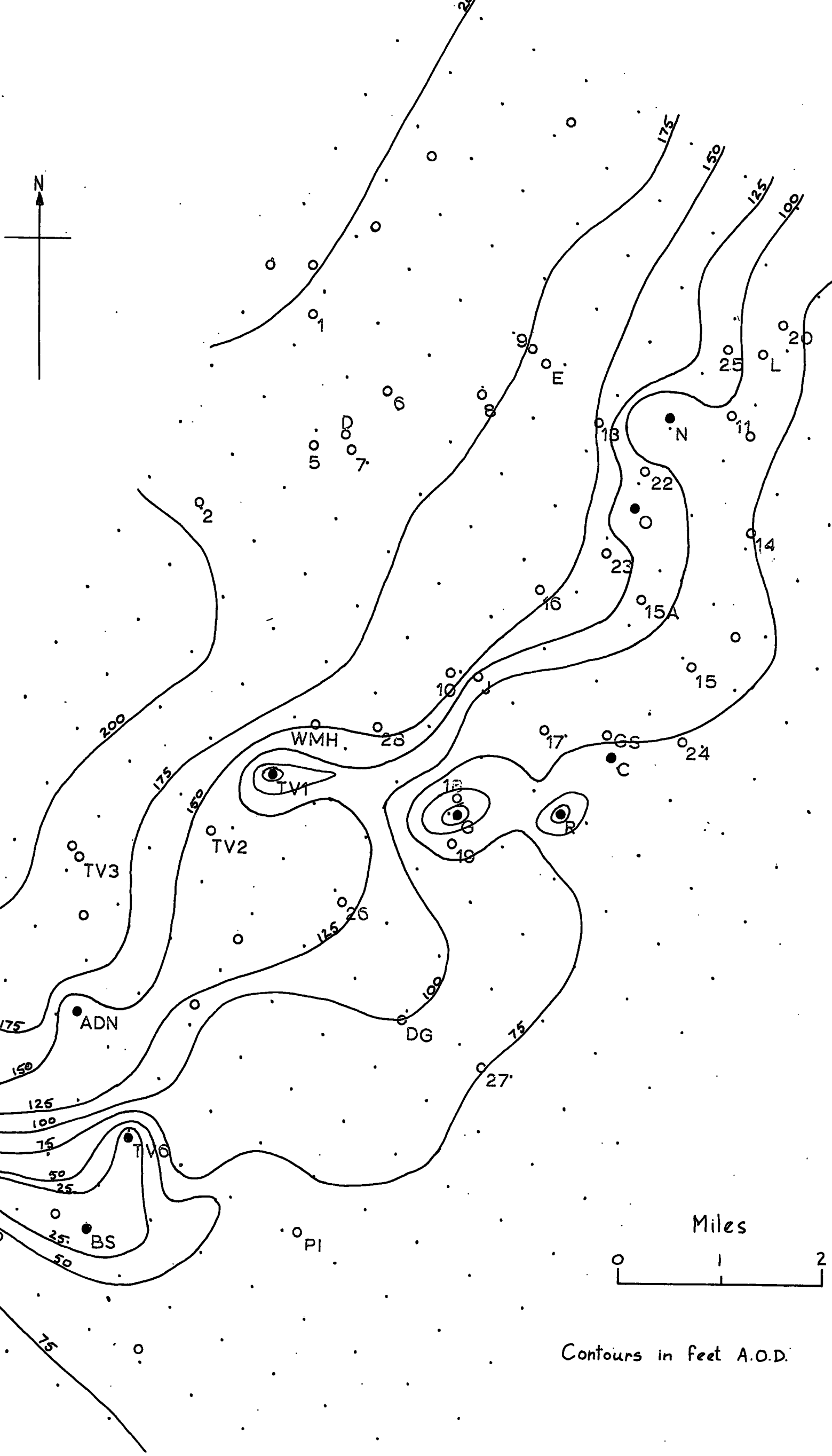

Fig. 3.16. Scheme 1, piezometric contours.

(b) Scheme No. 2. (Fig. 3.17)

Well	Proposed pumping rate (m.g.d).	Current (μ A)	Current available (μ A)	Suggested rate (m.g.d.)
Broken Scar	4.0	73.0	36	2.0
TV6	0.7	12.7	9.0	0.5
Archdeacon Newton	0.7	12.7	12.7	0.7
TV1	1.0	18.0	18.0	1.0
G	2.0	36.0	20.0	1.1
C	2.5	45.5	30.0	1.6
R	1.0	18.0	8.0	0.4
0	0.7	12.7	12.7	0.7
N	1.4	25.5	25.5	1.4
Preston-le-Skerne ($\equiv$ J)	1.2	21.8	15.0	0.8
obs 8	2.0	36.0	36.0	2.0

Total proposed yield 17.2 m.g.d.

Model yield 12.2 m.g.d.

This pumping scheme shows deficiencies at many wells, and for the yields obtainable it may not be economical to pump wells such as TV6 and R. However, the main point of interest lies in the effect of abstraction from the Carr Lands area (obs. 8). The cone of depression appears to be very large and coupled with the intense pumping in the central area, the piezometric head in the Carr Lands is reduced by some 60ft and the flow to Hartlepool is

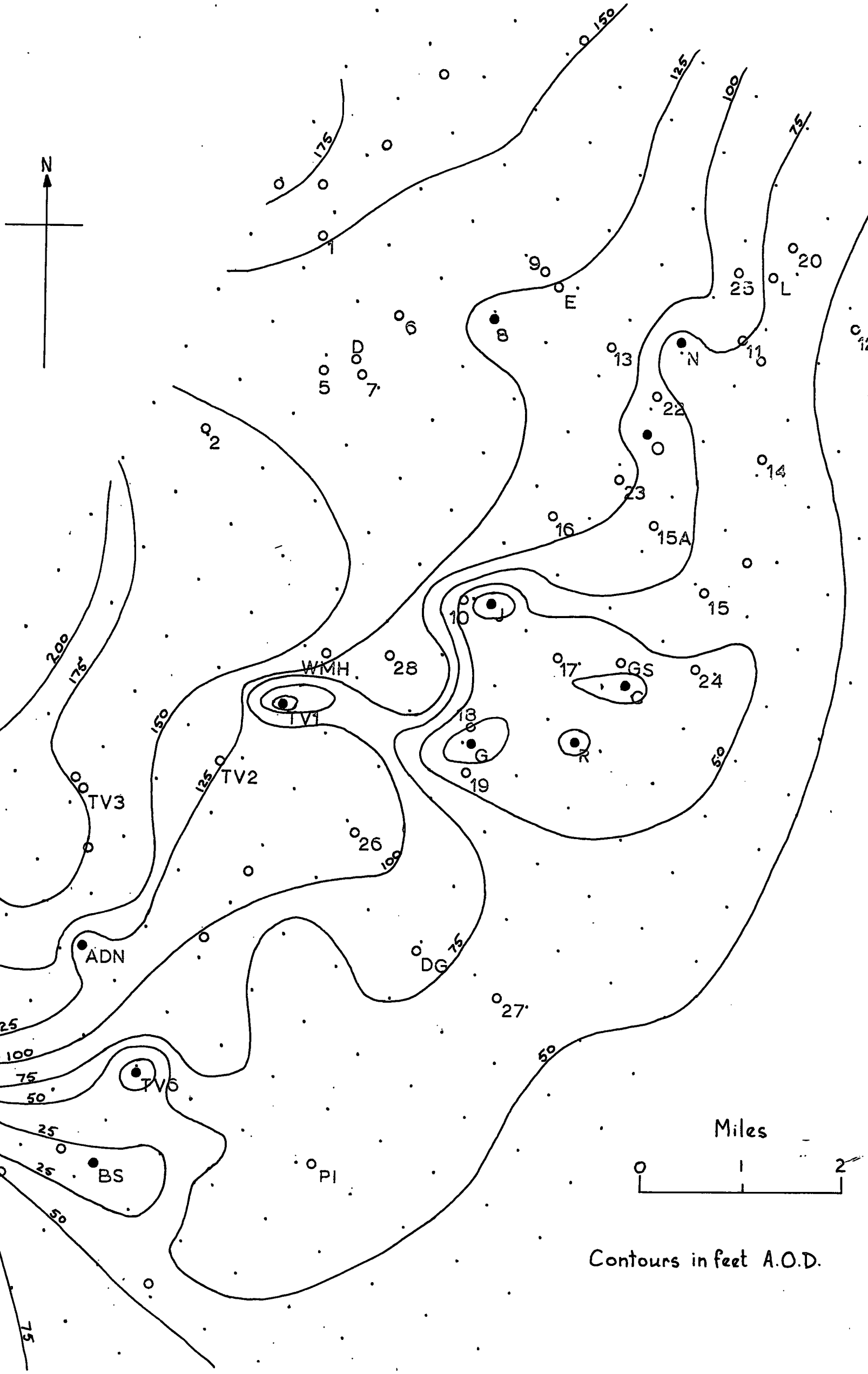

Fig. 3.17. Scheme 2, piezometric contours.

decreased to just over 2 m.g.d. Thus the total abstraction in the northern part (obs 8, 0, N) of 4.1 m.g.d. would require a derating at Hartlepool of 2 m.g.d. Whether it would be an economic proposition to obtain this extra 2.1 m.g.d. depends largely upon the capital cost of pipelaying, and the expense of pumping. As with Scheme No. 1 it is apparent that the artesian head will be removed at most pumped wells.

(c) Scheme No. 3 (Fig. 3.18)

Well	Proposed pumping rate (m.g.d)	Current (μ A)	Current available (μ A)	Suggested rate (m.g.d)
Broken Scar	4.0	73.0	40.0	2.2
TV6	0.7	12.7	12.7	0.7
Arch-deacon Newton	0.7	12.7	12.7	0.7
TV1	1.0	18.0	18.0	1.0
G	4.0	73.0	50.0	2.7
Preston-le-Skerne ($\equiv$ J)	1.2	21.6	21.6	1.2
obs. 8	1.5	27.0	27.0	1.5

Total proposed yield 13.1 m.g.d.

Model yield 10.0 m.g.d.

Increased pumping at obs. 8 could alleviate the deficiency, but this would result in a further decrease in the flow to Hartlepool. This appears to be the most rational of the medium yield schemes, It is interesting to note that under Scheme No. 2 the total yield from the central area (TV1, G, C, R, J) is 4.9 m.g.d., which is also the yield from the same area in Scheme No. 3,

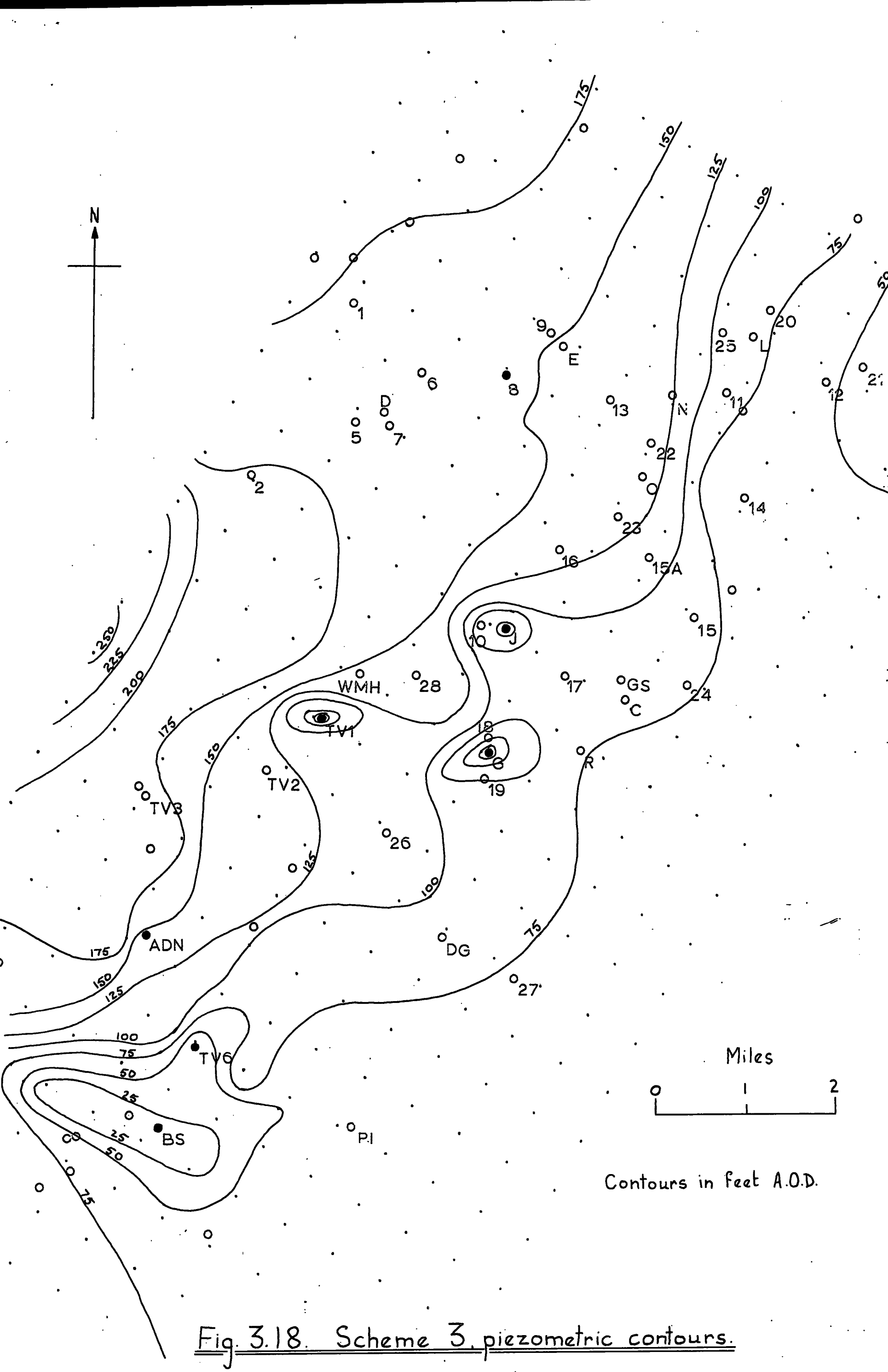

Contours in feet A.O.D.

Fig. 3.18. Scheme 3, piezometric contours.

(TV1, G, J), and must therefore represent the maximum possible for that area.

3.3.2.3. Pumping scheme conclusions - The total potential of the area modelled (some 16 m.g.d.) cannot be fully utilized since compensation flow to Hartlepool must be maintained. The nett maximum yield from the area is therefore 12 m.g.d. Of this, about 4 m.g.d. may be drawn from the southern area of Broken Scar, TV6 and Archdeacon Newton, 5 m.g.d. from the central area (TV1, C, G, R, J) and the remainder from the north., Since the model can only simulate confined conditions, the yield-drawdown ratio will increase rapidly as the aquifer is drawn into water-table conditions; however, this will result in dewatering which may be detrimental to the long-term performance of the aquifer. If pumping is only going to take place for limited periods, such as during summer low-flow conditions, then some dewatering could be tolerated, especially if provision were made for artificial recharge when available. In order to simulate these time dependent cond itions, a model capable of simulating both confined and unconfined conditions would be required (Hunter Blair, in press).

3.4. Simulation: summary, conclusions & proposals

Both digital and electrical methods have been used in the study of an area in south Durham. Simulation methods are particularly useful where complex variations in the aquifer parameters render normal idealized analytical techniques untenable. For one given set of boundary conditions, there is no unique solution for the transmissibility. By satisfying different boundary conditions, however, a particular solution may be obtained. This can only be done by iterative procedures which are time consuming using an electrical analogue, and costly by digital methods. Nevertheless, it is felt that the logical constraints imposed on a digital solution result in more

uniform solutions. Once the transmissibility elements have been determined, the electrical analogue offers much wider versatility, as well as rapid results and enabling the operator to 'get the feel' of the area. The ideal method would therefore be a hybrid of digital and analogue techniques, the former being employed for the transmissibility element iterations, and the electrical analogue built and scaled to these results, and used for the simulation of abstraction regimes.

For the area investigated in south-east Durham, the bulk of the results were obtained for steady state conditions, since the aquifer had a low storage coefficient. Calibration of the model indicated a flow through the area of some 16 m.g.d. Of this, 4 m.g.d. discharged in the north-east of the area, and therefore constituted a source of supply for wells in the Hartlepool area. Thus over the area modelled, a nett 12 m.g.d. may be abstracted. From the schemes investigated it may be seen that there is a maximum yield in an area, which is irrespective of the number of wells pumped. Thus in the central area, optimum yield is obtained from TV1, G, J. In the south, the high abstraction at Broken Scar affects the production of TV6, and thus improved, yields may be gained by replacing TV6 by a well at Darlington Golf. A possible scheme, deduced from the model, producing almost 11 m.g.d. but decreasing the Hartlepool flow by less than 2 m.g.d. is given below:

Proposed scheme No. 4 (Fig. 3.19)

Well	Current available (μ A)	Suggested pumping rate (m.g.d.)
Broken Scar	24.0	1.30
Archdeacon Newton	15.0	0.85
Darlington Golf	20.0	1.14
TV1	21.0	1.16
G	18.0	1.0
C	26.0	1.42
R	18.0	1.0
J	18.0	1.0
0	38.0	2.1

The electrical analogue therefore enables the effects of complex abstraction regimes to be rapidly simulated, and possible schemes to be optimised. As more data from the aquifer becomes available, especially with regard to quantity and location of recharge, and the production characteristics, the model may be updated, thereby reflecting the contemporary state of knowledge.

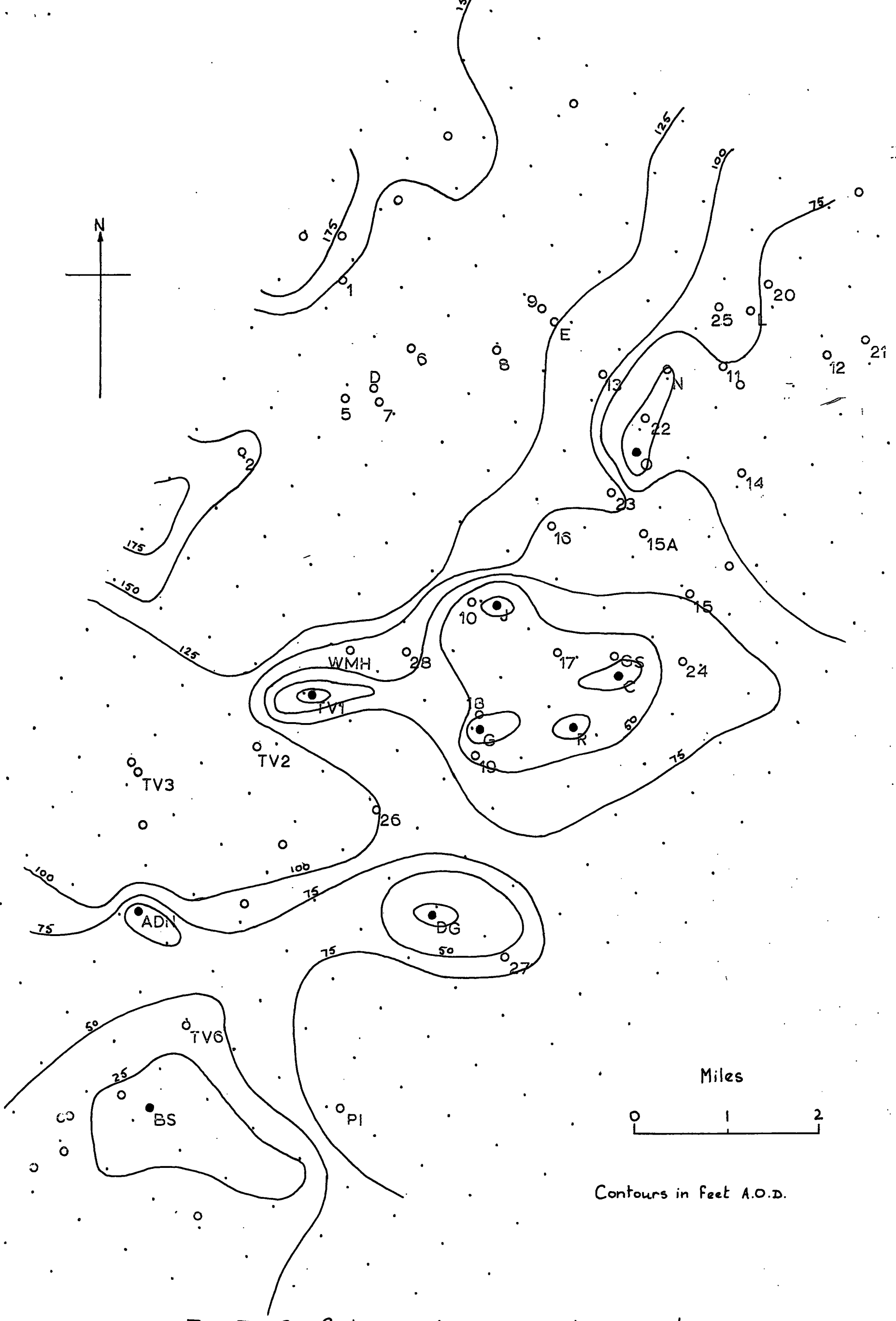

Fig. 3.19. Scheme 4, piezometric contours.

SECTION III

ENGINEERING GEOLOGY

CHAPTER I

INTRODUCTION AND THEORETICAL CONSIDERATIONS

1.1. Introduction

Since the object of the study of the Magnesian Limestone was to investigate the effects and problems of a variable and often highly fractured material, an evaluation of the engineering geology is complementary to the hydrological aspects already discussed. As with the geohydrology, the underlying control has proved to be the geology, with the palaeogeography controlling the lithology, which, in turn, affects the mechanical parameters of the rock. However, the fractured nature of the strata is likely to have a deleterious effect upon the desirable properties in an engineering sense, rather than the reverse as was the case with groundwater flow, and thus requires a more precise analysis and evaluation. The role of discontinuities in the en-masse failure of rock has therefore received an initial theoretical investigation as part of this work.

Laboratory tests have been carried out on a number of typical samples to determine the characteristic parameters relating to strength and deformational behaviour. In general, test conditions have been limited to values likely to occur in normal civil engineering practice, and the Magnesian Limestone may thus be considered as an essentially brittle material.

Since quarrying for industrial and constructional requirements represents the second largest extractive industry in eastern Co. Durham, some of the associated problems were investigated. These included an

assessment of the vibration levels induced during normal production and blasting, and a comparison of the aggregate properties from various quarries.

1.2. Theoretical considerations

Basic stress analysis and elasticity theory as applied to rock mechanics are adequately covered by the several text books on the subject (see Price, 1966; Obert & Duvall, 1967; Coates, 1967; Farmer, 1968; Jaeger & Cook, 1969; also see Timoshenko and Goodier (1951), as an entirely satisfactory text for projection into problems of rock elasticity). Standard theory is therefore taken as read and an acquaintance with it assumed.

1.2.1. Rheological properties

The actual behaviour of any material may be simulated by combinations of Hookean, Newtonian and St. Venant substances, representing respectively the properties of elasticity, viscosity and plasticity.

In many instances, it is necessary only to consider the elastic effects. The value of Young's modulus defined by:

$$d\sigma/dE = E \qquad (1.1)$$

is a complex function of temperature, pressure, and rate of strain. However, in the routine 'static' tests under normal conditions, variations may generally be attributed to a change in the material constitution.

Time-dependent creep effects are proportional to the principal stress difference, for a given material. Under most surface civil engineering works, their effects are small, although for semi-elastic

rocks the strain induced by creep over a period of, say, 10 years, is approximately the same as the immediate elastic strain. Where small displacements are critical, viscous effects must therefore be considered. Assuming a similar behaviour between concrete and rock, Zienkiewicz, (1968) notes that the Alfrey-McHenry theorem holds, which states that in a homogeneous situation, no stress redistribution occurs due to sustained loading. The implication of this is that elastic analysis may be used to determine the stress distribution, which will remain unchanged with time, even though creep displacements are continuing. However, in non-homogeneous states, for example a tunnel lining, creep in the rock will tend to transfer stresses to the lining.

True plastic deformation by intracrystalline dislocations have not been investigated, but are unlikely to occur in the low stress regimes used. However, cyclic stress-strain curves do exhibit some permanent set which is usually attributed to non-recoverable frictional effects as grains over-ride each other during compression. The brittle shear failure of rock generally results in a loss of strength, producing large strains across the failure plane.

1.2.2. Strength & failure criteria

The ideal failure criterion, not yet realized, must be able to reconcile theoretical considerations with the observed behaviour of a wide variety of rocks and their relative strengths in compression, tension and shear, under different stress and temperature conditions.

1.2.2.1. Coulomb-Navier failure criterion - This is widely used in soil mechanics and rock mechanics analyses and may be expressed as:

$$T = C + \sigma \tan \phi' \qquad (1.2)$$

where T = shear stress

C = cohesion

σ = normal stress

ϕ' = friction angle.

In terms of effective stress parameters (defined by primes),

$$T = C + \sigma' \tan \phi' \qquad (1.3)$$

In rock mechanics, the main criticisms of the Coulomb-Navier criterion are that it fails to predict the experimental high compressive/tensile strength ratio, and also it does not directly accommodate a non-linear failure envelope. Nevertheless, it does have widespread application over a limited normal stress range, and especially in fractured material.

1.2.2.2. Griffith failure criterion - This was originally expounded in a theoretical manner to explain the observed failure of glass at stress levels well below theoretical failure strengths. The existence of minute flaws, (Griffith cracks) was shown to be responsible for this strength reduction, since as a result of their geometry, high tensile stresses were induced at their tips. Under the influence of stress fields, compressive or tensile, of increasing magnitude, the cracks tend to propagate leading to total material failure. The relationship between the normal and shear stresses at Griffith failure results in a parabolic Mohr envelope (Murrell, 1958) and is given by:

$$T^2 - 4S_T\sigma - 4S_T 2 = 0 \qquad (1.4)$$

where S_T is the tensile strength.

Thus when $\sigma = 0$, $T = C$ (by definition)

and therefore $C = 2S_T \qquad (1.5)$

From the above, the compressive -to- tensile strength ratio is eight, which is in good agreement with the behaviour of many rock types.

1.2.2.3. Development from the basis of the Griffith criterion - McLintock & Walsh (1962) improved the Griffith criterion to take account of the frictional stresses which occur when a crack is closed under compression, and Brace (1960) showed that, in compression, the relationship between stresses at failure would thus be:

$$T = 2C + \mu\sigma \qquad (1.6)$$

where μ = coefficient of friction

For tensile stresses, Equation 1.4 still holds.

In the failure criteria so far considered, the intermediate principal stress has no effect upon the stresses at failure. Murrell (1963) showed from theoretical considerations that the intermediate principal stress has a small but measurable effect upon the failure envelope, and confirmed it by tests conducted with $\sigma_2 = \sigma_3$ and $\sigma_2 = \sigma_1$. More recent research (Wiebols & Cook, 1968) proposes a criterion based on the storage of energy around Griffith cracks, due to the sliding of crack surfaces over one another. In this, as the intermediate principal stress increases from $\sigma_2 = \sigma_3$ to $\sigma_2 = \sigma_1$, the strength increases to a maximum before decreasing to a value somewhat higher than at the beginning of the stress history. Laboratory tests show a good correlation with the theory.

1.2.2.4. Mohr circles and failure envelopes - Mohr circle construction has been widely used for plotting stresses at failure, and the failure envelope constructed tangentially to the principal stress circles. In many cases, especially at low confining pressures and with high friction angles, it is almost impossible to fit visually the best line to the group of circles. An alternative method, more amenable to statistical treatment is to plot q

against p defined by:

$$p = \tfrac{1}{2}(\sigma_1 + \sigma_3) \tag{1.7}$$

$$q = \tfrac{1}{2}(\sigma_1 - \sigma_3) \tag{1.8}$$

Each combination of failure stresses is thus represented by a pair of (p_f, q_f) co-ordinates, and the resulting curve is termed the K_f line (Lambe & Whitman, 1969). In many cases the points may be described by a linear relationship of the form:

$$q_f = a + p_f \,.\, \tan\alpha \tag{1.9}$$

The corresponding friction angle and cohesion may be obtained from:

$$\phi = \sin^{-1}(\tan\alpha) \tag{1.10}$$

$$C = a/\cos\phi) \tag{1.11}$$

Where the Mohr failure envelope is non-linear, a logarithmic plot must be employed. Hoek (1968), in his investigation of a semi-empirical failure criterion based on Griffith, proposed plotting logarithmically dimensionless ratios normalised by the unconfined compressive strength (S_c) thus

$$x = \log.(\bar{p}_f/S_c) \tag{1.12}$$

$$y = \log.\frac{(q_f - a)}{S_c} \tag{1.13}$$

The relationship between stresses at failure is thus of the form:

$$\log.\frac{(q_f - a)}{S_c} = \log.d + b\,\log.\frac{(p_f)}{S_c} \tag{1.14}$$

The constants b and d therefore define the material. Where a is not known a value of 0.1 for a/S_c is suggested to give a reasonable estimate. By normalising with the unconfined compressive strength, Hoek shows that many different sandstones plot on the same line, and this therefore represents

a method of assigning typical and realistic values to different rock types.

1.2.3. Discontinuities

The effects of discontinuities are important in a material like the Magnesian Limestone, which is typically highly jointed and well bedded. A discontinuity may be represented by a joint, bedding plane, fault, or, on a smaller scale, a flaw in a sample chosen for testing.

1.2.3.1. Effects on the rheological properties - This is very difficult to assess on a strictly quantitative basis. Walsh & Brace (1966) in a review of contemporary theoretical studies, show that the effect of planar cracks is more pronounced than that of the equivalent volume of spherical pores. For similar concentrations of cracks and pores, the difference between the effective and intrinsic bulk moduli is approximately the same. However, in contrast, pores have but a slight effect upon Young's modulus and Poisson's ratio. Neglecting pores, the ratio between the elastic moduli for various parts of the stress-strain curve may be theoretically predicted from:

$$\frac{E_2^{-1} - E_3^{-1}}{E_1^{-1} - E_3^{-1}} = 0.2 \left[\frac{2 + 3\mu^2 + 2\mu^4}{(1 - \mu^2)^{3/2}} - 2\mu \right] \qquad (1.15)$$

where E_1 = initial slope of curve

E_2 = ascending slope at maximum stress

E_3 = descending slope at maximum stress.

On a small laboratory sample, the intrinsic elastic properties (E_3) are those of the mineral constituents, and the effective elastic parameters (E_1, cracks open; E_2, cracks closed) those measured for the sample. However, the scale may be expanded so that the former becomes the

properties of the intact material, and the latter the properties for the en-masse discontinuous material. For this to hold, the crack concentration must be the same for all sample sizes, in which case the relationship between initial and final moduli for small samples and for large masses will be similar. If the subscript s denotes sample, and m rock mass then:

$$\left(\frac{E_2^{-1} - E_3^{-1}}{E_1^{-1} - E_3^{-1}}\right)_s = \left(\frac{E_2^{-1} - E_3^{-1}}{E_1^{-1} - E_3^{-1}}\right)_m \qquad (1.16)$$

Now if

$$(E_2)_s = (E_3)_m \qquad (1.17)$$

and

$$(E_1:E_2:E_3)_s = (E_1:E_2:E_3)_m \qquad (1.18)$$

then these relationships allow an estimate to be made of the en-masse reduction of Young's modulus. Inherent in the assumptions are many possible errors, for example the relationship:

$$\left(E_{3/E_2}\right)_s = \left(E_{3/E_2}\right)_m \qquad (1.19)$$

However, it may provide an easily applied guide to possible behaviour.

As might be expected, the increase in overburden stress with depth produces a closure of horizontally aligned cracks and bedding planes, and it follows from the above that this must increase the stiffness. Gibson (1967) has computed the settlement of a loaded pad and the surrounding area on the basis of an increase in stiffness with depth, and compared the resulting deflections with Boussinesq predictions. In the former, most of the deflection occurs under and very close to the loaded area. Large scale loading tests carried out on chalk in Norfolk (Ward, Burland and Gallois, 1969) show a remarkably close coincidence with Gibson's model. Geological evidence from boreholes associated with the project shows that the rock becomes tighter and less jointed with depth.

The effect of discontinuities on the other rheological properties is less documented. Recent work (Scholz, 1968) has shown that at low stress levels, creep may be a function of brittle failure and intergranular movements. Discontinuities will also tend to promote the free passage of circulating fluids which can lead to an increase in the viscous nature of the rock. Irrecoverable deformation following failure often takes place along a well defined plane which may be determined by discontinuities prior to rupture (see below). Movement along these planes is often of a stick-slip nature (Byerlee & Brace, 1967), and may, on a global scale, be responsible for earthquakes.

1.2.3.2. Effects upon failure characteristics - The effects of discontinuities has been examined theoretically by Jaeger (Jaeger & Cook, 1969) and experimentally by Donath (1964). In considering low stress conditions, the Coulomb-Navier criterion will be assumed to hold along the discontinuity.

(a) Biaxial system - Jaeger (op. cit.) has shown that failure will take place preferentially along a discontinuity for $\beta_1 < \theta < \beta_2$ (Fig. 1.1).

The principal stresses and C - ϕ parameters may be reduced to dimensionless factors based on the ratios of their magnitudes as illustrated by the geometry of the Mohr diagram, by a transfer of origin to the point of intersection of the extrapolated discontinuity envelope and the normal stress (σ) axis. Defining new symbols:

$$\sigma_1^* = \sigma_1 + C \cot \phi \qquad (1.20)$$

$$\sigma_2^* = \sigma_2 + C \cot \phi \qquad (1.21)$$

$$\sigma_3^* = \sigma_3 + C \cot \phi \qquad (1.22)$$

and

$$F^* = \frac{\sigma_1^* - \sigma_3^*}{\sigma_1^* + \sigma_3^*} \qquad (1.23)$$

It follows that:

$$\sin (2\beta + \theta) = \sin \phi / F^* \qquad (1.24)$$

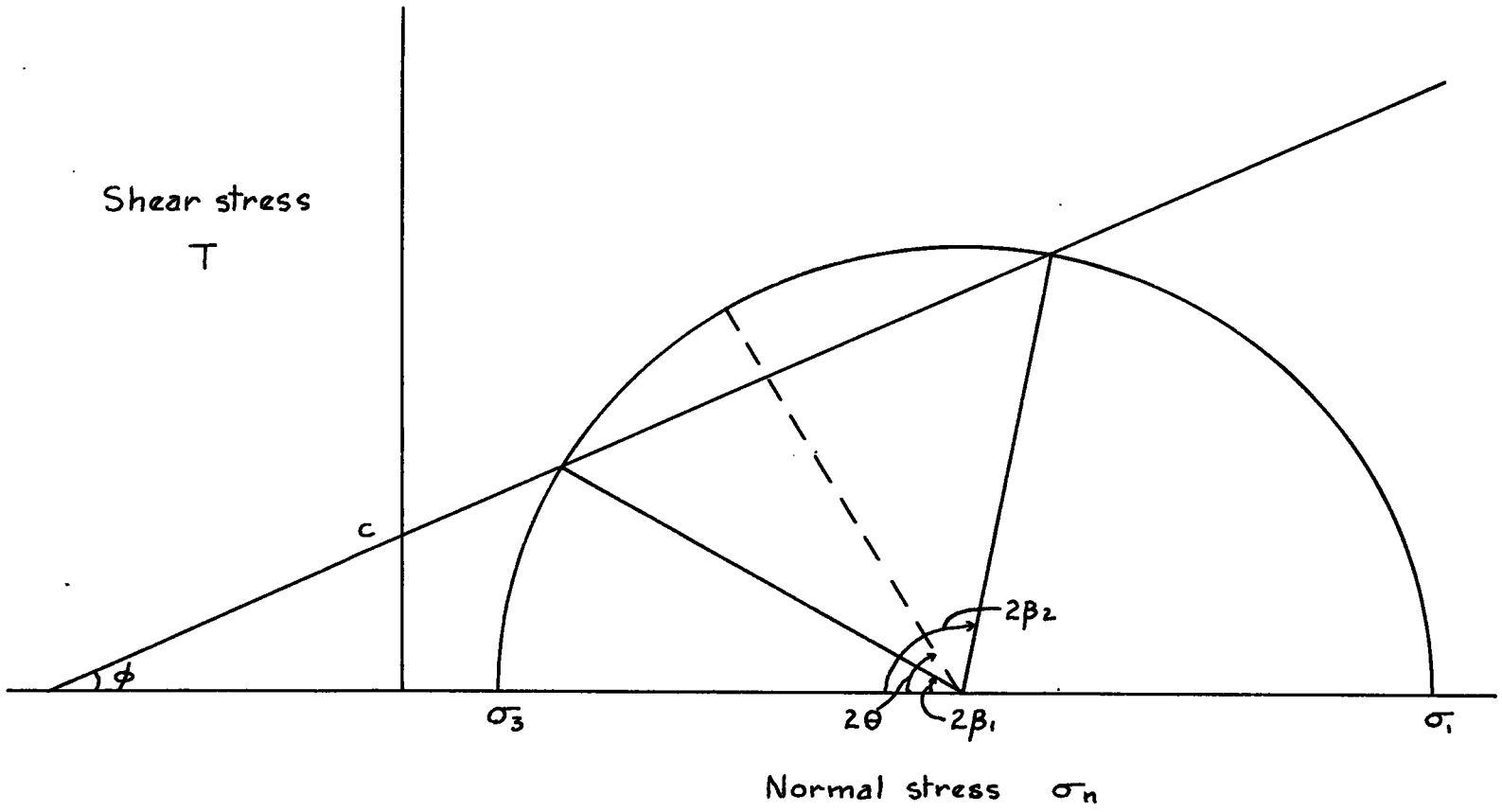

Fig. 1.1. Planar discontinuity : biaxial stress field.

The solution of this equation for β enables the locus of failure preferentially along a discontinuity to be located with respect to ϕ, F* and the angle the planar discontinuity makes with the σ_1 direction, θ, (Fig. 1.2).

When $\theta = 0$ the above Equation 1.24 is no longer applicable since $C \cot \phi = \infty$. For this case, failure along the discontinuity will take place for

$$\tfrac{1}{2} \sin^{-1}\left(\frac{2C}{\sigma_1 - \sigma_3}\right) < \theta < 90 - \tfrac{1}{2} \sin^{-1}\left(\frac{2C}{\sigma_1 - \sigma_3}\right) \qquad (1.25)$$

(b) Triaxial system - The above approach may readily be extended to the general triaxial case of $\sigma_1 > \sigma_2 > \sigma_3$. The stresses on any plane where direction cosines l, m, n, describe the angles θ, γ, ψ, may be represented on the Mohr diagram (Fig 1.3).

Now $$F^* = (\sigma_1^* - \sigma_3^*)/(\sigma_1^* + \sigma_3^*)$$

thus $$\sigma_1^* = \sigma_3^* (1 + F^*)/(1 - F^*)$$

$$\sigma_1^* = K_1 \sigma_3^* \qquad (1.26)$$

Let σ^* vary between σ_3^* and σ_1^* such that

$$\sigma^* = \sigma_3^* + N (\sigma_1^* - \sigma_3^*) \quad \text{for } 0<N<1$$

$$\sigma^* = \sigma_3^* \left[1 + N\left(\frac{2F^*}{1-F^*}\right)\right]$$

$$\sigma^* = K\sigma_3^* \qquad (1.27)$$

In a similar manner, σ_2^* may vary between σ_3^* and σ_1^*, and thus for $0 < P < 1$

$$\sigma_2^* = \sigma_3^* \left[1 + P\left(\frac{2F^*}{1-F^*}\right)\right]$$

$$\sigma_2^* = K_2\sigma_3^* \qquad (1.28)$$

The direction cosines on any plane in a triaxial system may be

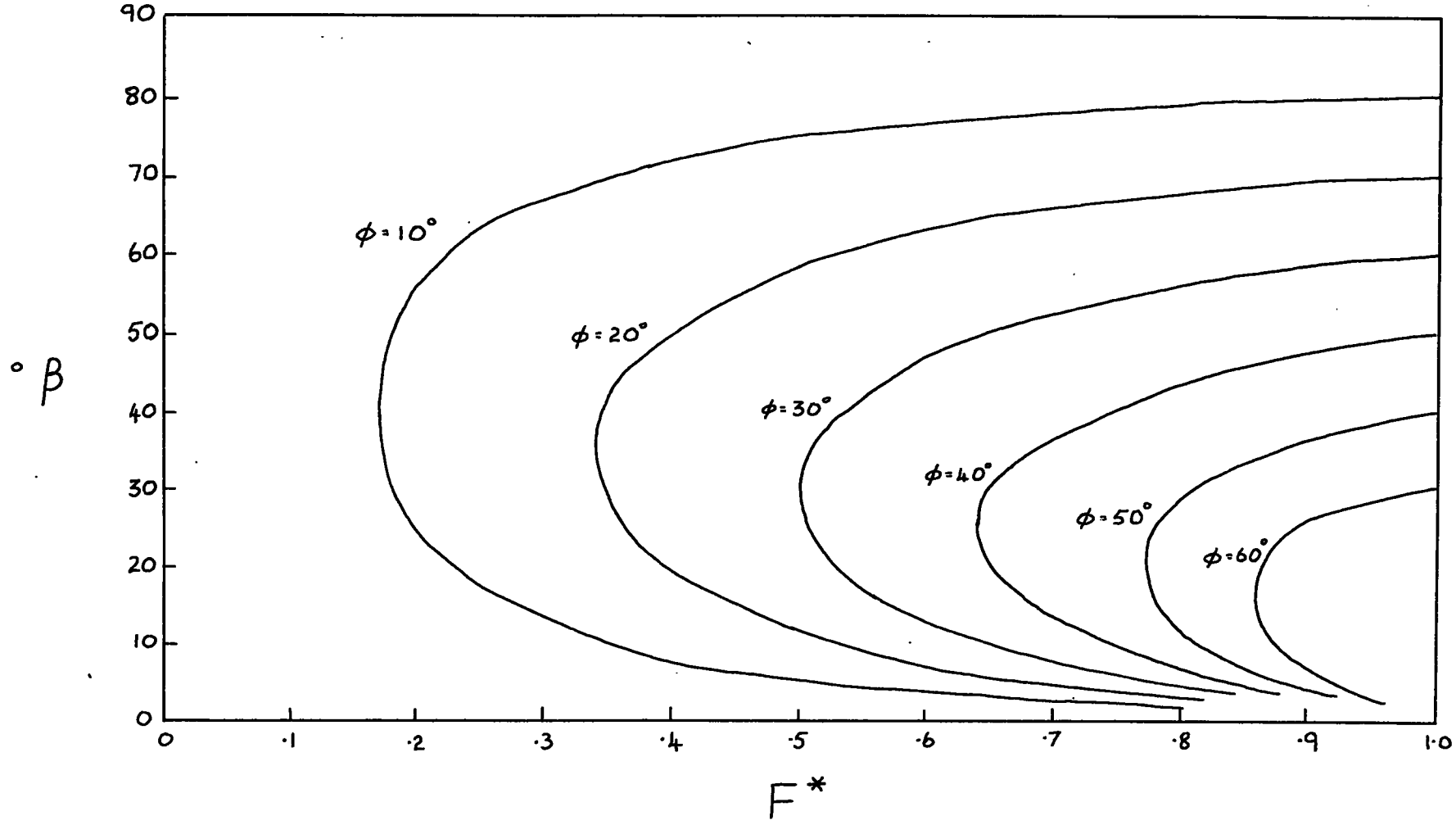

Fig. 1.2. Stability regimes: biaxial stress field.

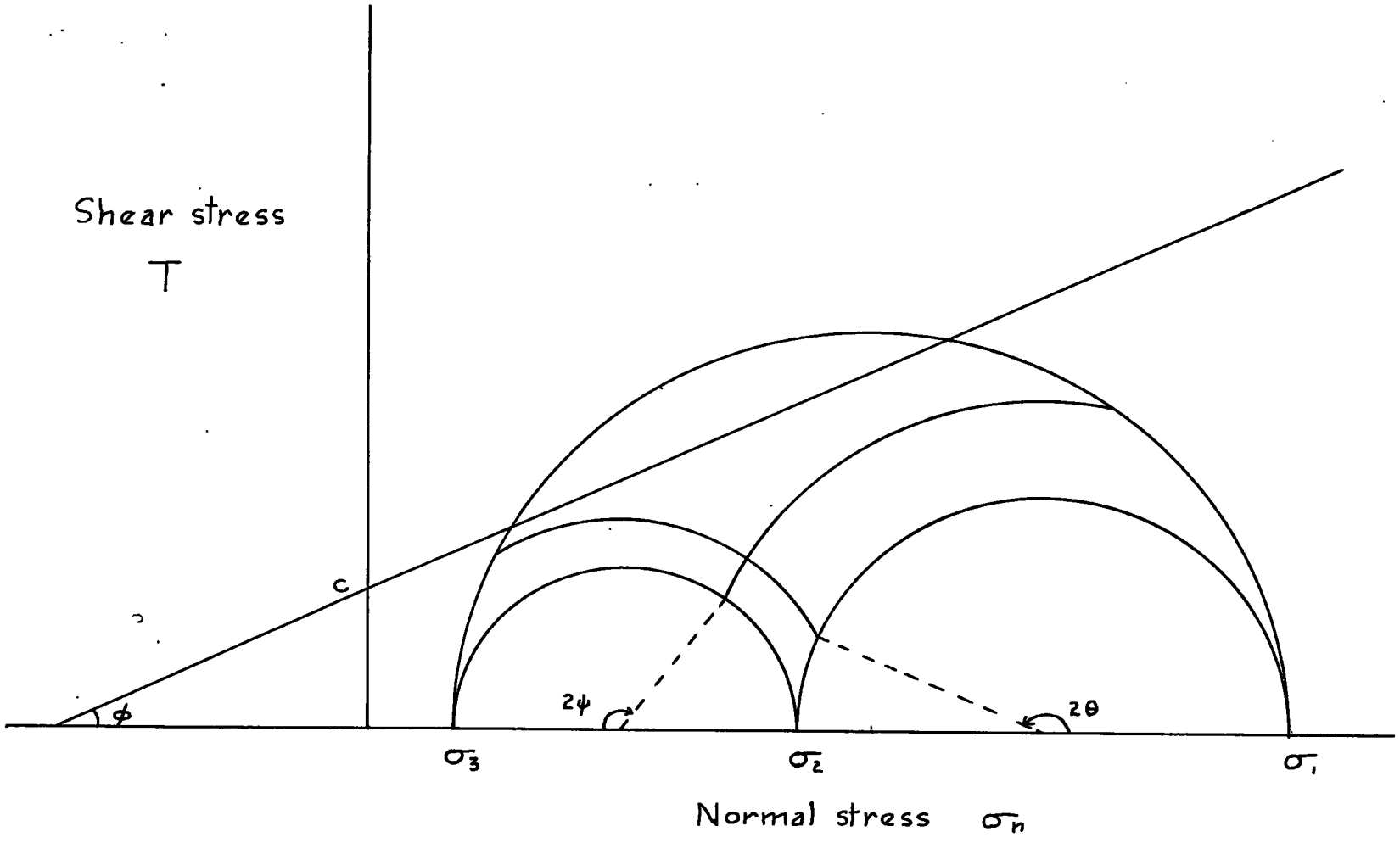

Fig. 1.3. Planar discontinuity: triaxial stress field.

determined from the magnitude of the normal and shear stress on the plane.

Thus

$$l^2 = \frac{(\sigma_2^* - \sigma^*)(\sigma_3^* - \sigma^*) + T^2}{(\sigma_2^* - \sigma_1^*)\,(\sigma_3^* - \sigma_1^*)} \tag{1.29}$$

and

$$n^2 = \frac{(\sigma_1^* - \sigma^*)\,(\sigma_2^* - \sigma^*) + T^2}{(\sigma_1^* - \sigma_3^*)\,(\sigma_2^* - \sigma_3^*)} \tag{1.30}$$

For limiting equilibrium on the planar discontinuity

$$T = \sigma^* \tan \phi \tag{1.31}$$

Substituting for σ_1^*, σ_2^*, σ^* and T

$$l = \frac{(K_2 - K)\,(K_3 - K) + K^2 \tan^2\phi}{(K_2 - K_1)\,(K_3 - K_1)}^{\frac{1}{2}} \tag{1.32}$$

$$n = \frac{(K_1 - K)\,(K_2 - K) + K^2 \tan^2\phi}{(K_1 - K_3)\,(K_2 - K_3)}^{\frac{1}{2}} \tag{1.33}$$

For the $\phi = 0$ case a similar procedure is followed except that a new dimensionless parameter is developed:

$$G = 2C/(\sigma_1 - \sigma_3) \tag{1.34}$$

from which

$$\sigma_3 = \sigma_1 - 2C/G \tag{1.35}$$

$$\sigma_2 = \sigma_1 + 2C(P-1)/G \tag{1.36}$$

$$\sigma_3 = \sigma_1 + 2C(N-1)/G \tag{1.37}$$

The direction cosines at limiting equilibrium are then given by:

$$l = \left[\frac{N(N-P) + G^2/4}{1 - P}\right]^{\frac{1}{2}} \tag{1.38}$$

$$n = \left[\frac{(1 - N)\,(P - N) - G^2/4}{P}\right]^{\frac{1}{2}} \tag{1.39}$$

Stereographic methods represent the most convenient method of plotting fail and no-fail regimes, since joint orientation and frequency diagrams usually employ lower hemisphere equal-area Schmidt projection. For plotting, the direction cosine angles θ and ψ must be converted to θ and α (Fig 1.4) using the relationship:

$$\alpha = \cos^{-1} (\cos.\theta / \sin\psi) \qquad (1.40)$$

For the present study, a PL/1 program was written to compute the stereographic co-ordinates of the limiting conditions for various combinations of F* and ϕ, and a description of the method and results are given in Appendix C.

In the general case, the global axes to which the discontinuities are referred are non-coincident with the principal stress directions, σ_1, σ_2, σ_3. A modified version of the previous program was therefore written which will rotate the failure diagram and the associated principal stress axes so that the directions are referrable to global axes (Appendix C). The advantage of this is that a joint survey may be carried out over the area of interest so that a statistically viable distribution may be built up. The principal stress magnitudes and directions at points of interest are determined either theoretically using, for example, finite element or photoelastic techniques, or directly by borehole stress plugs or strain gauge rosettes. The failure regimes for these stress combinations and C - ϕ characteristics of the discontinuities are then plotted and rotated into global co-ordinate directions. The concentration of the discontinuity directions which may give rise to instability at each location may then be assessed. The ultimate development of this method would be to determine the most susceptible failure surface from a summation of the safety factors along probable paths. Such an approach based on the development of the necessary finite element technique

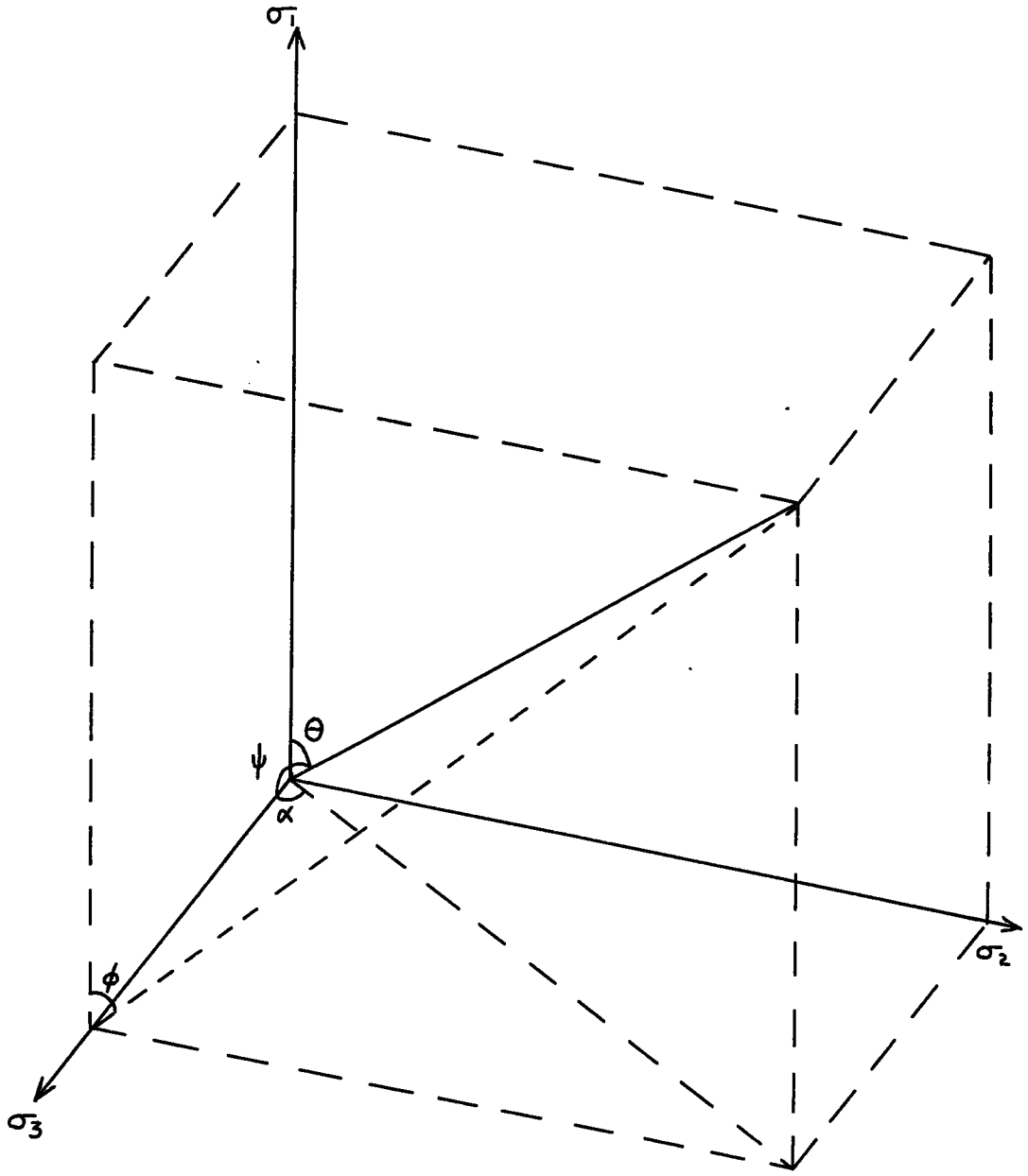

$\cos\theta = l \qquad \cos\psi = n$

Fig. 1.4. Axes and angle notation.

is recommended as appropriate for further work.

1.3. Summary and conclusions

Even though much research in rock mechanics has been directed towards an understanding of rheological and failure characteristics, there is not, as yet, a completely satisfactory overall theorem. Nevertheless, some failure criteria, such as the Griffith and its derivatives, based essentially upon theoretical considerations, do show reasonable agreement with the observed behaviour of rocks. For low compressive stress regimes and fractured material, the semi-empirical Coulomb-Navier criterion may be employed, and this results in simplified conclusions.

Since the Magnesian Limestone is essentially highly jointed and discontinuous, the associated theoretical aspects have been examined in some detail. The effect of discontinuities is to reduce the elastic and strength parameters, the degree of reduction being a function of size, concentration and directions of the discontinuities.

Digital computer methods have been used to facilitate the plotting and rotation of stability regime stereograms determined for typical dimensionless strength parameters in a triaxial stress field.

CHAPTER 2

LABORATORY TESTS

2.1. Objects

Since the engineering behaviour of a material is governed by its rheological nature and failure characteristics, laboratory tests are directed towards determining these parameters so that structures on or within the rock may be economically and safely designed. The rock may then be classified on the basis of these parameters (Deere, 1968) enabling comparisons to be made with other areas and utilising previous experience.

Various samples of Magnesian Limestone have been tested in an attempt to cover as many different lithologies as possible. Probably 75% of the exposure is represented by a buff, granular, silt-grade dolomite which occurs at all horizons. In the selection of samples there is doubtless a bias towards the more competent material since these are less of a problem to core and test. Nevertheless a representative range of lithologies and mechanical properties has been covered.

Laboratory methods have been used throughout, coupled with a visual inspection and classification of the strata at many localities. Ideally, full scale field tests should be carried out, but the high cost obviates their use in all but the largest and most critical schemes.

2.2. Tests

It is proposed to deal with each type of test individually, with the emphasis on the suitability and problems posed in each case.

2.2.1. Compression tests on intact samples

This form of test is usually employed for the investigation of both the elastic and strength characteristics of the sample. It is generally inherent in the test that the sample tested is macroscopically intact, although even small flaws may lead to a wide range of results for similar test conditions.

2.2.1.1 Sample preparation - Samples are cored using diamond tipped core barrels of either 1 inch or 1.5 inches nominal internal diameter. Water-flush was generally used, although some samples which tended to break down in water were air-flush cored. The ends were lapped parallel using push-fit holders to ensure axial perpendicularity, finishing with grade 800 carborundum powder. The cylinders had a nominal 2:1 length to diameter ratio, although shorter samples were tested and normalised using the expression, (Obert et al, 1946) :

$$S_c = S_{co} \left(0.8 + \frac{0.2}{L/D}\right) \qquad (2.1)$$

where S_{co} = compressive strength for L/D = 1

S_c = observed compressive strength.

The cylinders were oven dried at 110°C for 24 hours and tested dry. Rubber sheaths were used during triaxial test to prevent ingress of the pressurizing medium.

2.2.1.2. Measurement of stress - Most tests were carried out on a Clockhouse 10 ton machine (Fig. 2.1) on which the bottom platen is raised at a constant speed by a synchro-motor, infinitely variable between 7.4×10^{-6} ins/min and 2.5×10^{-3} ins/min, a speed of 5×10^{-3} ins/min being employed. The end load was calculated from the deflection of a calibrated proving ring. Initially, a dial gauge was used, but this was later replaced by a d.c. linear variable differential transformer (L.V.D.T.) having a one inch travel. The makers' calibration was accepted after checking with a micrometer and digital voltmeter. From the respective calibrations of the proving ring and L.V.D.T. (Appendix D) the load could be computed from changes in the output voltage, since the input voltage was maintained at the specified 24V d.c. by a Farnell stabilised power source.

For the 1.5 ins diameter samples it was sometimes necessary to use a Denison 300 ton hydraulic test rig, in which case the end load was read directly from the control panel dial.

2.2.1.3. Measurement of strain - Two methods were used:

(a) Strain gauges - T.M.L. foil type resistance strain gauges, 120Ω resistance, were bonded to the sample with epoxy resin, and held until set by a standard rubber sheath over the sample to ensure contact over all the substrate. Two axial gauges were placed diametrically opposite one another and connected in series so as to average strains across the diameter. Readout was via a Croyden Instruments Cropico Bridge, which was manually adjusted to maintain null deflection on the galvanometer. Where lateral strain gauges were used for the determination of Poisson's ratio, a two-pole two-way switch was tried so that alternate axial and

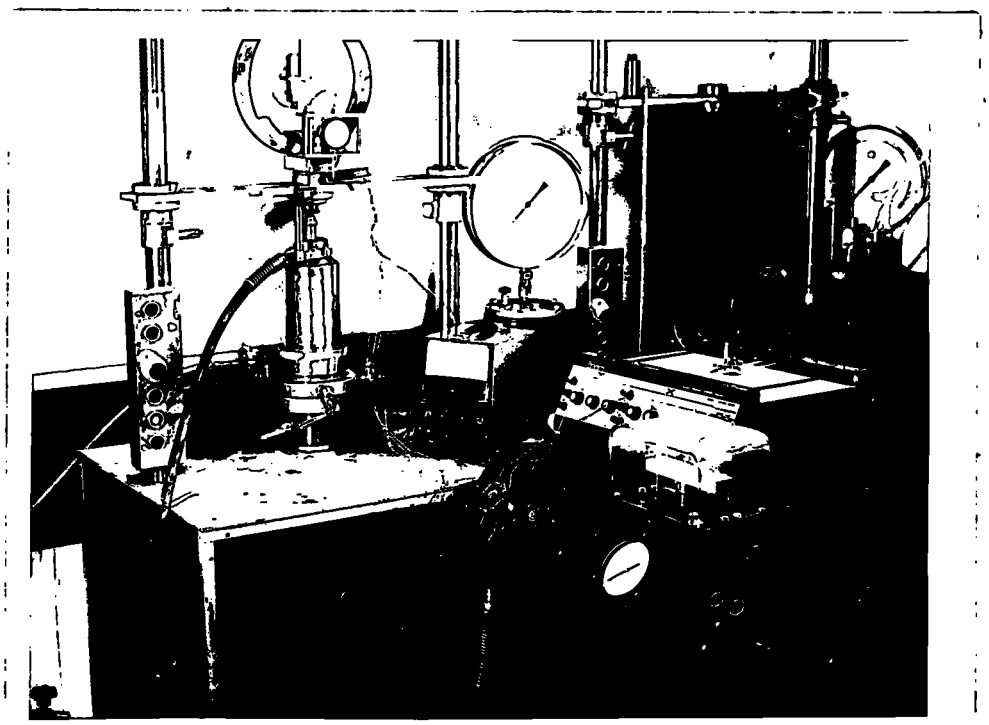

Fig. 2.1. Triaxial test arrangement.

lateral readings could be taken. However, the change in resistance of the strain gauge was masked by different contact resistances as the switch was thrown, resulting in very erratic readings. An alternative method was to monitor each gauge using a half bridge circuit, operational amplifier and attenuator, the out-of-balance current being measured using an ultra-violet galvanometric recorder, calibrated directly in terms of strain.

(b) Direct current L. V. D. T. - This was arranged to measure the displacement between the base of the proving ring and the machine bottom platen. As with the stress L. V. D. T. it may be calibrated to read directly in % strain (Appendix D). The main advantage of this method of strain measurement is that it does not require lengthy preparation and may be readily used for confined or unconfined tests. By taking the output from both the strain and stress L. V. D. T. s to the X and Y axes respectively of a potentiometric plotter, the stress-strain curve is directly and permanently displayed. However, possible errors may arise due to strain within the machine platens and loading piston. To reduce these effects as far as possible, all experiments, both confined and unconfined, were carried out using the same platens inside a triaxial cell, thus making the results comparable one with another. In most instances, since the material tested has a low Young's modulus in comparison with steel, the effect was neglected.

For $\sigma = 10^4$ lb/in^2

Rock $E_R = 5 \times 10^5$ lb/in^2

Steel $E_s = 30 \times 10^6$ lb/in^2

Taking a sample length, h_r = 2 ins, and for the steel, h_s = 3ins, then:

$$\Delta h_s = 3 \times 10^4 / 30 \times 10^6$$

$$= 1 \times 10^{-3} \text{ ins}$$

$$\Delta h_r = 2 \times 10^4 / 5 \times 10^5$$

$$= 4 \times 10^{-2} \text{ ins}$$

thus $$\Delta h = \Delta h_s + \Delta h_r = 4.1 \times 10^{-2} \text{ ins}$$

The error in calculating the rock in Young's modulus if the strain in the steel is neglected is thus only 2.5%, which was acceptable for the studies undertaken.

Fairhurst (1961) has shown that due to the stress distribution induced in the sample, the strain measured by strain gauges may be up to 10% higher than the strain calculated from the sample shortening. Numerous methods have been attempted which combine the benefit of the L.V.D.T. gauge with measuring the strain over the more uniformly stressed central third of the sample (Fairhurst, op. cit., Hobbs, 1967a) but most suffer from the disadvantages implicit in the techniques when used under confined conditions, as well as a likelihood of damage when the sample fails.

2.2.1.4. 'End effects' - The sample-platen interface and its effect on the measured properties has been the subject of a great deal of research and hypotheses, but, as yet, a complete appraisal has not been published. The fundamental dissension arises over whether the sample should be free to expand laterally or should be constrained at the platens. Mogi (1966) has shown that with 2:1 samples end effects were considerable, and suggested the use of an epoxy resin fillet into which the large stress concentrations could be diverted.

Under normal testing conditions, the sample faces are ground parallel and flat, and are in contact with steel whose lateral expansion

is, say, $^1/_{50}$th of that of the sample. The result is a complex stress distribution which may lead to indefinable failure stresses. On some stress-strain curves (Fig. 2.2) a 'knee' is apparent, interpreted as sample-platen slip under the generated shear stresses.

Brown & Trollope (1967) have demonstrated both theoretically and experimentally that when there are no constraints upon the strains, then for a triaxial stress system

$$\sigma_x^1 = \sigma_x - \nu(\sigma_y + \sigma_z) \tag{2.2}$$

$$\sigma_y^1 = \sigma_y - \nu(\sigma_x + \sigma_z) \tag{2.3}$$

$$\sigma_z^1 = \sigma_z - \nu(\sigma_x + \sigma_y) \tag{2.4}$$

where ν = Poisson's ratio and the primes indicate 'effective' stresses defined as above by considering the elastic effects of the orthogonal stresses. For an unconfined condition with perfect movement along the platen-sample interface:

$$\sigma_x = \sigma_y = 0$$

thus

$$\sigma_x^1 = \sigma_y^1 = -\nu\sigma_z \tag{2.5}$$

The negative sign indicates that a tensile intergranular stress has been generated. If the sample is not free to expand at the interfaces, then a stress of $\nu\sigma_z$ must be generated by friction to prohibit movement. For limiting equilibrium:

$$\sigma_x^1 / \sigma_z^1 = \mu \tag{2.6}$$

For many rocks, ν is not a constant but increases from zero to about 0.2 as the cracks close (Walsh & Brace, 1966). The true interface stress should thus be:

$$\sigma_x^1 = \int_0^{\sigma_z} f(\nu).d\sigma \tag{2.7}$$

Sample TH4 1V

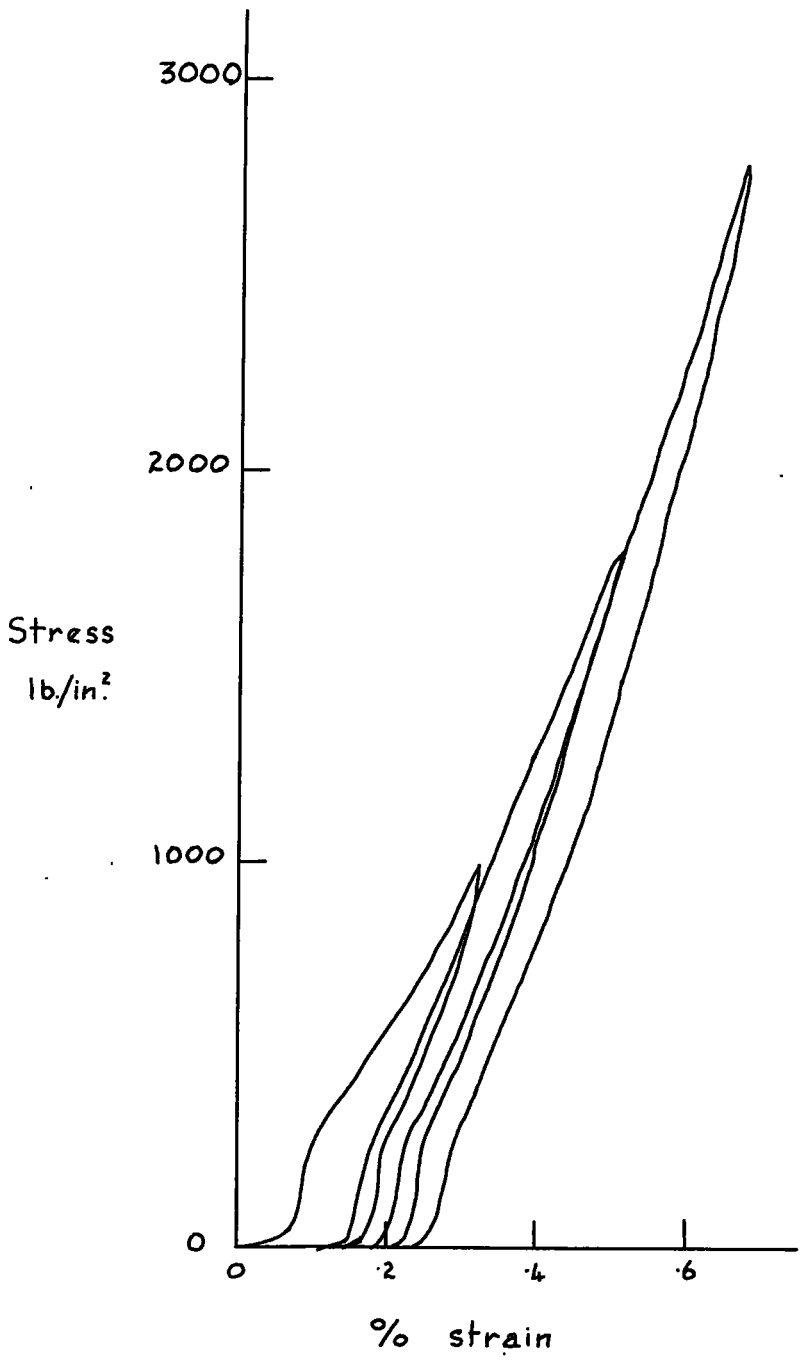

Fig. 2.2. Stress-strain curve.

Movement at the interface will be initiated when:

$$\sigma^{1}_{x}/\sigma^{1}_{z} \geqslant \mu \qquad (2.8)$$

and for a polished rock-steel junction a value of $\mu = 0.2$ is probably acceptable. The 'knee' in the stress-strain curve is thus attributed to this slippage which shows as an increased shortening for a slight change in stress as some of the strain energy is transferred from axial to lateral storage.

When the platen-sample surface is perfectly lubricated, the unconfined crushing strength is recorded on and 'effective' stress basis. However, long before the total stress crushing strength is reached, the sample would have failed in 'effective' tension, i.e. when $)\sigma_z \gg S_T$. When there is a frictional restraint between the sample and platens, the 'effective' stresses are indeterminable although the vertical mode of failure is indicative of a dominant tensile component (Fig. 2.3). As the confining pressure is increased the effective lateral stresses change from tensile to compressive. Mohr failure envelopes plotted on a total stress basis, show that at low confining stresses, the friction angle is very high. However, on an effective stress basis, these high-ϕ angles would occur for 'effective' normal stresses in the tensile region, as would be expected.

2.2.1.5. Summary and conclusions - The compression test as carried out in the present work is unsatisfactory on a number of theoretical points:

(a) The conditions along the platen-sample interface have a great effect upon rheological and failure parameters, especially the latter.

(b) The elastic moduli determined from the test are dependent upon the method of measurement. This is mainly due to (a) above, but also the strains within the loading system should be allowed for in a rigorous analysis.

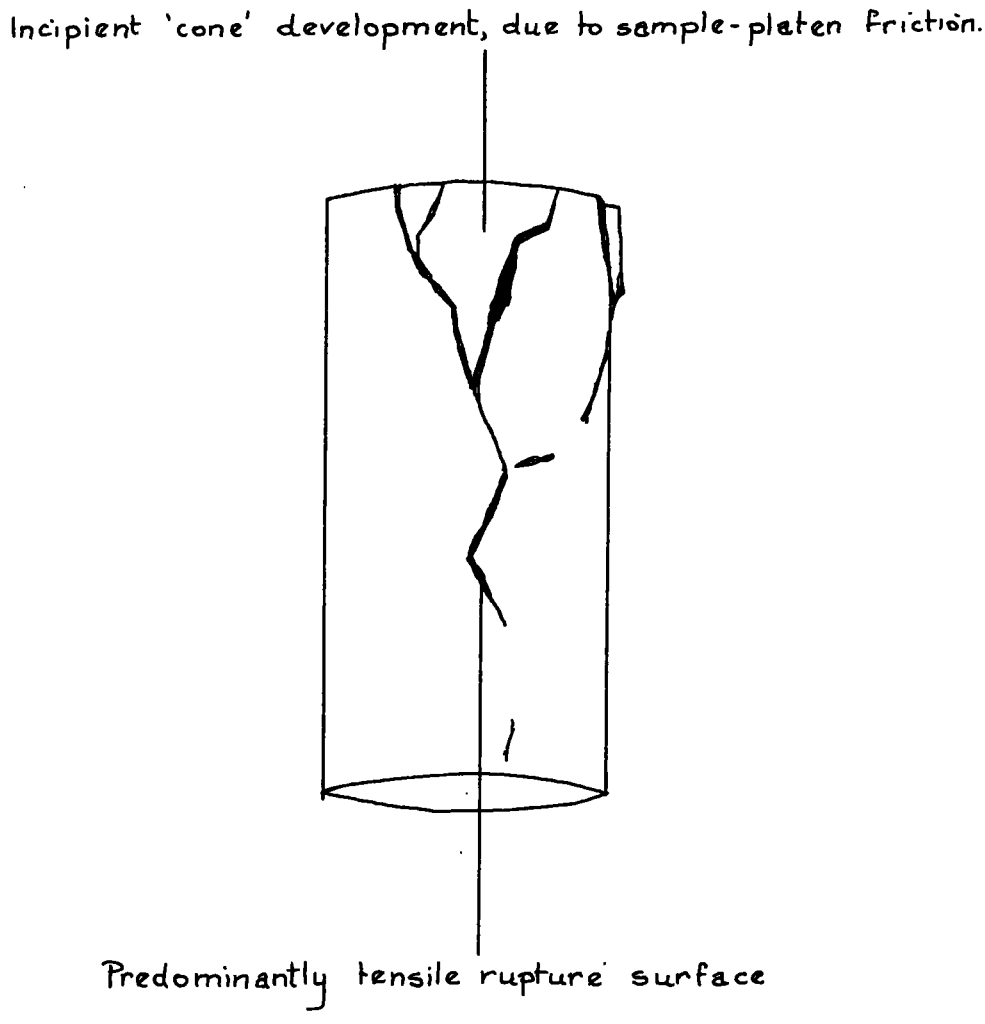

Fig. 2.3. Vertical tensile splitting in unconfined compression test.

(c) Discontinuities and flaws within the sample, if critically disposed (see 1. 2. 3. 2) may result in premature failure utilizing the plane of weakness.

(d) The stiffness of the testing machine can affect the failure, since, when low, energy is fed back into the sample as failure is approached, accelerating the propagation of rupture.

Besides the above, there are more mundane, although very real, experimental difficulties, for example, voltage stabilization, of measuring equipment, mechanical backlash in L. V. D. T. 's, bubbles beneath strain gauges, punctured sheaths, and sample face parallelism.

In conclusion, the compression test requires very diligent preparation of the sample and rigorously controlled testing conditions. Whilst such requirements may be acceptable in the academic study of rock mechanics, it is doubtful if the care and expense are justifiable in many civil engineering circumstances, where an indication of probable en-masse behaviour is wanted.

2. 2. 2. Tensile tests on intact samples

The tensile parameters of a brittle material may be measured by either direct or indirect methods.

2. 2. 2. 1. Direct methods - In these, a tensile stress is applied to the sample, and the deflections and failure stress recorded by methods similar to those outlined above. Sample preparation and the arrangement for transferring the stress are even more important than in the compression test. The simple direct pull experiment which has been employed consists of cementing a $\frac{1}{2}$ ins diameter, 3 ins long cylindrical sample into push-fit steel sleeve holders.

A Hounsfield Tensometer was used, and if the retaining pins are set at 90^{o} to each other, a small amount of out-of-line can be tolerated (Fig. 2.4). Even so, failure is often concentrated near the ends, indicating stress concentrations. Dumb-bell shaped samples have been used (Brace, 1964), designed to limit stress concentrations to the shoulders and larger diameter zones near the platens, and providing uniform stress conditions over the central, waisted area. However, sample preparation becomes more difficult and the method is limited to relatively intact, homogeneous materisl.

2.2.2.2. Indirect methods - The most common indirect method is the Brazilian test, where a sample disc is compressed diametrically inducing tensile stresses perpendicular to the direction of compression (Fig. 2.5). The stress distribution within the disc was computed by Hondros (1959) and Fairhurst (1964) showed that loading should be over a strip angle, $\alpha = \tan^{-1} 1/8$, to ensure a tensile value representative of the whole sample. The tensile stress is calculated from:

$$S_T = \frac{2P}{\pi DL} \qquad (2.9)$$

where P = applied load

D = diameter

L = length or thickness

Trollope (1968) shows that if 'effective' tensile stresses due to Poisson's ratio effects are also considered, then the tensile stress generated perpendicular to the loading axis may be twice as large as predicted by Hondros (op. cit.)

The relationship between the tensile strength and other alternative measures of rock strength has been investigated by Hobbs (1967b) and he demonstrated correlations with compressive strength, irregular lump strength and impact strength index.

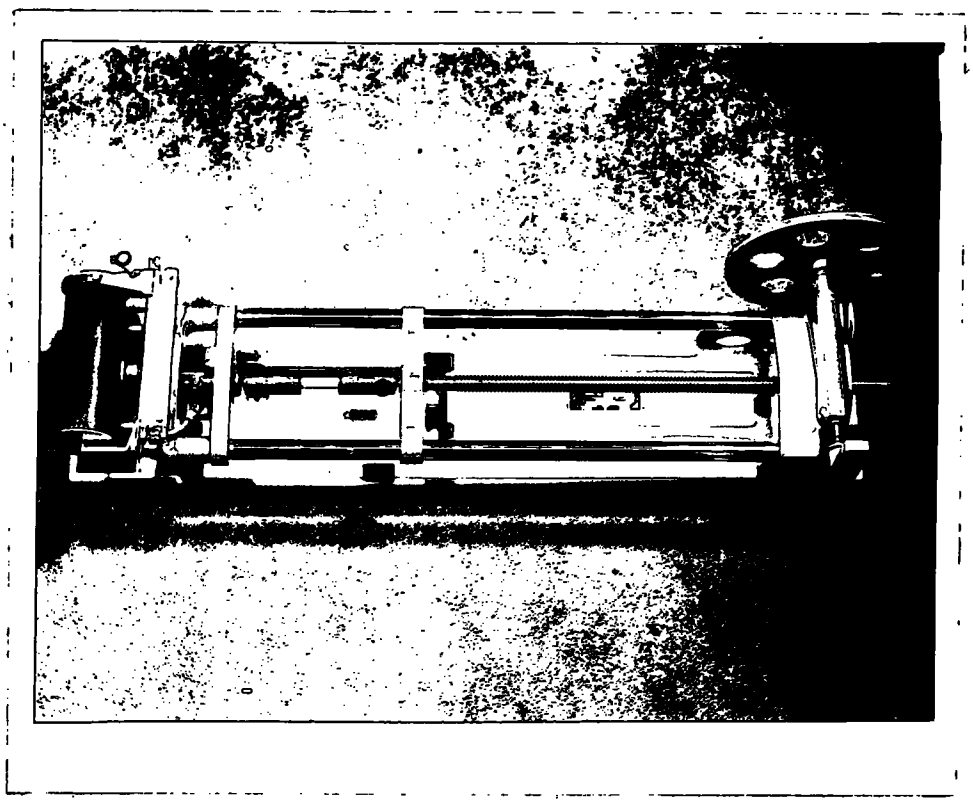

Fig. 2.4. Straight pull tensile test.

Fig. 2.5. Brazillian tensile test.

2. 2. 2. 3. Summary and conclusions - The tensile strength of rock is inherently difficult to measure. In many instances this uncertainty is overcome by a conservative design which treats the rock as a no-tension material. However, for a truly economic design, the benefits afforded by the tensile strength must be included. Either direct or indirect methods may be used, providing adequate care is taken with sample preparation, and all the experimental factors are taken into consideration.

2. 2. 3. Shear strength tests

The shear strength of a rock or soil may be obtained from the triaxial test. However, it is sometimes more convenient to carry out tests which measure the shear strength and frictional parameters more directly. If the Coulomb-Navier failure criterion is assumed operative at low confining stresses, then by measuring the shear stress necessary for failure at various normal stresses, the C and ϕ parameters may be established. The soil shear box represented one of the earliest techniques used for soil mechanics. After going through a period of disenchantment, it has recently returned to favour, especially for the study of long term, ultimate parameters. For most tests on intact rock, however, the normal soil shear box is insufficient. Specially designed machines are required, but they are costly and cumbersome, (Krsmanovic, 1967). A straightforward alternative is the double shear test (see for example, Lundborg, 1966), where an axially clamped cylindrical specimen is sheared in a special jig (Figs. 2. 6, 2. 7). The chief criticism of the test is that the stresses on the failure planes are unlikely to be as simple as that assumed in the analysis. Nevertheless, the method offers many advantages over the standard triaxial test. It is especially useful for separating the frictional and cohesive components, and

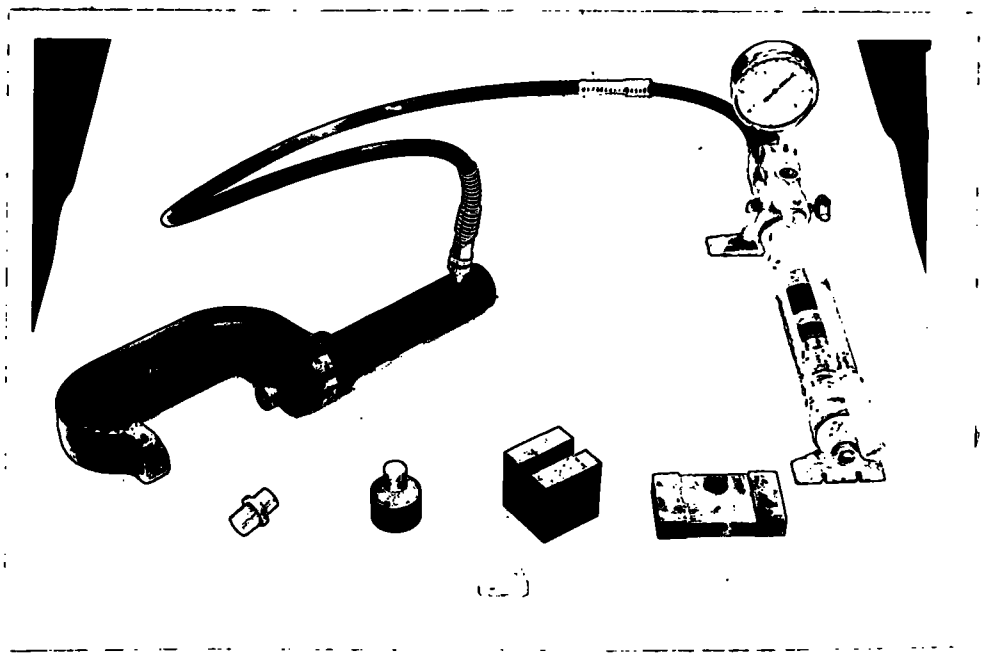

Fig. 2.6. Double shear test: jig components.

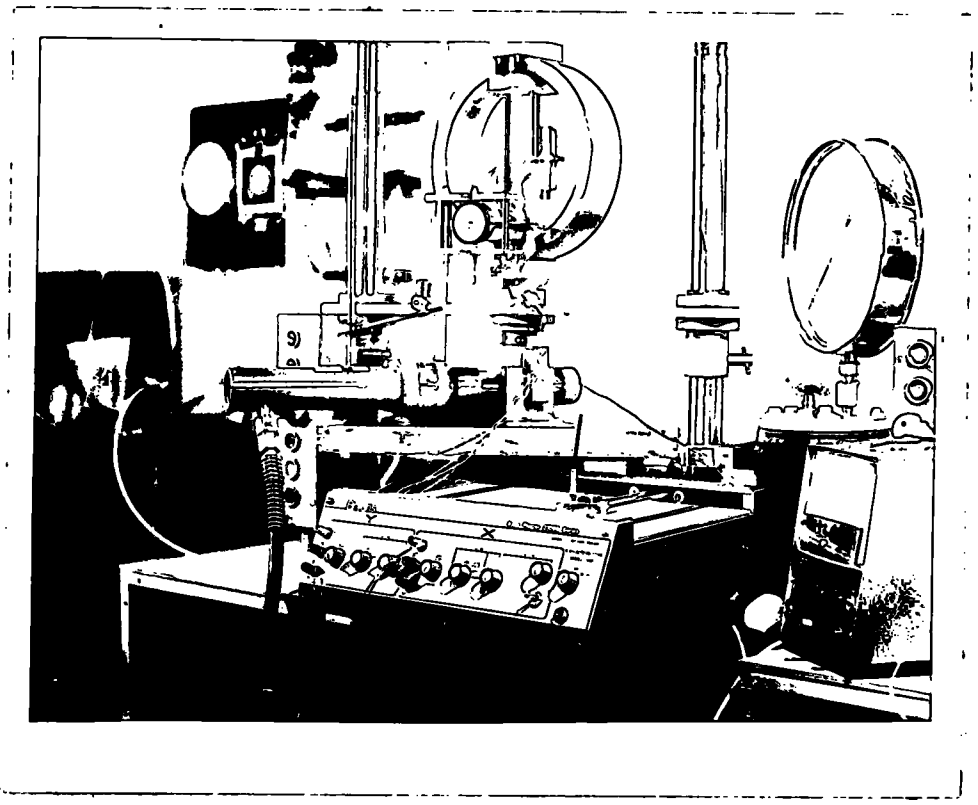

Fig. 2.7. Double shear test arrangement.

for studying the change in the former with increasing strain. Sample preparation need not be precise, and in many cases samples with unfinished ends have been used, with dolomite powder between the ram and sample. The normal pressure was applied by hydraulic jack, and unfortunately stresses below 1000 lb/in^2 could not be accurately applied and maintained. An alternative method would be to use a jig and sample with larger cross-sectional area, or to construct a jack to work of a standard mercury constant pressure unit.

2.2.4. Aggregate tests

These have been carried out for two reasons:

(a) the Magnesian Limestone represents an important source of roadmaking and concrete aggregates, and

(b) intact samples are notoriously unrepresentative of the site from which they are taken; aggregates however should include rock of various grades. By definition, aggregates are formed by mechanical breakdown of larger particles, and their strength is ultimately dependent upon a similar mechanism.

2.2.4.1. Comminution theory - Rock fragmentation theory is important in the study of drilling, crushing and blasting, but is, as yet, incompletely understood. The energy required in comminution is dependent upon the resulting increase in surface area. This represents only a small fraction of the total energy input, the bulk being dissipated as heat (Cheatham, 1968; Harris 1966). A number of empirical laws relating to the size distribution of particles subject to impact have been devised, the best known being the Rosin-Rammler:

$$R = 100ek^{-bx^n} \qquad (2.10)$$

where R = % particles in a sample larger than size x

b = an inverse parameter of size

n = sorting coefficient equal to the slope on Rosin Law probability paper

e = base of natural logs

This means that the size distribution is heavily skewed towards the larger particles. By constructing Rosin Law graph paper (Kittleman, 1964) the goodness-of-fit of an aggregate sizing to the Rosin distribution may be estimated, since the points will then plot on a straight line.

2.2.4.2. Irregular lump crushing strength - This has been employed by a number of workers as an alternative method of assessing the strength of rock (see, for example, Hobbs 1967b). Unfortunately, the method suffers from many drawbacks. The sample size appears to have an effect upon the measured strength (Attewell, personal communication). Whilst the crushing load may be used as a measure of the strength, a more precise figure is obtained if the contact stress is employed. This is most easily calculated by interposing carbon paper and graph paper between the sample and platens, the contact stress being the load divided by the average contact area. Experimentally, difficulties arise in determining exactly the stress at which failure occurs, since progressive crushing and consequent increase in contact area can result in an increase in load but a drop in contact stress. A minimum of twenty lumps should be crushed, and in many cases even this is insufficient to give a statistically meaningful result. The tedious counting of contact squares coupled with the factors noted above make this test of doubtful value.

2.2.4.3. Aggregate impact test - The equipment and procedure for carrying out this test are described in the relevant British Standard dealing with mineral aggregates, sands and fillers (British Standards Institution, 1967). It was found that the results were very susceptible to non-standard conditions, especially with regard to the nature of the base the impacter rests upon. Nevertheless, with careful control, close agreement with two other laboratories (Durham County Council and Tarmac Roadstone, Stockton) for tests using the same aggregate were obtained. The test is only really suitable for material with an aggregate impact value (A. I. V.) of less than 40, since for various soft materials there is but slight change in the A. I. V. An alternative method (Shergold & Hosking, 1963) of using less than 15 blows and normalising the result to 15 blows is erroneous, since it is dependent upon the number of blows delivered. From a graph of the percentage of fines v number of blows (Fig. 2.8) for a typical aggregate it can be seen that the linear portions have relationships of the form:

$$F = mN_B + C_F \qquad (2.11)$$

where F = % fines

m = gradient (constant)

N_B = number of blows

C_F = intersection on the F axis

For the relationship proposed by Shergold et. al. to hold, C_F must be zero, whereas C_F appears to increase as F increases, i. e. as the material becomes softer.

The aggregate impact test thus offers a rapid method of assessing the average strength of the rock from a limited locality. A more detailed knowledge of fragmentation mechanics may result in aggregate tests being used for the assessment of the failure characteristics of the intact material.

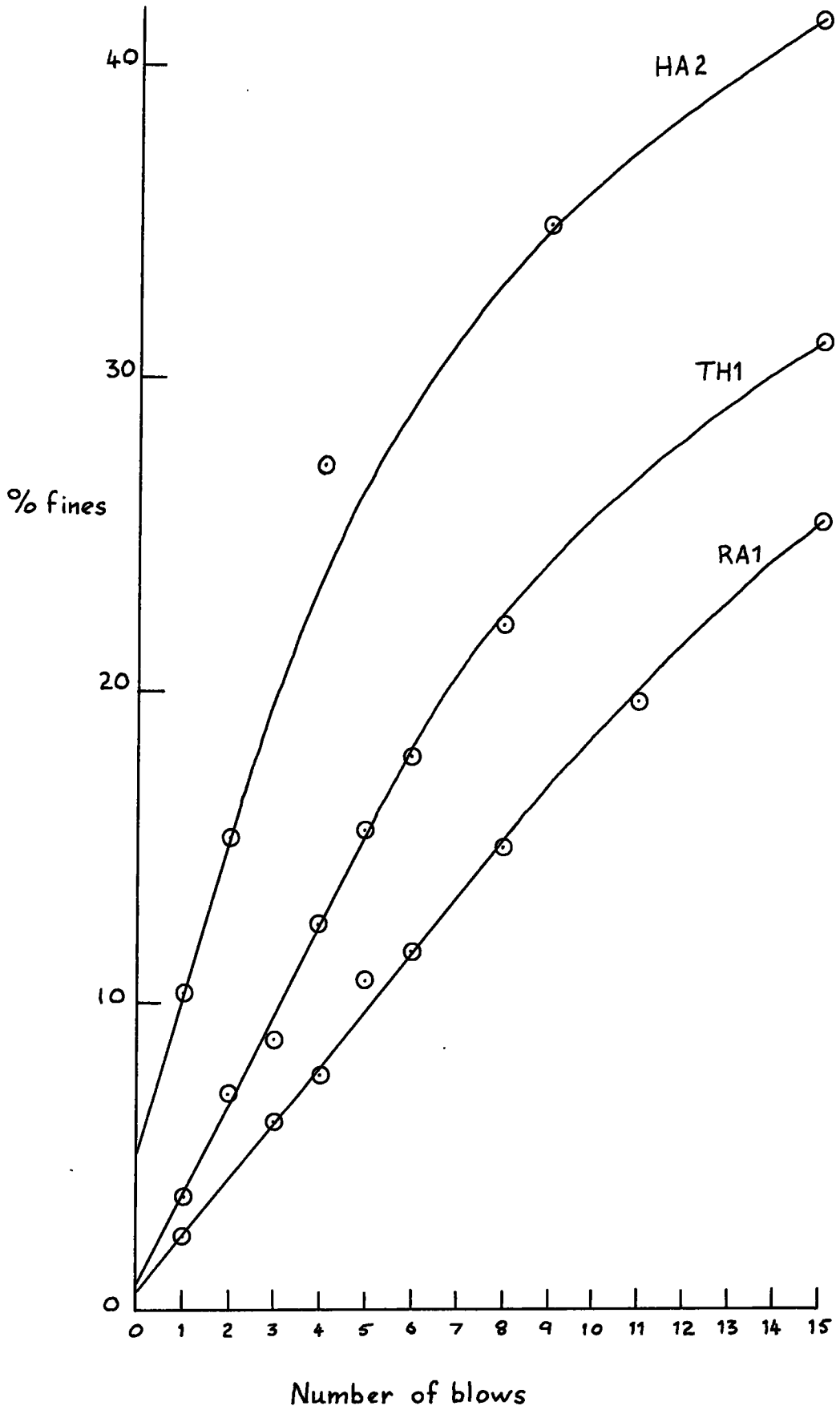

Fig. 2.8. Aggregate breakdown.

2.2.5 Other tests

Standard tests for porosity, specific gravity and permeability were carried out on various samples, and the methods employed have already been outlined (Section II, 2.4.1.), and are detailed in Ackroyd (1964), and in the British Standard on soil testing (British Standards Institution, 1968).

Various hardness indicators have been used in rock mechanics, for example the Shore scleroscope (Obert et. al. 1946), but with a coarse grained and often soft material like the Magnesian Limestone, they have little useful application. However, when the contact area is increased, a more accurate guide may be obtained. This constitutes the basis of the Schmidt rebound hammer (Hucka, 1965; Kolek, 1958). It has the advantage of field portability, and a large number of readings may be accumulated fairly rapidly. Care must be exercised in selecting test reports and it was especially noticeable that quarry faces gave significantly lower readings than large blocks on the quarry floor, attributed to the tendency for the rock to spall parallel to the face and open up fissures, which are accentuated by blasting. With experience, however, an estimate accurate to within $\pm$ 2000 lb/in^2 may be made using only a geological hammer and visual examination, and in many cases this would be within the 95%confidence limits of the Schmidt hammer.

2.3. Results and interpretations

These will be considered in a similar sequence to the above, namely, rheological nature, strength parameters of intact material in compression, tension and shear, and the behaviour of aggregates. Since the lithology is the controlling factor, the relationship with the diagenetic history and the inter-dependence of parameters will be considered. A summary of the main results is given in Table 2.1.

Sample	Horizon	Classification	γ_d lb./ft^3	n %	K cm./sec.	S_c lb./in.^{2}	S_T lb./in.^{2}	σ_3 lb./in.^{2}	σ_1 lb./in.^{2}	E_1 lb./in.^{2}	E_2 lb./in.^{2}	E_3 lb./in.^{2}	ϵ_s %e/lb./in.^{2}	A.I.V.	10% fines	S_c/S_T
BL1	U.M.L.	Slightly impure, pre-diag. dolomite.	152·5	7·3	$1·44\times10^{-6}$	11570	617 (SP)	0		$1·99\times10^6$ (S)	$3·85\times10^6$ (S)					18·75 (SP)
							1842	0	11570	$9·5\times10^5$	$1·5\times10^6$	$1·5\times10^6$	$4·85\times10^{-5}$			6·38
										4×10^5			$1·10\times10^{-5}$			
CH1	M.M.L.	Partly recrystallised calcite dolomite.	151·1	6·4	$6·07\times10^{-6}$	5658		0	8050	2×10^5	$1·75\times10^6$		$2·2\times10^{-5}$			
								0	4125	$7·75\times10^5$	$1·28\times10^6$	$1·78\times10^6$	$1·4\times10^{-5}$			
								0	4800	5×10^5	$1·25\times10^6$		$1·25\times10^{-5}$			
CH2	M.M.L.	Oolitic pre-diag. dolomite	143·3	10·3	$3·7\times10^{-6}$	5275		0	5275	3×10^5	1×10^6	$1·5\times10^6$	$4·48\times10^{-5}$		1·8	
FO1	M.M.L.	Shelly pre-diag dolomite	134·7	22·6	$4·29\times10^{-5}$	1850	360·9	0	1850	$4·5\times10^5$	$7·3\times10^5$	9×10^5	1×10^{-4}	41·8	1·35	5·13
HA1	M.M.L.	Oolitic pre-diag. dolomite		20·9	$2·23\times10^{-4}$	2688	531	0	1628	$2·17\times10^5$	$4·83\times10^5$	7×10^5	$2·5\times10^{-5}$		0·54	5·06
								0	1050	$2·75\times10^5$	$5·75\times10^5$					
								0	1120	$1·4\times10^5$	$5·2\times10^5$					
								0	7250	$3·1\times10^5$	$1·3\times10^6$	$1·63\times10^6$	$3·36\times10^{-5}$			
								0	580	$2·2\times10^5$	$2·9\times10^5$	$5·4\times10^5$	$2·25\times10^{-4}$			
								0	4500	$4·5\times10^5$	$8·3\times10^5$	$1·63\times10^6$	$7·5\times10^{-4}$			
HA2	M.M.L.	Pre-diag. dolomite		23·4	$5·22\times10^{-5}$	2750	433	0	2750	$1·74\times10^5$	$5·8\times10^5$	$6·67\times10^5$		4·2	0·9	6·35
HO1	L.M.L.	Fine grain post-diag. granular dolomite	149	15·5		4574 (mean)	463	0	2750	$1·75\times10^5$	$6·25\times10^5$	$3·25\times10^6$	$1·4\times10^{-4}$	34		5·88
						2490(recalc)		0	4435							
								0	6435							
								0	5124							
								284·4	4896							
								284·4	7666							
								284·4	5041							
								284·4	7481							
								284·4	4835							
								568·8	5787							
								568·8	3708							
								568·8	4818							
								853·2	11238							
								853·2	8869							
								853·2	8104							
								853·2	3229							
								853·2	18651							
								1137·6	9986							
								1137·6	18353							
								1137·6	10738							
								1422·0	17227							
								1422·0	6673							
								1422·0	7998							
								1422·0	11520							
MH5	L.M.L.	Post-diag. dolomite.	159·4	6·2		4000		0	4000	5×10^5	$1·35\times10^6$	$2·2\times10^6$	6×10^{-5}			
MH9	M.M.L.	Gran. pre-diag dol.	139·5	14·4		5850		0	5850	6×10^5	$1·15\times10^6$	$1·5\times10^6$	$7·07\times10^{-6}$			
RA1	L.M.L.	Micrite limestone	158	1·5		12538	843·4	0	8325	$7·75\times10^5$	$4·5\times10^6$			25·3	5·2	14·87
								0	16750	$3·4\times10^5$	$1·65\times10^6$	2×10^6	$2·28\times10^{-5}$			
								284·4	—	$1·15\times10^6$	2×10^6	3×10^6				
								1137·6	—	$1·05\times10^6$	$1·8\times10^6$	$1·95\times10^6$				
TH1	L.M.L.	Pre-diag. dolomite	142·8	18·3		5850	661	0	5850	$6·75\times10^5$	$1·45\times10^6$	$1·75\times10^6$		31·9	3·2	6·24
						4123 (recalc)		284·4	5634	$4·65\times10^5$	8×10^5	$1·63\times10^6$	$2·33\times10^{-5}$			
								568·8	5619	3×10^5	1×10^6	$1·05\times10^6$				
								853·2	9503	$2·6\times10^5$	$1·25\times10^6$	$1·25\times10^6$				
TH2	L.M.L.	Post-diag. dolomitic limestone	164	9·25		13600	790·2	0	13600	$1·3\times10^6$	$1·85\times10^6$	$1·9\times10^6$	$4·17\times10^{-6}$	25·6	4·5	10·12
						8000(recalc)		284·4	11104	7×10^6	$1·25\times10^6$					
								568·8	20369	$2·1\times10^6$	8×10^6	$9·4\times10^6$				
								853·2	22853	1×10^6	2×10^6					
								1137·6	17888	3×10^6	$6·2\times10^6$	$7·2\times10^6$				
TH4	L.M.L.	Post-diag. dolomite	151·9	12·3	$2·76\times10^{-6}$	2950	838	0	2950	$2·1\times10^5$	$3·8\times10^5$	$6·5\times10^5$	$1·4\times10^{-4}$	31·7		3·52
								0	—	$2·49\times10^5$	$6·3\times10^5$	$1·54\times10^6$				
								284·4	6652	$3·2\times10^5$	6×10^5	$9·8\times10^5$				
								568·8	—	$5·3\times10^5$	$9·2\times10^5$	$1·6\times10^6$				
								853·2	—	$3·5\times10^5$	$9·6\times10^5$	$1·46\times10^6$				
TR1	L.M.L.	Pre-diag granular dolomite (some calcite?)	147·2	15·1		12840	600·5	0	11700	7×10^5	$1·75\times10^6$	$2·6\times10^6$	$2·74\times10^{-5}$			17·4
						10449 (recalc)		0	13980							
								284·4	29284	$1·25\times10^6$	$3·1\times10^6$	$3·4\times10^6$				
								284·4	—	$6·75\times10^5$	$3·2\times10^6$	$3·4\times10^6$				
								284·4	20504		$9·45\times10^5$					
								568·8	12569							
								853·2	20683							
								1137·6	21528							
								1422·0	20402							

Table 2.1.

2.3.1. Rheological properties

Measurement of time dependent effects were not carried, and thus elastic parameters form the bulk of the results.

The tangent Young's modulus was measured at three points on the stress-strain curve (Fig. 2.9), using purely visual estimates of tangency, the values for the initial loading (E_1), highest loading (E_2) and highest unloading (E_3) being recorded. Adopting the interpretation of Walsh and Brace (1966), E_3 should represent the intrinsic elastic parameter of the minerals. E_1 and E_2, however, are much more a function of the crack concentration.

As expected, the limestones show a much higher Young's modulus than the dolomites, with E_2 up to 4.5×10^6 lb/in^2 for a micrite limestone from Raisby (RA1) and 8×10^6 lb/in^2 for the partially dolomitised limestone from Thrislington (TH2).

The dolomites show a large variation in E_2 due to crack and voids formed either as primary depositional features, for example oolites, or by dolomitisation. The pre-diagenetic granular dolomites thus show the highest Young's modulus, E_2 being generally greater than 1×10^6 lb/in^2 and even up to 3.2×10^6 lb/in^2 (TR1) under confined conditions. This is attributed to the high degree of interlocking between individual dolomite rhombohedra. Where dolomitised allochems produce a generally open texture, for example, shell debris (F01) or oolites (HA1, CH2), the E_2 values are much reduced to about 5×10^5 lb/in^2. Post-diagenetic dolomitisation reduces the Young's modulus providing it is far enough advanced to produce vughs and cracks, due to the volume decrease. These may be subsequently partially or wholly infilled by

Sample TH1 2V

$\sigma_3 = 284{\cdot}4$ lb./in.^{2}

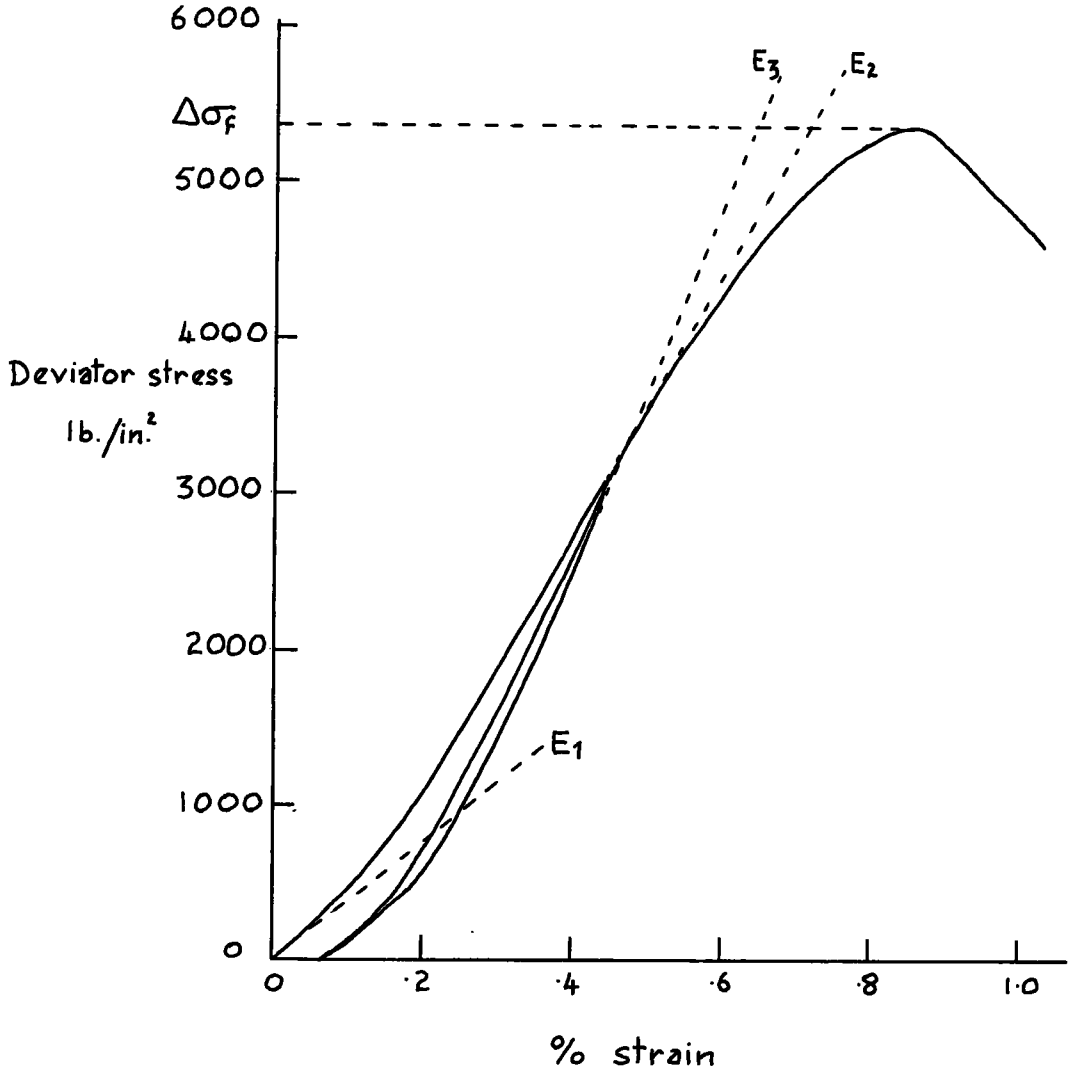

Fig. 2.9. Elastic and strength parameter definitions.

secondary calcite. E_2 for this type of rock varies greatly, from 2.1×10^5 lb/in^2 (TH4) to 1.35×10^6 lb/in^2 (MH5), and is a function of the degree of cracking and amount of infilling.

For most samples, the inherent variability masks any increase in the Young's modulus with confining pressure.

Poisson's ratio was determined for only two samples (BL1 and H01), and showed an average value of 0.2. In the latter there was evidence of an increase from zero to 0.2, which was sustained until the onset of cracking, when the lateral strain rose rapidly, presumably due to the gauge being cemented across an incipient fracture.

The pseudo-plastic component in the rheological nature was estimated from the permanent set (% strain) per lb/in^2 (ϵ_s) produced during cyclic loading to approximately half the failure stress. From the plot of log ϵ_s v log E_2 (Fig. 2.10) there is a poorly defined negative trend. This is as expected, since the amount of permanent set induced in a sample is a function of the crack concentration, which also largely controls the recorded Young's modulus.

The elastic and pseudo-plastic parameters thus appear to be controlled principally by the crack and/or pore concentration of the rock, which is, in turn determined by the depositional environment and subsequent pre-diagenetic and post-diagenetic changes.

2.3 2 Compressive strength parameters

The unconfined compressive strengths (S_c) show a wide variation from 580 lb/in^2 (HA1) to 16,750 lb/in^2 (RA1). It is quite likely that there is a sampling bias towards the more intact and therefore stronger material, and thus the distribution of values depicted is doubtless optimistic.

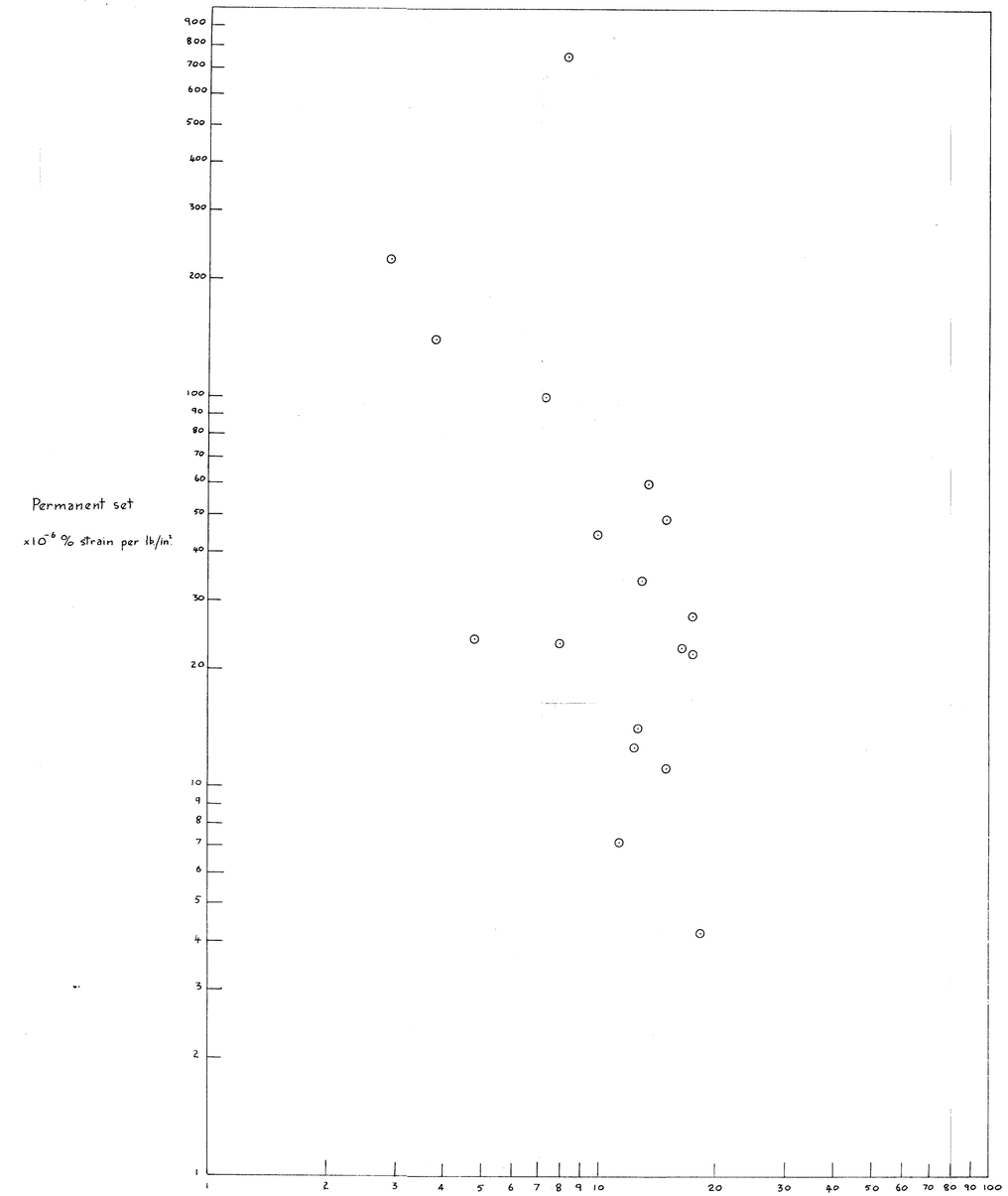

Fig. 2.10. Permanent set v Young's modulus

As with the rheological parameters, the dominant factor is the lithology. Where there is little or no dolomitisation the strengths are highest (RA1, TH2). Post-diagenetic dolomitisation (TH4, H01), however greatly reduces the strength to about 5000 lb/in^2, principally because of the formation of vughs and cracks. The strength of pre-diagenetically dolomitised material is mainly a function of the absence or presence and nature of the allochems. The oolitic material is often so weakly cemented that there is no core recovery at all during drilling. Outcrops of this material are rare, being limited to quarries and cliff sections. Nevertheless, samples of the more resistant material have been obtained and tested, and show a variation of unconfined compressive strength from 580 lb/in^2 to 7250 lb/in^2, the latter being exceptional. Shelly allochems (F01) have a similar effect, and for this type of lithology an unconfined compressive strength of 1850 lb/in^2 has been recorded. Where pre-diagenetically dolomitised material does not contain allochems, strengths up to 13980 lb/in^2 (TR1) may be obtained, but it is probable that for the majority of samples (TH1, MH9) the crushing strength is approximately 5000 lb/in^2.

Triaxial tests up to 10,000 lb/in^2 have only been carried out on one sample, TH1 (Welham, 1969). Confining pressures up to 1400 lb/in^2 however, have been employed for a number of samples, but in general, the results are unsatisfactory due to large sample variability and end effects. The Mohr envelope cannot be constructed from the principal stress circles since it is impossible to gauge visually the best fit tangent. However, if ϕ' is assumed constant over the range of confining pressures used, then a $p_f - q_f$ plot and linear regression line may be employed. The cohesion and friction angle are simply obtained from a and by:

$$\phi' = \sin^{-1} \tan \alpha \qquad (2.12)$$

$$c = a/\cos \phi' \qquad (2.13)$$

Another advantage of this method of assessing results is that an improved estimate of the unconfined crushing strength can be made, utilising all the test points. Thus for ϕ' constant:

$$S_c = \frac{2c \cos \phi'}{1 - \sin \phi'} \qquad (2.14)$$

and substituting from above:

$$S_c = 2a/(1 - \tan \alpha) \qquad (2.15)$$

This value may then be used to normalize the data (see later).

The c-ϕ' parameters obtained from the test appear unreliable because the cohesion intercept is so susceptible to small changes in ϕ' when the latter is greater than 50^o. Nevertheless, the indications are that the silt grade dolomite TH1 is much lower in strength than the post-diagenetic calcite-dolomite TH2. The post-diagenetic dolomite H01, however, shows a relatively high friction angle, but very low cohesion. In fact the latter is less than the Brazilian tensile strength, indicating that the cohesion has probably been underestimated for the reasons outlined above.

Despite these difficulties and errors in assessing the compressive strength parameters, the underlying influence of lithology and the effects of dolomitisation upon the strength may be recognized.

2. 3. 3. Tensile strength parameters

These generally employed the Brazilian test on solid discs, and unless otherwise stated, represent rupture planes perpendicular to the bedding. Straight pull tests produce much lower values, and the results of the two methods are not comparable.

The tensile strengths show a similar variation to the crushing strengths, ranging from 361 lb/in^2 for shelly, dolomitised reef limestone (F01) to 843 lb/in^2 for undolomitised limestone (RA1). The relatively smaller range is probably due to the existence of micro-flaws in even the most compact rock, the effect of which is to drastically reduce the tensile strength.

2.3.4. Shear strength parameters

These may be determined from the triaxial test (q. v), or more directly from the double shear test. Investigations by Welham (op. cit.) using sample TH1 show a reasonable match between the failure envelopes at normal stresses up to 10,000 lb/in^2, above that, the decrease in ϕ exhibited in the triaxial test was not apparent in the double shear test, which continued to show brittle-type failure. The results of triaxial and double shear tests on TR1, (Fig. 2.11) show a lower c - ϕ envelope for the latter for which c = 3096 lb/in^2, $\phi = 38^o$ compared with c = 1559 lb/in^2, $\phi = 57^o$ for the triaxial test. Tests on samples too soft to allow adequate preparation for triaxial tests may be undertaken (viz. WI1, OB1). ϕ values for these materials are very greatly reduced at normal pressures above 2000 lb/in^2 to about 25^o (Fig. 2.12) which compares closely with the polished value for TH1 (Welham, op. cit.)

The double shear test and the triaxial test do not give closely comparable results; the former emphasising cohesion, the latter high friction angles as being primarily responsible for strength. Shear box tests on Magnesian Limestone aggregate (> 200 and < 7 mesh) show a peak ϕ_p of 45^o degrees, and an ultimate ϕ_u of 38^o (Turner, 1967), and shear box tests on Carboniferous Limestone reveal similar parameters (Edwards, 1969). Drained triaxial and shear box tests on a Magnesian Limestone waste slurry show friction angles

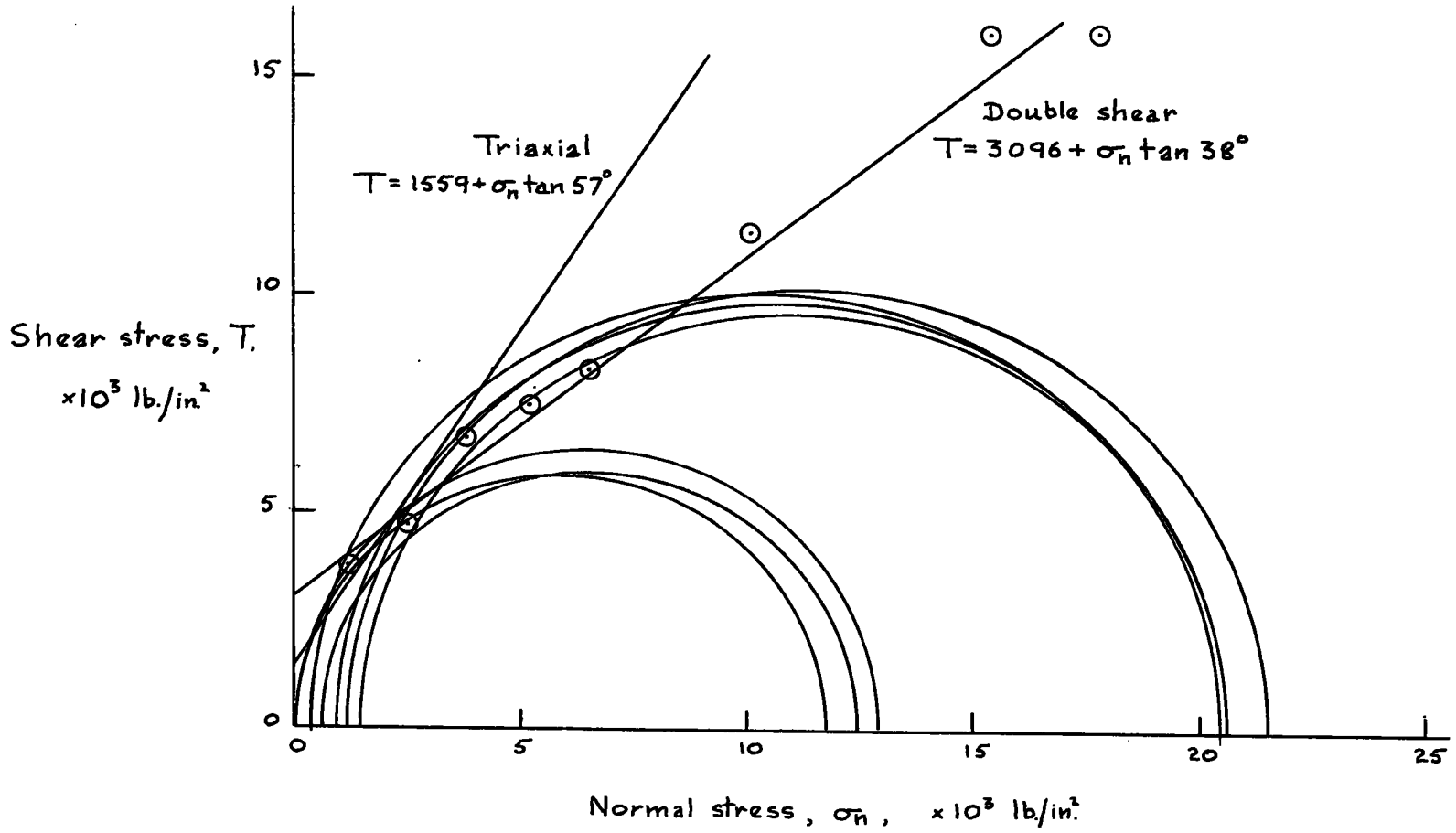

Fig. 2.11. Triaxial and double shear results for sample TR1.

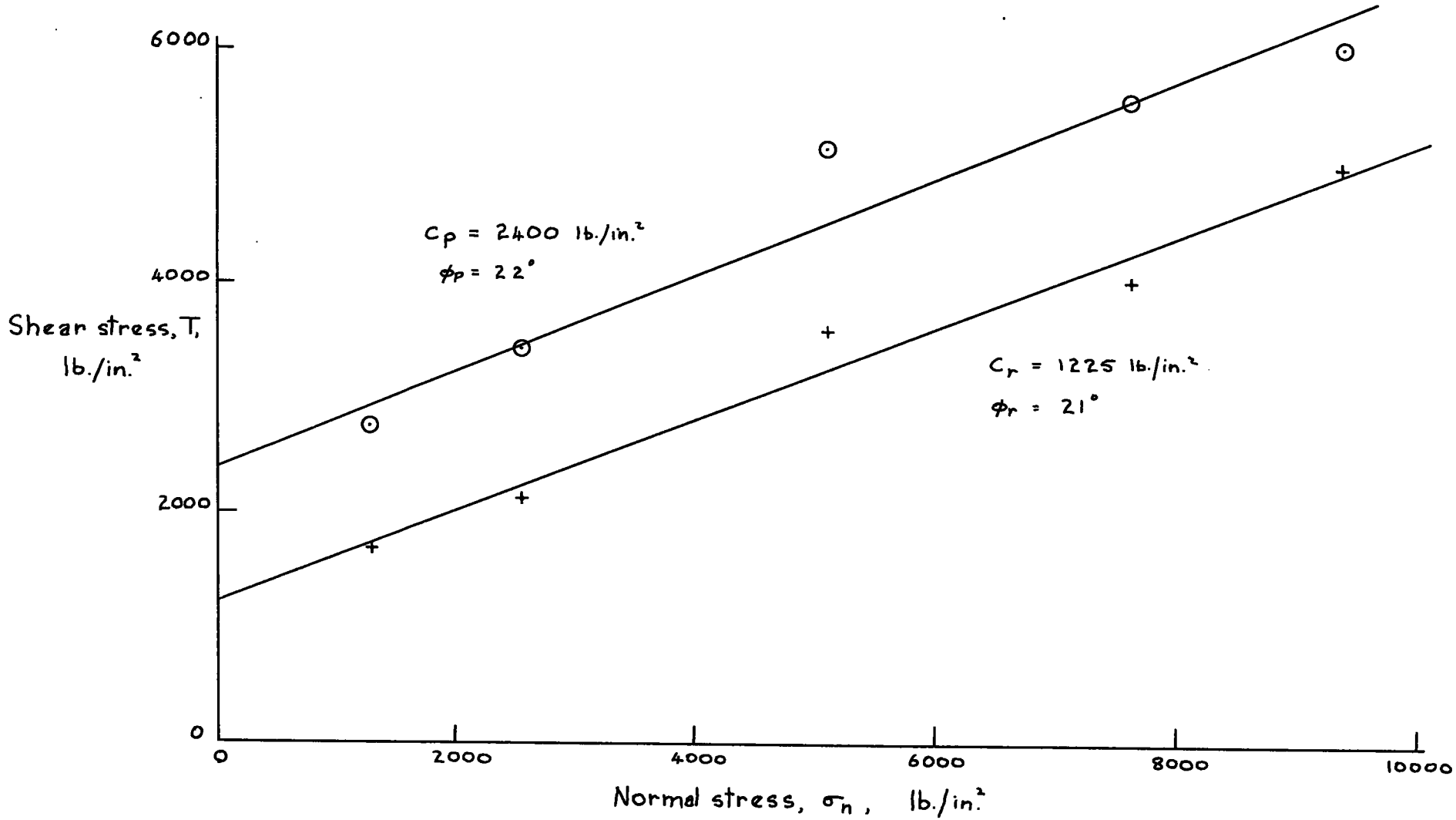

Fig. 2.12. Double shear test, sample WI1.

ϕ_p of 45^o and ϕ_u of 38^o (Wild, 1969). A value of 38^o for the ultimate friction angle would thus appear to be realistic on the basis of a number of independent assessments. The variations in strength between various samples are thus due principally to a change in the cohesion, although the friction angle does decrease with increasing normal pressure and decreasing grain size, to about 25^o. Since asperity influence is reduced for very fine grained material or polished samples (Byerlee, 1967; Patton, 1966), the ϕ value so obtained may be close to the intrinsic friction angle of the dolomite grains.

2.3.5. Aggregate tests

Irregular sample crushing tests were carried out on some samples, the results being expressed in arbitrary stress units. The test appears to be very insensitive to variations in the compressive strength.

Sample	Compressive strength (lb/in^2)	Irregular sample crushing strength (arbitrary units)
TH1	4123	5.99
TH2	8000	7.39
TH4	2950	5.73
RA1	12538	6.09

2.3.5.1. Aggregate impact test - This was carried out in accordance with British Standard Specification BS 812 (op. cit) . For hard material, the A.I.V. is expressed as the percentage fines produced by 15 blows, but for softer materials this is unsatisfactory. The blow-by-blow breakdown of various aggregates was therefore investigated. A comparison between the breakdown for hard (RA1) and softer (TH1, HA2) aggregates (Fig. 2.8), shows

that for the former, the breakdown is fairly linear, even up to 15 blows. However, the relationship becomes increasingly curved with softer materials. The suggested method of Shergold and Hosking (op. cit) for recalculating a modified aggregate impact value is therefore unsatisfactory.

A study of the grading and its change for different numbers of blows showed that after an initial accentuated skewness due to starting with single size particles, the subsequent grading closely approximated the Rosin distribution (Figs. 2.13, 2.14). The effect of increasing the number of blows was to produce more fines, but a similar distribution relationship was maintained. Different materials naturally yielded different graphical relationships, but they all appeared to belong to the same family of curves. Thus a particular grading attained from 15 blows on MA1, only requires 8 blows on F01.

Assuming that there is a constant partition of energy used for breaking down the sample, to energy expended within the system, the number of blows required to produce a particular grading should be proportional to certain physical parameters of the material, such as the surface energy, and hence the crushing strength.

Since all materials pass through similar gradings for various numbers of blows, a particular grading may be defined by only one point. The '10% fines' has been chosen since this is already employed in the aggregate crushing test, and the 10% fines value is therefore given by the interpolating of the number of blows required.

The standard aggregate impact values were determined for various samples, and showed a marked increase upon dolomitisation. Thus for the sequence undolomitised, partially dolomitised and completely dolomitised afforded by RA1, TH2, TH4, corresponding A. I. V. 's were 25, 26, 32. As the grain size of granular dolomite increases to silt grade, there is a further

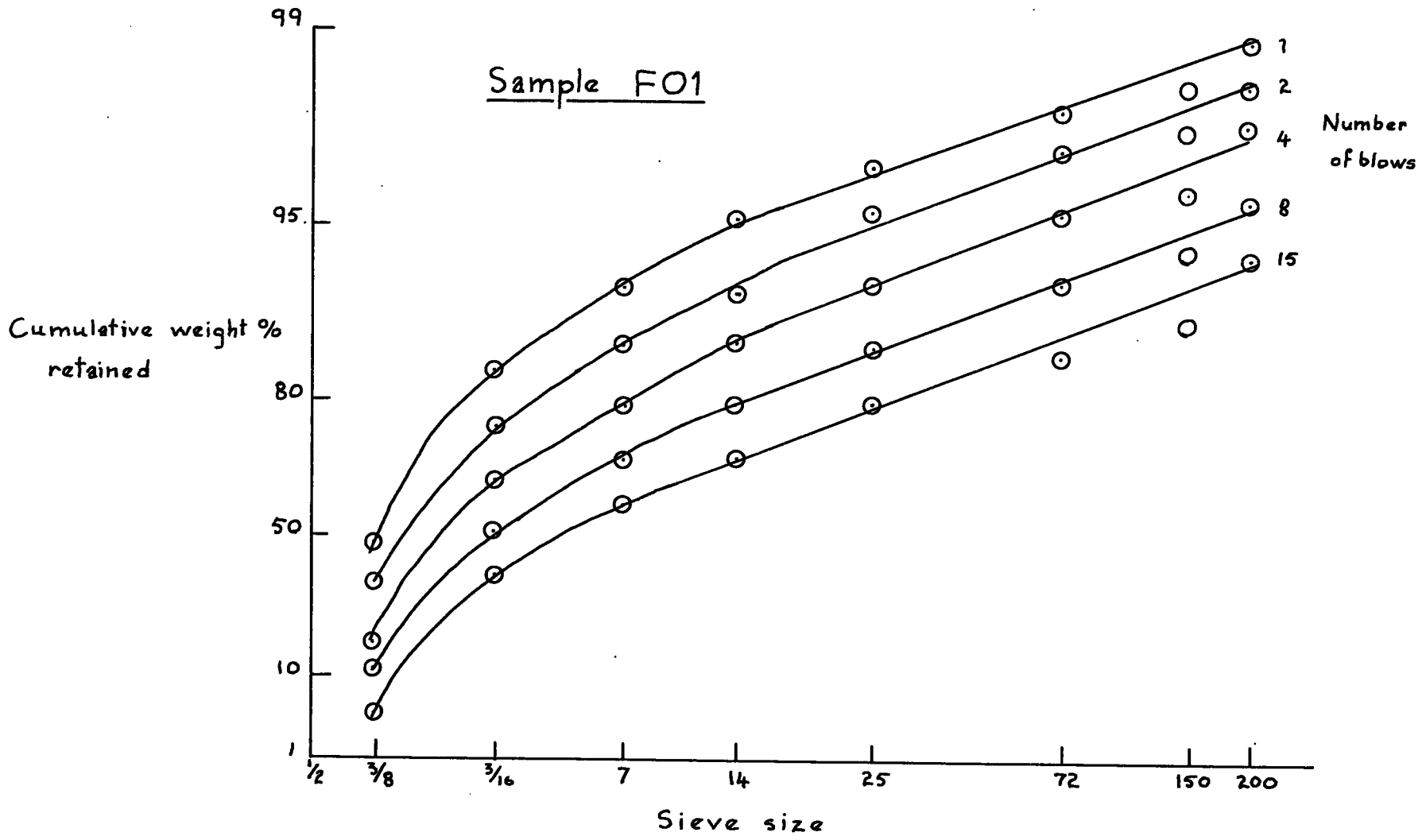

Fig. 2.13. Aggregate breakdown gradings.

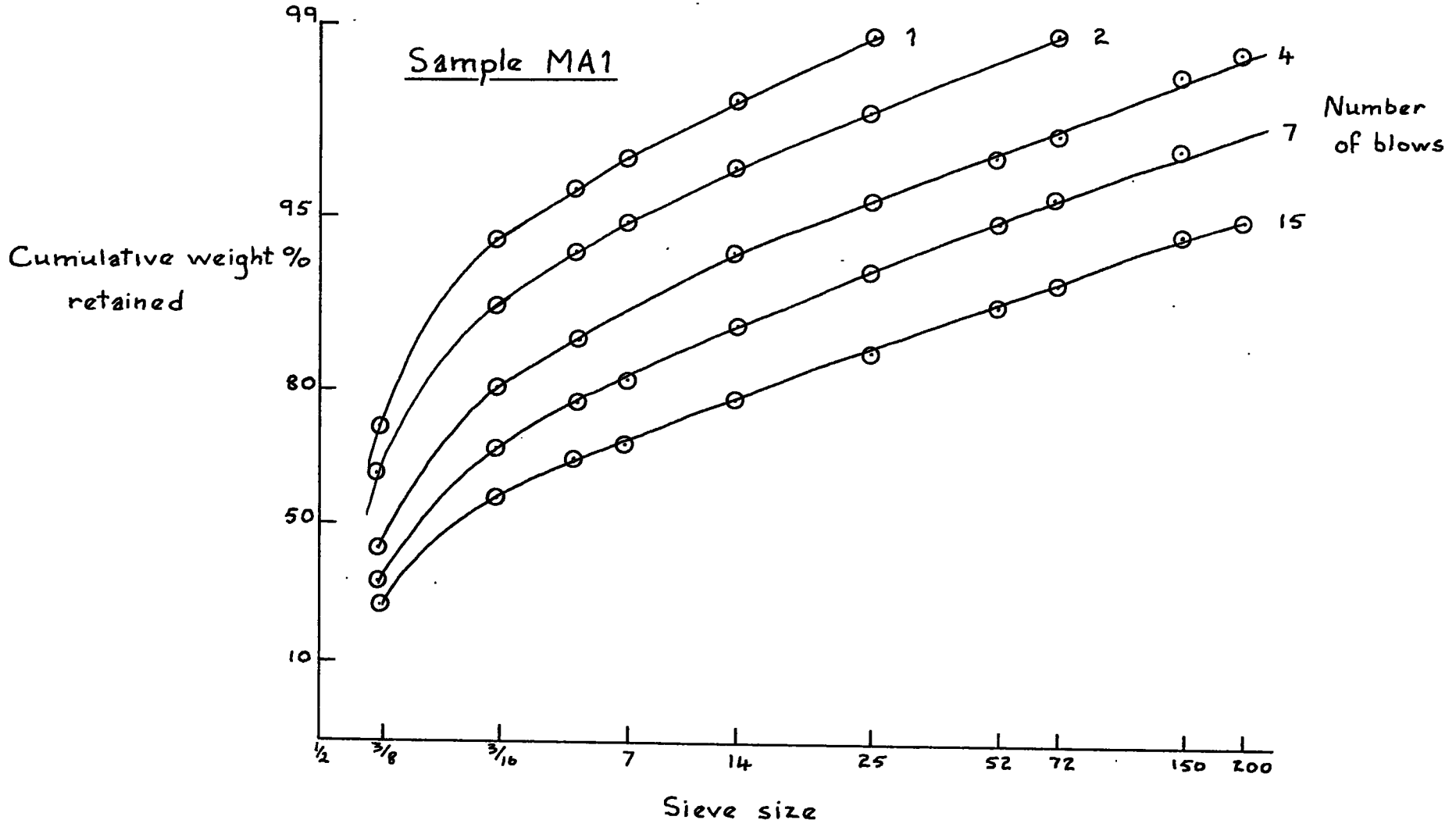

Fig. 2.14. Aggregate breakdown gradings.

drop to 35 (TH1). Where allochems are held by a weak dolomitic cement (F01, HA1) the A. I. V. is commonly greater than 40.

2.4. Inter-relationships

As has been hinted in the above consideration of results, there are often distinct relationships between different measurable parameters. Since the most fundamental is the unconfined compressive strength, it is not surprising that many parameters exhibit a linear plot with S_c as abscissa, employing either linear-linear or log-log scales. Where possible, the parameters obtained from the same sample are compared.

2.4.1. Correlations with the unconfined compressive strength - These include intrinsic, rheological, strength and aggregate parameters.

2.4.1.1. Porosity v S_c - This linear-linear plot (Fig. 2.15) exhibits the expected decrease in strength with increase in porosity. The linear regression line, however, shows a low correlation coefficient and the relationship can hardly be described as more than a trend. In many cases, average points were plotted: by dividing the samples into their petrographic units and considering each sample tested separately, a closer correlation may be obtainable.

2.4.1.2. Young's modulus v S_c - The E_2 value was taken as being most characteristic of the material. For a particular sample (e.g. HA1) the increase in Young's modulus shows very good linearity with S_c (Fig. 2.16). However, when all rock types are plotted, there is a far greater scatter (Fig. 2.17). In particular, the linear trend exhibited for low compressive strengths is not continued for $S_c > 10000$ lb/in^2. This is possibly a reflection upon the errors inherent in the method of measurement (cf Section 2.2.1.3) which would attain greater proportions as the sample Young's modulus increases. It is interesting to note that the E_2 value deduced from

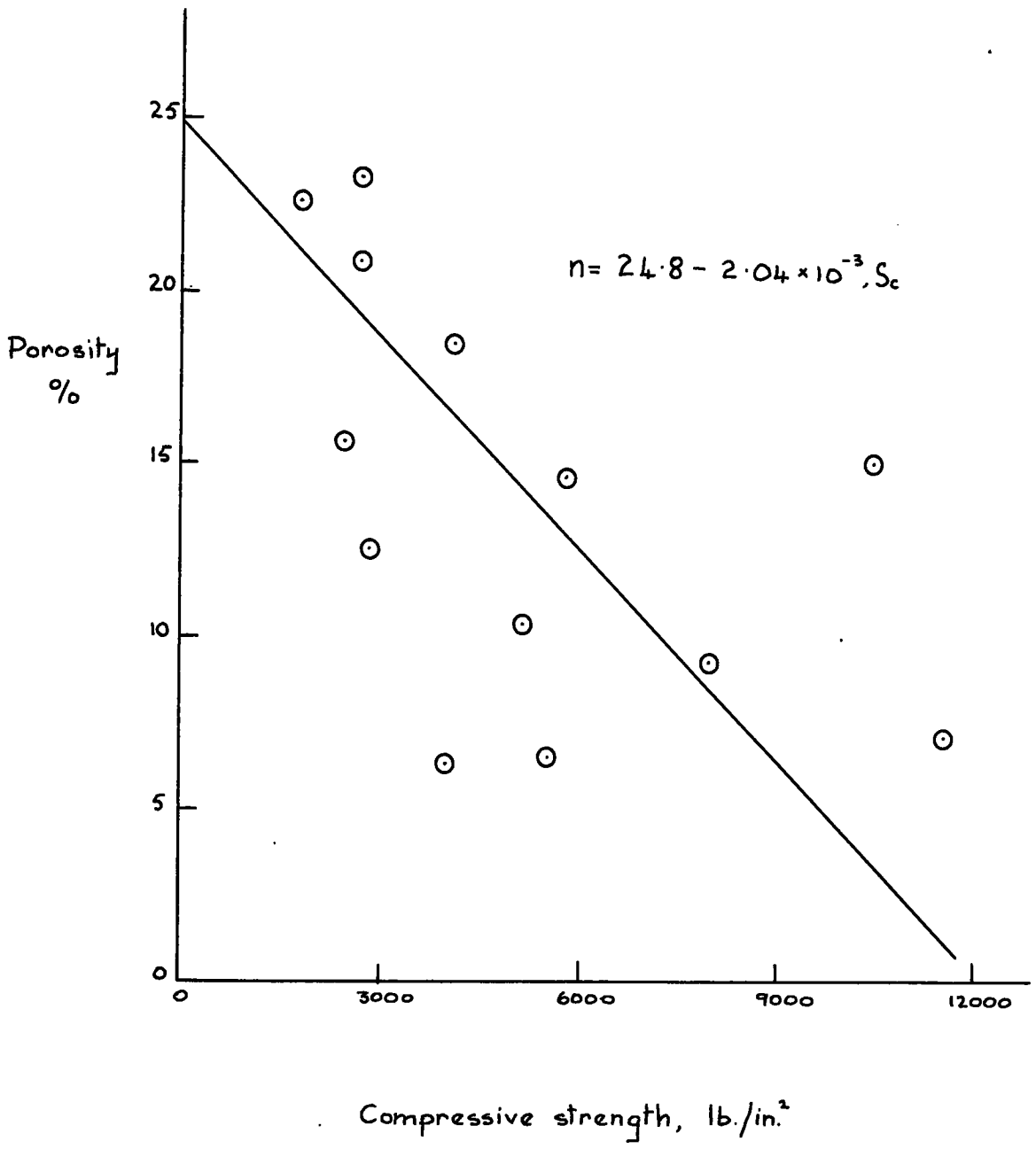

Fig. 2.15. Porosity v compressive strength.

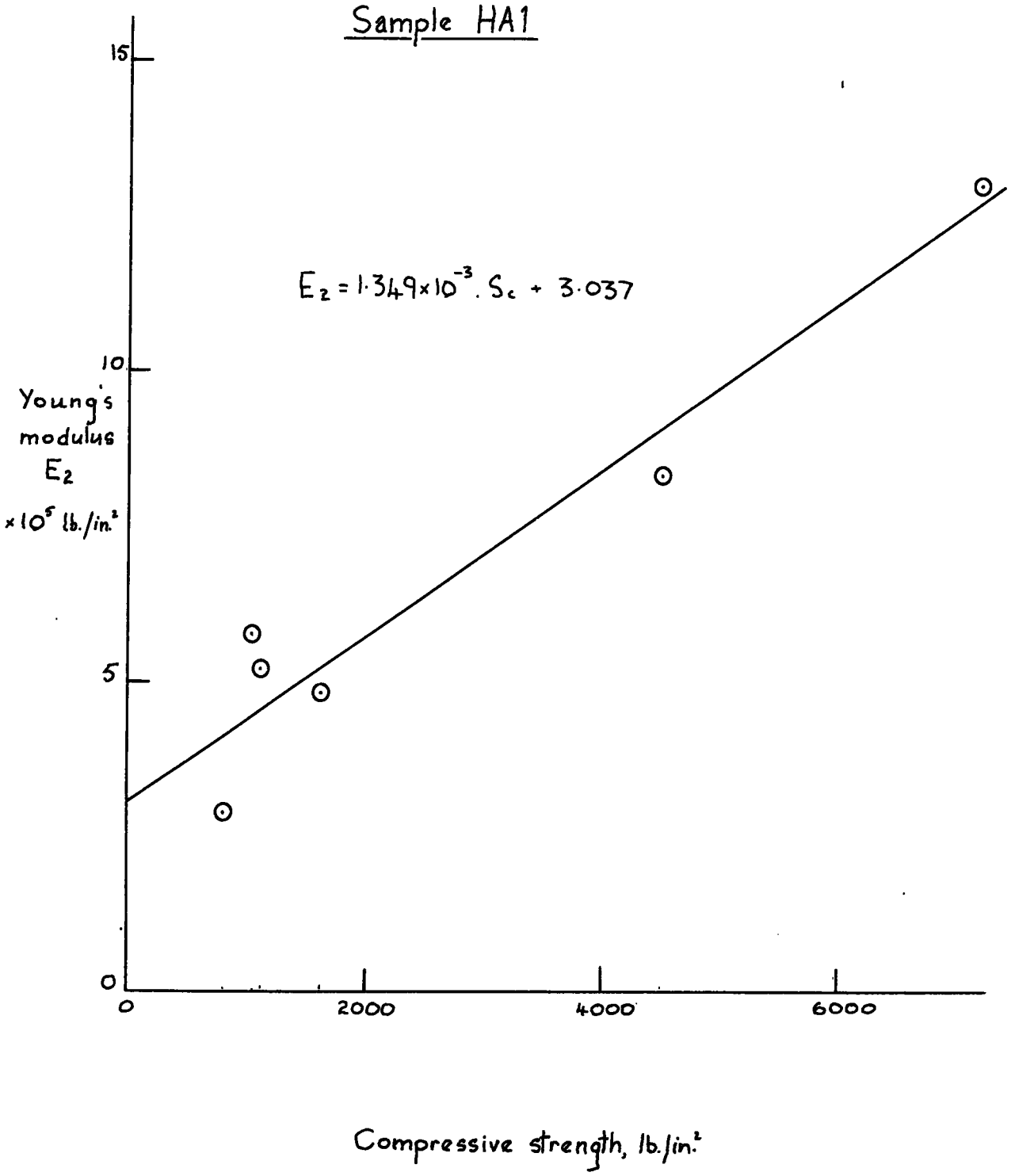

Fig. 2.16. Young's modulus v compressive strength.

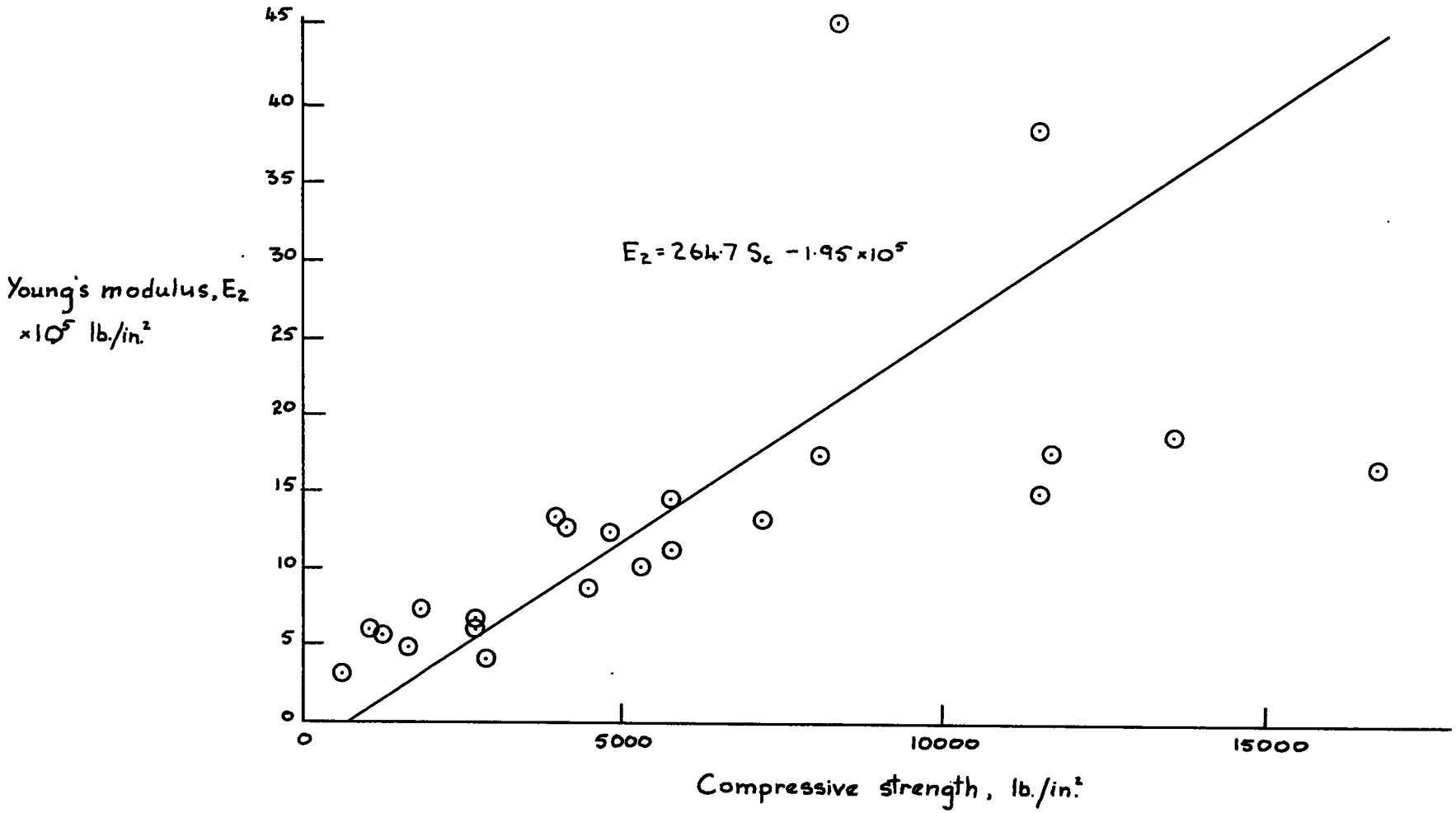

Fig. 2.17 Young's modulus v compressive strength.

strain gauge methods for BL1 is more in line with the expected trend than the corresponding point from L. V. D. T. measurements. The relationship for all measurements is given by:

$$E_2 = 264.7\ S_c - 1.95 \times 10^5 \qquad (2.16)$$

2.4.1.3. Compressive to tensile strength ratio v S_c - For this particular graph (Fig. 2.18) only tensile strengths determined by the Brazilian method were included. The more competent materials with $S_c > 8000$ lb/in^2 show a S_c/S_T ratio of approximately 10. The weaker rocks have a considerably reduced S_c/S_T ratio, generally 6 or below.

2.4.1.4. Aggregate strength parameters v S_c - The aggregates used in this limited study were often bulk samples taken from quarry stockpiles. For a rigorous investigation of this interrelationship the compressive strength samples should be cored from a block which is then crushed to produce the aggregate for comparison. The '10% fines' v S_c relationship appears to be linear (Fig. 2.19), compared with the A. I. V. v S_c which is probably exponential or second order (Fig. 2 20). Thus as noted before on deductions from comminution theory, the '10% fines' value is a better indicator or the relative strengths of rocks than is the aggregate impact value.

2.5. Normalised parameters

The linear relationship of most parameters with the unconfined compressive strength, enable this value to be used to normalize other measured parameters. The ultimate objective of this is that for a given rock type, a range of likely values for particular parameters may be considered in a preliminary design, without the need for expensive testing.

Using Hoek's (1968) conclusion (considered in Section 1.2.2.4) that the empirical failure envelope for sandstones may be determined from a plot of

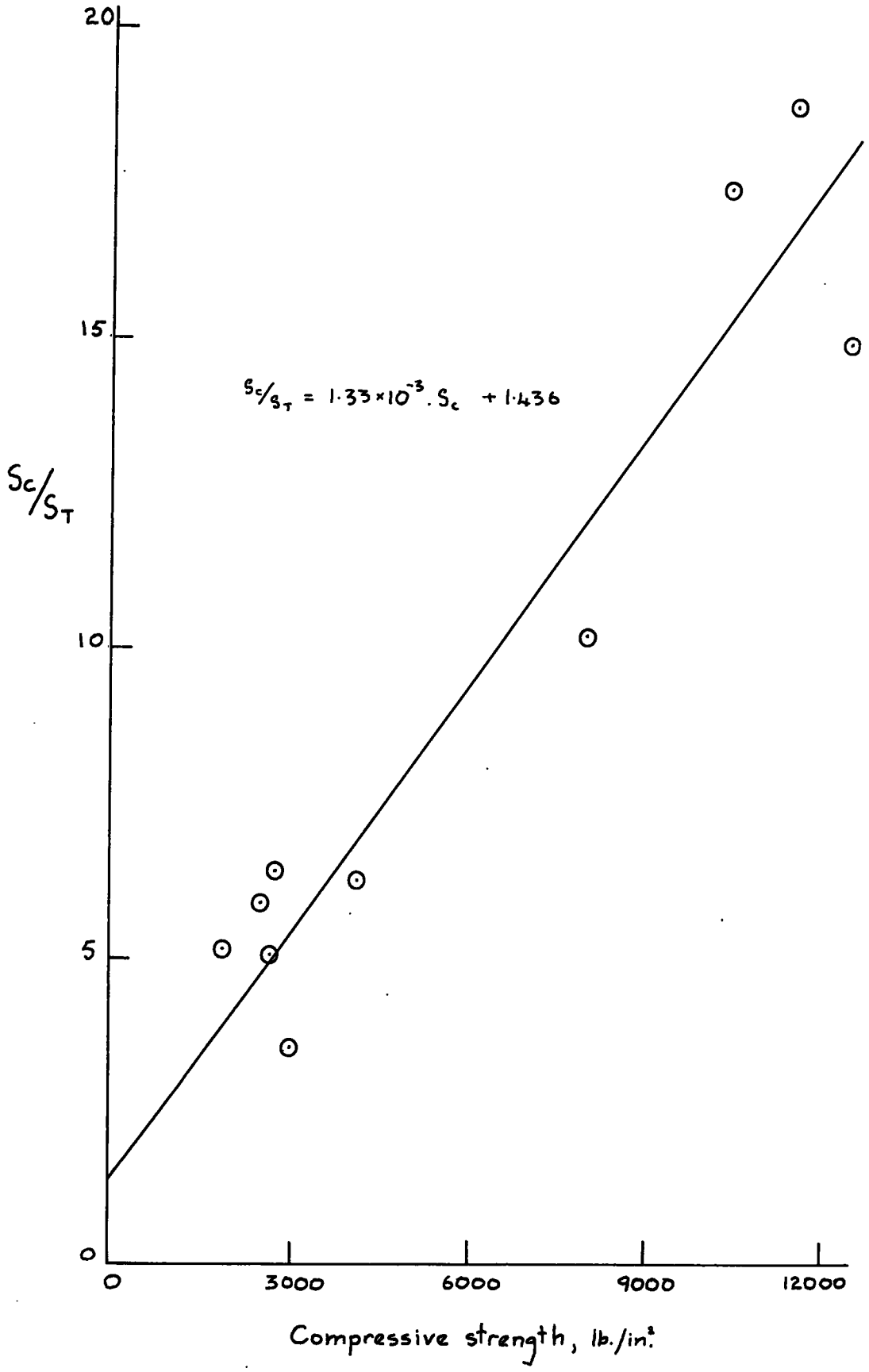

Fig. 2.18. Compressive to tensile strength ratio v compressive strength.

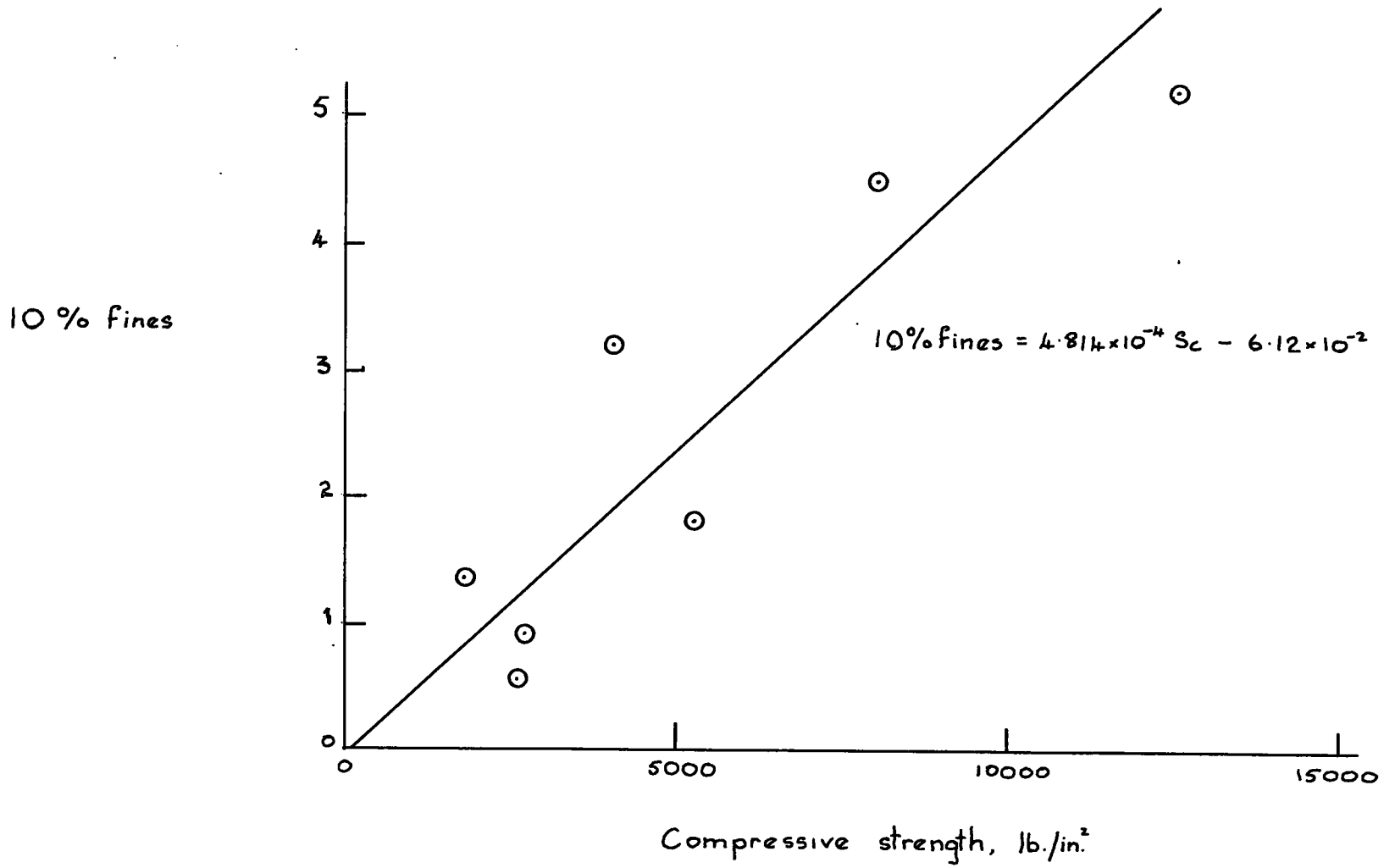

Fig. 2.19. 10% fines v compressive strength.

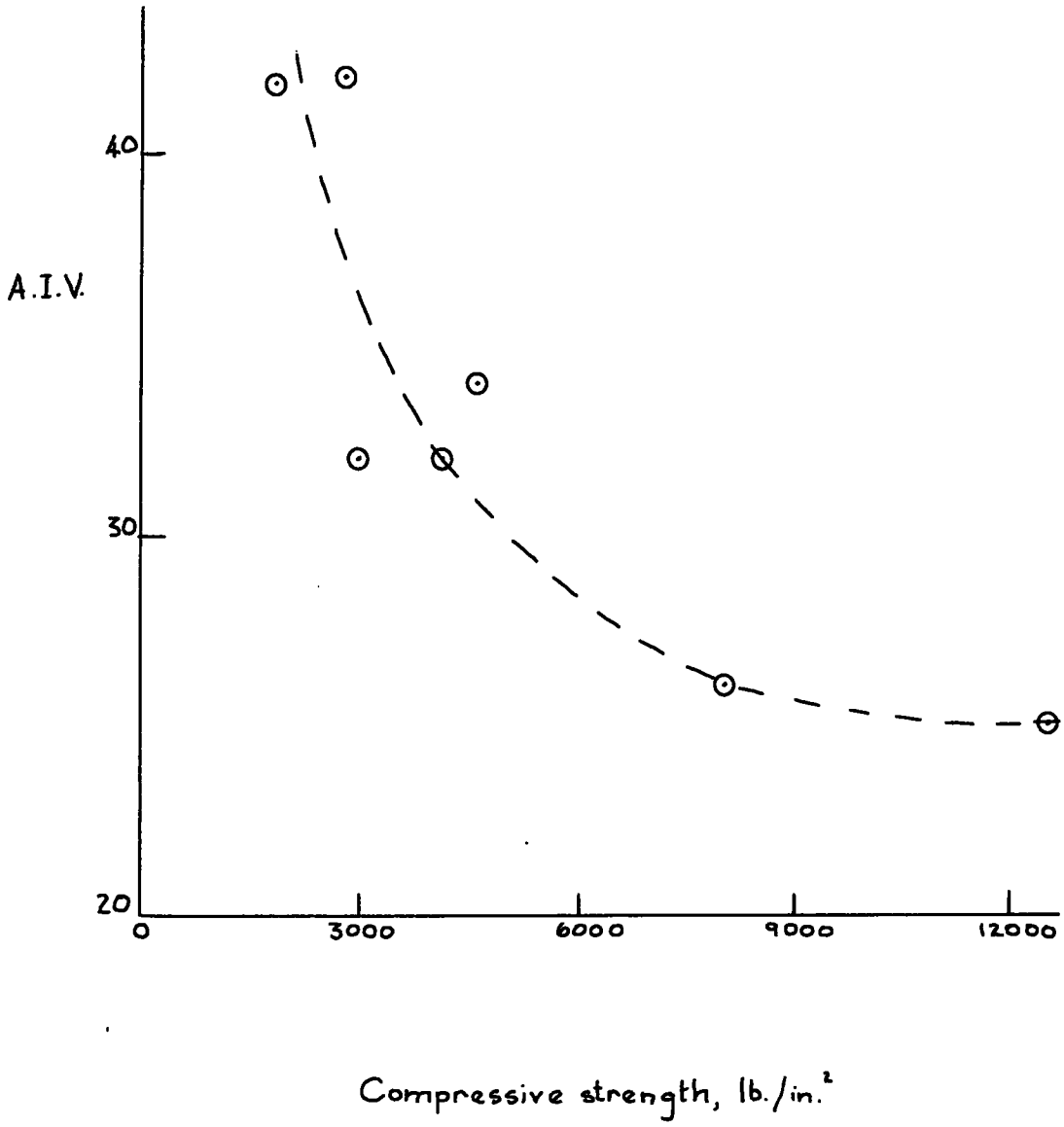

Fig. 2.20. Aggregate impact value v compressive strength.

$\log (p_f/S_c)$ v $\log((q_f - a)/S_c)$, the corresponding graph for Permian dolomites and limestones is given in Fig. 2.21 and follows the relationship:

$$q_f/S_c = 0.07933 + 0.7839\ (p_f/S_c)^{1.0672} \qquad (2.17)$$

Since an exponent greater than unity is invalid (it would imply that the Mohr envelope was convex to the σ_n axis), a linear relationship must be assumed. This enables q_f/S_c v p_f/S_c to be plotted (Fig. 2.22), for which the equation is:

$$q_f/S_c = 0.8510\ p_f/S_c + 0.0218 \qquad (2.18)$$

From this, $\phi = 58.5^o$ and $c/S_c = 0.0416$. The average envelope for low normal stresses is thus given by:

$$T = \tan 58.5^o + 0.0416\ S_c \qquad (2.19)$$

The normalised principal stress circles and envelope are shown in Fig. 2.23.

2.6. Summary and conclusions

A variety of laboratory tests was carried out on the Magnesian Limestone, and the results provide information about the tests themselves, as well as furnishing rheological and strength parameters for the different lithological types. The uniaxial and triaxial compression tests require extremely careful sample preparation for the results to be completely meaningful. Since economic considerations generally preclude such an approach, the results obtained from a greater number of more loosely conducted tests must be correspondingly treated on a statistical basis to obtain meaningful parameters. Amongst the other methods used for assessing rock strength, the double shear and aggregate tests appear to offer the greatest potential.

By treating all the triaxial test results statistically and normalizing the parameters with the unconfined compressive strength, a 'grand average'

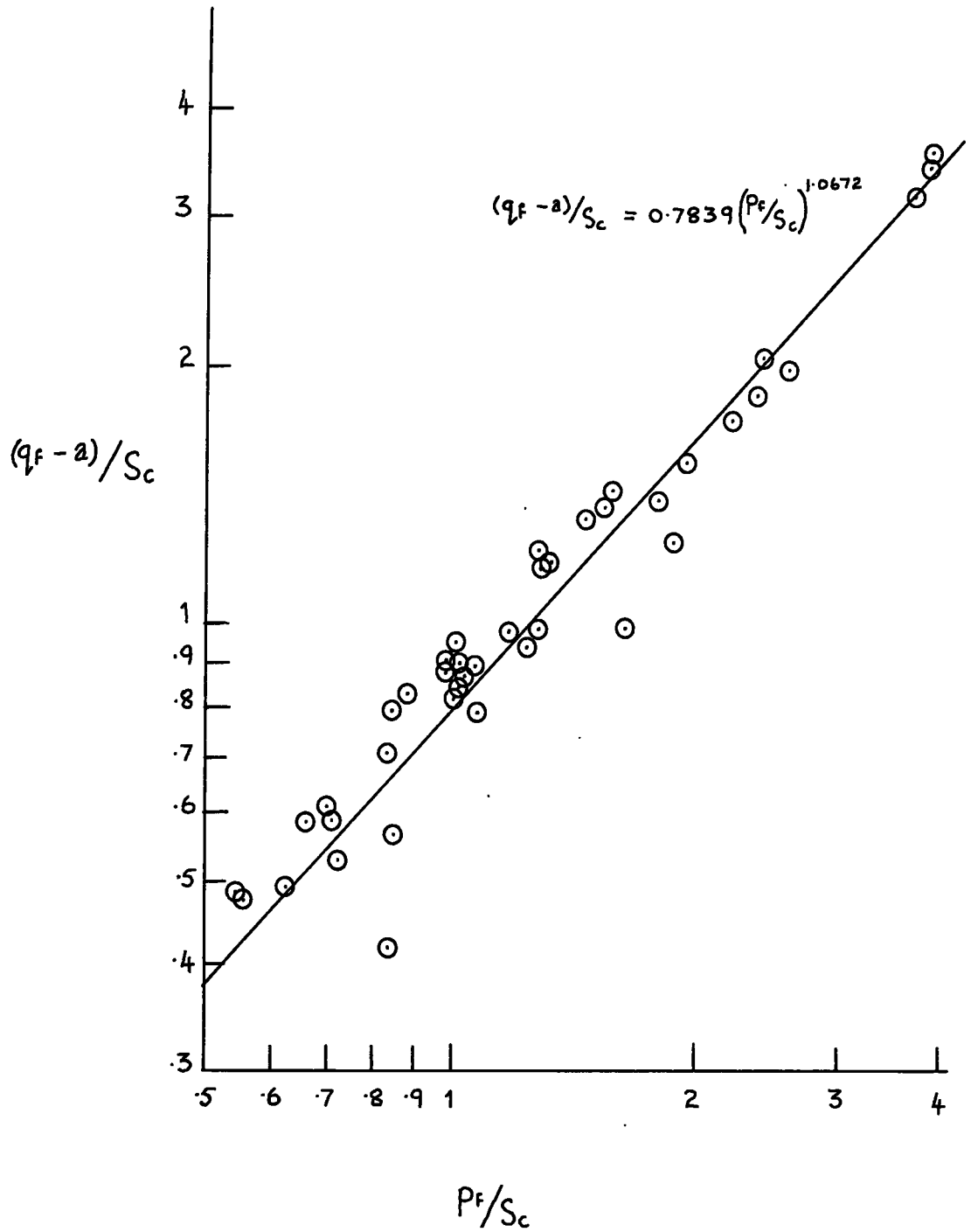

Fig. 2.21. 'Hoek plot' for all triaxial test results.

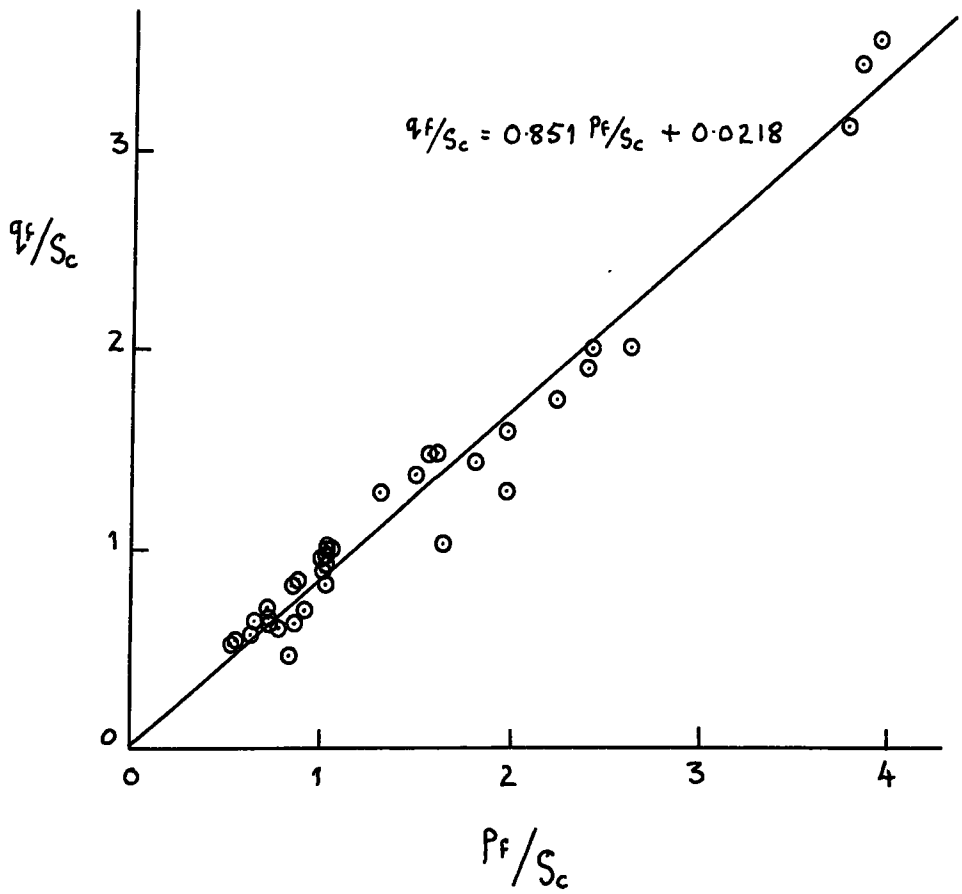

Fig. 2.22. Normalized maximum shear stress v mean normal stress.

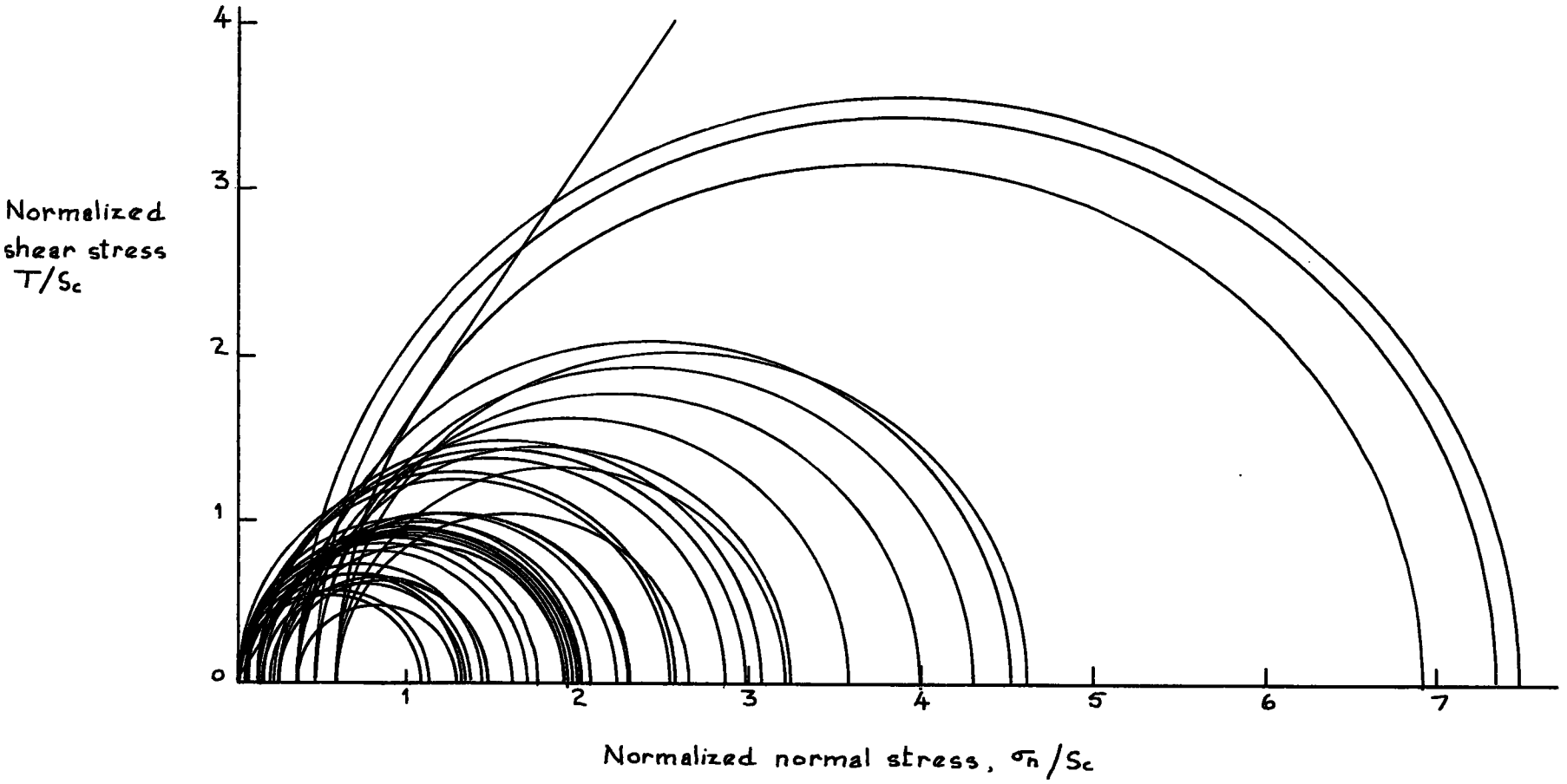

Fig. 2.23. Normalized Mohr circles for all triaxial tests.

failure envelope for the Magnesian Limestone may be obtained. The friction angle, $\emptyset$ so deduced, is 58.5°, which is far higher than the friction angles recorded during the double shear test, of 38°. This is interpreted as a reflection upon the triaxial test itself and the possible 'effective' tensile-type failure as postulated by Trollope (op. cit.)

CHAPTER 3

APPLICATIONS

3.1. Quarrying

Since quarrying of the Magnesian Limestone represents the second largest extractive industry in the east of Co. Durham, various pertinent aspects have been investigated. The sites and applications of present-day working quarries are given in Fig. 3.1. The majority of quarries work the Lower Magnesian Limestone for the construction and/or chemical industries.

3.1.1. Siting

The siting of quarries from a technical standpoint is governed by the mechanical properties and chemical composition which, combined with economic and planning considerations, dictate possible localities.

3.1.1.1. Chemical and strength considerations - These effects are so interrelated that they are most conveniently dealt with together. The Magnesian Limestone may be considered to consist of combinations of its two end members, calcite and dolomite, although most compositions tend to approach either of the extremes. Intermediate compositions exist where either of the processes of dolomitisation or dedolomitisation are incomplete, and as such represent only a small proportion of the total strata. Besides carbonates of calcium and magnesium, calcium sulphate and its relict textures may be identified (Jones, 1969) and in areas east of the reef and around Teesside the evaporites attain economic dimensions.

The chemical composition is obviously of principal importance to the extractors for the chemical industry. However, it does have applications in the

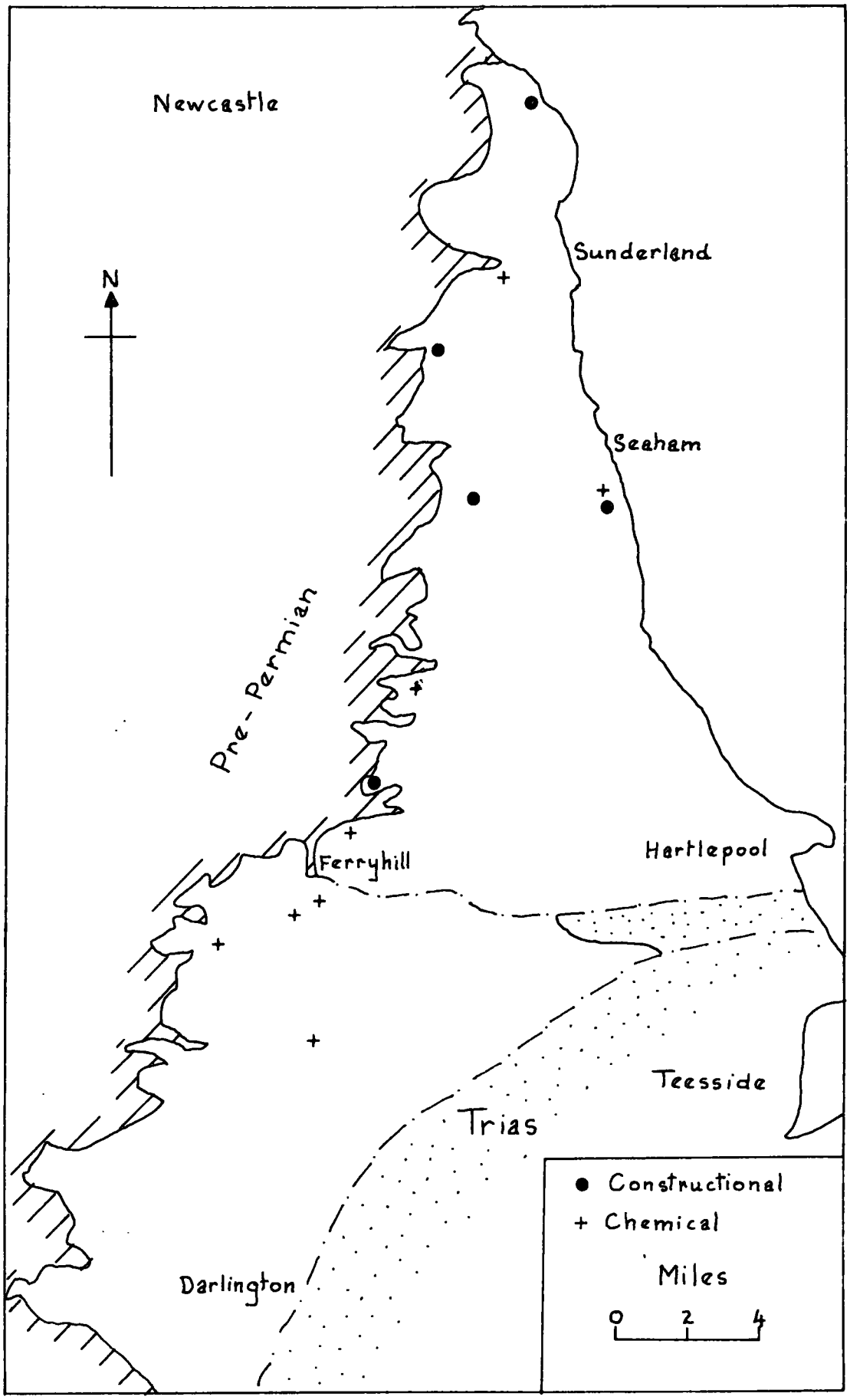

Fig. 3.1. Working quarry locations.

construction industry, especially with regard to strength, bitumen adhesion and frost susceptibility. Areas of primary limestone are extremely local and unpredictable, occurring only in the Lower Magnesian Limestone. They have been recorded from Raisby Hill, near Coxhoe, and East Thickley, near Shildon, although chemical analyses of borehole material often show a high calcite content near the base of the Lower Magnesian Limestone from other localities in the south of Co. Durham. (Smith & Francis, 1968). Dedolomitised limestones occur widely in the Upper Magnesian Limestone, where solution of the underlying evaporites has produced sulphate-rich brines which invaded the often collapse brecciated dolomites to produce calc-rudites and concretionary limestones. Limited dedolomitisation occurs in the Middle Magnesian Limestone, but it appears to be largely structurally controlled along fault and fracture lines, for instance at Tuthill Quarry near Haswell. At Hawthorn Quarry, calcite-dolomites of the reef-top beds are quarried for the steel industry of Teesside. The crushing of the rock improves the composition, since the dolomite fraction is concentrated in the 'scalpings'.

Apart from the above, dolomite is ubiquitous, its principal varieties being dictated by the nature of any allochems and the time of dolomitisation. Some of the country's purest dolomites are quarried at Thrislington Quarry by the Steetly Company Limited for refractory purposes. The principal requirements here are low iron and silica, and the best horizon is the upper division of the Lower Magnesian Limestone, since the detrital material available during the initial transgression would have been depleted. At Aycliffe Quarry, Lower Magnesian Limestone dolomite is worked for Darlington Chemicals, and at Ford Quarry, Sunderland, reef dolomite is quarried for use at Turner and Newalls insulation works at Washington. Dolomite is also used in the steel industry, and a powder produced at Middridge Quarry is transported to Skinningrove

steel works. Some dolomite finds an application in agriculture, although increased production of synthetic fertilisers with the additional beneficial components has resulted in a reduced demand.

The strength and suitability of aggregates employed in the construction industry are governed by the chemical composition and petrography of the rock. Aggregate tests indicate that the calcite rich horizons are superior to the dolomites in all respects. Primary limestones of the Permian are dense micrites with a low porosity (about 1%), and dedolomitization produces recrystallized calc-rudites and concretionary limestones of similar properties. On the other hand, dolomites are generally weaker and more porous, due to the strong tendency to produce enhedral crystals which lack the high interlocking character of calc-sparites and micrites. Nevertheless, some dolomites of the Lower Magnesian Limestone have an A. I. V. as low as 30 and may well find applications in road construction and as concrete aggregates.

From a consideration of the above factors and a knowledge of the geology, the potential of various areas may be assessed.

(a) Limestones and high calcite - Primary limestones are limited, as far as is known, to the Raisby and East Thickley localities mentioned above. However, at other localities in south Durham there may be up to 50ft of calcite rich strata near the base. Unfortunately, thick drift, especially east of the A1, severely restricts the economic viability of possible sites. In the northern part of the county there is no indication of a similar calcite enrichment near the base. The largest development of limestones formed by dedolomitisation occurs in the Upper Magnesian Limestone. The Concretionary Limestone shows varying degrees of dedolomitisation, and to the north of the River Wear, large areas of calc-rudites occur. South of this, collapse brecciation and subsequent dedolomitisation occurs on a more limited scale, with collapse sequences of up to 100 yds. occurring intermittently with well bedded dolomites. The reef-top

beds are often calcite rich, but their disposition is notoriously difficult to predict. Within the Middle Magnesian Limestone lagoonal facies, recrystallized limestone occur locally, but their distribution is limited and unpredictable.

(b) 'Hard' dolomites - These are post-diagenetic dolomites and in some cases the dolomitisation is incomplete. They are limited to the basal Lower Magnesian Limestone in the south of the county. Whilst having a much higher porosity than limestone (about 9%), they nevertheless have strength parameters quite acceptable for many purposes (A. I. V. $\approx$ 30, S_c > 8000 lb/in^2).

(c) Average dolomites - These represent the largest proportion of dolomites, containing both pre-diagenetic and post-diagenetic types. They have a crushing strength of less than 5000 lb/in^2, porosity of 12-18%, and A. I. V. > 34. Whilst attaining their largest development in the Lower Magnesian Limestone, they also occur widely in the Middle and Upper divisions. At some horizons they are remarkably free from impurities, but elsewhere sulphates, calcite, quartz, iron and manganese have been noted.

(d) 'Soft' dolomites - These are restricted to the Middle Magnesian Limestone, although east of the reef, beds of ? Upper Magnesian Limestone exhibit similar properties. They are weakly cemented and crumble easily. They often contain a high proportion of allochems such as shell debris or oolites, but the algal stromatolite horizons are stronger, with properties akin to the average dolomite. Boreholes sunk through the Middle Magnesian Limestone frequently show no recovery from these 'soft' dolomites, since they are slurried and return with the water.

3.1.1.2. Blast damage considerations - Recordings of ground vibrations from a number of routine blasts in the Magnesian Limestone were made and analysed by the author and Wijesinghe, and reported by Wijesinghe (1968). Only vertical vibrations were measured, using Dawe and Hall Sears seismometers with performances of 120 mV/in/sec and 500 mV/in/sec (r.m.s) respectively. The signals were fed via calibrated leads to attenuator/matching units, and the traces recorded on a Southern Instruments 10 channel U.V. recorder. An external trigger allowed remote starting of the chart from a position within visual range of the shotfirer.

From the record (Fig. 3.2) a travel-time graph can be constructed using first arrivals, and hence the surface layer velocity calculated from the gradient (Fig. 3.3). A value of 7850 ft/sec was found for the Magnesian Limestone at Thrislington. Amplitude velocity rather than displacement is now taken as being the most reliable damage criterion (Langefors and Kihlstrom 1963; Attewell and Farmer 1964; Ambraseys and Hendron, 1968) and this can be determined directly from the trace amplitude. The empirical propagation equation may be expressed as:

$$A_v = k\,(w/D^2)^n \qquad (3.1)$$

A graph of log A_v v log (w/D^2) enables the factors k and n to be determined (Fig. 3.4). The attenuation factor has an average value of 2×10^{-4} dB/cm at 10 c/s for the Magnesian Limestone, based on blasts monitored and this is typical for a sedimentary rock (Attewell and Ramana, 1966).

The limiting safe working distance of a face from liable property may be computed from the attenuation factor, for various charge weights. In practice, it is quite likely that subjective considerations would limit the working distance before the safe vibration level was exceeded.

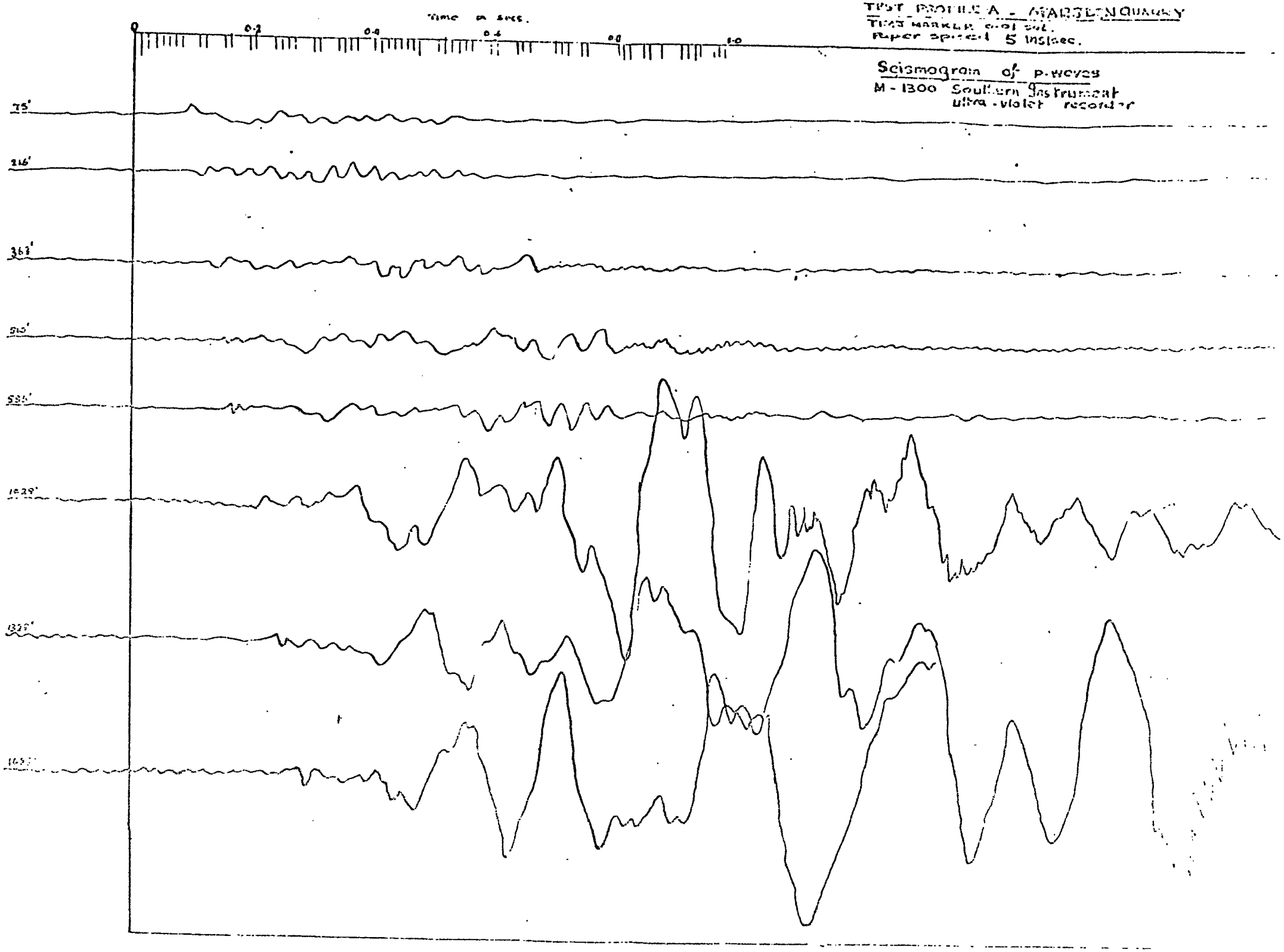

Fig. 3.2. Blast vibration record.

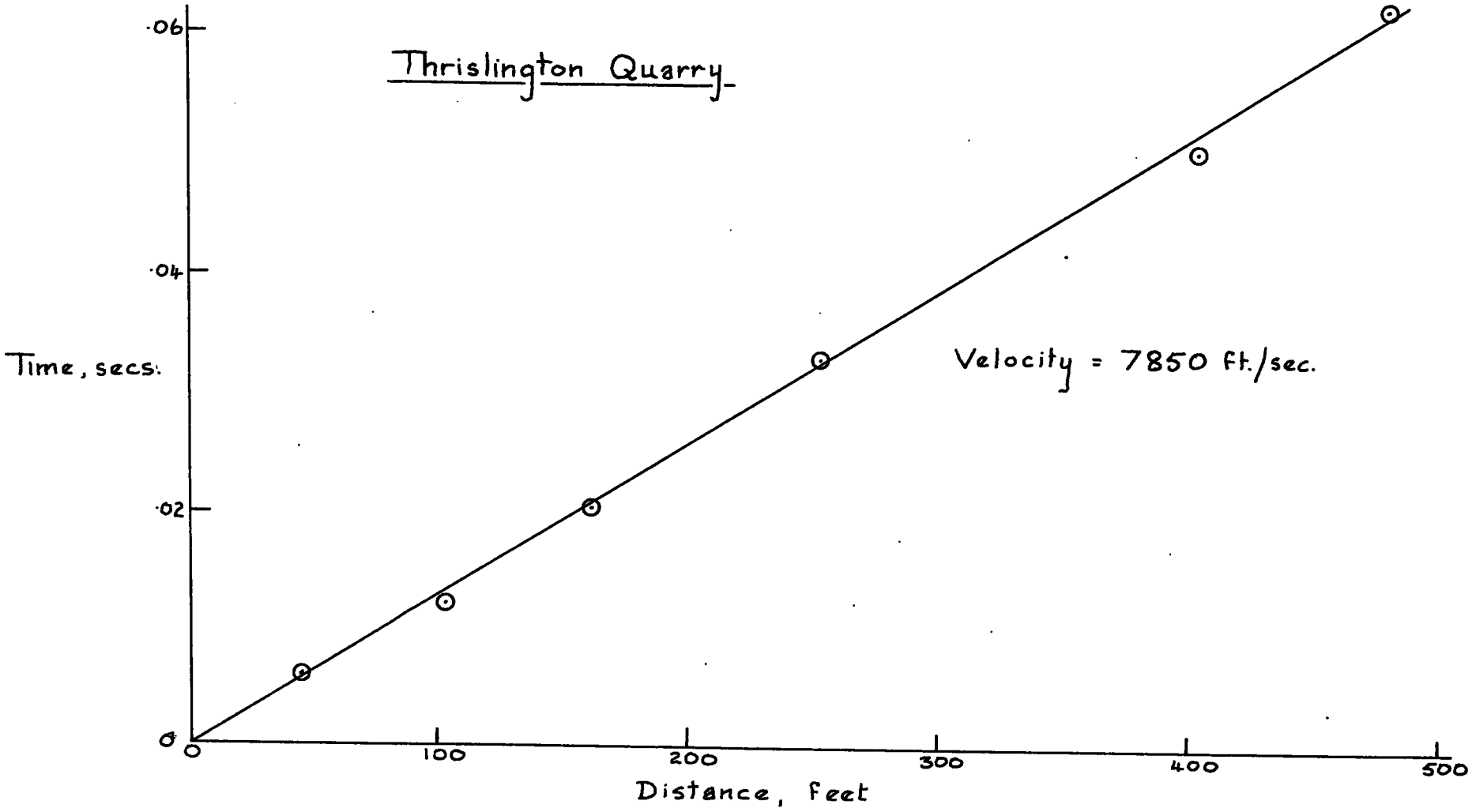

Fig. 3.3. Distance-time graph.

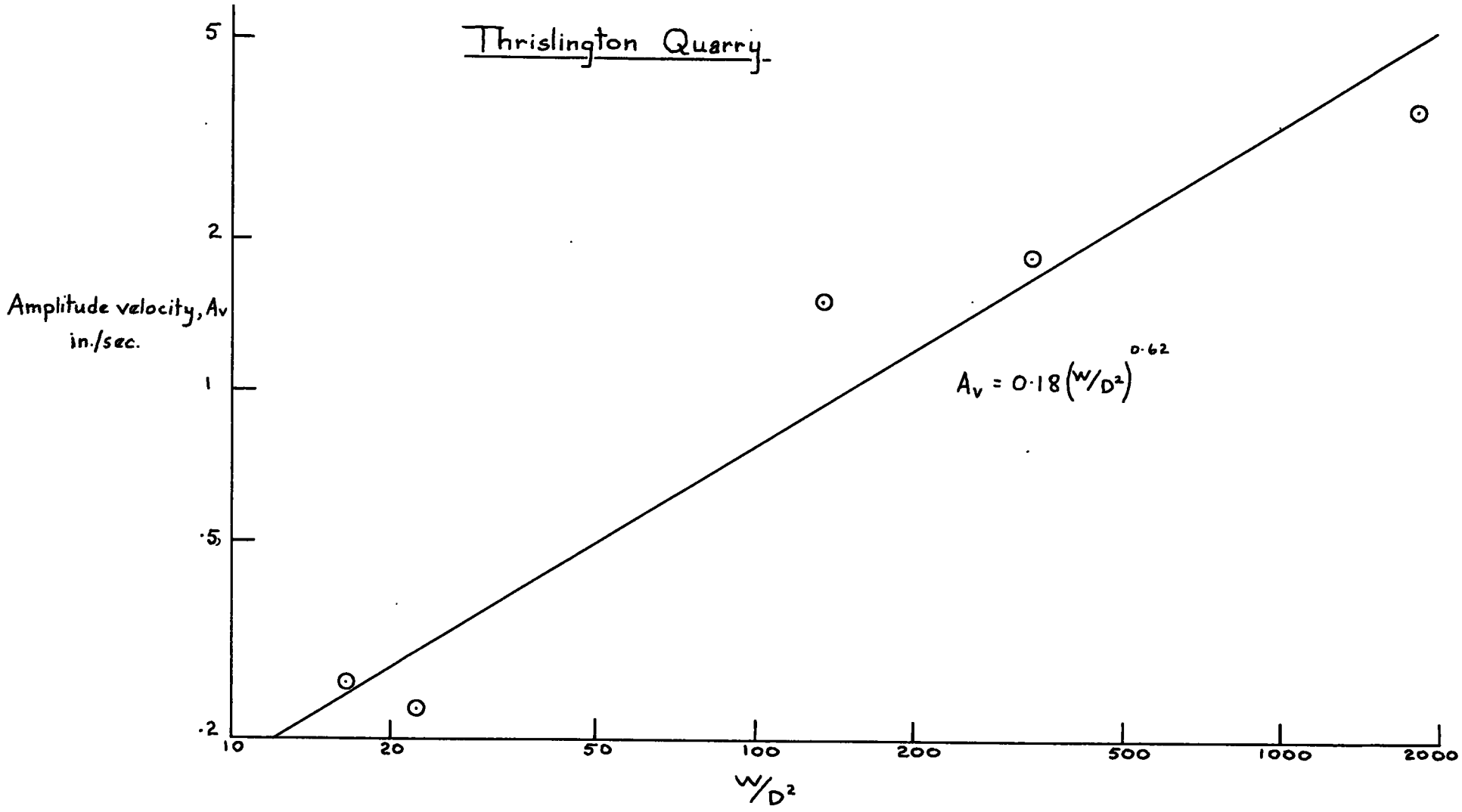

Fig. 3.4. Wave propagation parameters.

3.1.2. Waste disposal

As with most basically extractive industries, waste disposal within the stipulated planning limits may present difficulties. In many quarries, scalpings from the crushers and washers represent an ever present problem, and research has recently been directed towards an understanding of the physical nature and properties of the material (Wild, 1969), together with a search for possible applications. Whilst there is the obvious use as a fill, frost susceptibility and high air voids when compacted prevent its general use as a roadmaking material. A degree of stabilisation may be achieved with cement and, less successfully, with sodium silicate, but bitumen is ineffective. Ultimately, quarry spoil may be used in the final backfilling and landscaping of the disused parts of the quarries, but unless this can be designed into the quarry operation, the heaps will remain a feature for many years.

3.1.3. Economic considerations

The high capital investment required in an aggregate quarry can generally only be considered if the reserves of high grade stone are greater than 1 million tons. However, if the quarry is sited exceptionally close to the market, lower tonnages may be feasible. At present, the main markets are Tyneside, Wearside and Teesside, together with the development areas of Washington, Peterlee and Newton Aycliffe. With transport costs of 2/6 $\pm$ 4d. per ton mile, the Permian has distinct advantages over the limestones of Weardale and Teesdale. However, apart from a few exceptions, Magnesian Limestone aggregates lack the high strength properties of the Carboniferous Limestones, and require more binder when used in asphalt. It may be that improved mix designs could reduce some of the disadvantages, or that

Magnesian Limestone could be used where the specifications are not too rigorous.

3.1.4. Quarrying: summary and conclusions

The Magnesian Limestone quarries for both chemical and constructional purposes appear to have a guaranteed future. With further research and experience it may be possible to utilise lower grade aggregates at a reduced cost where some slight decrease in strength is acceptable. If this is the case, there are numerous sites in the Magnesian Limestone which offer possibilities. However, the siting of new quarries must take due consideration beforehand of the problems of possible variations in rock quality, overburden thickness, vibration damage, waste disposal and loss of amenity value for the district.

3.2. Slope stability

The varied nature of the Magnesian Limestone makes analysis difficult and generalisations necessary. The rock may be treated as being basically either a continuum, or else a discontinuum.

3.2.1. Continuum approach

In this the inherent property is taken to be the continuous nature of the strata, upon which the effects of discontinuities such as bedding and joints may be determined. Prior to the advent of large, high speed digital computers, continuum mechanics was chiefly studied from analogue models employing either mechanical, electrical or photoelastic techniques. Contemporary studies are chiefly directed towards the finite element method (Zienkiewicz and Cheung, 1967), which has the advantage of being able to simulate differing properties within the model. Unfortunately, the shortage of time did not permit the development of a program for the present study.

The effect of discontinuities under biaxial and triaxial stress conditions has already been covered (1. 2. 3. 2) and the use of the prepared stereograms requires only a knowledge of the pertinent stresses.

A graphical method of stability analysis based on the stereographic projection of joint orientation has also been described by John (1968).

3. 2. 2. Discontinuum approach

This considers the discontinuities to be the controlling influence on the mechanical behaviour. However, difficulties arise in assigning distributions and patterns varying between ordered and random to fit the observed features. Bray (1966) by utilising polar co-ordinates has shown that the friction angle is controlled by the ordering of the discontinuities. Other workers (Trollope, 1968; Hayashi, 1966; Goodman et al, 1968) have tended to concentrate on the square or rectangular 'building block', studying the self-weight interlocking characteristics. None of these methods have, however, been directly applicable to the Magnesian Limestone.

3. 2. 3. Semi-discontinuum approach

Whilst the methods outlined above treat the rock as either of the extremes, this analysis uses features of both techniques.

Most of the slope stability problems in the Magnesian Limestone are concerned with rock falls and long term degradation, rather than large scale, catastrophic slides. Since many rock excavations are required to be stable over a long period of time, it will be assumed that drained conditions hold, and the cohesion is negligible along failure surfaces. The idealised arrangement (Fig. 3. 5) therefore consists of a block, size H x t, with one free vertical face, and the active earth pressure from the cohesionless material acting on the other face. The stable slope angle is thus obtained by analysing limiting equilibrium conditions and is given by:

$$\beta = \tan^{-1} H/t \qquad (3.2)$$

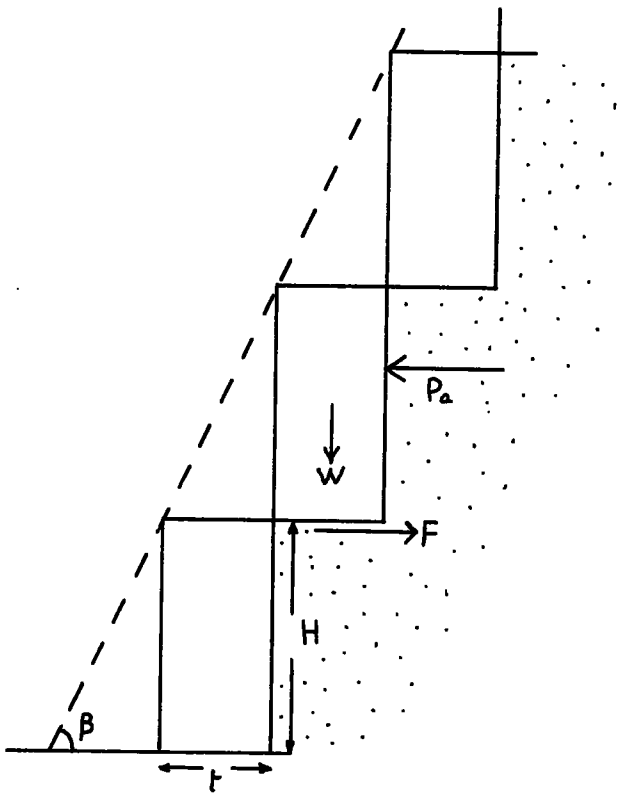

Fig. 3.5. Block slope: horizontal lower face.

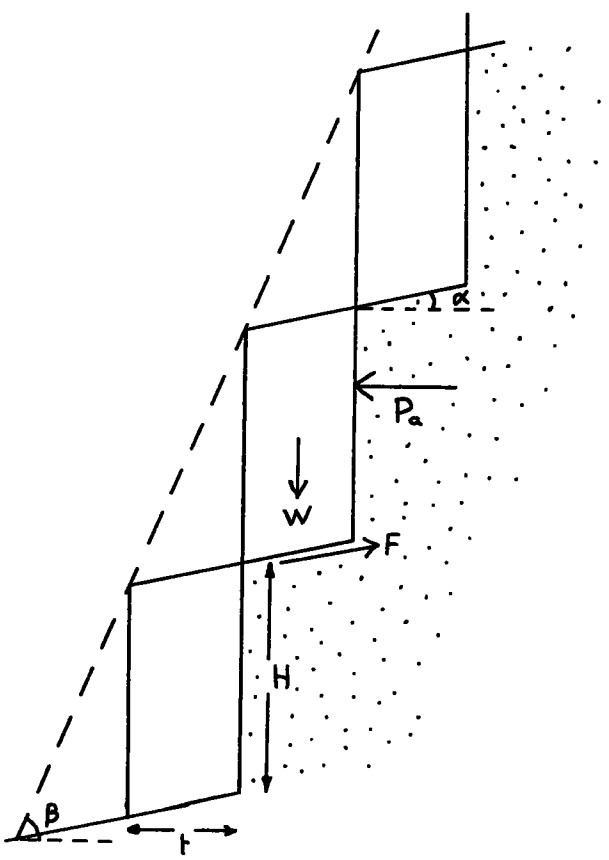

Fig. 3.6. Block slope: inclined lower face.

From a consideration of the forces parallel to the block base, assuming simple Rankine theory and therefore Pa horizontal:

$$Pa = F \qquad (3.3.)$$

For the active earth pressure, a depth of overburden of 2H must be taken, therefore:

$$2Ka \cdot H^2 = Ht \tan \phi$$

For a cohesionless material:

$$Ka = (1-\sin \phi)/(1+\sin \phi) \qquad (3.4)$$

Thus
$$H/t = \frac{\tan \phi \,(1+\sin \phi)}{2.(1-\sin \phi)} \qquad (3.5)$$

By a similar analysis for a sloping lower face (Fig 3.6)

$$H/t = \frac{(\tan \phi - \tan \alpha)(H \sin \phi)}{2\,(1 - \sin \phi)} \qquad (3.6)$$

Failure may also be by overturning, therefore taking moments about the lower left hand corner for limiting condition (horizontal base):

$$Pa.\,2H/3 = Wt/2 \qquad (3.7)$$

Therefore
$$H/t = \sqrt{\frac{3}{8}\,\frac{1}{ka}}$$

$$H/t = 0.6124 \sqrt{\frac{1 + \sin \phi}{1 - \sin \phi}} \qquad (3.8)$$

For an inclined lower face, the solution is rather more involved. Defining a new symbol:

$$Mi = 1 + \frac{t}{H} \cdot \frac{3 \tan \alpha}{2} \qquad (3.9)$$

then proceeding as above

$$H/t = 0.6124 \sqrt{Mi. \frac{1 + \sin \phi}{1 - \sin \phi}} \qquad (3.10)$$

As H and t occur on both sides, a trial and error method of solution is required.

Since the Magnesian Limestone is almost universally flat lying, only this case will be considered numerically. Fig. 3.7 indicates the stability regimes against sliding and overturning, and it will be immediately obvious that whilst the former dictates the slope angle for low - ϕ conditions, overturning is the dominant factor for $\phi > 34^{o}$. For very long term stability (i.e. geologically significant) the ultimate friction angle of 26^{o} would be used, and slopes as low as 30^{o} could be expected. For the civil engineering long term requirements, a friction angle of 38^{o} would be applicable, indicating slopes controlled by overturning, with a slope angle of 51^{o}.

3.2.4. Slope stability problems

There are no records of slope stability problems in the Magnesian Limestone, due largely to the low dips throughout the outcrop area. Turner (1967) examined an escarpment slope near Houghton-le-Spring, but concluded that there were unlikely to be any large scale stability problems within the Magnesian Limestone. Indeed the lowest factor of safety occurred for circular arc type failure through the underlying Basal Permian Sands.

Since glacial drift masks much of the solid geological features, it is difficult to estimate the natural slope angle. However, near Coxhoe an escarpment slope which shows signs of landslipping, probably immediately post-Pleistocene, has an angle of 25^{o}. Measurements of old quarry face angles are variable, being a function of the elapsed time since working, and also the rock nature. In the medium soft, granular dolomites, degraded slopes rarely exceed 60^{o}, although in some of the more resistant Lower Magnesian Limestone horizons, slopes of 70^{o} are common.

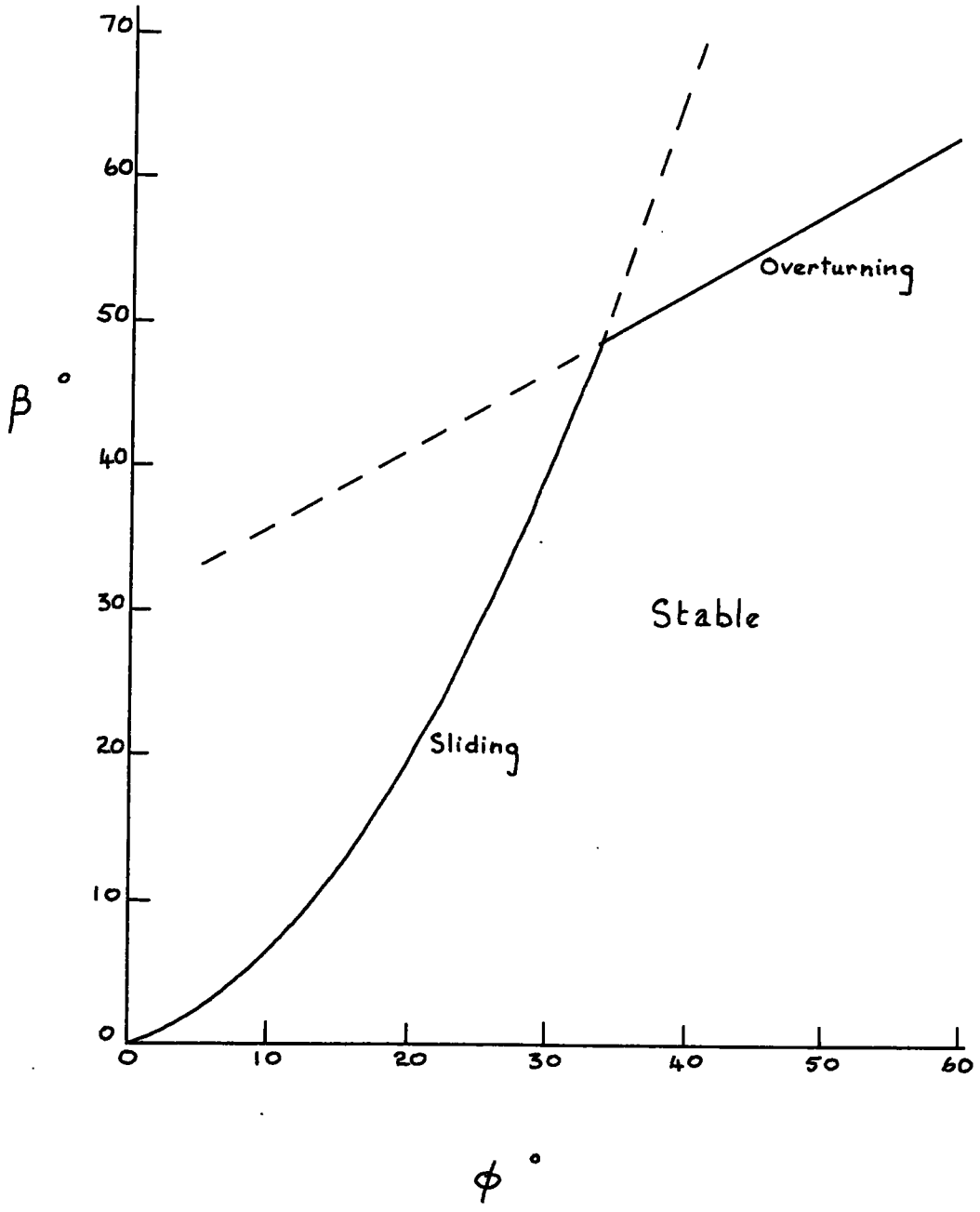

Fig. 3.7. Block slope : stability mode regimes.

The angle of repose of quarry waste heaps may be used as an indication of the long term stability. Measurements of dry waste in the field and on small samples in the laboratory give a value of 50^{o}.

The coastal cliffs represent the largest stability problem in the area. The horizons exposed range right through the Permian succession. In many places the more durable strata remains as headlands with the adjoining areas eroded into bays. In the majority of localities, the cliff line is currently receding and thus the slopes are oversteepened. The overlying boulder clay becomes washed down into joints and fissures, thus reducing the frictional resistance and leading to greater stability problems (Fig. 3. 8)

In cuttings through the Permian for the A1 (M) motorway near West Cornforth, slopes of 70^{o} were originally constructed in the Lower Magnesian Limestone, but this was reduced to 50^{o} in the less competent Middle Magnesian Limestone (Figs. 3. 9, 3. 10). Following the winter, degradation of the 70^{o} slopes was apparent, accelerated by frost action along fractures opened by blasting during excavation, and these slopes have recently been regraded.

3. 2. 5. Summary and conclusions

There is no evidence of large scale stability problems in the Magnesian Limestone, rock falls constituting the main type of failure. Two possibilities therefore exist:

(a) The slope may be angled such that the naturally formed blocks bounded by discontinuities are stable. A slope angle of 50^{o} would appear to be suitable for most horizons.

(b) The slope may be underdesigned, and any associated structures positioned so that the anticipated falls do not cause damage.

The problem of cliff stability would generally employ the latter method, coupled with action to prevent undercutting. This could be

Fig. 3.8. Cliff degradation, Shippersea Bay.

Fig. 3.9. Road cutting, A1(M), West Cornforth.

Fig. 3.10. Vertical view of above, showing talus.

achieved using 'tetrapods' or positioning large resistant rock blocks at the base of the cliff, to dissipate the wave energy.

In limited cases, surface treatment with Gunite or cement may help to stabilize a face (for example, Ferryhill Cut) but large scale grouting would probably be expensive, due to the high grout 'take'.

3.3. Foundations

In general, the Magnesian Limestone does not present any foundation problems. The brecciated Upper and the Lower Magnesian Limestones are able to support bored piles to the full allowable working stress of 750 lb/in^2. However, difficulty has been noted in obtaining a set with H-piles driven into the Magnesian Limestone (Taylor, personal communication). In this case the strata was oolitic Upper Magnesian Limestone and it was finally deemed better to found in the overlying boulder clay.

Where settlement is critical to the design of a structure, plate loading tests would be necessary. Experience from Chalk (Ward et al, 1968), shows that the settlements are more limited than predicted by Boussinesq. In weak horizons, the long term creep effects may be more important than the immediate elastic settlements.

As with many other characteristics, the type of foundation material likely to be encountered may be estimated from the stratigraphy. Thus the Lower Magnesian Limestone having a minimum crushing strength of about 3000 lb/in^2 is unlikely to present any problems. The Middle Magnesian Limestone, however, with its oolitic lagoonal facies, may be a difficult material, and where possible, foundations should be restricted to the boulder clay. In behaviour, it may be considered a loose, cohesionless sand, $\phi = 38^{\circ}$, and since leaching has often removed the evaporite cement a considerable strain

may be required to mobilise the full frictional bearing capacity. Spread foundations thus represent the best solution, and settlements may be limited by ground improvement using consolidation grouting or vibroflotation. The variable reef facies can give rise to a wide range of foundation characteristics, each requiring separate investigation. The Upper Magnesian Limestone is generally competent, although some oolitic dolomites near the top of the succession show similar properties and hence problems to the Middle Magnesian Limestone.

An added problem in some areas near evaporite sequences is the high concentration of dissolved salts in the groundwater. Where these include sulphates, high-alumina cement may be required to offset sulphate attack.

Properly conducted site investigations by diamond drilling should locate any possible problems due to soft cohesionless materials, particularly if the rock quality designation (R.Q.D.) is noted. (Deere, 1968). Estimates of settlement can only be made from plate bearing tests in this type of rock.

3.4. Summary and conclusions

Whilst the Magnesian Limestone exhibits a range of properties, the type of material liable to be encountered at a locality can be estimated from the local stratigraphy. This is of particular importance in the quarrying industry, but is also helpful in delimiting areas of possibly poor foundation characteristics. Where the rock is highly fractured and exposed to the atmosphere over long periods, it may be necessary to treat it as a soil, but elsewhere it exhibits the beneficial properties of a rock.

SECTION IV

SUMMARY AND CONCLUSIONS

1.1. Geology

(i) The subject of this study, the Magnesian Limestone, shows a great variety of lithologies and engineering properties, even though it is of only limited areal extent.

(ii) The succession can best be interpreted with reference to the palaeogeography and depositional environment, together with any chemical modifications which may have occurred either pre- or post-diagenesis.

(iii) Structurally the area is relatively simple, consisting essentially of a low angle dip toward the east or south-east upon which low amplitude folds are superimposed. The largest faults occur in the south of Co. Durham and result in an en-echelon total downthrow of strata to the south of over 2000 ft in places.

1.2. Geohydrology

(i) The dominant factor, the geology of the area, influences the overall groundwater regime in two ways. Firstly, variations in lithology result in changes in hydraulic conductivity and hence transmissibility and yield; secondly, faults and basement 'highs' affect the development of the cones of depression, and hence the yields.

(ii) The analytical methods which may be applied are determined by the aquifer type and the data available. Results obtained by different techniques are not directly comparable on an absolute basis, but may be viewed relatively.

(iii) In the northern part of the area, the average well permeability may be broken down into its constituent parts on the basis of the geological information. This enables the following parameters to be determined:

Horizon	Hydraulic conductivity (Dupuit-Forchheimer) - g.p.d./ft^2
Upper Magnesian Limestone, brecciated	300
Middle Magnesian Limestone	300
Lower Magnesian Limestone, except basal unit	110
Lower Magnesian Limestone, basal unit	40
Basal Permian Sands	40-120

(iv) In the south, the dominant aquifer is the oolitic Middle Magnesian Limestone, and is generally confined by either drift or marls of the Lower Evaporite Group. Some supplies may be obtained from the Upper Magnesian Limestone, but yields are unpredictable, being a function of the degree of collapse brecciation. Because of the complexity of barrier effects due to faults and basement 'highs', direct analysis and extrapolation becomes both difficult and dubious.

(v) Simulation techniques were adopted, since they are theoretically valid yet practically applicable to varying parameters. Both digital and analogue methods have been employed, the former producing a direct solution, but the expense incurred is only justifiable for large schemes where they may be used to reduce the tedious calibration necessary for electrical models. Resistance-capacitance analogues are both simple and cheap, but do require some expertise and a considerable amount of time. For the horizons studied, the time variant was unimportant for the confined conditions since the low storage coefficient resulted in fairly rapid stabilization.

(vi) Results from the electrical analogue indicate that over the area modelled, 16 m.g.d. are available without depleting resources. However, a discharge of 4 m.g.d. in the north-east of the area must be maintained for abstraction in the Hartlepool area, leaving a nett 12 m.g.d. If the abstraction is only for limited periods, then a certain amount of aquifer dewatering may be permissible, resulting in much increased yields.

1.3. Engineering geology

(i) The engineering geology, like the geohydrology, is principally controlled by the rock lithology, especially the extent and nature of any dolomitisation.

(ii) The probable behaviour of a rock may be readily deduced from a knowledge of its rheological and strength parameters. The former may be partially described by Young's modulus, determined from either laboratory tests on small samples, or large scale field loading tests. The results of strength tests may be interpreted by various failure criteria, although there is no unique criterion which completely describes all the observed characteristics of rocks. For the present study, under brittle low stress conditions, the Coulomb-Navier criterion has been used.

(iii) The Magnesian Limestone is typically highly fractured, the influence of discontinuities upon the rheological and strength parameters was investigated. In both cases the effect was to reduce the parameters to varying degrees, depending upon the size, concentration and disposition of the discontinuities. The theoretical aspects of planar discontinuity orientation and its role in inducing premature failure was investigated for both biaxial and triaxial stress systems, computer programs being written for the latter to facilitate plotting and geometrical processes such as rotation of axes.

(iv) Laboratory measurements carried out on a representative selection of lithologies from various horizons included uniaxial and triaxial compression, tensile, double shear and aggregate tests. The nett result was that most parameters showed a correlation with the unconfined compressive strength, even though the latter should be treated cautiously on absolute stress grounds due to complex stress distributions resulting from sample-platen interaction.

(v) By normalizing triaxial test data with the unconfined compressive strength a grand average failure envelope could be constructed for the Magnesian Limestone, defined by $c = 0.0416\ S_c$, $\phi = 58.5^{o}$. By comparison, the ϕ values determined from the double shear test were much lower, about 35^{o}, but with an increased cohesion. This is interpreted as being due to the 'effective' tensile triaxial failure under low confining pressures.

(vi) The results of the study of the engineering geology have various applications. In the quarrying industry, a knowledge of the type of rock likely at any locality is invaluable for estimating reserves and fixing new sites. A study of the effects of blast-induced vibrations indicate that damage to property is unlikely with the present location of faces and charges used at the quarries investigated.

(vii) Slope stability is not a major problem, most failures being of a relatively minor nature and consisting essentially of rockfalls. From theoretical considerations, it can be shown that for a friction angle $\phi > 34^{o}$, degradation is predominantly by an overturning mechanism, resulting in a slope angle of 50^{o} for the Magnesian Limestone.

(viii) Foundation difficulties are not usually experienced in the Magnesian Limestone, except where the evaporite cement has been leached. In these cases some form of ground improvement may be necessary by vibroflotation

or consolidation grouting, to reduce settlements to within tolerable limits. In all site investigations, tests for active sulphate content in the groundwater should be carried out.

REFERENCES

AKROYD, T. N. W. (1964) — 'Laboratory testing in soil engineering'. Soil Mechanics, Ltd., London.

AMBRASEYS, N. N. and HENDRON, A. J. (1968) — 'Dynamic behaviour of rock masses'. In 'Rock mechanics in engineering geology' eds. Stagg, K. C. and Zienkiewiez, O. C., Wiley, London, 203-36.

ANDERSON, W. (1941) — 'Water supply from underground sources of north-east England'. Wartime Pamphlet No. 19, Part III. Geological Survey of Great Britain.

ARMSTRONG, G., KIDD, R. R., and BUCHAN, S. (1959) — 'Dewatering scheme in the South Durham Coalfield'. Trans. Inst. Mining Engrs., 119, 141-52.

ATTEWELL, P. B. and FARMER, I. W. (1964) — 'Ground vibrations from blasting'. Quarry Mgrs' J., 48, 191-8.

ATTEWELL, P. B. and RAMANA, Y. V. (1966) — 'Wave attenuation and internal friction as functions of frequency in rocks'. Geophysics, 31 (6), 1049-56.

ATTEWELL, P. B., HIRST, D. M. and TAYLOR, R. K. (1968) — 'Diagenetic recrystallization and orientation of two carbonate species'. Sedimentology, 11, 237-47.

BAGNOLD, R. A. (1941) — 'The physics of blown sand and desert dunes'. Methuen, London, 265 pp.

BISHOP, A. W. and HENKEL D. J. (1957) — 'The measurement of soil properties in the triaxial test'. Arnold.

BOTT, M. H. P. and MASSON-SMITH, D. (1957) — 'The geological interpretation of a gravity survey of the Alston Block and Durham Coalfield'. Quart. J. Geol. Soc., 113, 93-117.

BOTT, M. H. P. (1967) — 'Geophysical investigation of the Northern Pennine basement rocks'. Proc. Yorks. Geol. Soc., 36, 139-68.

BOULTON, N.S. (1954) 'The drawdown of the water-table under non-steady conditions near a pumped well in an unconfined formation'. Proc. Inst. Civil Engrs., 3, 564-79.

BRACE, W. F. (1960) 'An extension of the Griffith theory of fracture to rocks'. J. Geophys. Res., 68, 3709.

BRACE, W.F (1964) Brittle fracture of rocks, in 'State of stress in the earth's crust', ed. Judd, W.R., New York, Elsevier, 111-74.

BRAY, J.W. (1966) 'Limiting equilibrium of fractured and jointed rocks'. Proc. 1st Int. Cong. Rock Mech. 531-35.

BRITISH STANDARDS INSTITUTION (1967) 'Sampling and testing of mineral aggregates, sands and fillers'. British Standard 812:1967, British Standards Institution, London.

BRITISH STANDARDS INSTITUTION (1967) 'Methods of testing soils for civil engineering purposes'. British Standard 1377:1967, British Standards Institution, London.

BROWN, E.T. and TROLLOPE (1967) 'The failure of linear brittle materials under effective tensile stress'. Rock Mech. and Engineering Geol., 4, 229-41.

BURGESS, A.S. and CAIRNEY, T. (in press). 'Ground-water investigations and simulation of the Magnesian Limestone of South Durham.' Proc. Geol. Soc. London.

BYERLEE, J.D. (1967) 'Frictional characteristics of granite under high confining pressure'. J. Geophys. Res. 72, 3639-48.

BYERLEE, J.D (1967) 'Theory of friction based on brittle fracture'. J. Appl. Phys., 38, 2928-34.

BYERLEE, J.D. (1968) 'Brittle - ductile transition in rocks'. J. Geophys. Res., 73, 4741-50.

BYERLEE, J.D. and BRACE, W.F. (1968)
'Stick slip, stable sliding, and earthquakes - effect of rock type pressure, strain rate, and stiffness'. J. Geophys. Res. 73, 6031-7.

CHAKRABARTI, A.K. and TAYLOR, R.K. (1968)
'The porosity and permeability of the Zawar Dolomites'. Int. J. Rock Mech. Min. Sci. 5, 261-73.

CHEATHAM, J.B. (1968)
'Rock breakage by crushing, blasting and drilling'. Engineering Geology, 2, 293-314.

CLARKE, A.M. (1962)
'Some structural, hydrological and safety aspects of recent developments in south-east Durham'. Mining Engineer, 27, 209-31.

COATES, D.F., (1966)
'Rock mechanics principles'. Mines Branch Monograph 874, Dept. of Energy, Mines and Resources, Ottawa.

DEERE, D.U. (1968)
Geological considerations, chapter 1 in 'Rock mechanics in engineering practice', eds. Stagg, K.C. and Zienkiewicz, O.C., Wiley, London, 1-20.

DE WIEST, R.J.M. (1965)
'Geohydrology'. Wiley, New York, XV + 366 pp.

DONATH, F.A. (1964)
'Strength variation and deformational behaviour in anisotropic rock,' in 'State of stress in the earth's crust', ed. Judd, W.R., New York, Elsevier, 281-97.

EASTWOOD, T. (1963)
'British Regional Geology:Northern England 3rd Ed., H.M.S.O., London, 72 + iv.

EVANS, W.B., WILSON, A.A., TAYLOR, B.J. PRICE, D. (1968)
'Geology of the country around Macclesfield, Congleton, Crewe and Middlewich'. Mem. Geol. Surv. Gt. Br., x + 328 pp. H.M.S.O. London.

FAIRHURST, C.
(1961)
'Laboratory measurements of some physical properties of rocks'.
Proc. 4th Symposium on Rock Mechanics.

FAIRHURST, C.
(1964)
On the validity of the 'Brazilian' test for brittle materials.
Int. J. Rock Mech. Mining Sci., 1, 535-46.

FARMER, I.W.
(1968)
'Engineering properties of rocks'.
Spon., London, 180 + vii.

FERRIS J.G., KNOWLES, D.B., BROWN, R.H., STALLMAN, R.W.
(1962)
'Theory of aquifer tests'.
U.S. Geol. Survey Water Supply.
Paper 1536-E.

GALLOWAY, R.L.
(1898)
'Annals of Coal Mining and the Coal Trade'.
London.

GIBSON, R.E.
(1967)
'Some results concerning displacements and stresses in a non-homogeneous elastic half-space'.
Geotechnique, 17, 58-67.

GOODMAN, R.E., TAYLOR, R.L., and BREKKE, T.L.
(1968)
'A model for the mechanics of jointed rocks'.
Proc. Amer. Soc. Civ. Engrs., 94 (SM3), 637-59.

HANDIN, J., HEARD, H.C., and MAGOUIRK, J.N.
(1967)
'Effects of the intermediate principal stress on the failure of limestone, dolomite and glass at different temperatures and strain rates'.
J. Geophys. Res., vol. 72, pp. 611-640.

HANTUSH, M.S.
(1964)
'Hydraulics of wells'.
Advances in Hydroscience, 1, 281-433.

HARRIS, C.C.
(1966)
On the role of energy in comminution; a review of physical and mathematical principles.
Trans. Inst. Min. & Metall. 75, C37-56.

HAYASHI, M.
(1966)
'A mechanism of stress distrubition in the fissured foundation'.
Proc. 1st Cong. Int. Soc. Rock Mechanics 2.

HERBERT, R. (1965)
'Well hydraulics - I'. Water Research Association Technical Paper, TP40, Water Research Association, Medmenham, Bucks. 34 pp.

HERBERT, R. and RUSHTON, K.R. (1966)
'Ground-water flow studies by resistance networks'. Geotechnique, 16, 53-75.

HERBERT, R. (1968)
'Time variant ground-water flow by resistance analogue'. J. Hydrol., 6, 237-64.

HIRST, D.M. and DUNHAM, K.C. (1963)
'Chemistry and petrography of the Marl Slate of S.E. Durham, England'. Econ. Geol., 58, 912-40.

HOBBS, D.W (1967a)
'Behaviour and simulation of sedimentary rocks'. J. of Strain Analysis, 2, 307-16.

HOBBS, D.W. (1967b)
'Rock tensile strength and its relationship to a number of alternative measures of rock strength'. Int. J. Rock Mech. Min. Sci., 4, 115-27.

HODGE, M.B. (1932)
'The Permian Yellow Sands of North-east England'. Proc. Univ. Durham Phil. Soc., 8, 410-58.

HOEK, E. (1968)
Brittle failure in rock, Chapter 4 in 'Rock mechanics in engineering practice', eds. Stagg, K.G. and Zienkiewicz, O.C., Wiley, London, 99-124.

HONDROS, G. (1959)
'The evaluation of Poisson's ratio and the modulus of materials of low tensile resistance by the Brazilian (indirect tensile) test with particular reference to concrete'. Aust. J. Appl. Sci. 10, 243.

HUCKA, V. (1965)
'A rapid method of determining the strength of rocks in situ'. Int. J. Rock Mech. Mining Sci., 2, 127-34.

HUNTER BLAIR A.
(in press)
'Simplification of groundwater data used for an analogue of a coastal aquifer'.
Paper presented at the General Assembly of the International Association of Scientific Hydrology, Berne, 1967, to be published in Gentbrugge Int. Assoc. Sci. Hydrol.

INESON, J.
(1953)
'Some observations on pumping tests carried out on chalk wells'.
J. Inst. Water Engrs., 7, 215-71.

INSTITUTION OF WATER ENGINEERS
(1961)
'Manual of British water engineering practice'.
3rd Edition, Heffer.

JACKSON, R.S.
(1968)
'Aquifer studies in Co. Durham and in the Nairobi area, Kenya'.
M.Sc. Thesis, University of Durham.

JACOB, C.E.
(1950)
'Flow of groundwater'.
'Engineering Hydraulics', H. Rouse (Ed.) Wiley.

JACOB, C.E.
(1963)
'Determining the permeability of water-table aquifers'.
U.S. Geol. Survey Water Supply Paper 1536-I.

JAEGER, J.C. and
COOK, N.G.W.,
(1968)
'Fundamentals of rock mechanics'.
Methuen, London, 513 + xiv.

JAMES, M.L., SMITH, G.M.
and WOLFORD, J.C.
(1967)
'Applied numerical methods for digital computation with Fortran'.
Scranton, Pa., Internation Textbook Co.

JOHN, K.W.
(1968)
'Graphical stability analysis of slopes in jointed rock'.
Proc. Amer. Soc. Civ. Engrs., 94 (SM2), 497-526.

JOHNSON, E.E.
(1966)
'Ground-water and wells'.
E.E. Johnson, Inc., St. Paul, Minn.

JONES, K.
(in preparation, 1969)
'The Mineralogy and geochemistry of the Middle Magnesian Limestone of County Durham'.
Ph. D. Thesis, University of Durham.

KARPLUS, W. J.
(1958)
'Analog simulation'
McGraw Hill, New York, 427 pp.

KITTLEMAN, L. R.
(1964)
Application of Rosin's Distribution in size-frequency analysis of clastic rocks'.
J. Sed. Pet., 34, 483-502.

KOLEK, J.
(1958)
An appreciation of the Schmidt rebound hammer.
Magazine of Concrete Research, 10, 27-36.

KRSMANOVIC, D.
(1967)
'Initial and residual shear strength of hard rocks'.
Geotechnique, 17, 145-60.

KRUMBEIN, W. C. and GRAYBILL, F. A.
(1965)
'An introduction to statistical models in geology'.
McGraw-Hill, New York.

LAMBE, T. W. and WHITMAN, R. V.
(1969)
Soil Mechanics.
Wiley, New York, 533 + xii.

LANGEFORS, U. and KIHLSTROM, B.
(1963)
'Rock blasting'.
Wiley.

LINDQUIST, E.
(1933)
On the flow of water through porous soil .
Premier Congres des grands banages, 81-101.

LOGAN, J.
(1964)
'Estimating transmissibility from routine production tests of water wells'.
Ground Water, Journ. National Water Well Assoc., 2, 35-37.

LUNDBORG, N.
(1966)
'Triaxial shear strength of some Swedish rocks and ores'.
Proc. 1st Cong. Int. Soc. Rock Mechanics, 251-55.

McCLINTOCK, F.A. and WALSH, J.B. (1962)
'Friction on Griffith cracks in rocks under pressure'. Proc. 4th U.S. Nat. Congr. App. Mech. 1015-21.

McCRACKEN, D.D. (1967)
Fortran with engineering applications. Wiley, New York.

MINISTRY OF HOUSING AND LOCAL GOVERNMENT (1961)
'Wear and Tees Hydrological Survey, Hydrometric Areas 24 and 25'. H.M.S O. London.

MOGI, K. (1966)
'Some precise measurements of fracture strength of rocks under uniform compressive stress'. Rock Mechanics & Engineering Geology. 4, 41-55.

MORGENSTERN, N.R. (1967)
'Submarine slumping and the initiation of turbidity currents' in Marine Geotechnique, ed. Richards, A. Univ. of Illinois Press, Urbana, 189-220.

MOSELEY, F. and AHMED, S.M. (1967)
'Carboniferous joints in the north of England and their relation to earlier and later structures'. Proc. Yorks. Geol. Soc. 36, 61-90.

MURRELL, S.A.F. (1958)
'The strength of coal under triaxial compression'. in Mechanical properties of non-metallic brittle materials, ed. Walton, W.H., Butterworths, London, 123-53.

NALIVKIN, D.V. (1937)
'Scientific results of the Permian Conference. In Problems of Soviet Geology, 7. Translated by T. Storichenko with comments and forward by J.S Williams. Bull. Amer:. Assoc. Petrol. Geol., 22, 771-6.

NOBLE, B. (1964)
'Numerical methods: 2 Differences, integration and differential equations'. Oliver & Boyd, Edinburgh.

NORTHUMBRIAN RIVER AUTHORITY (1969)

'Groundwater exploration of the Magnesian Limestone of south-east Durham'. Internal report, 32 pp.

OBERT, L. and DUVALL, W.I. (1967)

'Rock mechanics and the design of structures in rocks'. Wiley, New York.

OBERT, L., WINDES, S.L., and DUVALL, W.I. (1946)

'Standardized test for determining the physical properties of mine rock'. U.S. Bur. Mines Rept. Invest. 3891 67 pp.

PATTON, F.D. (1966)

'Multiple modes of shear failure in rock'. Proc. 1st Cong. Int. Soc. Rock Mechanics, 1, 509-13.

PINDER, G.F. and BREDEHOEFT, J.D. (1968)

'Application of the digital computer for aquifer evaluation'. Water Resources Research, 4(5), 1069-93.

PRICE, N.J. (1966)

'Fault and joint development in brittle and semi-brittle rock'. Pergamon, Oxford, x + 176 pp.

SCHOLZ, C.H., (1968)

'Mechanism of creep in brittle rock'. J. Geophys. Res., 73 (10), 3295-3302.

SEDGEWICK, A. (1829)

On the geological relations and internal structure of the Magnesian Limestone and the lower portions of the New Red Sandstone Series, in their range through Nottinghamshire, Derbyshire, Yorkshire, and Durham, to the southern extremity of Northumberland. Trans. Geol. Soc. (2), 3, 37-124.

SHERGOLD, F.A. and HOSKING, J.R. (1963)

'Investigation of test procedures for argillaceous and gritty rocks in relation to breakdown under traffic'. Road Research Laboratory, Note No. LN/385/FAS.JRH, Department of Scientific and Industrial Research, London.

SHERLOCK, R. L.
(1926)
'A correlation of the Permo-Triassic rocks'.
Proc. Geol. Assoc. 37, 1-72.

SHERLOCK, R. L.
(1928)
'A correlation of the Permo-Triassic rocks'.
Proc. Geol. Assoc., 39, 49-95.

SKIBITZKE, H. E.
(1963)
'The use of analogue computers for studies in ground-water hydrology'.
J. Inst. Wat. Engrs., 17, 216-30.

SKINNER, B. J., WHITE, D. E., ROSE, H. J., MAYS, R. E.
(1967)
'Sulfides associated with the Salton Sea geothermal brine'.
Econ. Geol., 62, 316-30.

SMITH, D. B. and FRANCIS, E. A.
(1967)
'The geology of the country between Durham and West Hartlepool'.
Mem. Geol. Surv. Gt. Br., viii+ 354 pp.
H. M. S. O., London.

SMITH, D. B.
(1968)
'The Hampole Beds - a significant marker in the Lower Magnesian Limestone of Yorkshire, Derbyshire and Nottinghamshire.
Proc. Yorks. Geol. Soc., 36, 463-477.

SMITH, D. B.
(in press)
'Foundered strata, collapse-breccias and subsidence features of the English Zechstein.'
Report on Symposium on the geology of of saline deposits, Hanover, 1968.

SMITH, D. B.
(in preparation)
'Submarine slumping and sliding in the Lower Magnesian Limestone of Durham and Northumberland.'

SOUTHWELL, R. V.
(1946)
'Relaxation methods in theoretical physics'.
Oxford.

STAGG, K. G. and ZIENKIEWICZ, O. C.
(editors), (1968).
'Rock mechanics in engineering practice'.
Wiley.

STALLMAN, R.W. (1963)
'Electric analog of 3-dimensional flow to wells and its application to unconfined aquifers'. U. S. Geol. Survey Water Supply Paper no. 1536-H.

TERZAGHI, K. and PECK, R B. (1967)
'Soil mechanics in engineering practice'. 2nd ed., Wiley, New York.

THEIS, C. V. (1935)
'Relation between the lowering of the piezometric surface and the rate and duration of discharge of a well using groundwater storage.' Am. Geophys. Union Trans. 16, 519-24.

TIMOSHENKO, S. P. and GOODIER, J. N. (1951)
'Theory of elasticity'. 2nd ed. McGraw-Hill, New York.

TRECHMANN, C. T. (1914)
On the lithology and composition of the Durham Magnesian Limestones. Quart. Journ. Geol. Soc., 52, 232-65.

TRECHMANN, C. T. (1925)
"The Permian Formation in Durham" Proc. Geol. Assoc., 36, 135-45.

TROLLOPE, D. H. (1968)
'Discontinua or elastic mechanics in rock problems', in 'Rock Mechanics in Engineering Practice', ed. Stagg and Zienkiewicz, p. 274, Wiley, London.

TURNER, M. J. (1967)
'Rock slope stability'. M. Sc. thesis, Univ. of Durham.

WALSH, J. B. and BRACE, W. F. (1966)
'Elasticity of rock: a review of some recent theoretical studies'. Rock Mechanics and Engineering Geology, 4, 283-97.

WALTON, W. C. and PRICKETT, T. A. (1963)
'Hydrogeologic electric analog computers'. Proc. Am. Soc. Civ. Engrs., H. Hydraul Div., 89 (HY6), 67-91.

WARD, W.H., BURLAND, J B., and GALLOIS, R.W (1968)
'Geotechnical assessment of a site at Mundford, Norfolk, for a large proton accelerator'. Geotechnique, 18, 399-431.

WATER RESOURCES BOARD (1967)
'Interim report on water resources in the North'. iii + 30 pp., H.M.S.O., London.

WELHAM, K. (1969)
'A study of the shear stress parameters of dolomite and microconcrete'. Engineering Science Final Year Project, Univ. of Durham.

WELLS, A.K. and KIRKALDY, J.F. (1966)
'Outline of historical geology'. 5th ed., Murby, London, 503 pp.

WIEBOLS, G.A. and COOK, N.G.W. (1968)
An energy criterion for the strength of rock in polyaxial compression'. Int. J. Rock Mech. Min. Sci., 5, 529-49.

WIJESINGHE (1968)
'Two geophysical techniques in engineering exploration'. M.Sc. Thesis, Univ. of Durham.

WILD, B.W. (1969)
M.Sc. Thesis, University of Durham.

WOOD, F.W. (1950)
'Recent information concerning the evaporites and the pre-Permian floor of south-east Durham'. Quart. J. Geol. Soc., 105, 327-46.

WOOD, W.O. (1923)
'The Permian Formation in East Durham'. Trans. Inst. Mining Engrs., 65, 178-86.

WOOLACOTT, D. (1919)
'The Magnesian Limestone of Durham'. Geol. Mag., 6, 452-65, 485-98.

WOOLACOTT, D. (1923)
On a boring at Roddymoor Colliery, near Crook, Co. Durham, Geol. Mag., 60, 50-62.

WYCKOFF, R.D. and REED, D.W. (1935)
'Electrical conduction models for the solution of water seepage problems'. Physics, 6, 395-401.

ZEE, C.H., PETERSON, D.F. and BECK, R.O. (1957)
'Flow into a well by electric and membrane analogy'. Trans. Amer. Soc. Civil Engineering, 122, 1088-1112.

ZIENKIEWICZ, O.C. and CHEUNG, Y.K. (1967)
'The finite element method in structural and continuum mechanics'. McGraw-Hill, London. ✓

ZIENKIEWICZ, O.C. (1968)
'Continuum mechanics as an approach to rock mass problems'. In 'Rock Mechanics in Engineering Practice', ed. Stagg, K.G. and Zienkiewicz, O.C., Wiley, 237-73.

APPENDICES

APPENDIX A

Data and Analyses of Wells

Contained in this appendix are the details of the geological succession, the rest and pumped water levels, and results of analyses by the pertinent methods.

Since much of the information dates to the time of sinking it may be in error today, due to the effects of mining subsidence on ground elevations, and the ground water depletion that has taken place.

Abbreviations

B. E. H. F.	Below engine-house floor
B. L. M. L.	Basal Lower Magnesian Limestone
B. P. S.	Basal Permian Sands
C. M.	Coal Measures
E. H. F.	Engine-house floor
I. G. S.	Institute of Geological Sciences
H	Thickness
K	Hydraulic conductivity
K_1, K_5	Hydraulic conductivities derived from assuming radius of influence (r_e) 1,000 ft and 5,000 ft respectively.
L. M. L.	Lower Magnesian Limestone
M. M. L.	Middle Magnesian Limestone
N. R. A. R.	Northumbrian River Authority Report

O. D.	Ordnance datum
R. W. L.	Rest water level
SC	Specific capacity
SC_{50}	Specific capacity recalculated for 50% maximum drawdown
T_1, T_5	Transmissibilities for K_1 & K_5 respectively
U. M L.	Upper Magnesian Limestone
W. T. P.	Wartime Pamphlet No. 19, Anderson, 1941.

Sunderland and South Shields Water Company

Humbledon Pumping Station

Grid reference NZ 382552

Geological succession (from W. T. P.)

	Thickness (ft)	Depth (ft)
Surface deposits	33	33
Magnesian Limestone	269	302
Marl Slate	?	302
Basal Permian Sands	20	322
Coal Measures	3	325

E. H. F. 212.93 ft OD

Well top 199.43 ft OD

Well bottom -20.07 ft OD

Well 10ft diameter to 233ft B. E. H. F., then 2, 3 ins diameter boreholes 42.5ft down from well bottom.

R. W. L. circa 1941 32.5 ft OD

1966 39.9 ft OD.

Analysis of data

It is unlikely that the boreholes are now effective, due to collapse. The Lower Magnesian Limestone is probably about 20ft thick in this area, and the well bottom will thus be in Middle Magnesian Limestone lagoon-reef facies.

Steady state $Q = 0.245$ m. g. d. $h_e = 40$ ft

$r_w = 5$ ft $h_w = 13.5$ft.

Dupuit-Forcheimer	K_1 = 291.5 g. p. d. /ft^2
	T_1 = 11659 g. p. d. /ft
	K_5 = 380 g. p. d. /ft^2
	T_5 = 15200 g. p. d. /ft
Herbert	K_1 = 205 g. p. d. /ft^2
	T_1 = 8200 g. p. d. /ft
	K_5 = 218 g. p. d. /ft^2
	T_5 = 8938 g. p. d. /ft
Non-steady state	Recovery with water table adjustment.
	K = 244.4 g. p. d /ft^2
	T = 1026 g. p. d. /ft
Specific capacity	In 1966 SC = 9245 g. p. d. /ft at 66.3% dewatered,
	giving SC_{50} = 10371 g. p. d. /ft.

Hydraulic conductivity models

Horizon	H (ft)	K (gpd/ft^2)
M. M. L.	40	300
Horizontal K (g. p. d. /ft^2)	300	

Fulwell Pumping Station

Grid Reference NZ 389606

Geological succession (from W. T. P.)

	Thickness (ft)	Depth (ft)
Surface deposits	73	73
Magnesian Limestone	52	125
Marl Slate	4	129
Basal Permian Sands	163	292
Coal Measures	3	295

E. H. F. 71. 8 ft OD

Well top 55. 29 ft OD

Well bottom -74. 79 ft OD

Well 10ft diameter to 146. 6ft B. E. H. F., then borehole of unknown diameter 155 ft down from well bottom.

Headings 120ft x 6ft x 4ft at 119ft B. E. H. F.

70ft x 5ft x 4ft at 119ft B. E. H. F.

235ft x 6ft x 5ft at 141ft B. E. H. F.

R. W. L. circa 1941 -27ft OD

1967 10ft OD

Analysis of data

It is unlikely that the borehole is now effective, due to collapse. The results obtained by neglecting the headings are of doubtful value.

Steady state $Q = 1$ m. g. d. $h_e = 84.8$ft.

$r_w = 5$ft $h_w = 30.3$ ft

Dupuit-Forcheimer $K_1 = 268.9$ g. p. d. /ft^2

$T_1 = 22802$ g. p. d. /ft

$K_5 = 350.6$ g. p. d. /ft^2

$T_5 = 29728$ g. p. d /ft

Herbert $K_1 = 275$ g. p. d. /ft^2

$T_1 = 23320$ g. p. d. /ft

$K_5 = 290$ g. p. d. /ft^2

$T_5 = 24621$ g. p. d. /ft

Non-steady state Recovery

Jacob approximation $K = 98.2$ g. p. d./ft^2

$T = 8347$ g. p. d. /ft

Water table adjustment $K = 118.8$ g. p. d. /ft^2

$T = 10110$ g. p. d. /ft

Specific capacity In 1941, SC = 25500 g. p. d. /ft for 63. 3% dewatered, and in 1967, SC = 18348 g. p. d. /ft for 64. 3% dewatered. For the latter, $SC_{50} = 20280$ g. p. d. /ft.

Hydraulic conductivity models

Horizon	H (ft)	K (gpd/ft^2)	H (ft)	K (gpd/ft^2)	H (ft)	K (gpd/ft^2)
U. M. L.	64. 8	300	64. 8	300	64. 8	300
L. M. L.	20	0	20	40	20	110
Horizontal K (g. p. d/ft^2)	229. 2		238. 7		255. 2	

Cleadon Pumping Station

Grid reference NZ 387636

Geological succession (from W. T. P.)

	Thickness (ft)	Depth (ft)
Surface deposits	14	14
Magnesian Limestone	314	328
Basal Permian Sands	49	377
Coal Measures	2	379

E. H. F. 218. 37 ft OD

Well top 206. 37 ft OD

Well bottom -49. 83 ft OD

R. W. L. circa 1941 7ft OD

1966 8. 4ft OD

Well 12ft diameter to 268 ft B. E. H. F., then borehole 36" - 14" diameter 109ft down from well bottom.

Analysis of data

Due to the very high chloride content the well is used only intermittently.

Specific capacity In 1965, SC = 42857 g. p. d. /ft for 24. 1% dewatered, giving SC_{50} = 36544 g. p. d. /ft.

Hydraulic conductivity model

Horizon	H (ft)	K (gpd/ft^2)
U. M. L.	58	300

Horizontal K ($g. p. d. /ft^2$) 300

Ryhope Pumping Station

Grid reference NZ 404524

Geological succession (from W. T. P.)

	Thickness (ft)	Depth (ft)
Surface deposits	20	20
Magnesian Limestone	338	358
Basal Permian Sands	30	388
Coal Measures	9	397

E. H. F. 228. 64 ft OD

Well top 219. 27 ft OD

Well bottom -22. 94 ft OD

Well 14ft diameter to 251. 6 ft B. E. H. F., then borehole of unknown diameter 136ft down from well bottom.

R. W. L. circa 1940 -5 ft OD

1966 8. 64 ft OD.

Analysis of data

It is unlikely that the borehole is now effective, due to collapse. The high value of permeability obtained in the analysis is probably due to the nearby sea acting as a recharge source, and this is borne out by the high chloride contamination of the pumped water.

Steady state $Q = 0.63$ m. g. d. $h_e = 31.64$ ft

$r_w = 7$ft $h_w = 25.09$ ft

Dupuit-Forcheimer $K_1 = 2679$ g. p. d. /ft^2

$T_1 = 84737$ g. p. d. /ft.

Herbert

K_1 = 430 g. p. d. /ft^2

T_1 = 13605 g. p. d. /ft

K_5 = 460 g. p. d. /ft^2

T_5 = 14559 g. p. d. /ft

Specific capacity

In 1965 SC = 96183 g. p. d. /ft for 20. 7% dewatered,

giving SC_{50} = 80457 g. p. d. /ft.

Hydraulic conductivity models

Horizon	H (ft)	K (gpd/ft^2)
?U. M. L.	31. 64	300
Horizontal K (g. p. d. /ft^2)		300

Dalton Pumping Station

Grid reference NZ 411469

Geological succession (from I. G. S. records)

Main shaft (north plant)

	Thickness (ft)	Depth (ft)
Surface deposits	26. 8	26. 8
Magnesian Limestone	442. 3	469. 1
Marl Slate	2	471. 1

Pilot shaft (south plant)

	Thickness (ft)	Depth (ft)
Surface deposits	?	?
Magnesian Limestone	?	465. 9
Marl Slate	0. 8	466. 7
Basal Permian Sands	83. 1	549. 8

Main shaft

E. H. F. 340. 31 ft OD

Well top 325. 56 ft OD

Well bottom -105. 89 ft OD

Well 20ft x 12. 5ft ellipse to 446. 2 ft B. E. H. F. then 1 ft diameter borehole 25ft down from well bottom.

Pilot shaft

E. H. F. 348. 3 ft OD

Well top 338. 41 ft OD

Well bottom -98. 7ft OD

Well 10ft diameter to 447ft B. E. H. F. then 2 boreholes, 12ins and 3ins diameter, 21ft down from well bottom.

R.W.L. in main shaft circa 1940 36ft OD

1966 48.3ft OD

Analysis of data

Neglecting any effects from the borehole, the main shaft penetrates to within 24ft of the base of the Lower Magnesian Limestone.

Steady state $Q = 1.53$ m.g.d. $h_e = 154$ ft

$r_w = 7.5$ft $h_w = 27.3$ ft

Dupuit-Forcheimer

$K_1 = 103.7$ g.p.d./ft^2

$T_1 = 15977$ g.p.d./ft

$K_5 = 137.9$ g.p.d./ft^2

$T_5 = 21232$ g.p.d./ft

Herbert

$K_1 = 105$ g.p.d./ft^2

$T_1 = 16170$ g.p.d./ft

$K_5 = 116$ g.p.d./ft^2

$T_5 = 17980$ g.p.d/ft

$Q = 1.75$ m.g.d. $h_e = 154$ ft

$r_w = 7.5$ ft $h_w = 12.2$ft

Dupuit-Forcheimer

$K_1 = 115.7$ g.p.d./ft^2

$T_1 = 17812$ g.p.d./ft

$K_5 = 153.7$ g.p.d./ft^2

$T_5 = 23671$ g.p.d./ft

Herbert

$K_1 = 116$ g.p.d./ft^2

$T_1 = 18096$ g.p.d./ft

$K_5 = 129$ g.p.d./ft^2

$T_5 = 20253$ g.p.d./ft

Specific capacity — In 1966:

for Q = 1.53 m.g.d. SC = 12056 g.p.d./ft for 82.3% dewatered

for Q = 1.75 m.g.d. SC = 12323 g.p.d./ft for .92% dewatered

Average SC_{50} = 16239 g.p.d./ft

Hydraulic conductivity models

Horizon	H (ft)	K (gpd/ft^2)	H (ft)	K (gpd/ft^2)	H (ft)	K (gpd/ft^2)
L.M.L.	154	110	149	110	149	110
B.L.M.L.	0	-	5	40	5	0
Horizontal K ($g.p.d./ft^2$)		110		107.7		106.4

Seaton Pumping Station

Grid reference NZ 393489

Geological succession (from W. T. P.)

	Thickness (ft)	Depth (ft)
Surface deposits	13	13
Magnesian Limestone	434	447

Coal Measures at base

E. H. F. 427.66 ft OD

Well top 415.15 ft OD

Well bottom -24.09 ft OD

Well 13 ft diameter to 452 ft B. E. H. F.

R. W. L. 1894 97 ft OD

1934 58 ft OD

1966 58 ft OD

Analysis of data

Since there are no effects from boreholes or from the Basal Permian Sands, the permeability value should be a good representation for the Lower Magnesian Limestone.

Steady state $Q = 0.205$ m. g. d. $h_e = 82$ ft

$r_w = 6.5$ ft $h_w = 34.1$ ft

Dupuit-Forcheimer $K_1 = 59.1$ g. p. d. /ft^2

$T_1 = 4846$ g. p. d. /ft

$K_5 = 78.0$ g. p. d. /ft^2

$T_5 = 6394$ g. p. d. /ft

Herbert $K_1 = 66$ g. p. d. /ft^2

$T_1 = 3076$ g. p. d. /ft

$K_5 = 70$ g. p. d. /ft^2

$T_5 = 3690$ g. p. d. /ft

Non-steady state Recovery:

Jacob approximation $K = 29.7$ g. p. d. /ft^2

$T = 1430$ g. p. d. /ft

Water table adjustment $K = 40.9$ g. p. d. /ft^2

$T = 2008$ g. p. d. /ft

Specific capacity In 1966 SC = 4279 g. p. d. /ft for 58.4% dewatered, giving $SC_{50} = 4533$ g. p. d. /ft.

Hydraulic conductivity models

Horizon	H (ft)	K (gpd/ft^2)	H (ft)	K (gpd/ft^2)	H (ft)	K (gpd/ft^2)
L. M. L.	69	110	59	110	49	110
B. L. M. L.	13	40	23	40	33	40
Horizontal K (g. p. d. /ft^2)		98.9		90.4		81.8

Horizon	H (ft)	K (gpd/ft^2)	H (ft)	K (gpd/ft^2)	H (ft)	K (gpd/ft^2)
L. M. L.	69	110	59	110	49	110
B. L. M. L.	13	0	23	0	33	0
Horizontal K (g. p. d. /ft^2)		92.6		79.1		65.7

Stonygate Pumping Station

Grid reference NZ 354417

Geological succession (from W. T. P.)

	Thickness (ft)	Depth (ft)
Surface deposits	12	12
Magnesian Limestone	344	356
Basal Permian Sands	32	388

E. H. F 365. 72 ft O. D.

Well top 347. 05 ft O. D.

Well bottom 28. 72 ft OD

Well 15 ft x 10. 7 ft ellipse to 337 ft B. E. H. F., then 2, 3ins diameter boreholes 59ft down from well bottom.

R. W. L.	1905	129 ft OD
	1931	117 ft OD
	1966	134 ft OD

Analysis of data

It is unlikely that the borehole is now effective, due to collapse. A value of r_w = 6ft has been used to approximate the elliptical shape.

Steady state $Q = 0.63$ m. g. d. $h_e = 105.3$ ft

$r_w = 6$ ft $h_w = 41.5$ ft.

Dupuit-Forcheimer $K_1 = 109.6$ g. p. d. /ft^2

$T_1 = 11536$ g. p. d. /ft.

$K_5 = 144.0$ g. p. d. /ft^2

$T_5 = 15165$ g. p. d/ft

Herbert

K_1 = 95 g. p. d. /ft^2

T_1 = 10003 g. p. d. /ft

K_5 = 110 g. p. d. /ft^2

T_5 = 11583 g. p. d. /ft

Specific capacity

In 1966 SC = 9874 g. p. d. /ft for 60. 6 dewatered, giving SC_{50} = 10624 g. p, d/ft.

Hydraulic conductivity models

Horizon	H (ft)	K (g. p. d. /ft^2)	H (ft)	K (gpd/ft^2)	H (ft)	K (gpd/ft^2)
L. M. L.	105	110	103	110	103	110
B. L. M. L.	0		2	40	2	0
Horizontal K (g. p. d. /ft^2)	110		108. 7		107. 9	

Thorpe Pumping Station

Grid reference NZ 427438

Geological succession (from W. T. P.)

	Thickness (ft)	Depth (ft)
Surface deposits	12	12
Magnesian Limestone	411	423
Basal Permian Sands	161	584

E. H. F. 370. 04 ft OD

Well top 359. 75 ft OD

Well bottom -103. 96 ft OD

Well 21 ft x 15 ft ellipse to 306 ft B. E. H. F. then 15ft diameter to 474 ft B. E. H. F., with borehole of unknown diameter 38 ft down from well bottom.

R. W. L. 1901 -44 ft OD

1966 -2 ft OD

Analysis of data

It is unlikely that the borehole is now effective, due to collapse. Since the saturated zone is penetrated only by the circular cross-section, the well radius is 7. 5 ft.

Steady state $Q = 0.7$ m. g. d. $h_e = 102$ ft

$r_w = 7.5$ ft $h_w = 15$ ft

$K_1 = 107.1$ g. p. d. /ft^2

$T_1 = 10926$ g. p. d. /ft

$K_5 = 142.4$ g. p. d. /ft^2

$T_5 = 14519$ g. p. d. /ft

Herbert $K_1 = 124$ g. p. d. /ft^2

$T_1 = 12648$ g. p. d. /ft

$K_5 = 140$ g. p. d. /ft^2

$T_5 = 14420$ g. p. d. /ft

Non-steady state Recovery:

Jacob approximation $K = 45.3$ g. p. d. /ft^2

$T = 4711$ g. p. d. /ft

Water table adjustment $K = 56.4$ g. p. d. /ft^2

$K = 5922$ g. p. d. /ft

Specific capacity In 1966, SC = 8046 g. p. d. /ft for 89.2% dewatered, giving $SC_{50} = 10891$ g. p. d. /ft.

Hydraulic conductivity models

Horizon	H (ft)	K (gpd/ft^2)	H (ft)	K (gpd/ft^2)	H (ft)	K (gpd/ft^2)
L. M. L.	402	110	32	110	22	110
B. L. M. L.	20	40	30	40	40	40
B. P. S.	40	120	40	120	40	120
Horizontal K (g. p. d. /ft^2)	100.2		93.3		86.5	

Horizon	H (ft)	K (gpd/ft^2)	H (ft)	K (gpd/ft^2)	H (ft)	K (gpd/ft^2)
L. M. L.	42	110	32	110	22	110
B. L. M. L.	20	0	30	0	40	0
B. P. S.	40	120	40	120	40	120
Horizontal K (gpd/ft^2)	92.4		81.6		70.8	

Burdon Pumping Station

Grid reference NZ 372513

Geological succession (from W. T. P.)

	Thickness (ft)	Depth (ft)
Surface deposits	57	57
Magnesian Limestone	366	423
Basal Permian Sands	34	457
Coal Measures	10	467

E. H. F. 462. 9 ft OD

Well top 444. 9 ft OD

Well bottom 50. 4 ft OD

Well 20ft x 14 ft ellipse to 293 ft B. E. H. F., then 14ft diameter to 472. 07 ft B. E. H. F., with a 12ins diameter borehole 27. 33 ft down from the well bottom.

R. W. L.	1900	115 ft OD
	1934	72 ft OD
	1966	39 ft OD

Analysis of data

The large variations in rest water levels render analysis doubtful. After the bottom was drawn out, the well was little used between 1920 and 1957. It was deepened by 40ft and a submersible pump installed in 1966.

Specific capacity In 1934 SC = 27450 g. p. d. /ft.

North Dalton Pumping Station

Grid reference NZ 408478

Geological succession (from I.G.S. records)

2 shafts and one borehole, for which the drillers records are identical.

	Thickness (ft)	Depth (ft)
Surface deposits	60	60
Magnesian Limestone	341	401
Basal Permian Sands	66	467
Coal Measures	1.5	468.5

Well tops 270.44 ft OD

East borehole top 275.3 ft OD

Twin shafts 14 ft diameter, 238 ft deep, with twin boreholes 31 ins - 24 ins diameter 221 ft down from each shaft bottom.

East borehole, 77ft from shafts, 24ins diameter, 468 ft deep.

A drift joins shafts and borehole at shaft bottom.

R.W.L.	Shafts	1909	33 ft OD
		1940	39 ft OD
		1966	26 ft OD
	Borehole	1906	33.5 ft OD

Analysis of data

The main shafts are 27 ft apart and the east borehole lies in line with them, 50.5 ft from the nearest.

Steady state Using multiple well methods

$Q_1 = Q_2 = 1.1$ m.g.d. $h_e = 215$ ft

$r_o = 64$ ft $h_o = 114$ ft

$r_1 = 13.5$ ft $r_2 = -13.5$ ft

$r_e = 1000$ ft

Dupuit-Forcheimer $K_1 = 99.4$ g. p. d. /ft^2

$T_1 = 21371$ g. p. d. /ft

Specific capacity This is difficult to determine since both shafts are pumped simultaneously.

Hydraulic conducitivity models

Horizon	H (ft)	K (gpd/ft^2)	H (ft)	K (gpd/ft^2)	H (ft)	K (gpd/ft^2)
L. M. L.	132	110	122	110	112	110
B. L. M. L.	20	40	30	40	40	40
B. P. S.	63	120	63	120	63	120
Horizontal K (g. p. d. /ft^2)	106.4		103.2		99.9	

Horizon	H (ft)	K (gpd/ft^2)	H (ft)	K (gpd/ft^2)	H (ft)	K (gpd/ft^2)
L. M L.	132	110	122	110	112	110
B. L. M. L.	20	0	30	0	40	0
B. P. S.	63	120	63	120	63	120
Horizontal K (g. p. d. /ft^2)	102.7		97.6		92.5	

New Winning Pumping Station

Grid reference NZ 407385

Geological succession (from W. T. P.) only one section given

	Thickness (ft)	Depth (ft)
Surface deposits	179	179
Magnesian Limestone	316	495
Basal Permian Sands	37	532 entered

E. H. F. 395.07 ft OD

No. 1 well 10 ft diameter to 477 ft B. E. H. F.

No. 2 well 14 ft diameter for 330 ft then remainder 9ft diameter to 503ft B. E. H. F.

R. W. L. No. 1 well 1924 185 ft OD

1949 70 ft OD

Analysis of data

Each well is generally pumped separately, allowing the standing well to be used as an observation well at 73 ft distance.

Steady state No. 1 $Q = 1.2$ m. g. d. $h_e = 151$ ft

$r_w = 5$ft $h_w = 22$ ft

Dupuit-Forcheimer $K_1 = 90.7$ g. p. d. /ft^2

$T_1 = 13696$ g. p. d. /ft

Herbert $K_1 = 75$ g. p. d. /ft^2

$T_1 = 11325$ g. p. d. /ft

$K_5 = 87$ g. p. d. /ft^2

$T_5 = 13137$ g. p. d. /ft

Hydraulic conductivity models

No. 1.

Horizon	H (ft)	K (gpd/ft^2)	H (ft)	K (gpd/ft^2)	H (ft)	K (gpd/ft^2)
L. M. L.	151	110	141	110	131	110
B. L. M. L.	0		10	40	20	40
Horizontal K (g. p. d. /ft^2)	110		105. 4		100. 7	

Horizon	H (ft)	K (gpd/ft^2)	H (ft)	K (gpd/ft^2)	H (ft)	K (gpd/ft^2)
L. M. L.	151	110	141	110		
B. L. M. L.	10	0	20	0		
Horizontal K (g. p. d. /ft^2)	102. 7		94. 4			

Herrington Pumping Station

Grid reference NZ 363528

Geological succession (from W. T. P.)

	Thickness (ft)	Depth (ft)
Surface deposits	?	?
Magnesian Limestone	?	300
Marl Slate	8	308
Basal Permian Sands	7	315
Coal Measures	19	334

E. H. F. 275.17 ft OD

Well 9 ft diameter to 162 ft B. E. H. F. then 2, 24ins diameter boreholes 167 ft and 272 ft down from well bottom.

R. W. L. circa 1940 115 ft OD

Analysis of data

Arrangement of well and boreholes makes analysis of doubtful value.

Peterlee Pumping Station

Grid reference NZ 425409

Geological succession

	Thickness (ft)	Depth (ft)
Surface deposits	164	164
Magnesian Limestone	338	502
Marl Slate	1.5	503.5
Basal Permian Sands	52.5	556
Coal Measures	4	560

Borehole top 330 ft OD

Borehole 33 ins - 24 ins diameter down 560 ft

R.W.L. 1966 20 ft OD

Analysis of data

The borehole diameter below the rest water level is 24 ins.

Steady state $Q = 0.49$ m.g.d. $h_e = 250$ ft

$r_w = 1$ft $h_w = 182$ ft

Dupuit-Forcheimer $K_1 = 36.7$ g.p.d./ft^2

$T_1 = 9170$ g.p.d./ft

$K_5 = 45.2$ g.p.d./ft^2

$T_5 = 11307$ g.p.d./ft

Herbert $K_1 = 25$ g.p.d./ft^2

$T_1 = 6250$ g.p.d./ft

$K_5 = 26$ g.p.d./ft^2

$T_5 = 6500$ g.p.d./ft

For $Q = 0.7$ m.g.d. $h_w = 141$ ft

Dupuit-Forcheimer $K_1 = 36.1$ g. p. d. /ft^2

$T_1 = 9030$ g. p. d. /ft

$K_5 = 44.5$ g. p. d. /ft^2

$T_5 = 11133$ g. p. d. /ft

Herbert Outside range of graphs

For Q = 0.8 m. g. d. $h_w = 122$ ft

Dupuit Forcheimer $K_1 = 37.0$ g. p. d. /ft^2

$T_1 = 9237$ g. p. d. /ft

$K_5 = 45.6$ g. p. d. /ft^2

$T_5 = 11388$ g. p. d. /ft

Herbert. Outside range of graphs.

Specific capacity The yield-drawdown curve is shown in fig 2.4.

For Q = 0.49 m. g. d. SC = 7205 g. p. d. /ft for 27.2% dewatered.

For Q = 0.7 m. g. d. SC = 6422 g. p. d /ft for 43.6% dewatered.

For Q = 0.8 m. g. d. SC = 6250 g. p. d. /ft for 51.2% dewatered.

Average SC_{50} = 6238 g. p. d. /ft.

Hydraulic conductivity models

Horizon	H (ft)	K (gpd/ft^2)	H (ft)	K (gpd/ft^2)	H (ft)	K (gpd/ft^2)
L. M. L.	153	110	153	110	153	110
B. L. M. L.	40	0	40	0	40	0
B. P. S.	53	120	53	40	53	0
C. M.	4	0	4	0	4	0
Horizontal K (g. p. d. /ft^2)	92.8		75.8		67.3	

Horizon	H (ft)	K (gpd/ft^2)	H (ft)	K (gpd/ft^2)	H (ft)	K (gpd/ft^2)
L. M. L.	113	110	63	110	0	
B. L. M. L.	80	40	130	40	193	40
B. P. S.	53	40	53	40	53	40
C. M.	4	0	4	0	4	0
Horizontal K (g. p. d. /ft^2)		71		57		39.4

Mill Hill Borehole

Grid reference NZ 412425

Geological succession (a comprehensive section is given in Smith & Francis, op. cit.)

	Thickness (ft)	Depth (ft)
Surface deposits	34	34
Magnesian Limestone	481	515
Marl Slate	2	517
Basal Permian Sands	120	637
Coal Measures	3	640

Borehole top 510 ft OD

Borehole 30 ins - 15 ins diameter, 640 ft deep.

R.W.L. 1962 on drilling 64 ft OD

1966 recovered to 33.5 ft OD

Analysis of data

Average radius below rest water level is 12 ins.

Steady state $Q = 0.61$ m.g.d. $h_e = 166.5$ ft

$r_w = 1$ ft $h_w = 115.5$ ft

Dupuit-Forcheimer $K_1 = 93.3$ g.p.d./ft^2

$T_1 = 15530$ g.p.d./ft

$K_5 = 115.0$ g.p.d./ft^2

$T_5 = 19148$ g.p.d./ft

Herbert $K_1 = 120$ g.p.d./ft^2

$T_1 = 19980$ g.p.d./ft

$K_5 = 123$ g.p.d./ft^2

$T_5 = 20479$ g.p.d./ft

Specific capacity SC = 11960 for 30.6% dewatered, giving $SC_{50} = 10589$ g.p.d./ft.

Hydraulic conductivity models

Horizon	H (ft)	K (gpd/ft^2)	H (ft)	K (gpd/ft^2)	H (ft)	K (gpd/ft^2)
L. M. L.	22	110	12	110	2	110
B. L. M. L.	20	40	30	40	40	40
B. P. S.	120	120	120	120	120	120
C. M.	5	0	5	0	5	0
Horizontal K (g. p. d. /ft^2)	105. 5		101. 3		97. 1	

Horizon	H (ft)	K (gpd/ft^2)	H (ft)	K (gpd/ft^2)	H (ft)	K (gpd/ft^2)
L. M. L.	22	110	12	110	2	110
B. L. M. L.	20	0	30	0	40	0
B. P. S.	120	120	120	120	120	120
C. M.	5	0	5	0	5	0
Horizontal K (g. p. d. /ft^2)	100. 7		94. 1		87. 5	

Hartlepools Water Company

Lancaster Road

Grid reference NZ 508334

Geological succession Disused Upper Magnesian Limestone quarry.

14 boreholes of varying lengths and diameters discharging into central adit.

Ground level 30 ft OD

R.W.L. up to 1949 2 ft OD artesian

1966 -11 ft OD

Analysis of data

Complexity of boreholes and pumping makes analysis impossible.

Specific capacity In 1966 drawdown 20 ft - 30 ft at Q = 1.08 m.g.d.

giving an approximate value SC = 45000 g.p.d./ft.

Howbeck Pumping Station

Grid reference NZ 500343

Geological succession No. 1 b.h.

	Thickness (ft)	Depth (ft)
Surface deposits	37	37
Magnesian Limestone	297	334

Ground level 37 ft OD

2, 21 ins diameter boreholes at 20 ft centres, pumped one at a time.

R.W.L. 1941 6 ft OD

1965 -1 ft OD

Analysis of data

The aquifer may be marginally confined by drift at this locality, the thickness of which varies from 37 ft to 57 ft for the various boreholes at the site.

Dalton Piercy Pumping Station

Grid reference

Geological succession, 7 boreholes

		Thickness (ft)	Depth (ft)
No. 1	Surface deposits	215	215
	Magnesian Limestone	85	300
No. 2	Surface deposits	126	126
	Magnesian Limestone	174	300
No. 3	Surface deposits	124. 5	124. 5
	Magnesian Limestone	195. 5	320
No. 4	Surface deposits	124	124
	Magnesian Limestone	197	321
No. 5	Surface deposits	124. 5	124. 5
	Magnesian Limestone	226	350. 5
No. 6	Surface deposits	132	132
	Magnesian Limestone	296	428
No. 7	Surface deposits	170	170
	Magnesian Limestone	280	450

Ground level 216 ft OD

R. W. L. average -21 ft OD

Analysis of results

At present, 4 boreholes are extracting up to 5.5 m.g.d. at rates depending upon demand. The interaction between holes and the varying pumping rates makes detailed analysis impossible. The aquifer is unconfined over the site area.

Specific capacity — At a total pumping rate of 5.5 m.g.d. the average drawdown is 30 ft giving an approximate value of SC = 1830000 g.p.d./ft.

Coal Lane

Grid reference NZ 431328

Geological succession (from I. G. S. records)

		Thickness (ft)	Depth (ft)
No. 1	Surface deposits	125	125
	Middle Magnesian Limestone	298. 5	423. 5
	Lower Magnesian Limestone	76. 5	500
No. 2	Surface deposits	103	103
	Middle Magnesian Limestone	302	405
	Lower Magnesian Limestone	45	450

Ground level No. 1 340 ft OD No. 2 340 ft OD.

Boreholes 18 ins diameter at 20 ft centres

R. W. L. 35 ft OD

Analysis of data

Both wells are generally pumped simultaneously.

Steady state No. 2. $Q = 1.1$. m. g. d. $h_e = 145$ ft

$r_w = 0.75$ ft $h_w = 112$ ft

Dupuit-Forcheimer $K_1 = 297.1$ g. p. d. /ft^2

$T_1 = 43080$ g. p. d. /ft

$K_5 = 363$ g. p. d. /ft^2

$T_5 = 52716$ g. p. d. /ft

Specific capacity SC = 33333 g. p. d. /ft for 22. 8% dewatered,

$SC_{50} = 29205$ g. p. d. /ft.

Hydraulic conductivity models

Horizon	H	K
M.M.L.	100	300
L.M.L.	45	110
Horizontal K ($g.p.d/ft^2$)	241.0	

Naisberry Pumping Station

Grid reference NZ 467337

Geological succession (from I. G. S. records)

		Thickness (ft)	Depth (ft)
No. 1	Surface deposits	30	30
	? Upper Magnesian Limestone	?30	?60
	Middle Magnesian Limestone	387	447
	Lower Magnesian Limestone	53	500

No. 2 Bore, 40 yd NW of No. 1 was sunk to 550 ft without penetrating Marl Slate.

E. H. F. 385.1 ft OD

Borehole top 381.72 ft OD

R. W. L. 5.7 ft OD

8.0 ft OD when drilled (1953).

Analysis of data

Both boreholes are generally pumped simultaneously

Steady state — Data for when only No. 1 abstracting.

$Q = 0.44$ m. g. d. $h_e = 125$ ft

$r_w = 0.75$ ft $h_w = 115$ ft

Dupuit-Forcheimer

$K_1 = 420.0$ g. p. d. /ft^2

$T_1 = 52494$ g. p. d. /ft

$K_5 = 513.9$ g. p. d. /ft^2

$T_5 = 64236$ g. p. d. /ft

	For Q = 0.538 m.g.d.	h_w = 111 ft
Dupuit-Forcheimer	K_1 = 373.0	
	T_1 = 46624	
	K_5 = 456.4	
	T_5 = 57053	
	For Q = 0.605 m.g.d.	h_w = 109 ft
Dupuit-Forcheimer	K_1 = 527.1	
	T_1 = 65893	
	K_5 = 645.1	
	T_5 = 80631	
	For Q = 0.48 m.g.d.	h_w = 114 ft
Dupuit-Forcheimer	K_1 = 418.2	
	T_1 = 52279	
	K_5 = 511.8	
	T_5 = 63972	
	For Q = 0.72 m.g.d.	h_w = 95 ft
Dupuit-Forcheimer	K_1 = 249.9	
	T_1 = 31237	
	K_5 = 305.8	
	T_5 = 38223	
	For Q = 0.868 m.g.d.	h_w = 85 ft
Dupuit-Forcheimer	K_1 = 236.7	
	T_1 = 29588	
	K_5 = 289.6	
	T_5 = 36206	
	Average K_1 = 370.8 g.p.d./ft^2	

Specific capacity — The specific capacities for the various pumping rates are:

Q = 0.44 m.g.d. — SC = 44000 g.p.d. /ft for 8.7% dewatered SC_{50} = 34500 gpd/f

Q = 0.538 m.g.d. — SC = 38429 g.p.d/ft for 12.1% dewatered SC_{50} = 30674 gpd/f

Q = 0.605 m.g.d. — SC = 37813 g.p.d. /ft for 13.8% dewatered SC_{50} = 30461 gpd/f

Q = 0.48 m.g.d. — SC = 43636 g.p.d/ft for 9.5% dewatered SC_{50} = 34359 gpd/f

Q = 0.72 m.g.d. — SC = 34286 g.p.d/ft for 18.1% dewatered SC_{50} = 28273 gpd/f

Q = 0.868 m.g.d. — SC = 2800 g.p.d/ft for 26.7% dewatered SC_{50} = 24234 gpd/ft

Average SC_{50} = 30417 g.p.d. /ft

Hydraulic conductivity models

Horizon	H	K
M.M.L.	72	300
L.M.L.	53	110
Horizontal K (g.p.d. /ft^2)	219.4	

Amerston Hall

Grid reference NZ 426304

Geological succession

	Thickness (ft)	Depth (ft)
Surface deposits	227	227
Red Marl	60	287
Magnesian Limestone	213	500

Ground Level 246 ft OD

R.W.L. 1965 50 ft OD

Analysis of data

The Magnesian Limestone aquifer is confined by the Upper Permian Marls, and has an artesian head of 91 ft.

Butterwick

Grid reference NZ 378298

Geological succession

	Thickness (ft)	Depth (ft)
Surface deposits	89	89
Magnesian Limestone	261	350
Marl Slate		350+

Ground level 310 ft OD

Borehole 15 ins - 12 ins diameter to 350 ft

R.W.L. 1966 82ft OD

Analysis of data

The groundwater level in this area has been lowered by about 150 ft since the mid 1930's, due to pumping at the nearby Fishburn Colliery.

Steady state $Q = 0.341$ m.g.d. $h_e = 120$ ft

$r_w = 0.5$ ft $h_w = 30$ ft

Dupuit-Forcheimer $K_1 = 61.1$ g.p.d./ft^2

$T_1 = 7334$ g.p.d./ft

$K_5 = 74.1$ g.p.d./ft^2

$T_5 = 8888$ g.p.d./ft

Herbert $K_1 = 46$ g.p.d./ft^2

$T_1 = 5520$ g.p.d./ft

Non-steady state Recovery

Jacob approximation $K = 20.4$ g.p.d./ft^2

$T = 2448$ g.p.d./ft

Specific capacity SC = 3786 g. p. d. /ft for 75% dewatered, giving

SC_{50} = 4543 g. p. d. /ft.

Hydraulic conductivity models

Horizon	H (ft)	K (gpd/ft^2)	H (ft)	K (gpd/ft^2)	H (ft)	K (gpd/ft^2)
L. M. L.	100	110	90	110	80	110
B. L. M. L.	20	40	30	40	40	40
Horizontal K ($g. p. d. /ft^2$)	98. 3		92. 5		86. 7	

Horizon	H (ft)	K (gpd/ft^2)	H (ft)	K (gpd/ft^2)	H (ft)	K (gpd/ft^2)
L. M. L.	100	110	90	110	80	110
B. L. M. L.	20	0	30	0	40	0
Horizontal K ($g. p. d/ft^2$)	91. 7		92. 5		73. 3	

Northumbrian River Authority: south-east Durham groundwater investigation

In this scheme, boreholes and observation wells were drilled by Tees Valley and Cleveland Water Board, Imperial Chemical Industries, and the Northumbrian River Authority, the latter processing most of the data (Northumbrian River Authority Report, 1969). The following results have been abstracted from this.

Borehole C

Grid reference NZ 337216

Geological succession

	Thickness (ft)	Depth (ft)
Surface deposits	179	179
Middle Magnesian Limestone	74	253
Lower Magnesian Limestone	9	262

Borehole 13 ins diameter reducing to 10 ins diameter

R.W.L. 180.46 ft OD

Non-steady state analysis From N.R.A.R., table 7

Plane	Method	T (gpd/ft)	K (gpd/ft^2)	S ($x10^{-4}$)	SC (gpd/ft)
C	Jacob	26000	351.4		25200
C-Gt. Stainton	Jacob	28427	379.0	0.98	
	Theis	21774	286.5	2.3	
C-17	Jacob	15194	197.3	1.7	
	Theis	24193	310.2	1.6	
C-G	Jacob	20352	257.6	0.2	
	Theis	25480	318.5	5.5	
C-19	Theis	1263	15.6	0.15	
C-R	Theis	44637	544.4	3.4	

Borehole D

Grid reference NZ 294263

Geological succession

	Thickness (ft)	Depth (ft)
Surface deposits	110	110
Middle Magnesian Limestone	52	162
Lower Magnesian Limestone	23	185

Borehole diameter 13 ins reducing to 10 ins.

R.W.L. 229.91 ft OD

Non-steady state analysis From N.R.A.R., table 7.

Plane	Method	T (gpd/ft)	K (gpd/ft^2)	S ($x10^{-4}$)	SC (gpd/ft)
D	Jacob	35800	688.5		26880
D-7	Theis	31908	602.0	0.3	

Borehole E

Grid reference NZ 323275

Geological succession

	Thickness (ft)	Depth (ft)
Surface deposits	124	124
Middle Magnesian Limestone	105.5	229.5
Lower Magnesian Limestone	5.5	234

Borehole diameter 13 ins reducing to 10 ins.

R.W.L. 202.21 ft OD

Non-steady state analysis From N.R.A.R., table 7.

Plane	Method	T (gpd/ft)	K (gpd/ft^2)	S ($x10^{-4}$)	SC (gpd/ft)
Pre-acidisation					
E	Jacob	4550	43.1		5856
E-13	Jacob	22494	213.0	1.7	
	Theis	13771	130.3	1.7	
Post-acidisation					
E	Jacob	7350	69.5		7632
E-13	Theis	7841	74.0	1.1	
E-9	Theis	47768?	450.6	13?	

Borehole G

Grid reference NZ 313207

Geological succession

	Thickness (ft)	Depth (ft)
Surface deposits	162	162
Upper Magnesian Limestone	65	227
Lower Evaporite Group	21	248
Middle Magnesian Limestone	69	317
Lower Magnesian Limestone	1	

Borehole diameter 13 ins reducing to 10 ins reducing to 8 ins.

R.W.L. 191.34 ft OD

Non-steady state analysis From N.R.A.R., table 7.

Plane	Method	T (gpd/ft)	K (gpd/ft^2)	S ($x10^{-4}$)	SC (gpd/ft)
G	Jacob	18458	267.5		31920
G-19	Jacob	33807	483.0	12	
	Theis	40081	564.5	13	
G-Gt. Stainton	Theis	28193	391.6	0.34	
G-17	Theis	9517	130.4	0.74	
G-18	Theis	48098	650.0	0.86	

Borehole J

Grid reference NZ 315227

Geological succession

	Thickness (ft)	Depth (ft)
Surface deposits	187	187
Middle Magnesian Limestone	59	246
Lower Magnesian Limestone	11	255

Borehole 13 ins reducing to 10 ins.

R.W.L. 213.96 ft OD

Non-steady state analysis From N.R.A.R., table 7.

Plane	Method	T (gpd/ft)	K (gpd/ft^2)	S ($x10^{-4}$)	SC (gpd/ft)
J	Jacob	12600	213.6		10560
J-10	Theis	5386	89.8	0.5	
J-18	Theis	13465	220.7	36	

Borehole K

Grid reference NZ 338265

Geological succession

	Thickness (ft)	Depth (ft)
Surface deposits	219	219
Middle Magnesian Limestone	92	311
Transitional Beds	6	317
Lower Magnesian Limestone	56	373

Borehole diameter 13 ins reducing to 10 ins.

R.W.L. 135.38 ft OD

Non-steady state analysis From N R.A.R., table 7.

Plane	Method	T (gpd/ft)	K (gpd/ft^2)	S ($x10^{-4}$)	SC (gpd/ft)
K	Jacob	3986	43.3		6384
K-11	Jacob	6165	66.3	1.9	
	Theis	5213	55.5	2.5	
K-L	Jacob	17109	180.1	3.5	
	Theis	17711	184.5	5.4	
K-O	Theis	8158	84.1	2.2	

Borehole L

Grid reference NZ 359277

Geological succession

	Thickness (ft)	Depth (ft)
Surface deposits	259.5	259.5
Upper Magnesian Limestone	69	328.5
Lower Evaporite Group	61.5	390
Middle Magnesian Limestone	124	514
Lower Magnesian Limestone	14	528

Borehole 10 ins reducing to 8 ins

R.W.L. 91.80 ft OD

Non-steady state analysis From N.R.A.R., table 7.

Plane	Method	T (gpd/ft)	K (gpd/ft^2)	S ($x10^{-4}$)	SC (gpd/ft)
L	Jacob	12800	103.2		11880
L-20	Jacob	20492	163.9	0.8	
L-25	Jacob	11557	91.7	0.7	
L-21	Jacob	15234	120.0	0.8	
L-K	Jacob	2268	17.7	0.4	
L-12	Jacob	11550	89.5	2.1	
L-11	Jacob	1892	14.6	0.4	
L-M	Jacob	3164	24.2	0.7	

Borehole N

Grid reference NZ 344267

Geological succession

	Thickness (ft)	Depth (ft)
Surface deposits	243	243
Middle Magnesian Limestone	101	344
Lower Magnesian Limestone	6	350

Borehole diameter 10 ins reducing to 9 ins, reducing to 8 ins.

R.W.L. 179.06 ft OD

Non-steady state analysis From N.R.A.R., table 7.

Plane	Method	T (gpd/ft)	K (gpd/ft^2)	S (x10^{-4})	SC (gpd/ft)
N	Jacob	9409	93.2		15768
N-11	Theis	7648	75.0	4.2	
	Jacob	13856	134.5	2.6	
N-13	Theis	12992	124.9	2.7	
	Jacob	19689	187.5	1.5	
N-O	Theis	11770	111.0	0.9	
	Jacob	19085	178.4	0.6	
N-22	Theis	10543	97.6	2.0	
	Jacob	15867	145.6	0.6	

Borehole 0

Grid reference NZ 340254

Geological succession

	Thickness (ft)	Depth (ft)
Surface deposits	223	223
Middle Magnesian Limestone	42.5	265.5
Lower Magnesian Limestone	62	327.5
Marl Slate	17.4	344.9
Carboniferous	4	348.9

Borehole diameter 10 ins reducing to 8 ins.

R.W.L. 192.0 ft OD

Non-steady state analysis From N.R.A.R, table 7.

Plane	Method	T (gpd/ft)	K (gpd/ft^2)	S ($x10^{-4}$)	SC (gpd/ft)
O	Jacob	7707	181.3		6912
O-13	Theis	7601	178	6.6	
	Jacob	14300	334.9	0.8	
O-23	Theis	2143	50.1	0.6	
	Jacob	12819	298.8	0.8	
O-22	Theis	6286	146.2	1.3	
	Jacob	5850	135.7	0.5	

Borehole R

Grid reference NZ 329206

Geological succession

	Thickness (ft)	Depth (ft)
Surface deposits	201	201
Upper Magnesian Limestone	35	236
Lower Evaporite Group	108	344
Middle Magnesian Limestone	61	405
Lower Magnesian Limestone	34.4	349.4

Borehole diameter 10 ins reducing to 8 ins.

R W.L. 170.00 ft OD

Non-steady state analysis From N.R.A.R., table 7.

Plane	Method	T (gpd/ft)	K' (gpd/ft^2)	S (x10^{-4})	SC (gpd/ft)
R	Jacob	8850	145.1		19560

APPENDIX B

AQUIFER SIMULATION: DIGITAL SOLUTION

B1. Logic

This has already been outlined in Section II 3.2.4.1.

B2. Deck setup

All input data is free format, using columns 1-80. There are basically two options, namely, potential determination and transmissibility determination.

B2.1. Potential determination - In this, the boundary conditions and all the transmissibility values are known (see Fig. 3.4 for numbering sequence). Input order

(B)	NCOD	O
	COL	No. of columns of nodes
	ROW	No. of rows of nodes
	A	Mesh length in feet
	NB	No. of boundary nodes at which the potential is known, otherwise assumed impermeable.
	NTFX	0 (Dummy)
	TOL	Solution tolerance, say 0.5 ft.
	F	2 (Dummy)
	NIT	Maximum no. of iterations in Gauss-Siedel solution, say 50.
	NNO(I)	Boundary potential pairs, of node number
	HBOUND(I)	and potential: NB pairs
	T(I)	Transmissibility values, total number given by (2 x COL x ROW) - COL - ROW.
(A)	NQR	No. of nodes at which flow is known. If NQR = 0 then

omit following input in square brackets.

[	NNQ	Node number and rate of flow pairs,
	QVAL	(+ recharge, - abstraction).
	RW	Well radius, ft. Only one value can be accommodated after all flow pairs input. Dummy required if recharge flow only.
	NUM	0 No transmissibility listings, or
		1 Full array, averaged array,
		1 and element listing.
	NDIR	0 Terminate, or
		1 Go to new pumping conditions (A), or
		3 Go to start and accept new input data, (B, C).

B.2.2. Transmissibility determination - In this, the boundary conditions and the potential distribution is known. However, the solution for transmissibility is not unique (cf 3.2.4).

Input order.

(C)	NCOD	1
	COL	No. of columns of nodes
	ROW	No. of rows of nodes.
	A	Mesh length, feet.
	NB	No. of boundary nodes at which the potential is known, otherwise assumed impermeable.
	NTFX	No. of transmissibility elements of known value.
	TOL	Solution tolerance, say 0.5 ft.
	F	Adjustment factor, 2.
	NIT	Maximum no. of iterations in Gauss-Siedel solution, say 50. The maximum no. of transmissibility iterations is then set at NIT/10.

NNO(I) HBOUN(I)	Boundary potential pairs of node numbers and potential: NB pairs.
HR (I, J)	Reference potentials: COL x ROW total.
NETF(I) TP(I)	Known transmissibilities, element number and value pairs. Omit if NTFX = 0.
NQR	No. of nodes at which flow is known. If NQR = 0 then omit following input in square brackets.
NNQ QVAL	Node number and rate of flow pairs, (+ recharge, - abstraction).
RW	Well radius, ft. Only one value can be accommodated after all flow pairs input. Dummy required if recharge flow only.
NUM	1 Transmissibility element array, and average transmissibility around each node, printed. 0 No listing of elements, or 1 Complete element listing.
NDIR	0 Terminate, or 1 Go to new pumping conditions, i. e. potential determination using calculated transmissibility values, (A), 3 Go to start and accept new input data, (B, C).

```
*
PROGRAM FOR THE SOLUTION OF TWO DIMENSIONAL LAPLACIAN FLOW BY GAUSS-
IDEAL METHOD, BY A.S.BURGESS. A SOLUTION FOR THE TRANSMISSIBILITY
ELEMENTS MAY ALSO BE OBTAINED.
                                                                    */
AQUIFT:PROCEDURE OPTIONS(MAIN);
       DCL (NOD(ROW,COL),NEL(NTOT,4),ANG(NB),NET(N,N),AHAC(NF))
       CONTROLLED FIXED BIN;
       DCL (T(TELEM),(TA,H,Q)(NTOT),(PA,HR,HP)(ROW,COL),FBCUR(NS),
       HVAL(NH))CONTROLLED FLOAT;
       DCL (CCL,ROW,NODO,N1,N2,N3,N4,E1,E2,E3,E4,I,J,KTR,NIT,NB,NC2,
      NR2,K,TELEM,NE(4))FIXED BIN;
       DCL ((ADIF,RDIF)(4),R1,R2,R3,R4,TTL,RES,DELH,TOL,WR(S)FLOAT;
       DCL NNO(NQR)CONTROLLED FIXED BIN,QVAL(NQR)CONTROLLED FLOAT;
       DCL NETF(NTFX)CONTROLLED FIXED BIN,TF(NTFX)CONTROLLED FLOAT;
       DCL TNOD(ROW,COL)CONTROLLED FLOAT;
 START:GET LIST(NODO,CCL,ROW,A,N2,NTFX,TOL,F,NIT);
       NTNIT=NIT/10;
       NTOT=COL*ROW;
       TELEM=(2*CCL*ROW)-CCL-ROW;
       M=(ROW*2)+1;
       N=(COL*2)+1;
       ALLOCATE NOD,NEL,ANG,NET,T,TA,P,Q,HA,HR,HP,HBOUN;
       ALLOCATE NETF,TF;
       ALLOCATE TNOD;
*
INITIALIZE ALL ARRAYS
                                                                    */
       NOD,HA,HR=0;
       NEL=0;
       ANG,HBOUN=0;
       NET=0;
       TA=0;
       Q=0;
       T=10000; H=100; KTR=1;
       NOIR=0;
*
THE NODES ARE NUMBERED FROM THE TOP LEFT ACROSS SUCCESSIVE ROWS
                                                                    */
       K=1;
         DO I=1 TO ROW;
           DO J=1 TO CCL;
           NOD(I,J)=K;
           K=K+1;
           END;
         END;
*
THE TRANSMISSIBILITY ELEMENTS ARE NUMBERED STARTING IN THE TOP LEFT AND
TERMINATING BOTTOM RIGHT. THE NUMBERS OF THE FOUR ELEMENTS AROUND EACH
NODE IN THE ORDER RIGHT,UP,LEFT,DOWN (I.E. ANTICLOCKWISE) ARE ENTERED
INTO ARRAY NEL. IF THERE IS NO ELEMENT IN A POSITION A 0 IS RETURNED
                                                                    */
       NC2=2*CCL;
       NR2=2*ROW;
       K=1-CCL;
         DO I=2 TO NR2 BY 2;
```

```
          K=K+CCL;
            DO J=2 TO (NC2-1) BY 2;
            NET(I,J)=K;
            K=K+1;
            END;
          END;
        K=1;
          DO I=3 TO (NR2-1) BY 2;
        K=K+CCL-1;
            DO J=2 TO NC2 BY 2;
            NET(I,J)=K;
            K=K+1;
            END;
          END;
        K=1;
          DO I=2 TO NR2 BY 2;
            DO J=2 TO NC2 BY 2;
            NEL(K,1)=NET(I,J+1);
            NEL(K,2)=NET(I-1,J);
            NEL(K,3)=NET(I,J-1);
            NEL(K,4)=NET(I+1,J);
            K=K+1;
            END;
          END;
        FREE NET;
*
-E BOUNDARY POTENTIALS ARE READ IN                                    */
          DO I=1 TO NB;
          GET LIST(NNC(I),HBOUN(I));
          H(NNC(I))=HBOUN(I);
          END;
*
-E INPUT DETAILS ARE PRINTED                                          */
        PUT PAGE;
        PUT EDIT('INPUT DETAILS')(X(40),A);
        PUT SKIP(4) EDIT('NUMBER OF COLUMNS=',CCL,'   NUMBER OF ROWS=',
        RCW)(A,F(2),A,F(2));
        PUT SKIP(2) EDIT('NUMBER OF NODAL POINTS=',NTOT,'    NUMBER OF
RANSMISSIBILITY ELEMENTS=',TELEM)(A,F(4),A,F(4));
        PUT SKIP(2) EDIT('MESH LENGTH=',A,'FEET')(A,F(7,1),A);
        PUT SKIP(2) EDIT('TOLERANCE IN SOLUTION OF EQUATIONS=',TOL,'FT
    MAXIMUM NUMBER OF ITERATIONS=',NIT,'   TRANSMISSIBILITY ADJUSTMENT
ACTOR=',F)(A,F(5,2),A,F(4),A,F(2));
        PUT SKIP(2) EDIT('BOUNDARY NODE NUMBER          FEET ABOVE D.D.')
        (A);
          DO I=1 TO NB;
          PUT SKIP EDIT(NNC(I),HBOUN(I))(X(6),F(4),X(23),F(7,2));
          END;
        PUT PAGE;
READ:IF NCOD=1 THEN DO;
          IF NDIR=0 THEN DO;
              DO I=1 TO RCW;
```

```
            DO J=1 TO COL;
            GET LIST(P(I,J));
            END;
          END;
        IF NTFX=0 THEN GO TO OPCT;
          DO I=1 TO NTFX;
          GET LIST (NETF(I),TF(I));
          END;
OPCT:   PUT PAGE EDIT('POTENTIAL ARRAY,FEET ABOVE U.D.')(A);
        PUT SKIP(3);
          DO I=1 TO ROW;
          PUT SKIP(2);
            DO J=1 TO COL;
            PUT EDIT(P(I,J))(F(6,1));
            END;
          END;
          END;
        IF NOIR>0 THEN DO;
          GET LIST(NH);
          ALLOCATE NHNO,HVAL;
            DO I=1 TO NH;
            GET LIST(NHNO(I),HVAL(I));
            END;
          END;
        END;
      ELSE IF NCOD=0 THEN DO;
          DO I=1 TO TELEM;
          GET LIST(T(I));
          END;
        END;
QREAD:GET LIST(NQR);
      IF NQR=0 THEN GO TO SOLN;
      FREE NNQ,QVAL;
      ALLOCATE NNQ,QVAL;
        DO I=1 TO NQR;
        GET LIST (NNQ(I),QVAL(I));
        END;
      GET LIST(RW);
NORPT:  DO I=1 TO NQR;
        Q(NNQ(I))=-QVAL(I);
        END;
*
RANSMISSIBILITY ELEMENTS AROUND A PUMPED WELL ARE ALTERED
                                                          */
      K=1;
        DO I=1 TO ROW;
          DO J=1 TO COL;
          IF Q(K)>0 THEN DO;
            NDOC=NOD(I,J);
            TC=3.1412/(2*LOG(A/RW));
              DO M=1 TO 4;
              T(NEL(NDOC,M))=T(NEL(NDOC,M))*TC;
              END;
            END;
```

```
            K=K+1;
            END;
          END;
  SOLN:NCTR=1;
TREAT:KTR=1;
*
PE TA MATRIX IS FORMULATED LINE BY LINE
                                                                    */
 AGAIN:BIG=0;
          DO I=1 TO ROW;
            DO J=1 TO COL;
            TA=0;
            NODO=NOD(I,J);
              DO K=1 TO NB;
              IF NBC(K)=NODO THEN GO TO SOLEND;
              END;
            E1=NEL(NODO,1);
            E2=NEL(NODO,2);
            E3=NEL(NODO,3);
            E4=NEL(NODO,4);
            R1,R2,R3,R4=1;
              DO K=1 TO NTEX;
              IF E1=NETF(K) THEN T(E1)=TF(K);
              IF E2=NETF(K) THEN T(E2)=TF(K);
              IF E3=NETF(K) THEN T(E3)=TF(K);
              IF E4=NETF(K) THEN T(E4)=TF(K);
              END;
              IF E1=0 THEN DO;
              R1=0;
              R2,R4=0.5;
              END;
              IF E2=0 THEN DO;
              R2=0;
              R1,R3=0.5;
              END;
              IF E3=0 THEN DO;
              R3=0;
              R2,R4=0.5;
              END;
              IF E4=0 THEN DO;
              R4=0;
              R1,R3=0.5;
              END;
            IF E1=0 THEN P1=0;
              ELSE DO;
              N1=NOD(I,J+1);
              P1=R1*T(E1);
              TA(N1)=P1;
              END;
            IF E2=0 THEN P2=0;
              ELSE DO;
              N2=NOD(I-1,J);
              P2=R2*T(E2);
              TA(N2)=P2;
```

```
            END;
          IF E3=0 THEN P3=C;
            ELSE DO;
            N3=NOD(I,J-1);
            P3=R3*T(E3);
            TA(N3)=P3;
            END;
          IF E4=0 THEN P4=C;
            ELSE DO;
            N4=NOD(I+1,J);
            P4=R4*T(E4);
            TA(N4)=P4;
            END;
          TA(NODO)=-P1-P2-P3-P4;
*
HE SOLUTION FOR THE HEAD AT THE NODE IS DETERMINED,AND THE VALUE
DJUSTED TO REDUCE THE RESIDUAL AT THE NODE TO ZERO (GAUSS-SIEDEL
TERATION)
                                                                    */
          TTL,RES,ARES=0;
            DO K=1 TO NTOT;
            TTL=TTL+TA(K)*H(K);
            END;
          RES=TTL-Q(NODO);
          DELH=-RES/TA(NODO);
          DELH=DELH*1.7;
          H(NODO)=H(NODO)+DELH;
*
HE MAXIMUM ABSOLUTE RESIDUAL IS TESTED. IF BIG>TOL ANOTHER ITERATION
S PERFORMED. IF BIG<TOL THEN THE SOLUTION IS ACCEPTABLE AND THE
ETAILS ARE PRINTED
                                                                    */
          IF ABS(DELH)>BIG THEN BIG=ABS(DELH);
SOL_END:    END;
        END;
      IF BIG<TOL THEN GO TO HPLOT;
      IF KTR>NIT THEN GO TO HPLOT;
      KTR=KTR+1;
      GO TO AGAIN;
HPLOT:PUT PAGE;
      PUT EDIT('NUMBER OF ITERATIONS IN GAUSS-SIEDEL SOLUTION=',KTR,'
      MAXIMUM ABSOLUTE RESIDUAL=',BIG,'FEET')(A,F(3),A,F(6,4),A);
      PUT SKIP(4);
      K=1;
        DO I=1 TO ROW;
          DO J=1 TO COL;
          HA(I,J)=H(K);
          K=K+1;
          END;
        END;
*
F NODO=0 (POTENTIAL DETERMINATION) THE RATE OF FLOW ARRAY AND
OTENTIAL ARRAY ARE PRINTED AND THE CURRENT COMPUTATION TERMINATED
                                                                    */
```

```
      IF NCCD=0 THEN DO;
        PUT SKIP(4);
        PUT EDIT('RATE OF FLOW ARRAY IN THOUSANDS OF GALLONS PER DAY'
      )(A);
        PUT SKIP(3);
        K=1;
          DO I=1 TO ROW;
          PUT SKIP(2);
            DO J=1 TO COL;
            QOPT=-Q(K)/1000;
            PUT EDIT(QOPT)(F(6));
            K=K+1;
            END;
          END;
        PUT PAGE EDIT('POTENTIAL ARRAY,HEAD ABOVE M.D.')(A);
        PUT SKIP(3);
          DO I=1 TO ROW;
          PUT SKIP(2);
            DO J=1 TO COL;
            PUT EDIT(HA(I,J))(F(6,1));
            END;
          END;
        PUT SKIP(6);
        PUT PAGE EDIT('DRAWDOWN IN FEET')(A);
        PUT SKIP(4);
          DO I=1 TO ROW;
          PUT SKIP(2);
            DO J=1 TO COL;
            DDN=HR(I,J)-HA(I,J);
            PUT EDIT(DDN)(F(7,3));
            END;
          END;
        GO TO TEAK;
        END;

* NCOD=1 (TRANSMISSIBILITY DETERMINATION) THE RESIDUALS BETWEEN THE
EAL VALUES AND THE CALCULATED VALUES ARE COMPUTED. IF BIG<TOL2 OR IF
E NUMBER OF TRANSMISSIBILITY ITERATIONS (NOTR) >NTRIT,THE T VALUES
F ACCEPTED. IF BIG>TOL2 THEN THE T VALUES ARE ADJUSTED
                                                                    */

      ELSE IF NCOD=1 THEN DO;
        BIG=0;
        TOL2=TOL*2;
        PUT EDIT('TRANSMISSIBILITY ITERATION NUMBER=',NOTR)(A,F(2));
        PUT SKIP(4);
        PUT EDIT('RESIDUAL ARRAY IN FEET')(A);
        PUT SKIP(3);
          IF NDIR=2 THEN DO;
          HP=HA;
            K=1;
              DO I=1 TO ROW;
              DO J=1 TO COL;
                DO L=1 TO NP;
                IF NHNO(L)=K THEN HP(I,J)=HVAL(L);
```

```
            END;
          K=K+1;
          END;
        END;
        DO I=1 TO ROW;
        PUT SKIP(2);
          DO J=1 TO COL;
          RES=HP(I,J)-HA(I,J);
            PUT EDIT(RES)(F(7,2));
          IF ABS(RES)>BIG THEN BIG=ABS(RES);
          END;
        END;
      END;
      ELSE DO;
      DO I=1 TO ROW;
      PUT SKIP(2);
        DO J=1 TO COL;
        RES=HR(I,J)-HA(I,J);
        PUT EDIT(RES)(F(7,2));
        IF ABS(RES)>BIG THEN BIG=ABS(RES);
        END;
      END;
      END;
  IF BIG<TOL2 THEN DO;
    IF NDIR=4 THEN DO;
        IF NNK>=2 THEN GO TO TOLT;
        ELSE DO;
          NDIR=2;
          NCOD=1;
          GO TO NORPT;
          END;
        END;
      ELSE GO TO TOLT;
      END;
/*
RANSMISSIBILITY ELEMENT ADJUSTMENT: REFERENCE AND CALCULATED POTENTIAL
ROP DETERMINED (RDIF,ADIF) AND USED TO FIX THE ADJUSTMENT FACTO..
                                                                    */
      K=1;
        DO I=1 TO ROW;
          DO J=1 TO COL;
          NCOO=K;
          E1=NEL(NCOO,1);
          E2=NEL(NCOO,2);
          E3=NEL(NCOO,3);
          E4=NEL(NCOO,4);
          HRC=HR(I,J);
          HAC=HA(I,J);
          IF E1>0 THEN DO;
            RDIF(1)=HR(I,J+1)-HRC;
            ADIF(1)=HA(I,J+1)-HAC;
            END;
          IF E2>0 THEN DO;
            RDIF(2)=HR(I-1,J)-HRC;
```

```
            RDIF(2)=RA(I-1,J)-RA0;
            END;
          IF E3>0 THEN DO;
            RDIF(3)=RR(I,J-1)-RR0;
            ADIF(3)=HA(I,J-1)-HA0;
            END;
          IF E4>0 THEN DO;
            RDIF(4)=RR(I+1,J)-RR0;
            ADIF(4)=HA(I+1,J)-HA0;
            END;
            DO L=1 TO 4;
            NE(L)=NEL(NODO,L);
            IF NE(L)=0 THEN GO TO LOOP1;
            IF ABS(RDIF(L))<0.05 THEN GO TO LOOP1;
            IF ABS(ADIF(L))<0.05 THEN GO TO LOOP1;
            ABAR=ABS(ADIF(L)-RDIF(L));
            TB=ABS(ADIF(L)/RDIF(L));
            TA=T(NE(L))*TB;
            DELT=TA-T(NE(L));
            T(NE(L))=T(NE(L))+(DELT*ABAR/40);
LOOP1:      END;
          K=K+1;
          END;
        END;
      IF NDIR=4 & NCTR>NTNIT THEN DO;
        IF NNK>=2 THEN GO TO TOUT;
          ELSE DO;
          NDIR=2;
          NCOD=1;
          GO TO NCRPT;
          END;
        END;
      IF NDIR=2 & NCTR>=1 THEN DO;
        K=1;
          DO I=1 TO ROW;
            DO J=1 TO COL;
            IF G(K)>0 THEN DO;
              NODO=NOD(I,J);
              TC=(2*LOG(A/AL))/3.1412;
                DO M=1 TO 4;
                T(NEL(NODO,M))=T(NEL(NODO,M))*TC;
                END;
              G(K)=0;
              END;
            K=K+1;
            END;
          END;
        NCOD=1;
        NDIR=4;
        NNK=NNK+1;
        GO TO SOLN;
        END;
      IF NCTR>NTNIT THEN GO TO TOUT;
      NCTR=NCTR+1;
```

```
          GO TO TREAPT;
*
PE TRANSMISSIBILITY ELEMENTS ARE OUTPUT EITHER ELEMENT BY ELEMENT,
'ERAGED AROUND EACH NODE, OR LISTED
                                                                    */
  TOUT:  PUT PAGE EDIT('RATE OF FLOW ARRAY IN THOUSANDS OF GALLONS PER
'AY')(A);
          PUT SKIP(3);
          K=1;
            DO I=1 TO ROW;
            PUT SKIP(3);
              DO J=1 TO COL;
              QOPT=-Q(K)/1000;
              PUT EDIT(QOPT)(F(6));
              K=K+1;
              END;
            END;
          END;
  TRAK:   K=1;
              DO I=1 TO NOW;
                DO J=1 TO COL;
                IF Q(K)>0 THEN DO;
                  NODC=NOD(I,J);
                  TC=(2*LOG(A/RW))/3.1412;
                    DO M=1 TO 4;
                    T(NEL(NODC,M))=T(NEL(NODC,M))*TC;
                    END;
                  END;
                K=K+1;
                END;
              END;
          GET LIST(NUM);
          IF NUM=0 THEN GO TO DIRECT;
          ELSE GO TO TPRINT;
TPRINT:   PUT PAGE EDIT('TRANSMISSIBILITY ARRAY IN THOUSANDS OF GALLONS
PER DAY PER FOOT')(A);
          PUT SKIP(3);
          K,L,M,N=0;
NXTLNE:   K=N+1;
          L=K+COL-2;
          PUT EDIT('    ')(A);
            DO I=K TO L;
            TVAL=(T(I)+500)/1000;
            PUT EDIT(TVAL)(F(7));
            END;
          PUT SKIP(2);
          IF L>=TELEM THEN GO TO DELIST;
          M=L+1;
          N=M+COL-1;
            DO I=M TO N;
            TVAL=(T(I)+500)/1000;
            PUT EDIT(TVAL)(F(7));
            END;
          PUT SKIP(2);
```

```
          IF N>=TELEM THEN GO TO DELIST;
          ELSE GO TO NXTLNG;
DELIST:   PUT SKIP(6);
          DO I=1 TO NOM;
            DO J=1 TO COL;
            NODO=NOD(I,J);
            TTOT=0;
            NC=4;
              DO K=1 TO 4;
              IF NEL(NODO,K)=0 THEN NC=NC-1;
              ELSE TTOT=T(NEL(NODO,K))+TTOT;
              END;
            TNOD(I,J)=TTOT/NC;
            END;
          END;
          PUT PAGE;
            DO I=1 TO NOW;
            PUT SKIP(3);
              DO J=1 TO COL;
              TVAL=TNOD(I,J)/1000;
              PUT EDIT(TVAL)(F(7));
              END;
            END;
          GET LIST(NUM);
          IF NUM=0 THEN GO TO DIRECT;
          ELSE GO TO LIST;
  LIST:   PUT PAGE EDIT('TRANSMISSIBILITY VALUES IN GALLONS PER DAY PER
FOOT')(A);
          PUT SKIP(4);
          PUT EDIT('ELEMENT NUMBER        TRANSMISSIBILITY')(A);
          PUT SKIP(2);
            DO I=1 TO TELEM;
            PUT SKIP(2) EDIT(I,T(I))(F(8),X(15),F(12,2));
            END;
          GO TO DIRECT;
*
* THE NEXT OPERATION REQUIRED IS DETERMINED FROM VALUE OF NDIR
                                                                    */

DIRECT:PUT SKIP;
       GET LIST(NDIR);
       IF NDIR=0 THEN GO TO FIN;
       IF NDIR=1 THEN DO;
        PUT PAGE;
         NCOL=0;
           DO I=1 TO NTOT;
           IF Q(I)>0 THEN Q(I)=0;
           END;
         GO TO QREAD;
         END;
       IF NDIR=2 THEN DO;
         FREE NPAC,HVAL;
         NNK=1;
         NCOL=1;
        PUT PAGE;
```

NUMBER OF ITERATIONS IN GAUSS-SIEDEL SOLUTION= 12   MAXIMUM ABSOLUTE RESIDUAL=0.3976FEET

RATE OF FLOW ARRAY IN THOUSANDS OF GALLONS PER DAY

0	0	0	0	0	0	0	0	0	0	0	0	0	0	0	0	0
0	0	0	0	0	0	0	0	0	0	0	0	0	0	0	0	0
0	0	0	0	0	0	0	0	0	0	0	0	0	0	0	0	0
0	0	0	0	0	0	0	0	0	0	0	0	0	0	0	0	0
0	0	0	0	0	0	0	0	0	0	0	0	0	0	0	0	0
0	0	0	0	0	0	0	0	0	0	0	0	0	0	0	0	0
0	0	0	0	0	0	0	0	0	0	0	0	0	0	0	0	0
0	0	0	0	0	0	0	0	0	0	0	0	0	0	0	0	0
0	0	0	0	0	0	0	0	-800	0	0	0	0	0	0	0	0
0	0	0	0	0	0	0	0	0	0	0	0	0	0	0	0	0
0	0	0	0	0	0	0	0	0	0	0	0	0	0	0	0	0
0	0	0	0	0	0	0	0	0	0	0	0	0	0	0	0	0
0	0	0	0	0	0	0	0	0	0	0	0	0	0	0	0	0
0	0	0	0	0	0	0	0	0	0	0	0	0	0	0	0	0
0	0	0	0	0	0	0	0	0	0	0	0	0	0	0	0	0
0	0	0	0	0	0	0	0	0	0	0	0	0	0	0	0	0
0	0	0	0	0	0	0	0	0	0	0	0	0	0	0	0	0

POTENTIAL ARRAY,HEAD ABOVE O.D.

200.0	200.0	200.0	200.0	200.0	200.0	200.0	200.0	200.0	200.0	200.0	200.0	200.0	200.0	200.0	200.0	200.0
200.0	199.7	199.5	199.2	198.7	198.4	198.2	198.1	198.0	198.0	198.1	198.4	198.7	199.0	199.3	199.6	200.0
200.0	199.5	199.0	198.1	197.5	196.8	196.3	195.9	195.8	195.9	196.2	196.7	197.4	198.0	198.7	199.3	200.0
200.0	199.2	198.1	197.2	196.0	195.1	194.2	193.6	193.3	193.5	194.1	194.9	195.9	196.9	198.0	199.0	200.0
200.0	198.7	197.5	196.0	194.7	193.1	191.8	190.8	190.4	190.7	191.7	193.0	194.5	195.9	197.3	198.7	200.0
200.0	198.4	196.8	195.1	193.1	191.2	189.1	187.4	186.6	187.3	189.0	191.0	193.0	194.9	196.7	198.4	200.0
200.0	198.2	196.3	194.2	191.8	189.1	186.1	183.0	181.1	183.0	186.0	189.0	191.7	194.0	196.2	198.1	200.0
200.0	198.1	195.9	193.6	190.8	187.4	183.0	177.6	172.0	177.5	182.9	187.2	190.6	193.4	195.8	197.9	200.0
200.0	198.0	195.8	193.3	190.4	186.6	181.1	172.0	84.1	172.0	181.1	186.4	190.2	193.2	195.6	197.9	200.0
200.0	198.0	195.9	193.5	190.7	187.3	183.0	177.5	172.0	177.5	182.9	187.2	190.6	193.4	195.8	197.9	200.0
200.0	198.1	196.2	194.1	191.7	189.0	186.0	182.9	181.1	182.9	185.9	188.9	191.6	194.0	196.1	198.1	200.0
200.0	198.4	196.7	195.0	193.0	191.0	189.0	187.2	186.4	187.2	188.9	191.0	193.0	194.9	196.7	198.4	200.0
200.0	198.7	197.4	195.9	194.5	193.0	191.7	190.6	190.2	190.6	191.6	193.0	194.4	195.9	197.3	198.7	200.0
200.0	199.0	198.0	196.9	195.9	194.9	194.0	193.4	193.2	193.4	194.0	194.9	195.9	196.9	198.0	199.0	200.0
200.0	199.3	198.7	198.0	197.3	196.7	196.2	195.8	195.6	195.8	196.1	196.7	197.3	198.0	198.6	199.3	200.0
200.0	199.6	199.3	199.0	198.7	198.4	198.1	197.9	197.9	197.9	198.1	198.4	198.7	199.0	199.3	199.7	200.0
200.0	200.0	200.0	200.0	200.0	200.0	200.0	200.0	200.0	200.0	200.0	200.0	200.0	200.0	200.0	200.0	200.0

NUMBER OF ITERATIONS IN GAUSS-SIEDEL SOLUTION= 12   MAXIMUM ABSOLUTE RESIDUAL=0.3977FEET

RATE OF FLOW ARRAY IN THOUSANDS OF GALLONS PER DAY

0	0	0	0	0	0	0	0	0	0	0	0	0	0	0	0	0
0	0	0	0	0	0	0	0	0	0	0	0	0	0	0	0	0
0	0	0	0	0	0	0	0	0	0	0	0	0	0	0	0	0
0	0	0	0	0	0	0	0	0	0	0	0	0	0	0	0	0
0	0	0	0	0	0	0	0	0	0	0	0	0	0	0	0	0
0	0	0	0	0	0	0	0	0	0	0	0	0	0	0	0	0
0	0	0	0	0	0	0	0	0	0	0	0	0	0	0	0	0
0	0	0	0	0	0	0	0	0	0	0	0	0	0	0	0	0
0	0	0	0	0	0	0	0	-1000	0	0	0	0	0	0	0	0
0	0	0	0	0	0	0	0	0	0	0	0	0	0	0	0	0
0	0	0	0	0	0	0	0	0	0	0	0	0	0	0	0	0
0	0	0	0	0	0	0	0	0	0	0	0	0	0	0	0	0
0	0	0	0	0	0	0	0	0	0	0	0	0	0	0	0	0
0	0	0	0	0	0	0	0	0	0	0	0	0	0	0	0	0
0	0	0	0	0	0	0	0	0	0	0	0	0	0	0	0	0
0	0	0	0	0	0	0	0	0	0	0	0	0	0	0	0	0
0	0	0	0	0	0	0	0	0	0	0	0	0	0	0	0	0

POTENTIAL ARRAY,HEAD ABOVE O.D.

200.0	200.0	200.0	200.0	200.0	200.0	200.0	200.0	200.0	200.0	200.0	200.0	200.0	200.0	200.0	200.0	200.0
200.0	199.7	199.3	199.0	198.4	198.0	197.8	197.6	197.4	197.5	197.7	198.0	198.4	198.7	199.2	199.6	200.0
200.0	199.3	198.6	197.6	196.8	196.0	195.3	194.9	194.7	194.8	195.2	195.9	196.7	197.5	198.3	199.2	200.0
200.0	199.0	197.6	196.4	195.0	193.8	192.7	191.9	191.6	191.9	192.6	193.7	194.9	196.2	197.5	198.7	200.0
200.0	198.4	196.8	195.0	193.3	191.4	189.7	188.5	187.9	188.4	189.6	191.3	193.1	194.9	196.6	198.3	200.0
200.0	198.0	196.0	193.8	191.4	188.9	186.3	184.2	183.2	184.1	186.2	188.7	191.3	193.6	195.9	198.0	200.0
200.0	197.8	195.3	192.7	189.7	186.3	182.6	178.8	176.4	178.7	182.5	186.2	189.6	192.5	195.2	197.6	200.0
200.0	197.6	194.9	191.9	188.5	184.2	178.8	171.9	165.0	171.8	178.7	184.1	188.3	191.8	194.7	197.4	200.0
200.0	197.4	194.7	191.6	187.9	183.2	176.4	165.0	55.1	165.0	176.3	183.1	187.8	191.5	194.6	197.4	200.0
200.0	197.5	194.8	191.9	188.4	184.1	178.7	171.8	165.0	171.8	178.7	184.0	188.3	191.7	194.7	197.4	200.0
200.0	197.7	195.2	192.6	189.6	186.2	182.5	178.7	176.3	178.7	182.4	186.2	189.5	192.5	195.2	197.6	200.0
200.0	198.0	195.9	193.7	191.3	188.7	186.2	184.1	183.1	184.0	186.2	188.7	191.2	193.6	195.8	197.9	200.0
200.0	198.4	196.7	194.9	193.1	191.3	189.6	188.3	187.8	188.3	189.5	191.2	193.0	194.9	196.6	198.3	200.0
200.0	198.7	197.5	196.2	194.9	193.6	192.5	191.8	191.5	191.7	192.5	193.6	194.9	196.2	197.5	198.7	200.0
200.0	199.2	198.3	197.5	196.6	195.9	195.2	194.7	194.6	194.7	195.2	195.8	196.6	197.5	198.3	199.2	200.0
200.0	199.6	199.2	198.7	198.3	198.0	197.6	197.4	197.4	197.4	197.6	197.9	198.3	198.7	199.2	199.6	200.0
200.0	200.0	200.0	200.0	200.0	200.0	200.0	200.0	200.0	200.0	200.0	200.0	200.0	200.0	200.0	200.0	200.0

INPUT DETAILS

NUMBER OF COLUMNS=17 NUMBER OF ROWS=17

NUMBER OF NODAL POINTS= 289 NUMBER OF TRANSMISSIBILITY ELEMENTS= 544

MESH LENGTH= 500.0FEET

TOLERANCE IN SOLUTION OF EQUATIONS= 0.50FT MAXIMUM NUMBER OF ITERATIONS= 100 TRANSMISSIBILITY ADJUSTMENTFACTOR= 2

BOUNDARY NODE NUMBER	FEET ABOVE D.D.
1	200.00
2	200.00
3	200.00
4	200.00
5	200.00
6	200.00
7	200.00
8	200.00
9	200.00
10	200.00
11	200.00
12	200.00
13	200.00
14	200.00
15	200.00
16	200.00
17	200.00
18	200.00
34	200.00
35	200.00
51	200.00
52	200.00
68	200.00
69	200.00
85	200.00
86	200.00
102	200.00
103	200.00
119	200.00
120	200.00
136	200.00
137	200.00
153	200.00
154	200.00
170	200.00
171	200.00
187	200.00
188	200.00
204	200.00
205	200.00
221	200.00
222	200.00
238	200.00
239	200.00
255	200.00
256	200.00
272	200.00
273	200.00
274	200.00
275	200.00
276	200.00
277	200.00
278	200.00
279	200.00
280	200.00
281	200.00
282	200.00
283	200.00
284	200.00
285	200.00
286	200.00
287	200.00
288	200.00
289	200.00

NUMBER OF ITERATIONS IN GAUSS-SIEDEL SOLUTION= 28   MAXIMUM ABSOLUTE RESIDUAL=0.4968FEET

RATE OF FLOW ARRAY IN THOUSANDS OF GALLONS PER DAY

0	0	0	0	0	0	0	0	0	0	0	0	0	0	0	0	0
0	0	0	0	0	0	0	0	0	0	0	0	0	0	0	0	0
0	0	0	0	0	0	0	0	0	0	0	0	0	0	0	0	0
0	0	0	0	0	0	0	0	0	0	0	0	0	0	0	0	0
0	0	0	0	0	0	0	0	0	0	0	0	0	0	0	0	0
0	0	0	0	0	0	0	0	0	0	0	0	0	0	0	0	0
0	0	0	0	0	0	0	0	0	0	0	0	0	0	0	0	0
0	0	0	0	0	0	0	0	0	0	0	0	0	0	0	0	0
0	0	0	0	0	0	0	0	-200	0	0	0	0	0	0	0	0
0	0	0	0	0	0	0	0	0	0	0	0	0	0	0	0	0
0	0	0	0	0	0	0	0	0	0	0	0	0	0	0	0	0
0	0	0	0	0	0	0	0	0	0	0	0	0	0	0	0	0
0	0	0	0	0	0	0	0	0	0	0	0	0	0	0	0	0
0	0	0	0	0	0	0	0	0	0	0	0	0	0	0	0	0
0	0	0	0	0	0	0	0	0	0	0	0	0	0	0	0	0
0	0	0	0	0	0	0	0	0	0	0	0	0	0	0	0	0
0	0	0	0	0	0	0	0	0	0	0	0	0	0	0	0	0

POTENTIAL ARRAY,HEAD ABOVE O.D.

200.0	200.0	200.0	200.0	200.0	200.0	200.0	200.0	200.0	200.0	200.0	200.0	200.0	200.0	200.0	200.0	200.0
200.0	200.0	200.1	199.6	199.7	199.6	199.5	199.5	199.5	199.5	199.5	199.6	199.7	199.8	199.8	199.9	200.0
200.0	200.1	199.6	199.3	199.3	199.2	199.0	199.0	198.9	199.0	199.1	199.2	199.3	199.5	199.7	199.8	200.0
200.0	199.6	199.3	199.0	198.9	198.7	198.5	198.3	198.3	198.4	198.5	198.7	199.0	199.2	199.5	199.7	200.0
200.0	199.7	199.3	198.9	198.6	198.2	197.9	197.7	197.6	197.7	197.9	198.3	198.6	199.0	199.3	199.7	200.0
200.0	199.6	199.2	198.7	198.2	197.8	197.3	196.8	196.6	196.8	197.3	197.8	198.3	198.7	199.2	199.6	200.0
200.0	199.5	199.0	198.5	197.9	197.3	196.5	195.8	195.3	195.8	196.5	197.3	197.9	198.5	199.0	199.5	200.0
200.0	199.5	199.0	198.3	197.7	196.8	195.8	194.4	193.0	194.4	195.8	196.8	197.7	198.3	198.9	199.5	200.0
200.0	199.5	198.9	198.3	197.6	196.6	195.3	193.0	171.0	193.0	195.3	196.6	197.6	198.3	198.9	199.5	200.0
200.0	199.5	199.0	198.4	197.7	196.8	195.8	194.4	193.0	194.4	195.7	196.8	197.7	198.3	198.9	199.5	200.0
200.0	199.5	199.1	198.5	197.9	197.3	196.5	195.8	195.3	195.7	196.5	197.2	197.9	198.5	199.0	199.5	200.0
200.0	199.6	199.2	198.7	198.3	197.8	197.3	196.8	196.6	196.8	197.2	197.7	198.2	198.7	199.2	199.6	200.0
200.0	199.7	199.3	199.0	198.6	198.3	197.9	197.7	197.6	197.7	197.9	198.2	198.6	199.0	199.3	199.7	200.0
200.0	199.8	199.5	199.2	199.0	198.7	198.5	198.3	198.3	198.3	198.5	198.7	199.0	199.2	199.5	199.7	200.0
200.0	199.8	199.7	199.5	199.3	199.2	199.0	198.9	198.9	198.9	199.0	199.2	199.3	199.5	199.7	199.8	200.0
200.0	199.9	199.8	199.7	199.7	199.6	199.5	199.5	199.5	199.5	199.5	199.6	199.7	199.7	199.8	199.9	200.0
200.0	200.0	200.0	200.0	200.0	200.0	200.0	200.0	200.0	200.0	200.0	200.0	200.0	200.0	200.0	200.0	200.0

NUMBER OF ITERATIONS IN GAUSS-SIEDEL SOLUTION= 12 MAXIMUM ABSOLUTE RESIDUAL=0.3980FEET

RATE OF FLOW ARRAY IN THOUSANDS OF GALLONS PER DAY

0	0	0	0	0	0	0	0	0	0	0	0	0	0	0	0	0
0	0	0	0	0	0	0	0	0	0	0	0	0	0	0	0	0
0	0	0	0	0	0	0	0	0	0	0	0	0	0	0	0	0
0	0	0	0	0	0	0	0	0	0	0	0	0	0	0	0	0
0	0	0	0	0	0	0	0	0	0	0	0	0	0	0	0	0
0	0	0	0	0	0	0	0	0	0	0	0	0	0	0	0	0
0	0	0	0	0	0	0	0	0	0	0	0	0	0	0	0	0
0	0	0	0	0	0	0	0	0	0	0	0	0	0	0	0	0
0	0	0	0	0	0	0	0	-400	0	0	0	0	0	0	0	0
0	0	0	0	0	0	0	0	0	0	0	0	0	0	0	0	0
0	0	0	0	0	0	0	0	0	0	0	0	0	0	0	0	0
0	0	0	0	0	0	0	0	0	0	0	0	0	0	0	0	0
0	0	0	0	0	0	0	0	0	0	0	0	0	0	0	0	0
0	0	0	0	0	0	0	0	0	0	0	0	0	0	0	0	0
0	0	0	0	0	0	0	0	0	0	0	0	0	0	0	0	0
0	0	0	0	0	0	0	0	0	0	0	0	0	0	0	0	0
0	0	0	0	0	0	0	0	0	0	0	0	0	0	0	0	0

POTENTIAL ARRAY,HEAD ABOVE O.D.

200.0	200.0	200.0	200.0	200.0	200.0	200.0	200.0	200.0	200.0	200.0	200.0	200.0	200.0	200.0	200.0	200.0
200.0	199.9	199.8	199.7	199.4	199.2	199.2	199.1	199.0	199.0	199.1	199.2	199.4	199.5	199.7	199.8	200.0
200.0	199.8	199.7	199.1	198.8	198.5	198.2	198.0	198.0	198.0	198.1	198.4	198.7	199.0	199.4	199.7	200.0
200.0	199.7	199.1	198.7	198.1	197.6	197.2	196.9	196.7	196.8	197.1	197.5	198.0	198.5	199.0	199.5	200.0
200.0	199.4	198.8	198.1	197.5	196.7	196.0	195.5	195.3	195.4	195.9	196.6	197.3	198.0	198.7	199.3	200.0
200.0	199.2	198.5	197.6	196.7	195.7	194.6	193.8	193.3	193.7	194.5	195.5	196.5	197.5	198.3	199.2	200.0
200.0	199.2	198.2	197.2	196.0	194.6	193.1	191.6	190.6	191.5	193.0	194.5	195.8	197.0	198.1	199.1	200.0
200.0	199.1	198.0	196.9	195.5	193.8	191.6	188.8	186.0	188.8	191.5	193.6	195.3	196.7	197.9	199.0	200.0
200.0	199.0	198.0	196.7	195.3	193.3	190.6	186.0	142.1	186.0	190.5	193.2	195.1	196.6	197.8	198.9	200.0
200.0	199.0	198.0	196.8	195.4	193.7	191.5	188.8	186.0	188.8	191.5	193.6	195.3	196.7	197.9	199.0	200.0
200.0	199.1	198.1	197.1	195.9	194.5	193.0	191.5	190.5	191.5	193.0	194.5	195.8	197.0	198.1	199.1	200.0
200.0	199.2	198.4	197.5	196.6	195.5	194.5	193.6	193.2	193.6	194.5	195.5	196.5	197.4	198.3	199.2	200.0
200.0	199.4	198.7	198.0	197.3	196.5	195.8	195.3	195.1	195.3	195.8	196.5	197.2	197.9	198.6	199.3	200.0
200.0	199.5	199.0	198.5	198.0	197.5	197.0	196.7	196.6	196.7	197.0	197.4	197.9	198.5	199.0	199.5	200.0
200.0	199.7	199.4	199.0	198.7	198.3	198.1	197.9	197.8	197.9	198.1	198.3	198.6	199.0	199.3	199.7	200.0
200.0	199.8	199.7	199.5	199.3	199.2	199.1	199.0	198.9	199.0	199.1	199.2	199.3	199.5	199.7	199.8	200.0
200.0	200.0	200.0	200.0	200.0	200.0	200.0	200.0	200.0	200.0	200.0	200.0	200.0	200.0	200.0	200.0	200.0

```
NUMBER OF ITERATIONS IN GAUSS-SIEDEL SOLUTION= 12        MAXIMUM ABSOLUTE RESIDUAL=0.3976FEET



RATE OF FLOW ARRAY IN THOUSANDS OF GALLONS PER DAY


    0    0    0    0    0    0    0    0    0    0    0    0    0    0    0    0    0
    0    0    0    0    0    0    0    0    0    0    0    0    0    0    0    0    0
    0    0    0    0    0    0    0    0    0    0    0    0    0    0    0    0    0
    0    0    0    0    0    0    0    0    0    0    0    0    0    0    0    0    0
    0    0    0    0    0    0    0    0    0    0    0    0    0    0    0    0    0
    0    0    0    0    0    0    0    0    0    0    0    0    0    0    0    0    0
    0    0    0    0    0    0    0    0    0    0    0    0    0    0    0    0    0
    0    0    0    0    0    0    0    0    0    0    0    0    0    0    0    0    0
    0    0    0    0    0    0    0    0 -600    0    0    0    0    0    0    0    0
    0    0    0    0    0    0    0    0    0    0    0    0    0    0    0    0    0
    0    0    0    0    0    0    0    0    0    0    0    0    0    0    0    0    0
    0    0    0    0    0    0    0    0    0    0    0    0    0    0    0    0    0
    0    0    0    0    0    0    0    0    0    0    0    0    0    0    0    0    0
    0    0    0    0    0    0    0    0    0    0    0    0    0    0    0    0    0
    0    0    0    0    0    0    0    0    0    0    0    0    0    0    0    0    0
    0    0    0    0    0    0    0    0    0    0    0    0    0    0    0    0    0
    0    0    0    0    0    0    0    0    0    0    0    0    0    0    0    0    0



POTENTIAL ARRAY,HEAD ABOVE O.D.


 200.0 200.0 200.0 200.0 200.0 200.0 200.0 200.0 200.0 200.0 200.0 200.0 200.0 200.0 200.0 200.0 200.0
 200.0 199.8 199.7 199.5 199.0 198.8 198.7 198.6 198.5 198.5 198.6 198.8 199.0 199.3 199.5 199.7 200.0
 200.0 199.7 199.3 198.6 198.1 197.7 197.2 197.0 196.9 196.9 197.2 197.5 198.0 198.5 199.0 199.5 200.0
 200.0 199.5 198.6 198.0 197.1 196.3 195.7 195.2 195.0 195.2 195.6 196.2 197.0 197.7 198.5 199.2 200.0
 200.0 199.0 198.1 197.1 196.1 194.9 193.9 193.2 192.8 193.1 193.8 194.8 195.9 196.9 198.0 199.0 200.0
 200.0 198.8 197.7 196.3 194.9 193.4 191.9 190.6 190.0 190.5 191.8 193.3 194.8 196.2 197.5 198.8 200.0
 200.0 198.7 197.2 195.7 193.9 191.9 189.6 187.3 185.9 187.3 189.5 191.7 193.7 195.5 197.1 198.6 200.0
 200.0 198.6 197.0 195.2 193.2 190.6 187.3 183.2 179.0 183.1 187.2 190.4 193.0 195.1 196.8 198.5 200.0
 200.0 198.5 196.9 195.0 192.8 190.0 185.9 179.0 113.1 179.0 185.8 189.8 192.7 194.9 196.7 198.4 200.0
 200.0 198.5 196.9 195.2 193.1 190.5 187.3 183.1 179.0 183.1 187.2 190.4 193.0 195.0 196.8 198.5 200.0
 200.0 198.6 197.2 195.6 193.8 191.8 189.5 187.2 185.8 187.2 189.5 191.7 193.7 195.5 197.1 198.6 200.0
 200.0 198.8 197.5 196.2 194.8 193.3 191.7 190.4 189.8 190.4 191.7 193.2 194.7 196.2 197.5 198.8 200.0
 200.0 199.0 198.0 197.0 195.9 194.8 193.7 193.0 192.7 193.0 193.7 194.7 195.8 196.9 198.0 199.0 200.0
 200.0 199.3 198.5 197.7 196.9 196.2 195.5 195.1 194.9 195.0 195.5 196.2 196.9 197.7 198.5 199.2 200.0
 200.0 199.5 199.0 198.5 198.0 197.5 197.1 196.8 196.7 196.8 197.1 197.5 198.0 198.5 199.0 199.5 200.0
 200.0 199.7 199.5 199.2 199.0 198.8 198.6 198.5 198.4 198.5 198.6 198.8 199.0 199.2 199.5 199.7 200.0
 200.0 200.0 200.0 200.0 200.0 200.0 200.0 200.0 200.0 200.0 200.0 200.0 200.0 200.0 200.0 200.0 200.0
```

```
      GO TO PREAD;
      END;
    IF NDIR=3 THEN DO;
      FREE NOD,NEL,NNO,T,TA,H,C,FA,HR,HBOUN,NPNO,HVAL;
     PUT PAGE;
      GO TO START;
      END;
    IF NDIR=4 THEN DO;
        DO I=1 TO NTOT;
        IF G(I)>0 THEN G(I)=C;
        END;
      NDIR=0;
      NOOD=1;
      PUT PAGE;
      GO TO SOLN;
      END;
FIN:END AQUDET;
```

APPENDIX C

COMPUTER PLOTTED STEREOGRAPHIC STABILITY REGIMES FOR A PLANE DISCONTINUITY

C1. Introduction

Two programs have been written using the principles described in Section III, 1.2.3.2. Program STAB computes and plots the stability regimes for particular F* and ϕ combinations. Program JTSTAB employs a similar method to determine the stability regime for a particular C-ϕ, σ_1, σ_2, σ_3, set of conditions, and has the facility for rotating this plot, using the known principal stress directions, into global axes.

C2. Program STAB

Using the notation of Fig. 1.3, an orientation may be considered in limiting equilibrium when it satisfies all the following conditions:

$$0 \leqslant l^2 \leqslant 1$$

$$0 \leqslant n^2 \leqslant 1$$

$$l^2 + n^2 \leqslant 1$$

For the present study, P values of 0, 0.33, 0.67, 1 have been used: N is incremented in 999 steps between σ_3 and σ_1. If the P-N combination satisfies the limiting conditions, l and n are converted into the corresponding angles α & θ (see Fig. 1.4).

All plotting is done using the standard characters & line printer. Because there are 10 characters/inch horizontally, but only 6 characters/inch vertically, locations in the output character array B must be scaled accordingly. The cartesian coordinates, before scaling, are calculated for an equal area Schmidt net by,

$$x = \sqrt{2}.\ r.\ \sin(\theta/2).\ \sin\alpha$$

$$y = \sqrt{2}.\ r.\ \sin(\theta/2).\ \cos\alpha$$

These coordinates are entered into B as '+', together with the circle and axes as '*', '-', '|' respectively. Successive quadrants are used for each P value, and when complete, array B is printed.

Input details are simple, consisting of only a F*-ϕ pair for each stability regime stereogram required. The source listing and a representative selection of stability diagrams are given.

```
 OPTIONS(MAIN);


 STAB:PROC OPTIONS(MAIN);
*******************************************************************************
IS PROGRAMME PLOTS THE FAIL AND NO-FAIL REGIMES FOR A PLANAR
SCONTINUITY IN A TRIAXIAL STRESS FIELD.(REF:JAEGER,J.C.,ELASTICITY,
ACTURE AND FLOW,METHUEN,1962) THE RESULTANT PLOT IS BASED ON A
HMIDT EQUAL AREA PROJECTION.
*******************************************************************************
                              INPUT DETAILS
 A DIMENSIONLESS PARAMETER DESCRIBING THE STRESS-FAILURE RELATIONSHIP
((SIGMA1-SIGMA3)/2)/(((SIGMA1+SIGMA3)/2)+C*COT(PHI))
   FRICTION ANGLE
*******************************************************************************/
      DCL((F,PHI,K1,K2,K,P,M1,LL,L,NN,N,RA,THETA,ALPHA,A1,A2,F1,
      BETA1,BETA2)FLOAT,((PHI1,PSI1,A,T)(88))FLOAT,(COL,ROW,PP,M,I,
      XC(-24:24),X,Y,MM)FIXED BIN,B(-24:24,-40:40)CHAR(1));
      DCL STEPOL ENTRY((*)FLOAT,(*)FLOAT,(*)FLOAT,(*)FLOAT,FIXED
      BIN);
TEPOL:PROCEDURE(R1,R2,R3,R4,M);

OCEDURE STEPOL CONVERTS A PAIR OF EQUATORIAL PROJECTION ANGLES INTO
E CORRESPONDING PAIR OF POLAR PROJECTION ANGLES
                                                                      */
      DCL((R1,R2,R3,R4)(M)FLOAT,(I,M)FIXED BIN);
      DO I=1 TO M;
      IF R1(I)=7777 THEN DO;
                  R3(I)=7777; R4(I)=7777; GOTO ST1; END;
      IF ABS(R1(I))>90 THEN DO;
            R2(I)=-R2(I);
            IF R1(I)>0 THEN R1(I)=R1(I)-180;
            ELSE R1(I)=180+R1(I);
            END;

N THE ARGUMENT OF THE GENERIC FUNCTION TAND APPROACHES 90 DEGREES
 VALUE OF THE FUNCTION BECOMES TOO LARGE AND THE OVERFLOW CONDITION
RAISED. THIS MAY BE AVOIDED BY THE USE OF CONDITIONAL STATEMENTS
                                                                      */
      IF (ABS(R2(I))>89.999 & ABS(R2(I))<90.001) THEN DO;
      IF (ABS(R1(I))>89.999 & ABS(R1(I))<90.001) THEN DO;
            R4(I)=90; GOTO STO; END;
      ELSE R4(I)=ATAND(TAND(R1(I)));
            R4(I)=ABS(ATAND(TAND(R1(I))));
 STO:       IF SIND(R1(I))>0 THEN R3(I)=90;
            ELSE R3(I)=270; GOTO ST1; END;
      F1=SIND(R1(I));
      F2=TAND(R2(I));
      R3(I)=ATAND(F1*F2);
      IF F2<0 THEN DO;R3(I)=180+R3(I);END;
      ON ZERODIVIDE BEGIN;
            R4(I)=90; GOTO ST1; END;
            F3=(COSD(R1(I)))*(TAND(R2(I)))*COSD(R3(I));
            R4(I)=ATAND(1/F3);
 ST1:       END;
      END STEPOL;
TART:THETA,ALPHA=0;
      GET LIST(F,PHI); IF F= 9999.0 THEN GOTO FINISH;ELSE
      B=' ';
```

```
 OPTIONS(MAIN);



      ROW=24; COL=40;

E COORDINATES OF THE CIRCLE ARE CALCULATED,AND TOGETHER WITH THE X
D Y AXES ARE ENTERED INTO THE CHARACTER ARRAY AS * - | RESPECTIVELY
                                                                    */
      DO I=0 TO ROW;
      XC(I)=((SQRT((ROW*ROW)-(I*I)))*COL/ROW)+0.5;
      XC(-I)=XC(I); END;
      DO I=0 TO ROW; B(I,XC(I))='*'; B(I,-XC(I))='*'; END;
      DO I=0 TO -ROW BY -1; B(I,XC(I))='*'; B(I,-XC(I))='*'; END;
      DO I=-ROW TO ROW; B(I,0)='|'; END;
      DO J=-COL TO COL; B(0,J)='-'; END;

 THERE IS NO INTERSECTION OF THE PRINCIPAL STESS CIRCLE BY THE
ILURE ENVELOPE FOR THE DISCONTINUITY,THE RUN IS TERMINATED
                                                                    */
      IF F<=SIND(PHI) THEN GOTO FIN;

E ANGLES BETA1 AND BETA2 BETWEEN THE DISCONTINUITY FAILURE AND THE
GMA1 DIRECTION ARE COMPUTED
                                                                    */
      F1=(SIND(PHI))/F;
      W1=ATAND(F1/(SQRT(1-F1*F1)));
      W2=180-W1;
      BETA1=(W1-PHI)/2;
      BETA2=(W2-PHI)/2;

 VALUE OF THE INTERMEDIATE PRINCIPAL STRESS WILL BE BETWEEN SIGMA1
 SIGMA2. FOUR VALUES ARE USED, INCLUDING THE END VALUES OF SIGMA2=
GMA3 AND SIGMA2=SIGMA1,WITH TWO EQUALLY SPACED INTERMEDIATE VALUES
                                                                    */
OOP1:DO PP=0 TO 3; M=44;P=PP/3;

E STABILITY REGIME FOR SIGMA2=SIGMA3 IS COMPUTED
                                                                    */
           IF PP=0 THEN DO;
                DO I=1 TO M;
                ALPHA=I*2; THETA=BETA1;
                RA=1.4142*ROW*SIND(THETA/2);
                X=((RA*SIND(ALPHA))*COL/ROW)+0.5;
                Y=(RA*COSD(ALPHA))+0.5;
                B(Y,X)='+';
                ALPHA=(I*2)-1; THETA=BETA2;
                RA=1.4142*ROW*SIND(THETA/2);
                X=((RA*SIND(ALPHA))*COL/ROW)+0.5;
                Y=(RA*COSD(ALPHA))+0.5;
                B(Y,X)='+';
                END;
           END;

 STABILITY REGIME FOR SIGMA2=SIGMA1 IS COMPUTED
                                                                    */
     ELSE IF PP=3 THEN DO;
           DO I=1 TO M;
```

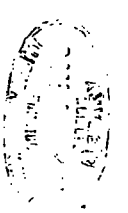

```
OPTIONS(MAIN);



            PHI1(2*I)=2*I; PSI1(2*I)=BETA1;
            PHI1((2*I)-1)=(2*I)-1; PSI1((2*I)-1)=BETA2; END;
            M=2*M;
            CALL STEPOL(PHI1,PSI1,A,T,M);
            DO I=1 TO M;
            RA=1.4142*ROW*SIND((T(I))/2);
            X=((RA*SIND(A(I)))*COL/ROW)+0.5;
            Y=(RA*COSD(A(I)))+0.5;
            B(-Y,X)='+';
            END;
      END;

E STABILITY REGIMES FOR SIGMA2=SIGMA3+(SIGMA1-SIGMA3)/3 AND FOR
GMA2=SIGMA3+(SIGMA1-SIGMA3)*2/3 ARE COMPUTED
                                                                    */
      ELSE DO;
      DO MM=1 TO 999;  M1=MM/1000;
            K=1+M1*(2*F/(1-F));
            K1=(1+F)/(1-F);
            K2=1+P*(2*F/(1-F));
            LL=((K2-K)*(1-K)+(K*TAND(PHI))**2)/((K2-K1)*(1-K1));

NCE LL AND NN ARE THE SQUARES OF DIRECTION COSINES,THEY DO NOT EXIST
EATER THAN 1 OR LESS THAN 0
                                                                    */
            IF LL<=0|LL>1 THEN GOTO L2;
            L=SQRT(LL);
            NN=((K1-K)*(K2-K)+(K*TAND(PHI))**2)/((K1-1)*(K2-1));
            IF NN<=0|NN>1 THEN GOTO L2;
            N=SQRT(NN);

E SUM OF THE SQUARES OF THE THREE DIRECTION COSINES DESCRIBING A
NE IS UNITY. IF THE SUM OF TWO (LL AND NN) IS GREATER THAN 1 THEN
E OTHER DOES NOT EXIST AND THUS THE VALUES L AND N ARE ALSO
ENABLE
                                                                    */
            IF (1-LL-NN)<=0 THEN GO TO L2;
            THETA=ATAND((SQRT(1-L*L))/L);
            L=N/SIND(THETA);
            ALPHA=ATAND((SQRT(1-L*L))/L);
            RA=1.4142*ROW*SIND(THETA/2);
            X=((RA*SIND(ALPHA))*COL/ROW)+0.5;
            Y=(RA*COSD(ALPHA))+0.5;
            IF PP=1 THEN B(Y,-X)='+';
            ELSE B(-Y,-X)='+';
   L2:      END;
            END;
      END LOOP1;
      PUT PAGE EDIT('TRIAXIAL STABILITY ANALYSIS:STEREOGRAPHIC EQUAL
EA PROJECTION')(X(40),A);
      PUT SKIP(2) EDIT('F=',F,'PHI=',PHI,'P=0, 0.33, 0.67, 1')
      (X(50),A,F(5,3),X(5),A,F(4,1),X(5),A);
      PUT SKIP(6);
      DO I=ROW TO -ROW BY -1; PUT SKIP EDIT('
```

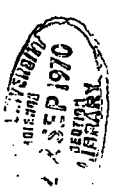
SEP 1970

```
OPTIONS(MAIN);



   ')(A);
      DO J=-COL TO COL BY 1;
       PUT EDIT(B(I,J))(A(1)); END; END;
  FIN:GOTO START;
IVISH:END STAB;
```

TRIAXIAL STABILITY ANALYSIS:STEREOGRAPHIC EQUAL AREA PROJECTION

F=0.300 PHI=10.0 P=0, 0.33, 0.67, 1

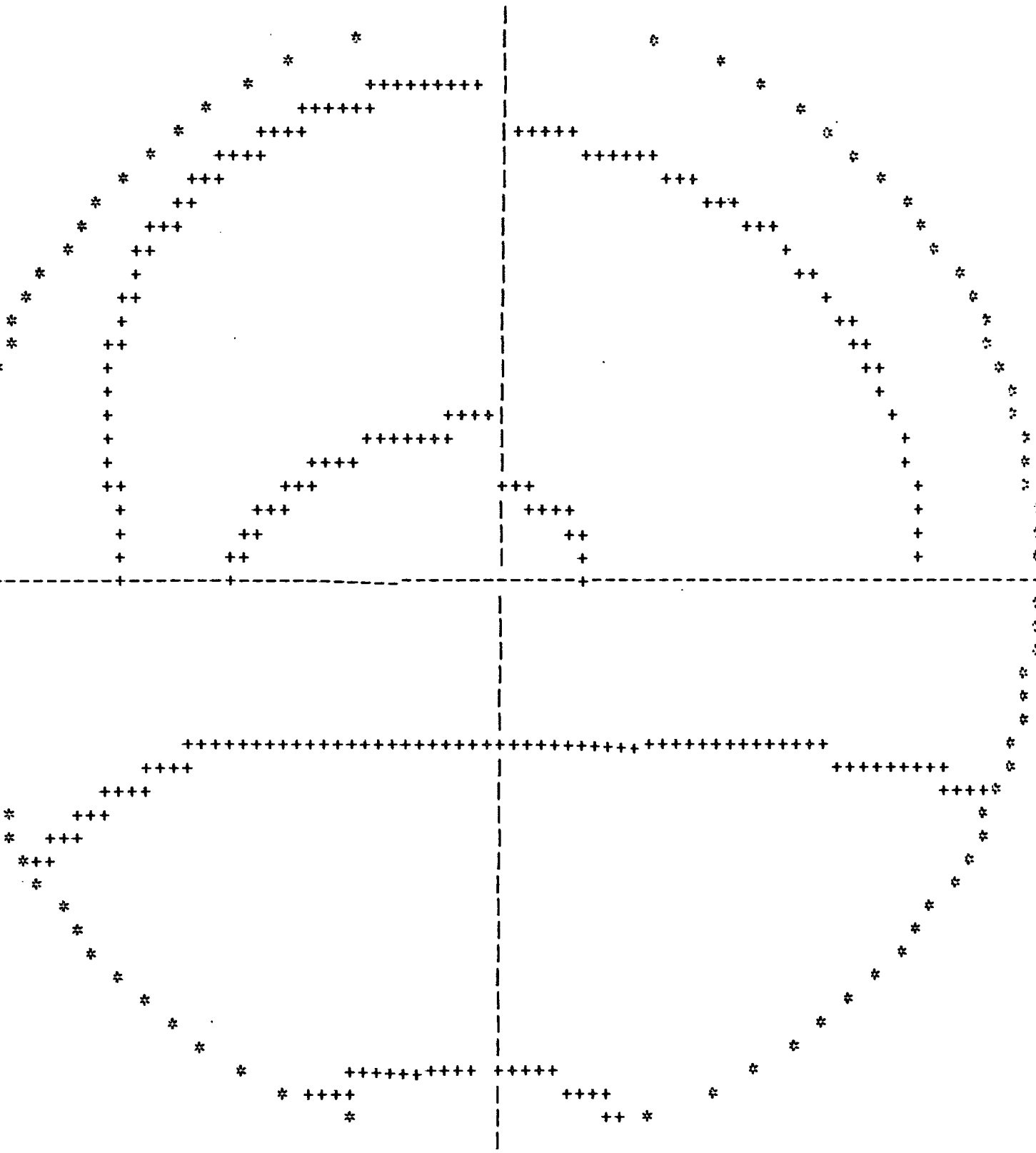

TRIAXIAL STABILITY ANALYSIS: STEREOGRAPHIC EQUAL AREA PROJECTION

F=0.600 PHI=10.0 P=0, 0.33, 0.67, 1

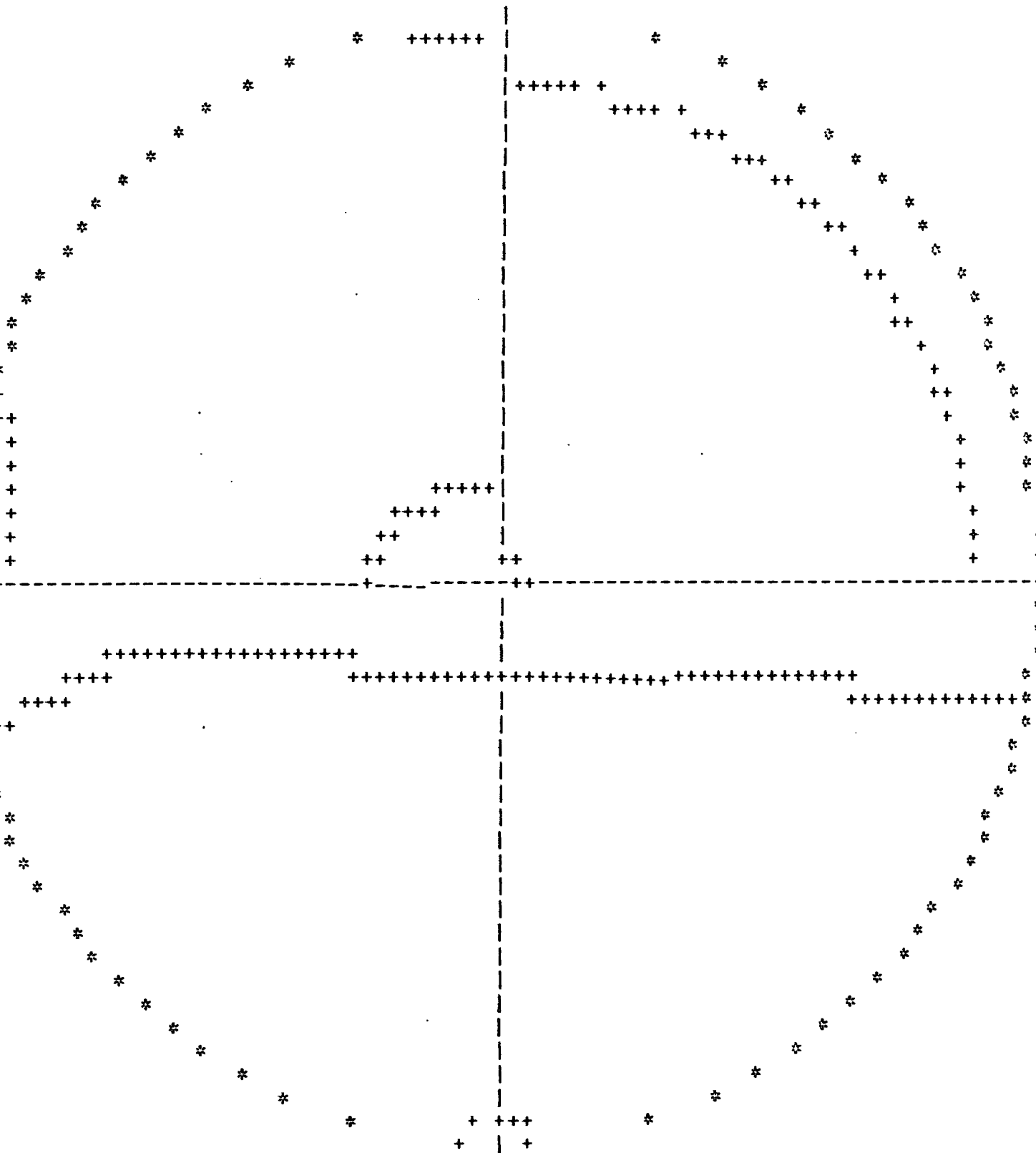

TRIAXIAL STABILITy ANALYSIS:STEREOGRAPHIC EQUAL AREA PROJECTION

F=0.600 PHI=20.0 P=0, 0.33, 0.67, 1

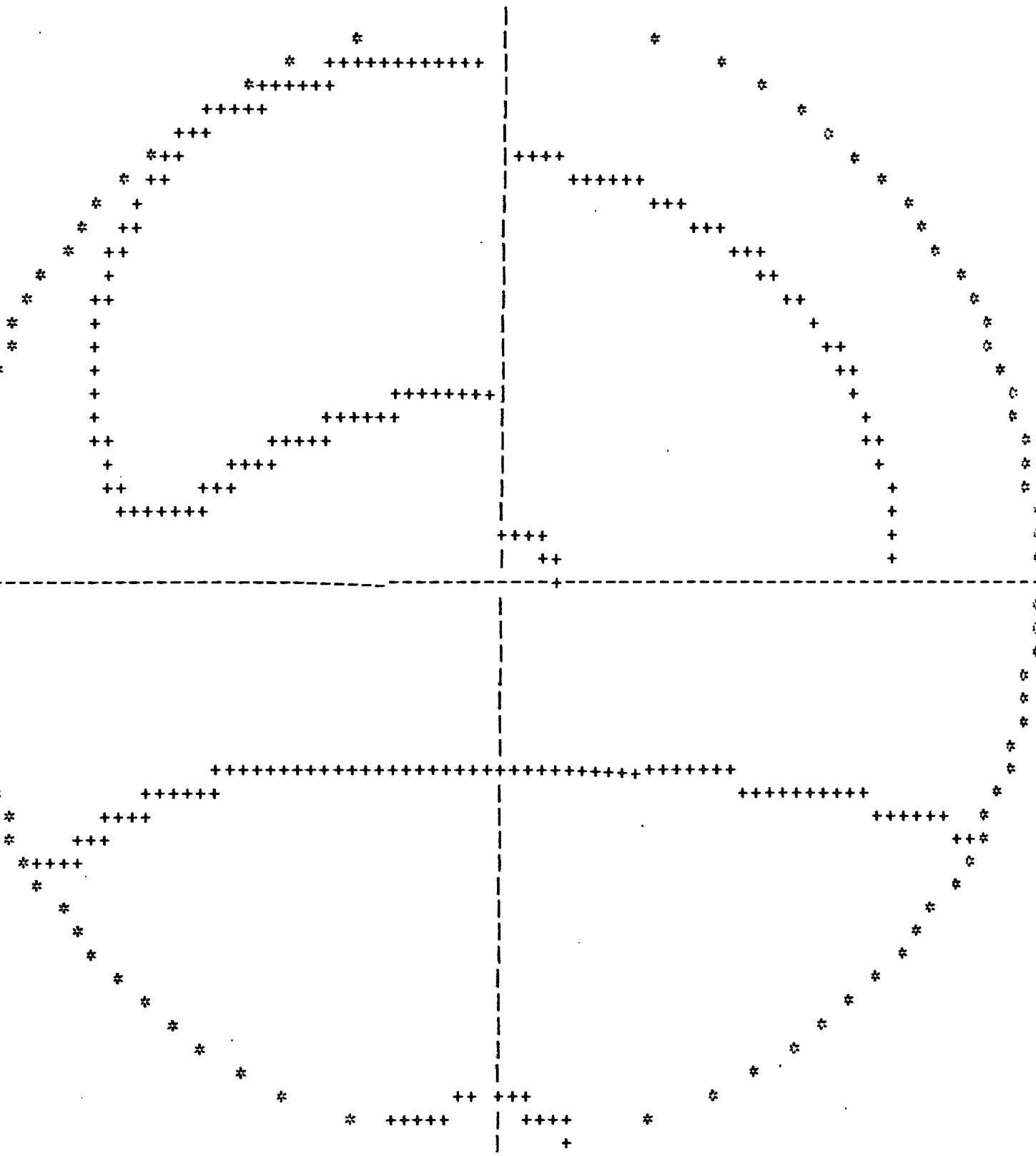

TRIAXIAL STABILITY ANALYSIS: STEREOGRAPHIC EQUAL AREA PROJECTION

F=0.600 PHI=30.0 P=0, 0.33, 0.67, 1

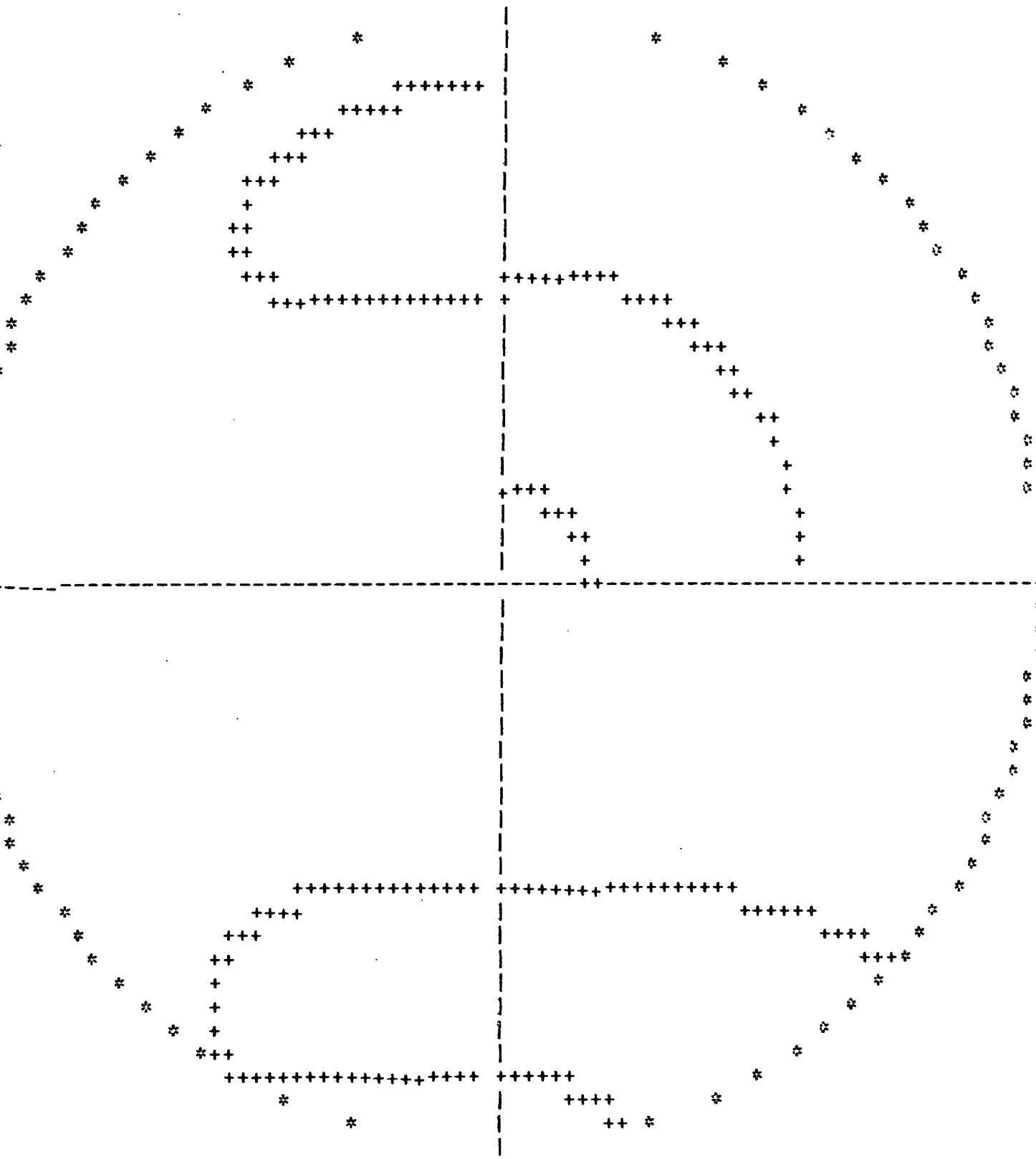

TRIAXIAL STABILITY ANALYSIS:STEREOGRAPHIC EQUAL AREA PROJECTION

F=0.800 PHI=10.0 P=0, 0.33, 0.67, 1

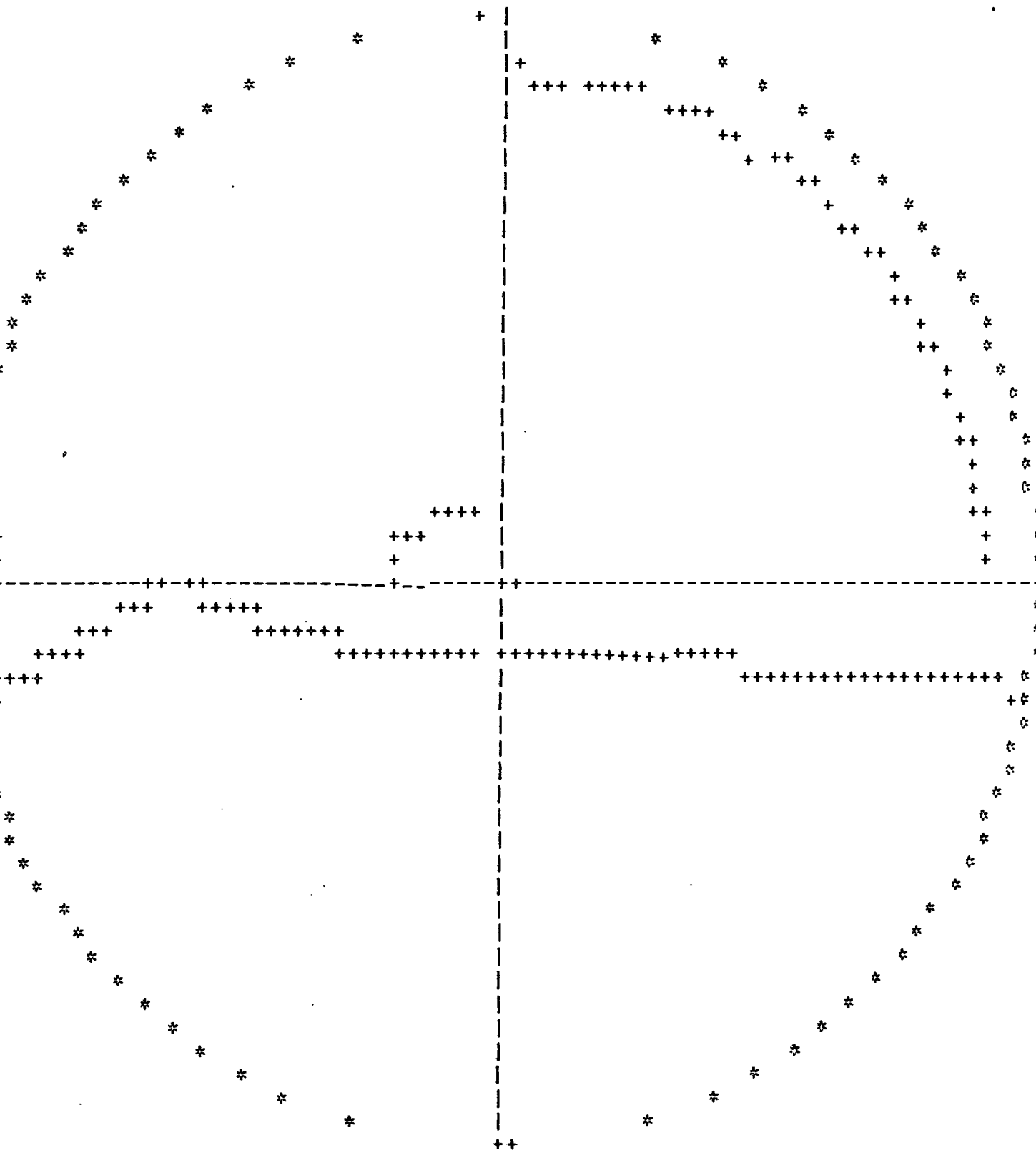

TRIAXIAL STABILITY ANALYSIS: STEREOGRAPHIC EQUAL AREA PROJECTION

F=0.800 PHI=20.0 P=0, 0.33, 0.67, 1

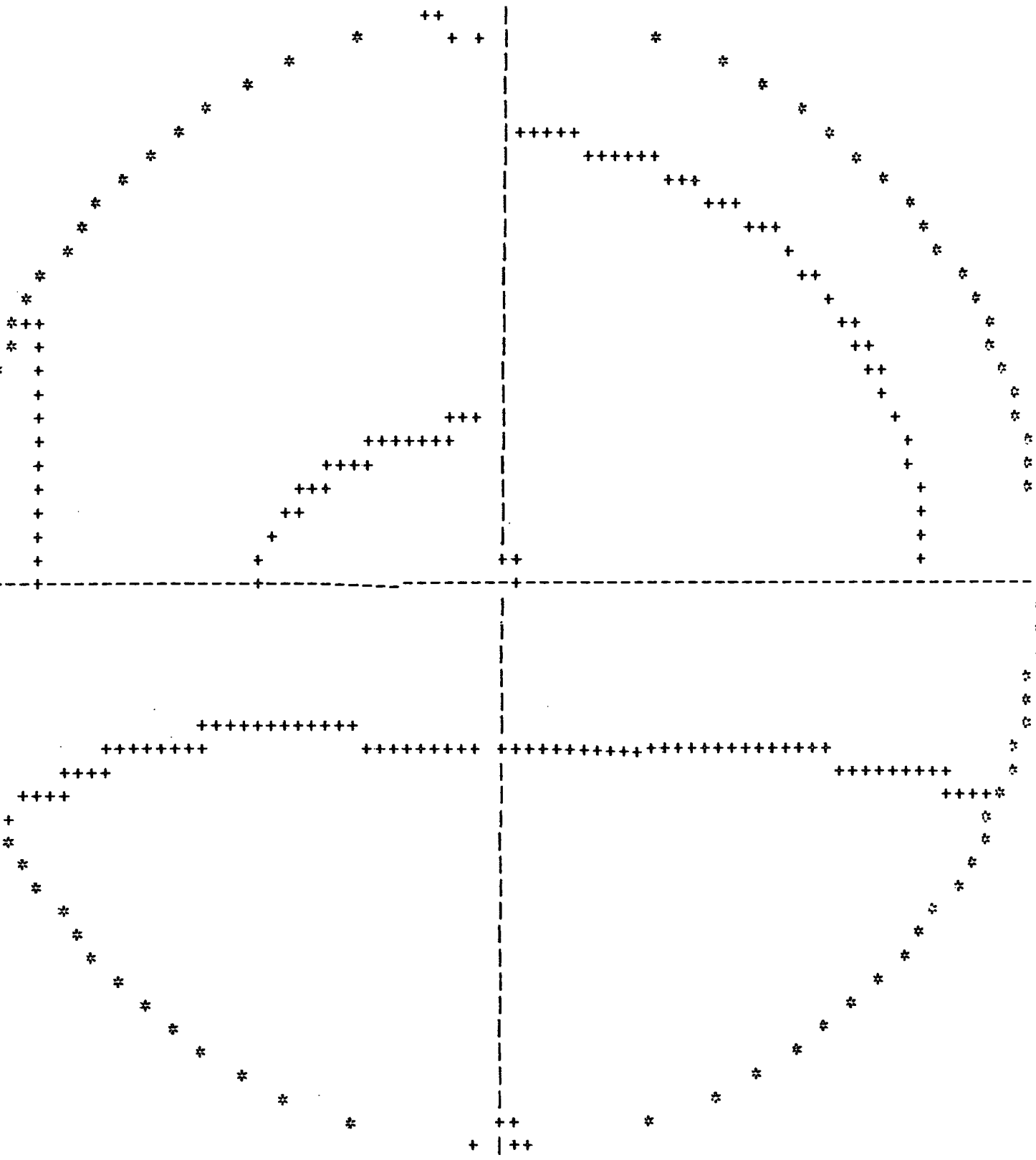

TRIAXIAL STABILITY ANALYSIS:STEREOGRAPHIC EQUAL AREA PROJECTION

F=0.800 PHI=30.0 P=0, 0.33, 0.67, 1

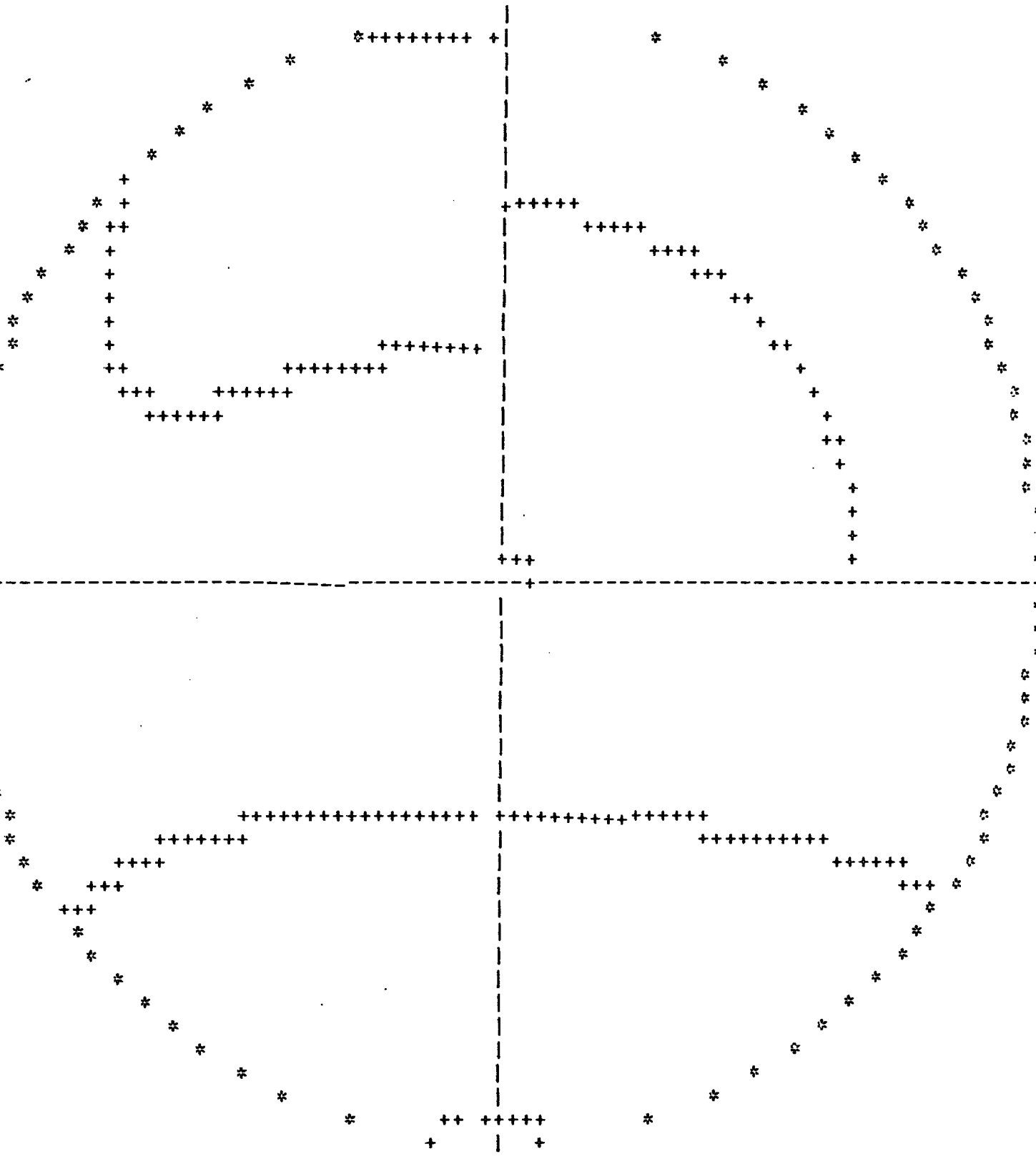

TRIAXIAL STABILITY ANALYSIS: STEREOGRAPHIC EQUAL AREA PROJECTION

F=0.800 PHI=40.0 P=0, 0.33, 0.67, 1

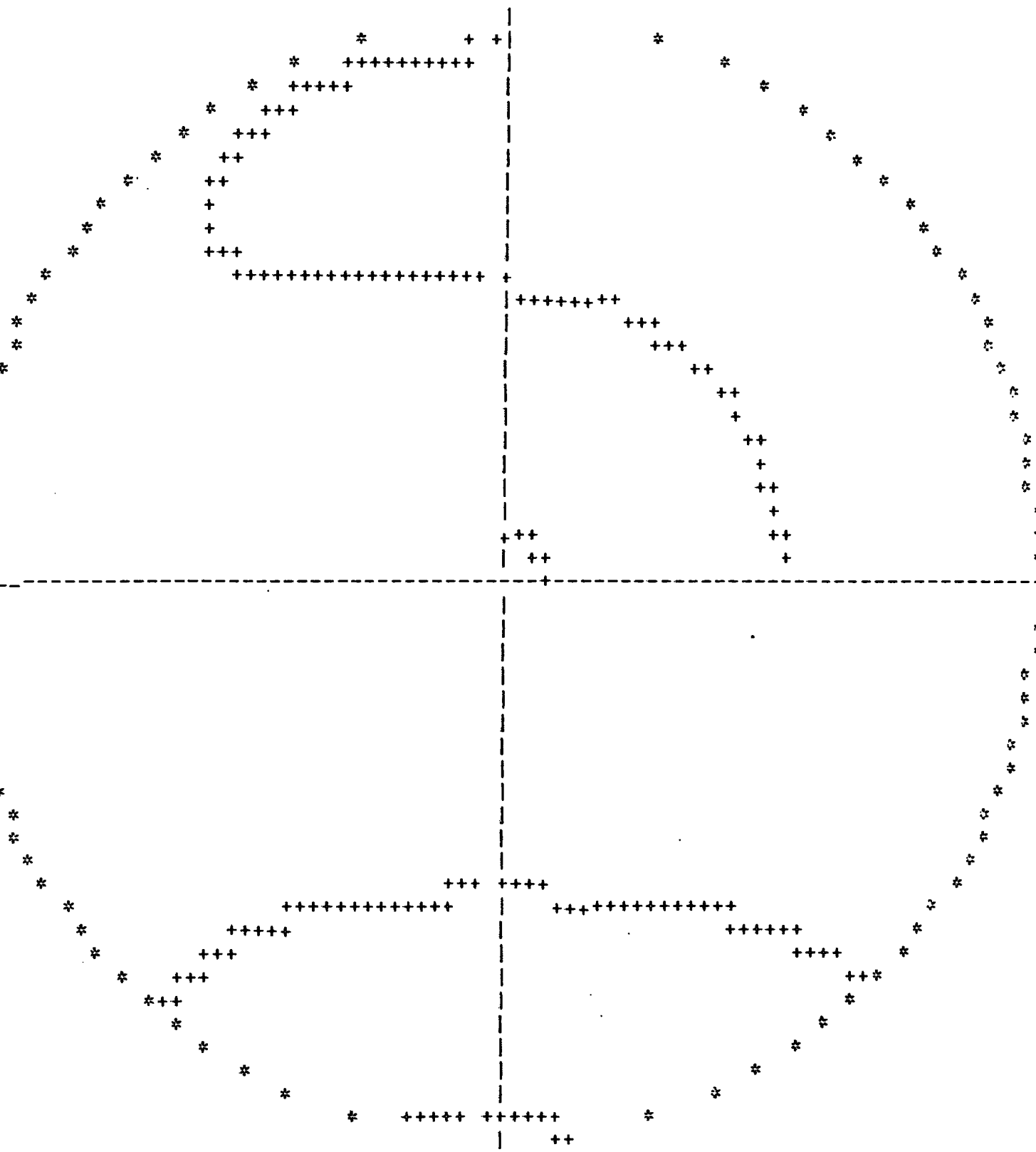

TRIAXIAL STABILITY ANALYSIS: STEREOGRAPHIC EQUAL AREA PROJECTION

F=0.800 PHI=50.0 P=0, 0.33, 0.67, 1

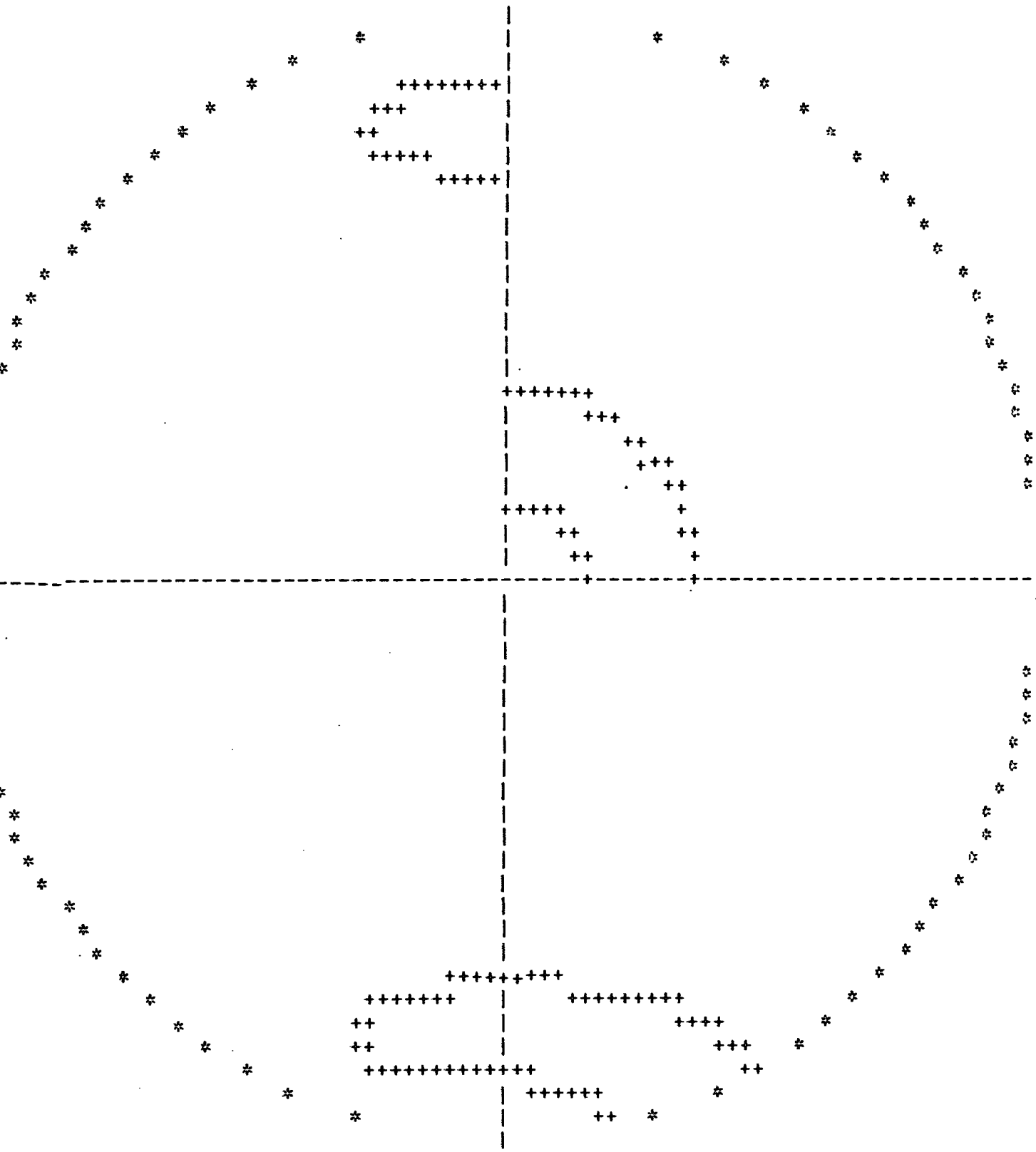


22 SEP 1970

TRIAXIAL STABILITY ANALYSIS:STEREOGRAPHIC EQUAL AREA PROJECTION

F=0.900 PHI=10.0 P=0, 0.33, 0.67, 1

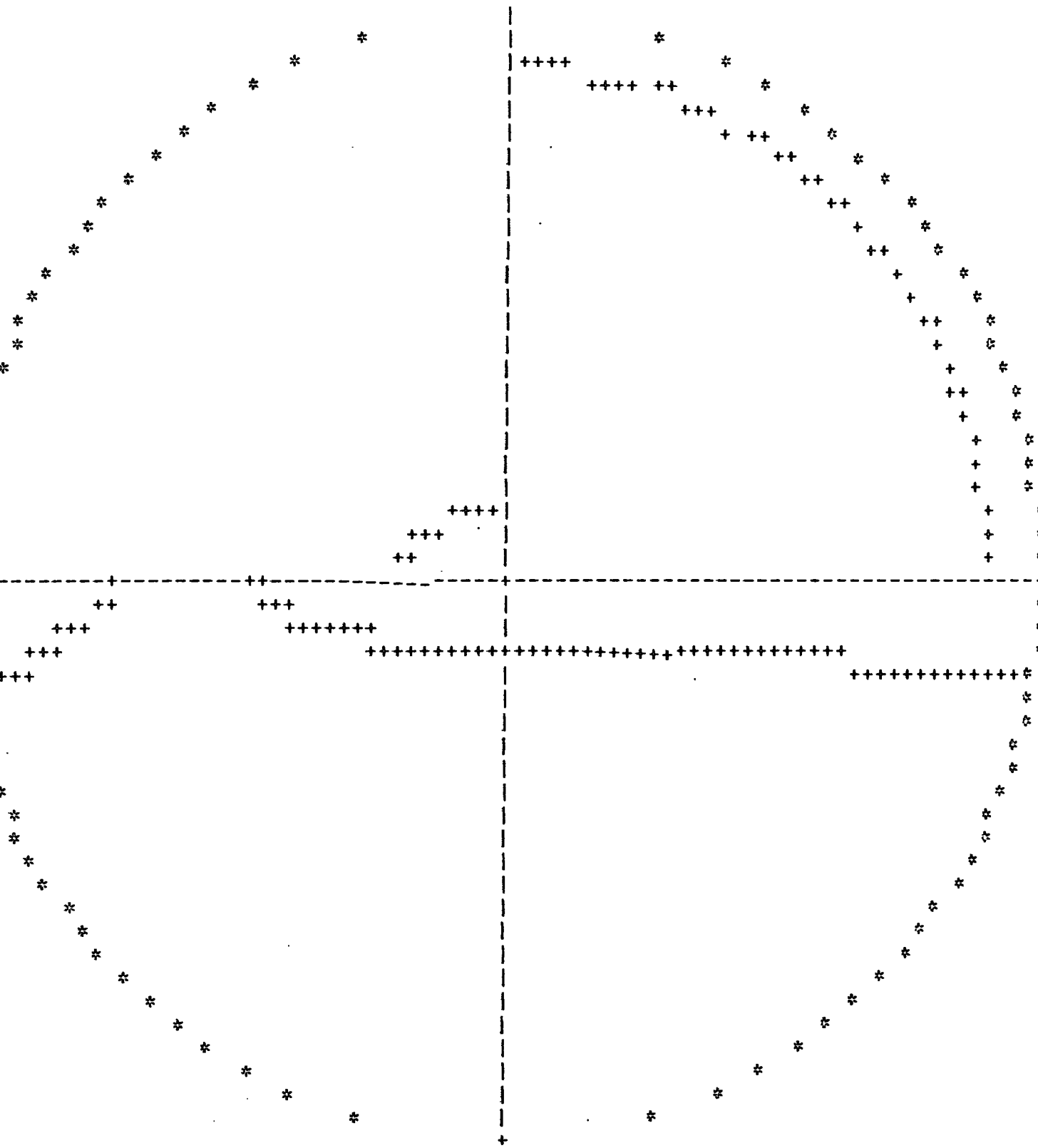


22 SEP 1970

TRIAXIAL STABILITY ANALYSIS:STEREOGRAPHIC EQUAL AREA PROJECTION

F=0.900 PHI=20.0 P=0, 0.33, 0.67, 1

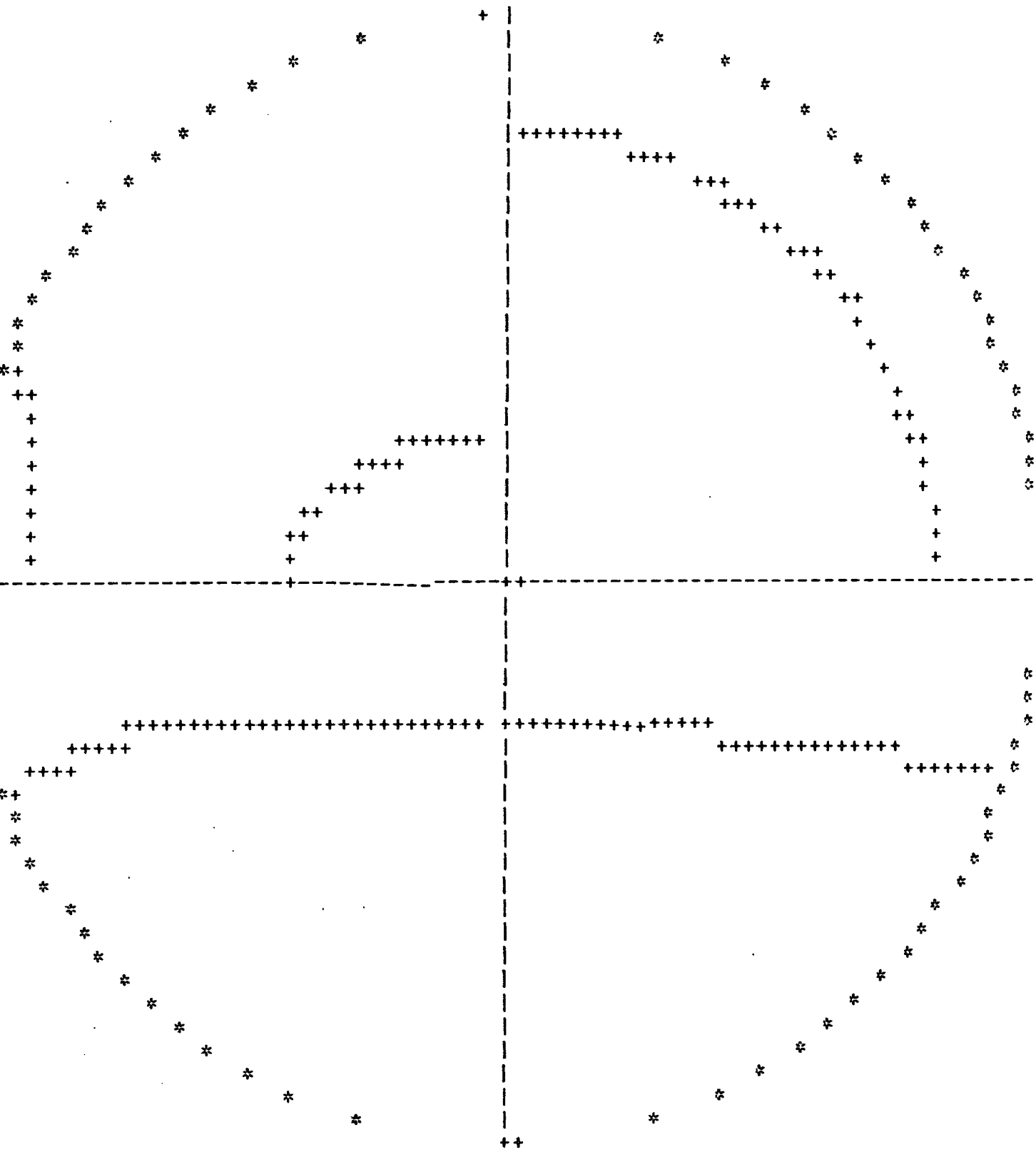

TRIAXIAL STABILITY ANALYSIS: STEREOGRAPHIC EQUAL AREA PROJECTION

F=0.900 PHI=30.0 P=0, 0.33, 0.67, 1

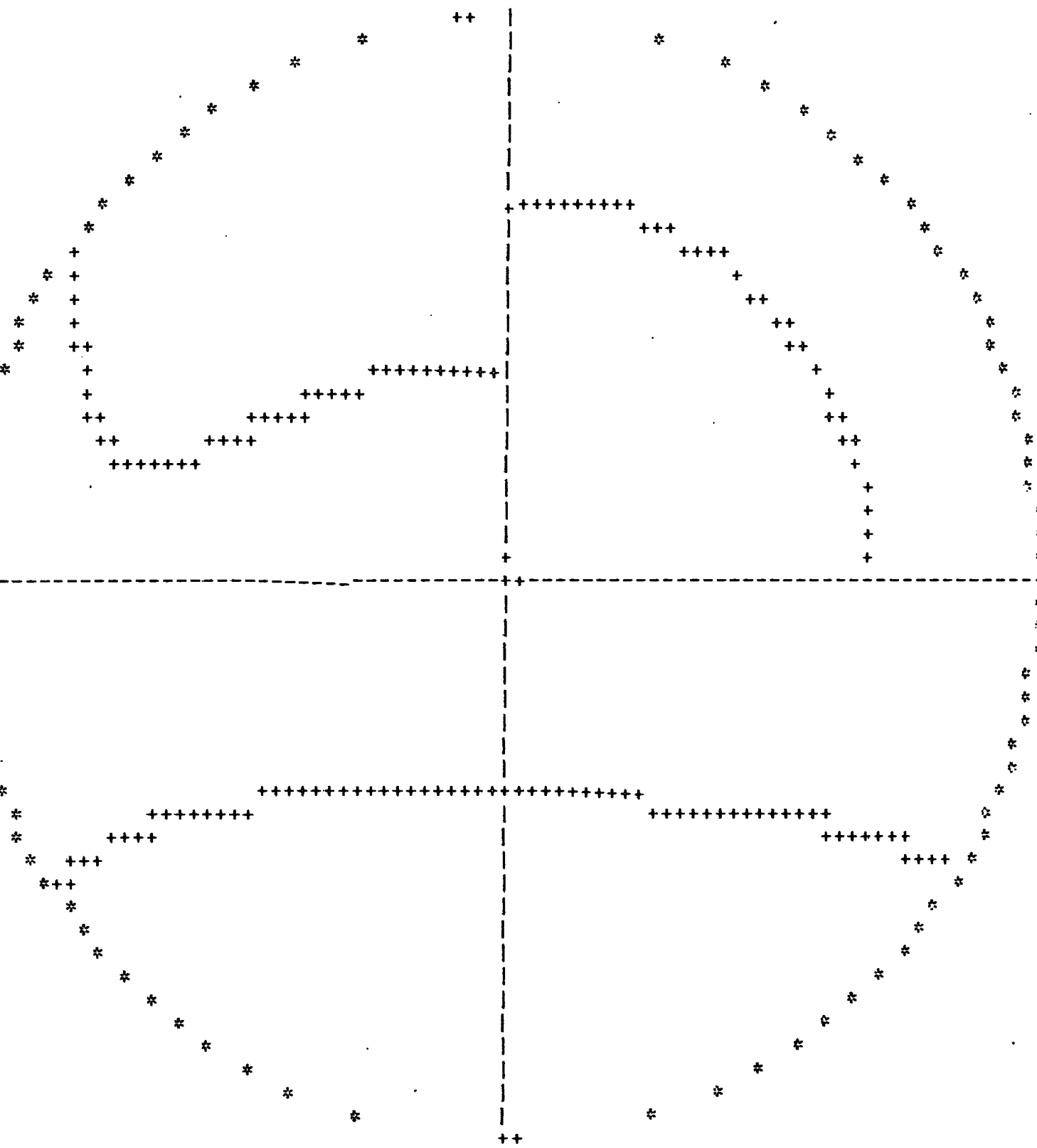

TRIAXIAL STABILITY ANALYSIS:STEREOGRAPHIC EQUAL AREA PROJECTION

F=0.900 PHI=40.0 P=0, 0.33, 0.67, 1

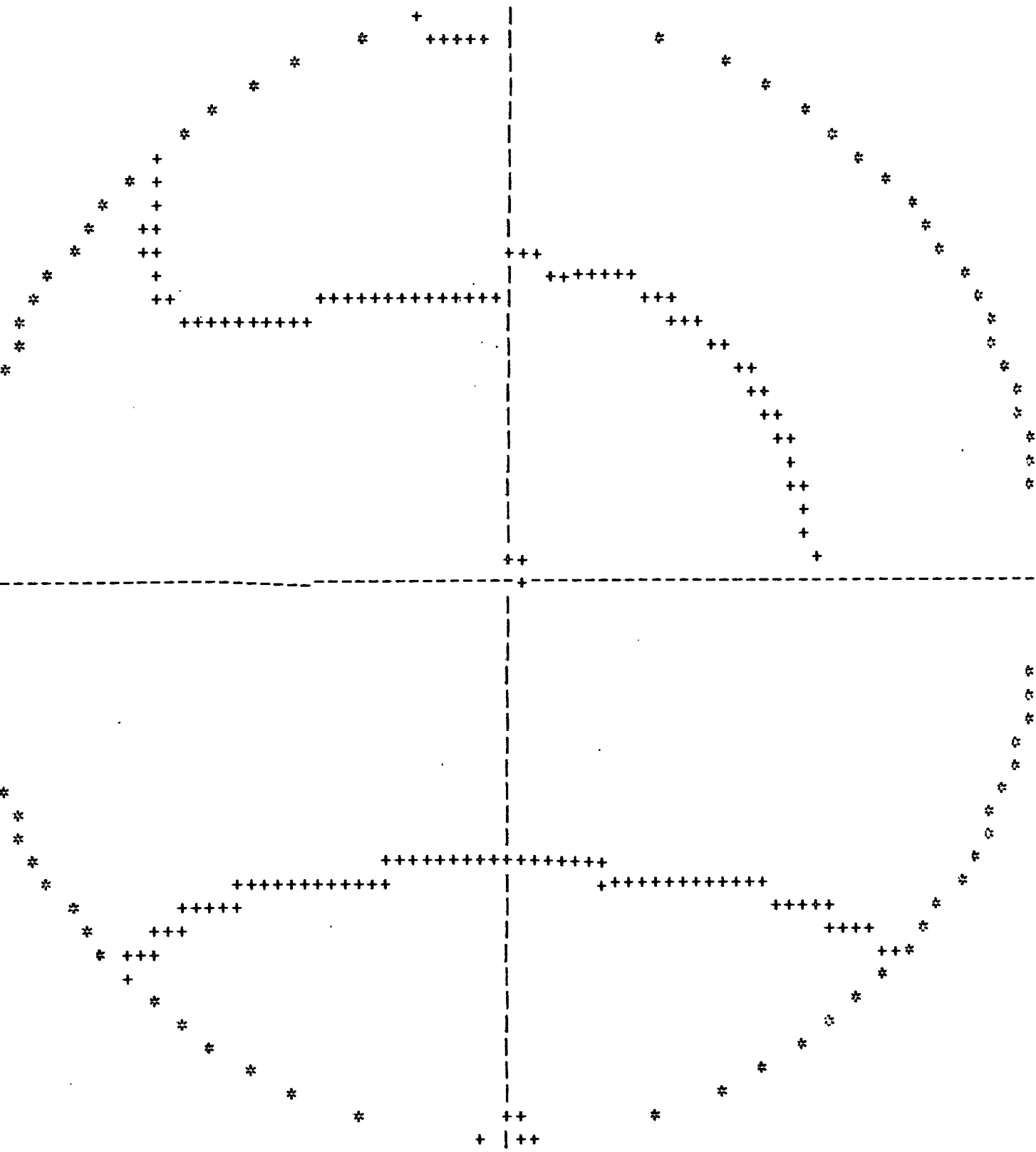

TRIAXIAL STABILITY ANALYSIS:STEREOGRAPHIC EQUAL AREA PROJECTION

F=0.900 PHI=50.0 P=0, 0.33, 0.67, 1

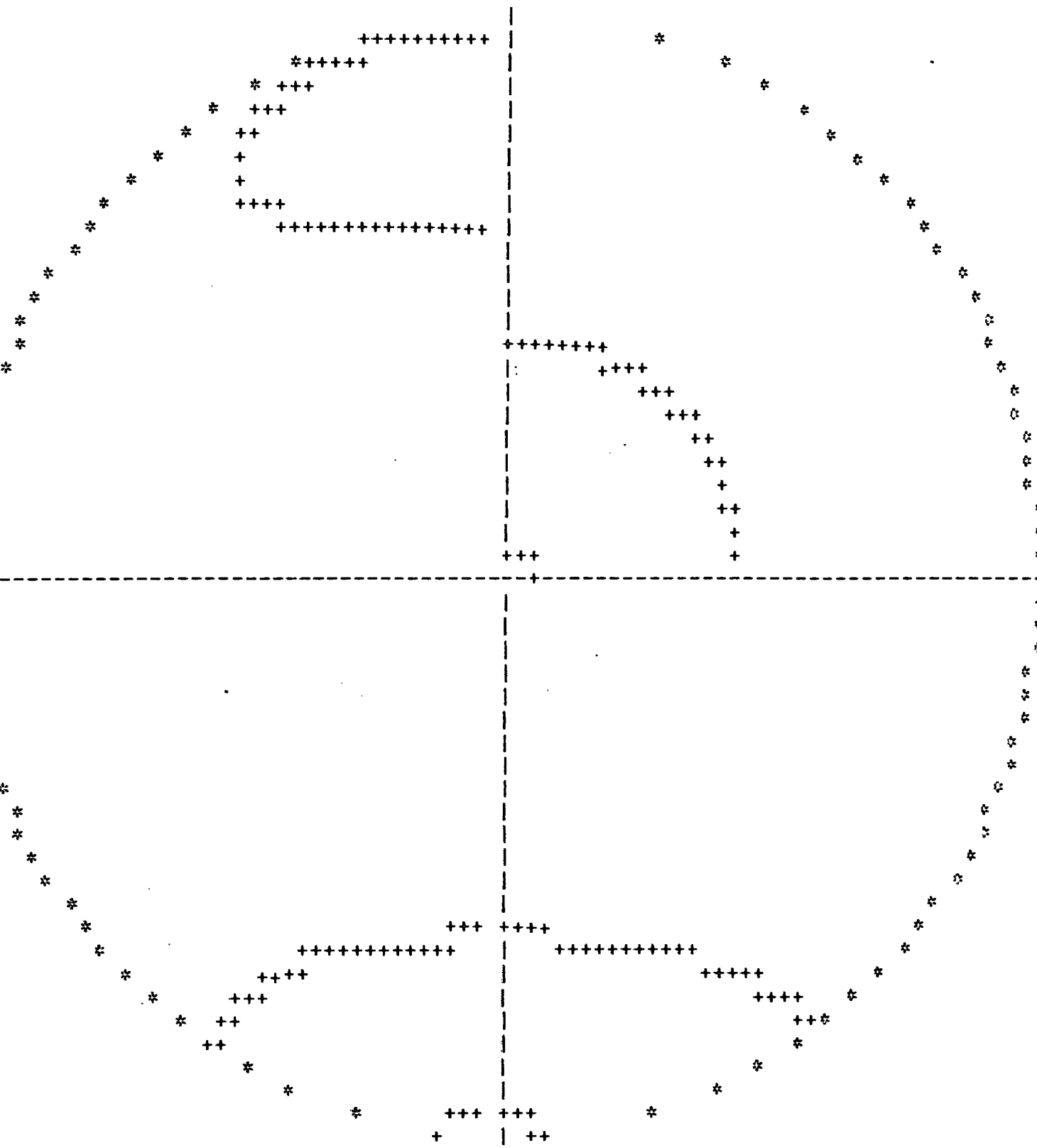

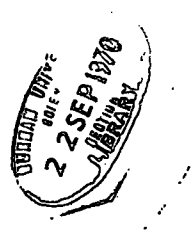
22SEP1970

TRIAXIAL STABILITY ANALYSIS:STEREOGRAPHIC EQUAL AREA PROJECTION

F=0.900 PHI=60.0 P=0, 0.33, 0.67, 1

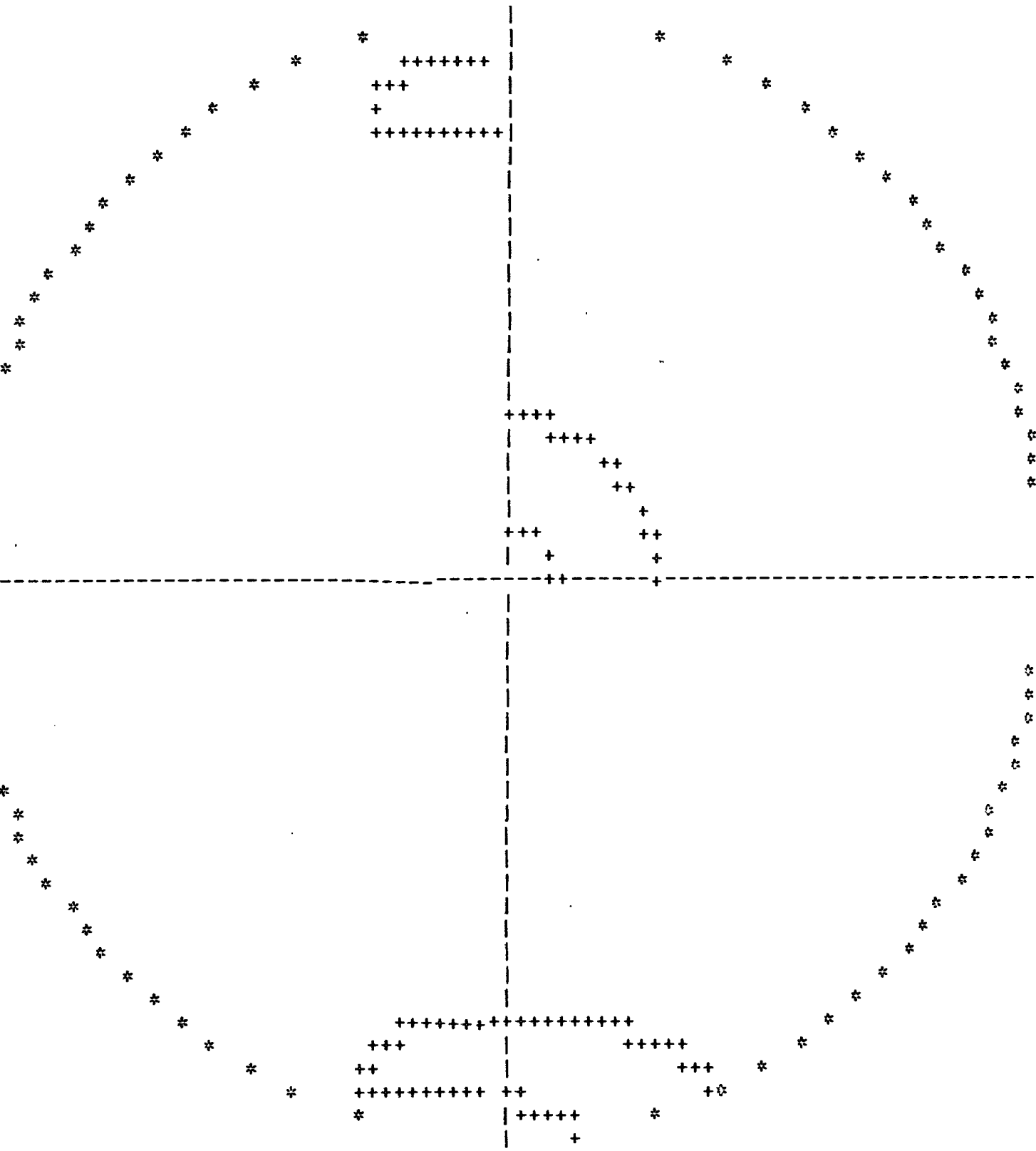

C3. Program JTSTAB

This employs similar methods to the above, and is extensively detailed by the comment cards contained in the source listing. To simplify to logic, three interrelated procedures (subroutines) are used. The orientation of a plane in space may be described by combinations of the angles α, θ, ϕ, ψ (Fig. 1.4). Thus (α , θ) are the polar coordinates, (ψ , ϕ) equatorial coordinates and (θ, ψ) direction cosine coordinates. For plotting purposes, polar coordinates are used, but equatorial coordinates are required for some rotations. Procedure POLSTE therefore converts from polar to equatorial coordinates, procedure STEPOL performing the reverse function.

Rotation is executed by procedure ROTATE, and may be about the vertical axis (azimuth rotation) or the N-S axis (elevation rotation). By a combination of elevation rotation, azimuth rotation and elevation rotation, any completely new orientation may be achieved. For elevation rotation, the coordinates are required in equatorial form, polar coordinates being used for azimuth rotation. At the end of each step, coordinates are converted into polar form.

C3.1. Logic - The planar discontinuity envelope is first tested for intersection of the principal stress circle, and the stress coordinates calculated. If there is no intersection, or the envelope is tangential to the circle, a termination message is printed and the run stopped.

The stability regime is calculated similarly to the above, and the limiting orientations stored in paired locations as (α, θ). The ROTATE procedure is then used to bring the σ_1, σ_2, σ_3, directions into coincidence with the vertical, E-W, and N-S axes respectively, and the required angular rotations stored, (BETAR 1, BETAR 2, BETAR 3). The (α , θ) pairs are then back-rotated in reverse sequence using the above rotation parameters.

Finally, the polar coordinates are translated into cartesian locations in the output character array using the definitions given in STAB above, and the final rotated stability regime is printed.

Details of input are contained in the program listing. The example given depicts to stability regimes at each stage of back rotation.

```
CEDURE OPTIONS(MAIN);


JTSTAB:PROCEDURE OPTIONS(MAIN);
/*
THIS PROGRAMME ANALYSES THE STABILITY OF A PLANAR DISCONTINUITY,
ESCRIBED BY ITS FAILURE STRENGTH PARAMETERS OF COHESION AND FRICTION
NGLE,AND ITS DIP AND DIP DIRECTION,IN TERMS OF THE TRIAXIAL STRESS
IELD ACTING UPON IT AT A POINT,DESCRIBED BY THE DIRECTIONS AND DIPS OF
HE THREE PRINCIPAL STRESSES.
                        SYMBOL DEFINITIONS
          DUMMY VARIABLE USED IN THE COMPUTATION OF INTERSECTION POINTS
CJ        DISTANCE FROM THE CENTRE OF THE PRINCIPAL STRESS CIRCLE TO THE
          PROJECTION ONTO THE NORMAL STRESS AXIS OF THE TWO INTERSECTION
          POINTS
LPHA      DIRECTION OF RADIUS VECTOR IN POLAR PLOT
LPHA1     GLOBAL DIRECTION OF SIGMA1
LPHA2     GLOBAL DIRECTION OF SIGMA2
LPHA3     GLOBAL DIRECTION OF SIGMA3
NG1       ANGLE BETWEEN THE SIGMA1 DIRECTION AND THE PLANAR FAILURE (<45
          DEGREES),THUS EQUAL TO HALF ANGLE SUBTENDED BY INTERSECTION
          POINTS AND SIGMA3 IN THE PRINCIPAL STRESS CIRCLE
NG2       45 ANG1 BUT <45 DEGREES SINCE CORRESPONDS TO INTERSECTION POINTS
          DUMMY VARIABLE USED IN THE COMPUTATION OF INTERSECTION POINTS
ETA       ROTATION ANGLE ABOUT THE POLE OF PROJECTION
ETA1      FIRST ROTATION ANGLE
ETA2      SECOND ROTATION ANGLE
ETA3      THIRD ROTATION ANGLE
          DUMMY VARIABLE USED IN COMPUTATION OF INTERSECTION POINTS
CL        NUMBER OF PRINT POSITIONS ACROSS THE PAGE FOR OUTPUT OF
          CHARACTER ARRAY GIVING STABILITY PLOT,AND THUS THE X DIMENSION
          OF E
          STEP INCREMENT IN SIGMA BETWEEN PT2 AND PT1
ELTA      ANGLE BETWEEN 'NORTH' AND THE REQUIRED AXIS OF ROTATION
          CHARACTER ARRAY CONTAINING STABILITY PLOT
I         FRICTION ANGLE FOR DISCONTINUITY MATERIAL
AMMA      ANGLE OF ROTATION,ABOUT AXIS DELTA FROM 'NORTH'
          DUMMY VARIABLE USED IN COMPUTATION OF INTERSECTION POINTS
          DIRECTION COSINE MEASURED FROM SIGMA1
L         L**2
          TOTAL NUMBER OF POINTS
          DIRECTION COSINE MEASURED FROM SIGMA3
N         N**2
OUNT      COUNTER USED IN ROTATION TESTING
1         EQUIVALENT TO ALPHA
2         EQUIVALENT TO THETA
3         EQUIVALENT TOPHI
4         EQUIVALENT TOPSI
I1        ANGLE IN EQUATORIAL PLOT
I1        ANGLE IN EQUATORIAL PLOT
T1        NORMAL STRESS VALUE OF THE HIGHEST INTERSECTION BETWEEN THE
          DISCONTINUITY ENVELOPE AND THE PRINCIPAL STRESS CIRCLE
T2        NORMAL STRESS VALUE OF THE LOWEST INTERSECTION BETWEEN THE
          DISCONTINUITY ENVELOPE AND THE PRINCIPAL STRESS CIRCLE
1         EQUIVALENT TO PHI
2         EQUIVALENT TO PSI
3         EQUIVALENT TO ALPHA
4         EQUIVALENT TO THETA
A         DUMMY VARIABLE USED IN COMPUTATION OF THE COORDINATES FOR
```

```
JCEDURE OPTIONS(MAIN);



        SCHMIDT EQUAL AREA PROJECTION
ACW     NUMBER OF PRINT POSITIONS ACROSS THE PAGE FOR OUTPUT OF
        CHARACTER ARRAY GIVING STABILITY PLOT,AND THUS THE Y DIMENSION
        OF E
SIGMA   NORMAL STRESS
SIGMA1  MAJOR PINCIPAL STRESS VALUE
SIGMA2  INTERMEDIATE PRINCIPAL STRESS VALUE
SIGMA3  MINOR PRINCIPAL STRESS VALUE
        SHEAR STRESS
THETA   ANGLE ALONG RADIUS VECTOR IN POLAR PLOT
THETA1  DIP OF SIGMA1
THETA2  DIP OF SIGMA2
THETA3  DIP OF SIGMA3
        X COORDINATE OF A CHARACTER IN ARRAY E
XC      X COORDINATE OF CIRCLE IN ARRAY C
        Y COORDINATE OF A CHARACTER IN ARRAY E
                        INPUT DETAILS
FREE FORMAT INPUT IN ORDER:- ALPHA1
                             THETA1
                             ALPHA2
                             THETA2
                             ALPHA3
                             THETA3
                             SIGMA1
                             SIGMA2
                             SIGMA3
                             SC
                             FI
                                                                        */
        DCL(((ALPHA1,THETA1,PHI1,PSI1,ALPHA2,THETA2,PHI2,PSI2,ALPHA3,
        THETA3,PHI3,PSI3)(M))FLOAT CONTROLLED,(BETA1,BETA2,BETA3)
        FLOAT,(M,I)FIXED BIN);
        DCL((SIGMA1,SIGMA2,SIGMA3,SC,FI,A,B,C,H)FLOAT);
        DCL (THETA,ALPHA,PHI,PSI)(359)FLOAT,(CCL,RCW,X,Y)FIXED BIN,
        XC(-RCW:RCW)CONTROLLED FIXED BIN,
        E(-RCW:RCW,-CCL:CCL)CONTROLLED CHAR(1),(LL,L,NN,N)FLOAT;
*
ROCEDURE POLSTE CONVERTS THE POLAR ANGLES P1 AND P2 INTO THE
ORRESPONDING EQUATORIAL ANGLES P3 AND P4
                                                                        */
        DCL POLSTE ENTRY((*)FLOAT,(*)FLOAT,(*)FLOAT,(*)FLOAT,FIXED
        BIN);
POLSTE:PROCEDURE(P1,P2,P3,P4,M);
        DCL((P1,P2,P3,P4)(M)FLOAT,(I,M)FIXED BIN);
*
NGLES UPON WHICH IT IS NOT REQUIRED TO OPERATE ARE GIVEN A VALUE 7777
                                                                        */
              DO I=1 TO M;
              IF P1(I)=7777 THEN DO;
                        P3(I)=7777; P4(I)=7777; GOTO POI; END;
*
HEN THE ARGUMENT OF THE GENERIC FUNCTION TAND IS CLOSE TO 90 DEGREES
R 270 DEGREES) THE VALUE OF THE FUNCTION IS VERY LARGE AND MAY LEAD
 THE OVERFLOW CONDITION. IN ORDER TO BYPASS THIS A CONDITIONAL
```

```
JCEDURE OPTIONS(MAIN);



STATEMENT IS USED
                                                                      */
            IF (P2(I)>89.99 & P2(I)<90.01) THEN DO;
                 IF SIND(P1(I))>0 THEN P3(I)=90;
                 ELSE P3(I)=-90;
                 IF ((ABS(P1(I))>89.99 & ABS(P1(I))<90.01) |
                 (ABS(P1(I))>269.99 & ABS(P1(I))<270.01)) THEN DO;
                      P4(I)=90; GO TO PO1; END;
                 ELSE P4(I)=ATAND(TAND(P1(I))); GOTO PO1; END;
            P3(I)=ATAND((SIND(P1(I)))*TAND(P2(I)));
            ON ZERODIVIDE BEGIN;
            P4(I)=90; GOTO PO1; END;
            P4(I)=ATAND(1/((COSD(P3(I)))*(COSD(P1(I)))*TAND(P2(I))));
   PO1:     END;
      END POLSTE;
/*
PROCEDURE STEPOL CONVERTS THE EQUATORIAL ANGLES R1 AND R2 INTO THE
CORRESPONDING POLAR ANGLES R3 AND R4
                                                                      */
      DCL STEPOL ENTRY((*)FLOAT,(*)FLOAT,(*)FLOAT,(*)FLOAT,FIXED
      BIN);
STEPOL:PROCEDURE(R1,R2,R3,R4,M);
      DCL((R1,R2,R3,R4)(M)FLOAT,(I,M)FIXED BIN);
      DO I=1 TO M;
      IF R1(I)=7777 THEN DO;
                 R3(I)=7777; R4(I)=7777; GOTO ST1; END;
/*
WHEN ABS(R1)>90 DEGREES IT INDICATES THAT DURING ROTATION THE POLE HAS
CROSSED THE PRIMITIVE CIRCLE AND THUS REAPPEARS IN THE DIAMETRICALLY
OPPOSITE QUADRANT
                                                                      */
      IF ABS(R1(I))>90 THEN DO;
           R2(I)=-R2(I); R1(I)=-R1(I); END;
      IF (ABS(R2(I))>89.99 & ABS(R2(I))<90.01) THEN DO;
      IF (ABS(R1(I))>89.99 & ABS(R1(I))<90.01) THEN DO;
           R4(I)=90; GO TO STO; END;
       ELSE R4(I)=ABS(ATAND(TAND(R1(I))));
   STO:    IF SIND(R1(I))>0 THEN R3(I)=90;
           ELSE R3(I)=270; GOTO ST1; END;
      IF (R2(I)>89.99 & R2(I)<90.01)|
      (R2(I)>269.99 & R2(I)<270.01) THEN DO; R3(I)=90; END;
      F1=SIND(R1(I));
      F2=TAND(R2(I));
      R3(I)=ATAND(F1*F2);
      IF F2<0 THEN DO;R3(I)=180+R3(I);END;
      ON ZERODIVIDE BEGIN;
           R4(I)=90; GOTO ST1; END;
           F3=(COSD(R1(I)))*(TAND(R2(I)))*COSD(R3(I));
           R4(I)=ATAND(1/F3);
           IF R4(I)<0 THEN R4(I)=-R4(I);
   ST1:    END;
      END STEPOL;
/*
PROCEDURE ROTATE COMPUTES THE NEW VALUES ALPHA1 AND THETA1 OF THE
```

```
CEDURE OPTIONS(MAIN);



POLAR ANGLES ALPHA AND THETA FOLLOWING ROTATION. THE AXIS AND DEGREE OF
OTATION ARE DETERMINED BY THE PARAMETERS BETA,GAMMA,DELTA.
                                                                      */
        DCL ROTATE ENTRY(FLOAT,FLOAT,FLOAT,(*)FLOAT,(*)FLOAT,(*)FLOAT,
        (*)FLOAT,FIXED BIN);
ROTATE:PROCEDURE(BETA,GAMMA,DELTA,ALPHA,THETA,ALPHA1,THETA1,M);
        DCL(((ALPHA,THETA,ALPHA1,THETA1,PHI,PSI)(M))FLOAT,
        (BETA,GAMMA,DELTA)FLOAT,(M,I)FIXED BIN);
/*
THE POLES ARE ROTATED ABOUT THE POLE OF PROJECTION TO LINE THE AXIS OF
OTATION 'NORTH-SOUTH'
                                                                      */
        DO I=1 TO M; THETA1(I)=THETA(I); ALPHA1(I)=ALPHA(I)-DELTA;END;
/*
THE POLAR ANGLES ALPHA1 AND THETA1 ARE CONVERTED TO THE CORRESPONDING
EQUATORIAL ANGLES PHI AND PSI
                                                                      */
        CALL POLSTE(ALPHA1,THETA1,PHI,PSI,M);
/*
THE EQUATORIAL ANGLES PHI AND PSI ARE ROTATED THROUGH AN ANGLE GAMMA
                                                                      */
        DO I=1 TO M; PHI(I)=PHI(I)+GAMMA; END;
/*
THE NEW POLAR ANGLES ALPHA1 AND THETA1 ARE COMPUTED FROM PHI AND PSI
                                                                      */
        CALL STEPOL(PHI,PSI,ALPHA1,THETA1,M);
/*
THE POLES ARE BACK ROTATED ABOUT THE POLE OF PROJECTION,AND BY
OTATION ABOUT THIS AXIS COMPLETED
                                                                      */
        DO I=1 TO M; ALPHA1(I)=ALPHA1(I)+DELTA+BETA; END;
        END ROTATE;
        M=1;
        COL=48; ROW=29;
        ALLOCATE ALPHA1,THETA1,ALPHA2,THETA2,ALPHA3,THETA3,PHI1,PSI1,
        PHI2,PSI2,PHI3,PSI3;
        ALLOCATE XC,YC;
        DO I=1 TO M;
/*
THE PRINCIPAL STRESS DIP AND DIP DIRECTIONS ARE READ IN
                                                                      */
        GET LIST(ALPHA1(I),THETA1(I),ALPHA2(I),THETA2(I),ALPHA3(I),
        THETA3(I)); END;
        DO I=1 TO M;
        PUT SKIP EDIT(ALPHA1(I),THETA1(I),ALPHA2(I),THETA2(I),
        ALPHA3(I),THETA3(I))
        (F(3,3),COLUMN(11),F(8,3),COLUMN(21),F(8,3),COLUMN(31),F(8,3),
        COLUMN(41),F(8,3),COLUMN(51),F(8,3));
/*
THE POLAR ANGLES ARE CONVERTED TO THE CORRESPONDING EQUATORIAL ANGLES
                                                                      */
        CALL POLSTE(ALPHA1,THETA1,PHI1,PSI1,M);
        CALL POLSTE(ALPHA2,THETA2,PHI2,PSI2,M);
        CALL POLSTE(ALPHA3,THETA3,PHI3,PSI3,M);
```


22 SEP 1970
LIBRARY

```
OCEDURE OPTICAS(MAIN);

        PUT SKIP EDIT(PHI1(I),PSI1(I),PHI2(I),PSI2(I),PHI3(I),PSI3(I))
        (F(8,3),COLUMN(11),F(8,3),COLUMN(21),F(8,3),COLUMN(31),F(8,3),
        COLUMN(41),F(8,3),COLUMN(51),F(8,3));
/*
THE POLES ARE ROTATED ABOUT A NORTH-SOUTH AXIS SO THAT SIGMA3 LIES ON
THE PRIMITIVE CIRCLE,AND THE ANGLE OF ROTATION IS BETAR1
                                                                    */
        IF PHI3(I)<0 THEN BETAR1=-90-PHI3(I);
        ELSE BETAR1=90-PHI3(I);
        PHI1(I)=PHI1(I)+BETAR1;
        PHI2(I)=PHI2(I)+BETAR1;
        PHI3(I)=PHI3(I)+BETAR1;
/*
THE EQUATORIAL ANGLES ARE CONVERTED TO THE CORRESPONDING POLAR ANGLES
                                                                    */
        CALL STEPOL(PHI1,PSI1,ALPHA1,THETA1,M);
        CALL STEPOL(PHI2,PSI2,ALPHA2,THETA2,M);
        CALL STEPOL(PHI3,PSI3,ALPHA3,THETA3,M);
        PUT SKIP EDIT(ALPHA1(I),THETA1(I),ALPHA2(I),THETA2(I),
        ALPHA3(I),THETA3(I))
        (F(8,3),COLUMN(11),F(8,3),COLUMN(21),F(8,3),COLUMN(31),F(8,3),
        COLUMN(41),F(8,3),COLUMN(51),F(8,3));
/*
THE POLES ARE ROTATED ABOUT THE POLE OF PROJECTION SUCH THAT SIGMA3
LIES IN THE NORTH OR SOUTH POSITION,AND THE ANGLE OF ROTATION IS BETAR2
                                                                    */
        IF PSI3(I)<0 THEN BETAR2=180-ALPHA3(I);
        ELSE IF ALPHA3(I)<90 THEN BETAR2=-ALPHA3(I);
             ELSE BETAR2=360-ALPHA3(I);
        ALPHA1(I)=ALPHA1(I)+BETAR2;
        ALPHA2(I)=ALPHA2(I)+BETAR2;
        ALPHA3(I)=ALPHA3(I)+BETAR2;
/*
THE POLAR ANGLES ARE CONVERTED TO THE CORRESPONDING EQUATORIAL ANGLES
                                                                    */
        CALL POLSTE(ALPHA1,THETA1,PHI1,PSI1,M);
        CALL POLSTE(ALPHA2,THETA2,PHI2,PSI2,M);
        CALL POLSTE(ALPHA3,THETA3,PHI3,PSI3,M);
        PUT SKIP EDIT(PHI1(I),PSI1(I),PHI2(I),PSI2(I),PHI3(I),PSI3(I))
        (F(8,3),COLUMN(11),F(8,3),COLUMN(21),F(8,3),COLUMN(31),F(8,3),
        COLUMN(41),F(8,3),COLUMN(51),F(8,3));
/*
THE POLES ARE ROTATED ABOUT A NORTH-SOUTH AXIS SUCH THAT SIGMA1 LIES
ON THE POLE OF PROJECTION,AND THE ANGLE OF ROTATION IS BETAR3
                                                                    */
        BETAR3=-PHI1(I);
        PHI1(I)=PHI1(I)+BETAR3;
        PHI2(I)=PHI2(I)+BETAR3;
        PHI3(I)=PHI3(I)+BETAR3;
        CALL STEPOL(PHI1,PSI1,ALPHA1,THETA1,M);
        CALL STEPOL(PHI2,PSI2,ALPHA2,THETA2,M);
        CALL STEPOL(PHI3,PSI3,ALPHA3,THETA3,M);
        PUT SKIP EDIT(ALPHA1(I),THETA1(I),ALPHA2(I),THETA2(I),
        ALPHA3(I),THETA3(I))
```

```
PROCEDURE OPTIONS(MAIN);

        (F(8,3),COLUMN(11),F(8,3),COLUMN(21),F(8,3),COLUMN(31),F(8,3),
        COLUMN(41),F(8,3),COLUMN(51),F(8,3));
        END;
        PUT SKIP DATA(BETAR1,BETAR2,BETAR3);
/*
THE THREE PRINCIPAL STRESSES AND THE COHESION AND FRICTION ANGLE OF
THE DISCONTINUITY ARE READ IN
                                                                    */
  START:GET LIST(SIGMA1,SIGMA2,SIGMA3,SO,FI);
/*
THE DUMMY VARIABLES A,B,AND C ARE COMPUTED FOR THE SOLUTION OF THE
INTERSECTION POINTS USING THE FORMULA FOR THE ROOTS OF A QUADRATIC
                                                                    */
        A=1+(TAND(FI))*TAND(FI);
        B=(2*SO*TAND(FI))-SIGMA1-SIGMA3;
        C=(SO*SO)+(SIGMA1*SIGMA3);
        H=(B**2)-4*A*C;
        PUT DATA(A,B,C,H);
/*
IF B**2 >4*A*C THEN THERE ARE NO ROOTS,I.E. NO INTERSECTION
                                                                    */
        IF H<0 THEN DO;
              PUT PAGE EDIT('NO INTERSECTION')(A);
              GOTO FIN; END;
*
IF B**2=4*A*C THEN THERE ARE TWO EQUAL ROOTS,I.E. THE DISCONTINUITY
FAILURE ENVELOPE IS TANGENTIAL TO THE PRINCIPAL STRESS CIRCLE
                                                                    */
        ELSE IF H=0 THEN DO;
              PUT PAGE EDIT('TANGENT AT SIGMA=',-B)(A,F(8,3));
              GOTO FIN; END;
*
OTHERWISE THERE ARE TWO ROOTS,I.E. INTERSECTION POINTS PT1 AND PT2
                                                                    */
        ELSE PT1=(-B+(SQRT(H)))/(2*A);
             PT2=(-B-(SQRT(H)))/(2*A);
              PUT PAGE EDIT('INTERSECTION AT SIGMA=',PT1,' AND SIGMA=',
        PT2)(A,F(8,3),A,F(8,3));
*
ALPHA AND THETA ARRAYS ARE INITIALIZED TO 7777 SO THAT VALUES UPON
WHICH IT IS NOT REQUIRED TO OPERATE MAY BE IDENTIFIED
                                                                    */
        ALPHA,THETA=7777;
*
THE TWO BIAXIAL CASES ARE TREATED FIRST
                                                                    */
        IF ((SIGMA2=SIGMA1) | (SIGMA2=SIGMA3)) THEN DO;
*
THE TWO ANGLES SUBTENDED BY THE INTERSECTION POINTS ARE COMPUTED FROM
THE SHEAR STRESS AND PROJECTION ONTO THE NORMAL STRESS AXIS OF THE
RADII TO THE POINTS PT1 AND PT2
                                                                    */
              T=SC+PT2*TAND(FI);
              ADJ=((SIGMA1+SIGMA2)/2)-PT2;
```

```
CEDURE OPTICAS(MAIN);


            ANG2=(ATAND(T/ADJ))/2;
            T=SC+PT1*TAND(FI);
            ADJ=PT1-((SIGMA1+SIGMA2)/2);
            ANG1=45+(ATAND(T/ADJ))/2;
/*
THE CASE WHEN SIGMA2=SIGMA3 IS CONSIDERED                              */
            IF SIGMA2=SIGMA3 THEN DO;
                 DO I=2 TO 88 BY 2;
                 THETA(I)=ANG2;
                 ALPHA(I)=I;
                 END;
                 DO I=1 TO 89 BY 2;
                 THETA(I)=ANG1;
                 ALPHA(I)=I;
                 END; END;
/*
THE CASE WHEN SIGMA2=SIGMA1 IS CONSIDERED                              */
            ELSE IF SIGMA2=SIGMA1 THEN DO;
                 DO I=2 TO 88 BY 2;
                 PSI(I)=ANG1;
                 PHI(I)=I;
                 END;
                 DO I=1 TO 89 BY 2;
                 PSI(I)=ANG2;
                 PHI(I)=I;
                 END;
                 CALL STEPOL(PHI,PSI,ALPHA,THETA,90);
                 END;
            END;
*
THE GENERAL TRIAXIAL CASE IS CONSIDERED                                */
       ELSE DO;
*
THE CHANGE IN NORMAL STRESS FROM PT2 TO PT1 IS INCREMENTED IN 89 STEPS
AND THE CORRESPONDING SHEAR STRESS AT EACH STEP COMPUTED               */
            D=(PT1-PT2)/90;
            DO I=1 TO 89;
                 SIGMA=PT2+I*D;
                 T=SIGMA*TAND(FI)+SC;
*
THE SQUARE OF THE DIRECTION COSINE CORRESPONDING TO THETA IS COMPUTED  */
                 LL=((SIGMA2-SIGMA)*(SIGMA3-SIGMA)+(T*T))/
                      ((SIGMA2-SIGMA1)*(SIGMA3-SIGMA1));
*
IF 0<LL<1 THEN COS(THETA)=SQRT(L). OTHERWISE THERE IS NO SOLUTION,AND
THETA AND ALPHA ARE BOTH ASSIGNED A VALUE 7777                         */
            IF LL<=0|LL>1 THEN DO;
            ALPHA(I)=7777;
```

```
CEDURE OPTIONS(MAIN);



            THETA(I)=7777;
            GO TO NOG;
            END;
                  L=SQRT(LL);
                  NN=((SIGMA1-SIGMA)*(SIGMA2-SIGMA)+(T*T))/
                        ((SIGMA1-SIGMA3)*(SIGMA2-SIGMA3));
/*
THE SQUARE OF THE SECOND DIRECTION COSINE IS COMPUTED,AND THIS ALSO
MUST LIE 0<NN<1 TO HAVE A SOLUTION. THE SUM OF LL AND NN MUST ALSO BE
<1 OR THE THIRD DIRECTION COSINE HAS NO SOLUTION. IN THE EVENT OF NO
SOLUTION,THETA AND ALPHA ARE BOTH ASSIGNED A VALUE 7777
                                                                    */
            IF NN<=0|NN>1 THEN DO;
            ALPHA(I)=7777;
            THETA(I)=7777;
            GO TO NOG;
            END;
                  N=SQRT(NN);
            IF (1-LL-NN)<=0 THEN DO;
            ALPHA(I)=7777;
            THETA(I)=7777;
            GO TO NOG;
            END;
/*
THETA AND ALPHA ARE COMPUTED FROM THE TWO DIRECTION COSINES
                                                                    */
                  THETA(I)=ATAND((SQRT(1-L*L))/L);
                  L=N/SIND(THETA(I));
                  ALPHA(I)=ATAND((SQRT(1-L*L))/L);
   NOG:     END;
      END;
/*
THE THETA AND ALPHA VALUES FOR THE OTHER THREE QUADRANTS ARE OBTAINED
FROM SYMMETRY
                                                                    */
      DO I=1 TO 89;
      IF ALPHA(I)=7777 | THETA(I)=7777 THEN GO TO NIG;
            ELSE DO;
            ALPHA(180-I)=180-ALPHA(I);
            THETA(180-I)=THETA(I);
            ALPHA(180+I)=180+ALPHA(I);
            THETA(180+I)=THETA(I);
            ALPHA(360-I)=360-ALPHA(I);
            THETA(360-I)=THETA(I);
            END;
   NIG:     END;
*
THE STABILITY PLOT IS ROTATED USING THE VALES -BETAR3,-BETAR2 AND
-BETAR1
                                                                    */
      BETAR1=-BETAR1; BETAR2=-BETAR2; BETAR3=-BETAR3;
      NCOL=4;
      GO TO PLOT;
  ROT3:CALL ROTATE(0,BETAR3,0,ALPHA,THETA,ALPHA,THETA,359);
```

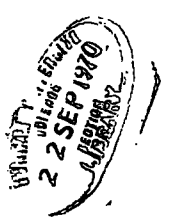
22 SEP 1970

```
:CEDURE OPTIONS(MAIN);



        GO TO PLOT;
   ROT2:CALL ROTATE(BETAR2,0,C,ALPHA,THETA,ALPHA,THETA,359);
        GO TO PLOT;
   ROT1:CALL ROTATE(0,BETAR1,C,ALPHA,THETA,ALPHA,THETA,359);
/*
THE CARTESIAN COORDINATES FOR EACH ALPHA THETA PAIR ARE COMPUTED FOR A
SCRIPT NET AND ENTERED INTO THE CHARACTER ARRAY E AS A +
                                                                      */
   PLOT:E=' ';
        DO I=1 TO 359;
        IF ALPHA(I)=7777 | THETA(I)=7777 THEN GO TO COEND;
              RA=1.4142*ROW*SIND(THETA(I)/2);
              X=((RA*SIND(ALPHA(I)))*COL/ROW)+0.5;
              Y=(RA*COSD(ALPHA(I)))+0.5;
              E(Y,X)='+';
 COEND:       END;
/*
THE CARTESIAN COORDINATES OF THE CIRCLE ARE COMPUTED AND ENTERED INTO
THE CHARACTER ARRAY E AS A *
                                                                      */
        DO I=0 TO ROW;
        XC(I)=((SQRT((ROW*ROW)-(I*I)))*COL/ROW)+0.5;
        XC(-I)=XC(I); END;
        DO I=0 TO ROW; E(I,XC(I))='*'; E(I,-XC(I))='*'; END;
        DO I=0 TO -ROW BY -1; E(I,XC(I))='*'; E(I,-XC(I))='*'; END;
/*
THE X AND Y AXES ARE ENTERED INTO E AS - AND | RESPECTIVELY
                                                                      */
        DO I=-ROW TO ROW; E(I,0)='|'; END;
        DO J=-COL TO COL; E(0,J)='-'; END;
/*
THE ROTATED STABILITY PLOT IS PRINTED
                                                                      */
        PUT PAGE;
        DO I=ROW TO -ROW BY -1; PUT SKIP EDIT('          ')(A);
        DO J=-COL TO COL;
        PUT EDIT(E(I,J))(A(1));
        END; END;
        NCOD=NCOD-1;
        IF NCOD=3 THEN GO TO ROT3;
        IF NCOD=2 THEN GO TO ROT2;
        IF NCOD=1 THEN GO TO ROT1;
   FIN:GOTO START;
        END JTSTAB;
```

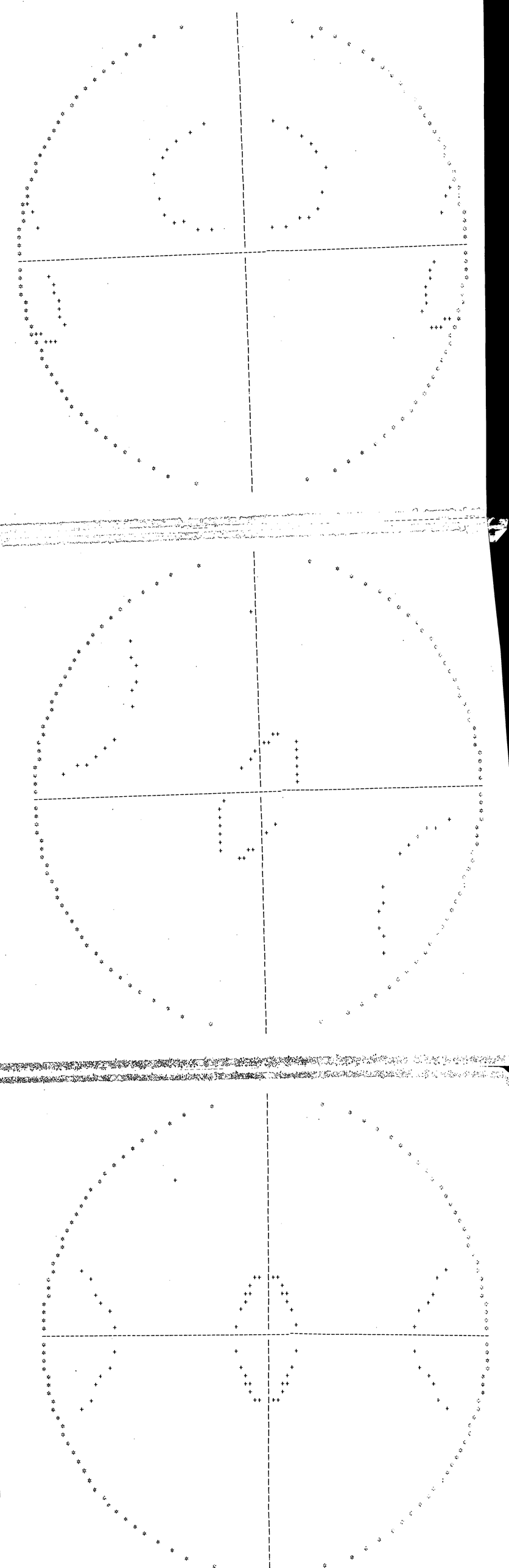

APPENDIX D

L. V. D. T. CALIBRATIONS FOR X-Y PLOTTER

STRESS-STRAIN CURVES

D1. Introduction

The L. V. D. T's used are Electromechanisms type 4035, serial numbers 049 , 050, and have a total travel of 1 inch. The makers calibration was checked and accepted. If the input voltage is maintained constant at 24V then the output voltage change may be monitored directly in terms of displacement, being 15.6×10^3 mV/ins. All the following stress calibrations refer only to Clockhouse proving-ring no. A.2393 (0-10000 kg).

D2. Stress

This is conventionally taken up the y-axis.

D2.1. Nominal 1.5 ins diameter sample - Deviator stress:

100 lb/in^2/cm = 15.15 mV/cm

200 lb/in^2/cm = 30.3 mV/cm

500 lb/in^2/cm = 75.75 mV/cm

Maximum permissible stress is 9000 lb/in^2, i. e. 18 cm on the latter setting.

D2.2. Nominal 1 ins diameter sample - Deviator stress:

100 lb/in^2/cm = 6.73 mV/cm

200 lb/in^2/cm = 13.47 mV/cm

500 lb/in^2/cm = 33.67 mV/cm

1000 lb/in^2/cm = 67.32 mV/cm

Maximum permissible stress is 25000 lb/in^2, which is 25 cm on the latter setting.

D2. 3. Double shear, nominal 1 ins diameter sample - Shear stress T:

50 lb/in^2/cm = 6. 73 mV/cm

100 lb/in^2/cm = 13. 47 mV/cm

200 lb/in^2/cm = 33. 67 mV/cm

500 lb/in^2/cm = 67. 32 mV/cm

Maximum permissible stress is 12500 lb/in^2, which is 25 cm on the latter setting.

D3. Strain

L = sample length, inches.

0. 05%/cm = L x 7. 8 mV/cm

0. 1 %/cm = L x 15. 6 mV/cm

0. 2 %/cm = L x 31. 2 mV/cm

0. 5 %/cm = L x 78 mV/cm

D4. Displacement

15. 6 x 10^3 mV/ins

APPENDIX E

SAMPLE LOCATIONS AND DETAILS

No.	Horizon	Grid Reference	Location	Details
BL1	U.M.L.	NZ 473 387	Blackhall Rocks	Impure dolomite
CH1	M.M.L.	NZ 443 466	Chourdon Point	Reef front breccia, partly dedolomitised.
CH2	M.M.L.	NZ 438 573	Between Chourdon Point & Dawdon	Post-reef dolomite oolite
FO1	M.M.L.	NZ 364 573	Ford Quarry, Sunderland	Shelly reef dolomite
HA1	M.M.L.	NZ 438 465	Hawthorn Quarry, Seaham	Oolitic reef dolomite
HA2	M.M.L.	NZ 436 464	Hawthorn Quarry, Seaham	Reef dolomite
HA3	M.M.L.	NZ 436 466	Hawthorn Quarry, Seaham	Post-reef calcitic dolomite
HA4	M.M.L.	NZ 436 466	Hawthorn Quarry, Seaham	100% cubic aggregate from calcitic dolomite
HA5	M.M.L.	NZ 436 464	Hawthorn Quarry, Seaham	Aggregate from reef dolomites
HO1	L.M.L.	NZ 345 505	Houghton Cut	Cavernous granular dolomite
MA1	U.M.L.	NZ 405 642	Marsden Quarry	Concretionary limestone
MA2	U.M.L.	NZ 399 650	Cliffs N. of Marsden Grotto	'Flexible' Limestone
RA1	L.M.L.	NZ 347 354	Raisby Hill Quarry	Micritic Limestone
TH1	L.M.L.	NZ 310 330	Thrislington Quarry	Buff granular dolomite
TH2	L.M.L.	NZ 310 330	Thrislington Quarry	Dolomitised limestone
TH4	L.M.L.	NZ 310 330	Thrislington Quarry	Dolomitised limestone

No.	Horizon	Grid Reference	Location	Details
TR1	L. M. L.	NZ 384 666	Trow Rocks, South Shields	Buff granular dolomite
TR2	U. M. L.	NZ 384 666	Trow Rocks, South Shields	Cellular breccia, limestone
WI1	M. M. L.	NZ 372 378	Old Wingate Quarry	Oolitic lagoonal dolomite